

FEB 3 1957

MOLECULAR VIBRATIONS IN THE EXCITON THEORY FOR  
MOLECULAR AGGREGATES

I. GENERAL THEORY

By E. G. MCRAE\*

[Manuscript received December 9, 1960]

*Summary*

A molecular aggregate is defined as an ordered array of identical molecules. This definition includes molecular crystals, dimers, and certain polymeric aggregates of dye molecules.

The vibronic states of an electronically excited molecular aggregate are studied theoretically. The aggregate is treated as an array of non-rigid molecules in a rigid lattice. The simplest form of the exciton theory is assumed to be correct except with regard to intramolecular vibrations. The molecules in the aggregate are considered as harmonic oscillators with one vibrational degree of freedom, whose individual wave functions are Born-Oppenheimer separable. The molecules are assumed to interact by a purely electronic mechanism.

Born-Oppenheimer separable wave functions for the whole aggregate, here called E-V functions, are defined. It is shown that the interaction integrals between E-V functions may be expressed in terms of integrals which depend only on the properties of individual molecules. Explicit expressions are given for the latter integrals.

The resonance interactions between E-V functions are described. On this basis, the limiting conditions under which the E-V functions steadily approach exact vibronic state functions of the aggregate are specified.

The vibrational overlap integrals between E-V and electronic ground-state wave functions are studied. These integrals may be expressed as sums of products of vibrational overlap integrals for individual molecules. Explicit expressions for the latter integrals are obtained through an approximation to Hirschmann's theory.

I. INTRODUCTION

We define a molecular aggregate as an ordered array of identical molecules. This definition includes molecular crystals, dimers, and certain polymeric aggregates of dye molecules.

The exciton theory of the electronically excited states of solids was first applied to molecular aggregates by Davydov (1948). A simplified version of the theory has been given by Craig and Hobbins (1955). Davydov's work made possible an interpretation of the effects of aggregation on electronic spectra, and has stimulated much recent work on that topic (Ganguly and Chaudhury 1959; McClure 1959; Wolf 1959).

The accumulated experimental information indicates that the exciton theory offers a basically correct description of the lower-energy excited states, but a

\* Division of Chemical Physics, C.S.I.R.O. Chemical Research Laboratories, Melbourne.

number of obstacles remains to be surmounted before the theory can be applied confidently in either quantitative or detailed interpretations. One of the chief difficulties is that of the inclusion of intramolecular vibrations in the exciton-theory description, and it is to this question that the present series of papers is addressed.

Lattice vibrations are not considered in this work. Our discussion thus refers to a model consisting of an array of non-rigid molecules in a rigid lattice.\*

The significance of intramolecular vibrations may be understood with reference to Davydov's original formulation, in which vibrational motions were not considered. The displacement and splitting of electronic bands were expressed there in terms of intermolecular interaction integrals involving the electronic wave functions of the component molecules. When molecular vibrations are included, each integral must be multiplied by a vibrational overlap factor whose magnitude is not in general equal to or even close to unity. Again, Davydov's theory applies to an electronic band as a whole, without reference to the extended system of vibrational structure ordinarily encountered in molecular spectra. The inclusion of molecular vibrations permits, in principle, an interpretation of vibrational structure within the electronic band envelope. From these considerations it is clear that the inclusion of molecular vibrations is necessary for either a quantitative or detailed application of the exciton theory to molecular aggregates.

Davydov (1948) suggested that vibrational motions might be taken into account by a method similar to that normally adopted for single molecules. However, the simplifying condition of Born-Oppenheimer separability, which ordinarily applies in a fairly good approximation to molecules, cannot be assumed to hold for electronically excited molecular aggregates. Born-Oppenheimer separability for a given state depends on the energy separation between it and neighbouring electronic states being large in comparison with a fundamental vibrational interval, a condition which is ordinarily encountered in molecules but never in the exciton states of molecular aggregates. Simpson and Peterson (1957) subsequently proposed that the correct description of an exciton state, including intramolecular vibrations, is in some sense intermediate between the following two limiting cases: in the first limiting case, Born-Oppenheimer separability applies to the individual molecules in the aggregate, and in the second the wave functions for the whole system are Born-Oppenheimer separable.

In Davydov's theory, i.e. neglecting vibrational motions, the stationary exciton-state wave functions are built up from simple products of electronic wave functions for individual molecules. Each product represents electronic excitation localized at a particular molecule, and the exciton wave functions are linear combinations of the products. For a representation of the first limiting case of Simpson and Peterson, the exciton wave functions are constructed, in the same way, from products of the vibronic (*vibrational plus electronic*) wave functions for individual molecules. The other limiting case may be represented

\* We refer here to the lattice of molecular centres. Were we to consider the lattice of atomic centres, our discussion would refer to the inclusion of the optical branch of the lattice vibrations.

by products of electronic and vibrational wave functions for the aggregate as a whole.

The formation of the wave functions may be indicated schematically as follows: let  $v$ ,  $e$ , and  $m$  signify vibrational, electronic, and vibronic types of wave function for an individual molecule, and let  $V$ ,  $E$ , and  $M$  signify the same types of wave function for an aggregate as a whole. Here, but not elsewhere in this paper, let  $\Pi$  denote the formation of a simple product function, and  $\Sigma$  the formation of a linear combination. The construction of Davydov's wave functions is summarized by

$$\Pi e \rightarrow \Sigma \Pi e = E.$$

For the inclusion of intramolecular vibrations, we have the following two schemes, corresponding respectively to the first and second limiting cases of Simpson and Peterson :

$$ev = m; \quad \Pi m \rightarrow \Sigma \Pi m = M \quad (m-m \text{ coupling}), \quad (1)$$

$$\begin{aligned} \Pi e \rightarrow \Sigma \Pi e &= E; \\ \Pi v \rightarrow \Sigma \Pi v &= V; \end{aligned} \quad \left\{ \begin{aligned} EV &= M && (\text{E-V coupling}). \end{aligned} \right. \quad (2)$$

It is proposed that, by analogy with  $j-j$  and  $L-S$  coupling in atoms, the above schemes should be called  $m-m$  and  $E-V$  coupling.\*

The wave functions corresponding to either of the limiting cases ( $m-m$  or  $E-V$  wave functions) may be adopted as zeroth-order wave functions for a perturbation treatment of the general case of intermediate coupling. Previous work on this topic has been confined mainly to the case of  $m-m$  coupling (Craig 1955; McClure and Schnepp 1955; Bingel 1959) and to the approach to intermediate coupling from the  $m-m$  coupling limit (McClure 1958). In the present work, we have considered the possibility of including intramolecular vibrations in the exciton theory, starting from the limiting case of  $E-V$  coupling. The theory given here is complementary to previous work based on  $m-m$  coupling.

The present work is reported in Parts I, II, and III. Part I of the series is devoted to the definition of Born-Oppenheimer separable wave functions for a molecular aggregate, and to interaction and overlap integrals involving the defined functions. The number,  $N$ , of molecules in the aggregate is retained in all formulae, so that the derivations apply to both large polymeric aggregates and dimers.† In Part II, the theory for dimeric systems is obtained by setting  $N=2$ , and in Part III the theory for polymeric systems is discussed as a limiting case of large  $N$ .‡

\* In Simpson and Peterson's (1957) nomenclature,  $m-m$  and  $E-V$  coupling correspond respectively to weak and strong (intermolecular) coupling. The present terminology offers a mnemonic description of the limiting cases, without anticipating any results of theory.

† In order to treat non-cyclic aggregates of intermediate size, it would be necessary to consider end or surface effects, which are beyond the scope of the present work.

‡ Since this paper was prepared for publication, a new treatment of the limiting coupling cases for a dimer has appeared (Witkowski and Moffitt 1960). It is shown in Appendix I that the special form of the present theory which is obtained by putting  $N=2$  is consistent with the theory of Witkowski and Moffitt.

## II. MODEL AND BASIC ASSUMPTIONS

Since E-V coupling has not previously been discussed in detail, it seems appropriate to keep the present treatment as simple as possible, and we propose to do this by assuming a simple model for the individual molecules and for the aggregate as a whole. The model, basic assumptions, and as much notation as practicable, are introduced here. A further simplifying assumption, which is not however essential to the theory, is introduced in Section VII.

### *(a) Model and Notation for Individual Molecules*

The model for the individual molecules is defined by the following properties :

- (i) Born-Oppenheimer separability applies exactly in all electronic states.
- (ii) The nuclear motion is restricted to one normal mode of vibration.
- (iii) The vibration is harmonic.

Properties (i) and (iii) of the model correspond to approximations which are frequently adopted in the description of molecules. Property (ii) applies strictly to diatomic molecules only. However, we show in Appendix II that the theory for the above model may be applied to systems of polyatomic molecules, as long as only one mode of vibration is excited in the electronic transition to the excited state under consideration, and all modes of vibration are harmonic.

The condition of Born-Oppenheimer separability (property (i)) will be understood to apply in the sense of the "static" approximation. This means that for a non-rotating molecule in its  $a$ th electronic state the total Hamiltonian  $\mathcal{H}$  can be written

$$\mathcal{H} = \mathcal{U}_a + \mathcal{V}_a, \quad (3)$$

where  $\mathcal{U}_a$  denotes the electronic Hamiltonian for a molecule rigidly fixed in the equilibrium nuclear configuration for the  $a$ th electronic state and  $\mathcal{V}_a$  denotes the Hamiltonian for vibrational motion about the equilibrium configuration.

A notation for the electronic and vibrational wave functions and for the corresponding energy eigenvalues may be introduced through the Schroedinger equations

$$\mathcal{U}_a \psi_a = u_a \psi_a, \quad (4)$$

$$\langle \mathcal{V}_a \rangle_b \chi_{am} = v_{am} \chi_{am}, \quad (5)$$

where in general

$$\langle \mathcal{V}_a \rangle_b = \int \psi_b^* \mathcal{V}_a \psi_b d\tau = (\psi_b | \mathcal{V}_a | \psi_b) \quad (6)$$

(the star denotes a complex conjugate and the integration is to be carried over all coordinates represented in the integrand).

Property (ii) of the model enables us to specify that the vibrational wave functions all belong to one normal mode. We denote the normal coordinate by  $R$ , and its equilibrium value in the  $a$ th electronic state by  $R_a$ . Property (iii) means that we can write

$$\mathcal{V}_a = \mathcal{T} + \frac{d\mathcal{H}}{dR} \Big|_{R_a} (R - R_a) + \frac{1}{2} \frac{d^2\mathcal{H}}{dR^2} \Big|_{R_a} (R - R_a)^2, \quad (7)$$

where  $\mathcal{T}$  denotes the vibrational kinetic energy operator.

We now derive an expression for  $\langle \mathcal{V}_a \rangle_b$ . This integral, though a property of an individual molecule, will be found to play a vital part in the exciton theory for molecular aggregates. We note that  $\psi_a$  is a "static" electronic wave function in the sense that

$$\frac{d\psi_a}{dR} = \frac{d^2\psi_a}{dR^2} = \dots = 0. \quad (8)$$

(This follows from equation (4) and the definition of  $\mathcal{U}_a$ .) Because of property (i) we can identify the integral  $(\psi_b | \mathcal{H} | \psi_b)$  with the total energy of a molecule with stationary nuclei in the  $b$ th electronic state. Using properties (ii) and (iii) we have

$$(\psi_b | \mathcal{H} | \psi_b) = u_b + \frac{1}{2}k_b(R - R_b)^2,$$

where  $k_b$  denotes the force constant for the  $b$ th electronic state. From this equation and equations (7) and (8) we obtain

$$\langle \mathcal{V}_a \rangle_b = \mathcal{T} + k_b(R_a - R_b)(R - R_a) + \frac{1}{2}k_b(R - R_a)^2. \quad (9)$$

In the above expression for  $\langle \mathcal{V}_a \rangle_b$ ,  $k_b$ ,  $R_a$ , and  $R_b$  should be understood to signify actual rather than calculated molecular constants.

Where  $a=b$ , equation (9) reduces to the harmonic oscillator Hamiltonian. The vibrational energy levels are given by

$$v_{am} = (m + \frac{1}{2})\hbar c v_a,$$

where  $v_a$  denotes the fundamental vibrational frequency ( $\text{cm}^{-1}$ ) for the  $a$ th electronic state,  $\hbar$  denotes Planck's constant, and  $c$  the velocity of light. The eigenfunctions  $\chi_{am}$  are Hermite orthogonal functions with argument  $\beta_a^{\frac{1}{2}}(R - R_a)$ , where, if  $\mu$  denotes the reduced mass,

$$\beta_a = 4\pi^2 \mu c v_a / \hbar.$$

Throughout this work, the electronic ground state is designated by  $a=0$ , and the energy scale is chosen so that  $u_0=0$ . The electronically excited state under consideration is designated by  $a=1$ . Finally, where it is necessary to distinguish between different molecules in an aggregate, we do so by means of superscripts in parentheses.

### *(b) Model and Assumptions for the Aggregate*

The lattice of an aggregate of  $N$  molecules is defined as the  $N$  points lying at the molecular centres. The model for the aggregate is defined by the following properties :

- (i') The lattice is rigid.
- (ii') Molecules lying at different sites in the unit cell have equivalent local environments.

Property (i') means that the model may be described as an ordered array of non-rigid molecules in a rigid lattice. Property (ii') is not unduly restrictive, since it is found in many real molecular aggregates.

The basic assumptions of the theory may be stated as follows: the simplest form of the exciton theory, as presented by Craig and Hobbins (1955), is assumed to be correct except with regard to intramolecular vibrations. In particular:

- (i) Cyclic boundary conditions are assumed.
- (ii) Interactions between states which correspond to different electronic states of the monomer are neglected.
- (iii) The part of the Hamiltonian operator representing the intermolecular interactions is assumed to be purely electronic in character—i.e. independent of intramolecular nuclear displacements.

Assumption (iii) has special relevance to the present work. It means that we are ignoring any possible mechanical coupling of the vibrational motions of neighbouring molecules.

### III. THEORY OF E-V COUPLING

The Hamiltonian operator for the aggregate is

$$\mathcal{H}_{\text{agg}} = \sum_j \mathcal{H}^{(j)} + \sum_j \sum_{i>j} \mathcal{W}^{(j,i)}, \quad (10)$$

where  $\mathcal{W}^{(j,i)}$  denotes the energy of non-electrostatic interaction between the  $i$ th and  $j$ th molecules. If electrostatic (i.e. permanent multipole) interaction terms are present, they may be absorbed into the first sum. For a description of the electronically excited aggregate, we propose to divide the Hamiltonian into an electronic part and a vibrational part in a manner formally similar to the partition for a single molecule (see eqn. (3)). Specifically, we choose the partition

$$\mathcal{H}_{\text{agg}} = \sum_j \mathcal{U}_\sigma^{(j)} + \sum_j \sum_{i>j} \mathcal{W}^{(j,i)} + \sum_j \mathcal{V}_\sigma^{(j)}, \quad (11)$$

where

$$\begin{aligned} \mathcal{U}_\sigma &= [\mathcal{U}_1 + (N-1)\mathcal{U}_0]/N, \\ \mathcal{V}_\sigma &= [\mathcal{V}_1 + (N-1)\mathcal{V}_0]/N. \end{aligned}$$

The right-hand side of equation (11) may be identified with the right-hand side of (10) through the use of (3) and the defining equations for  $\mathcal{U}_\sigma$  and  $\mathcal{V}_\sigma$ .

The above partition of the Hamiltonian  $\mathcal{H}_{\text{agg}}$  has no *a priori* justification, but it is an expression of the idea that in a stationary excited state the probability of electronic excitation is spread evenly over the  $N$  molecules of the aggregate. We shall define the E-V coupling wave functions with reference to equation (11), and the success of our method will be judged ultimately by the usefulness of the E-V functions as the basis for a perturbation expansion.

The E-V coupling wave functions are products of an electronic and a vibrational wave function for the aggregate as a whole. We define one-molecule electronic wave functions and energies through the Schrödinger equation

$$\mathcal{U}_\sigma \varphi_a = u'_a \varphi_a.$$

$\mathcal{U}_\sigma$  denotes the Hamiltonian corresponding to some fixed value of  $R$  intermediate between  $R_0$  and  $R_1$ . We shall not attempt to calculate this value of  $R$ , because to do so would require a too detailed analysis which is beyond the scope of the present

study. We do, however, note that because of equation (8),  $\varphi_a$  can be identified with  $\psi_a$ . This provision of the model will be exploited by replacing all integrals involving  $\varphi$ 's by the corresponding integrals involving  $\psi$ 's. However, the notational difference will be retained to emphasize that  $\varphi_a$  and  $\psi_a$  are regarded as eigenfunctions of different Schrödinger equations.

The electronic wave functions for the aggregate are eigenfunctions of the electronic part of the Hamiltonian (11). According to the exciton theory, they are given by

$$\Phi(\mathbf{k}) = N^{-\frac{1}{2}} \sum_j \exp i\mathbf{k} \cdot \mathbf{r}^{(j)} \Phi^{(j)}, \quad (12)$$

where  $\mathbf{r}^{(j)}$  denotes the position vector of the centre of the  $j$ th molecule, and

$$\Phi_1^{(j)} = (\prod_i \varphi_0^{(i)}) \varphi_1^{(j)} / \varphi_0^{(j)}.$$

The wave vector  $\mathbf{k}$  may take any one of  $N$  values lying within the first Brillouin zone. If the crystal is a parallelopiped, one edge of which contains  $N_\alpha$  lattice points, the corresponding component of  $\mathbf{k}$  may take any one of the  $N_\alpha$  values

$$0, \pm 2\pi b_\alpha / N_\alpha, \dots, \pm (N_\alpha - 1) 2\pi b_\alpha / N_\alpha, \pi b_\alpha,$$

where  $b_\alpha$  is the magnitude of the appropriate primitive translation in the reciprocal lattice.

The energy corresponding to  $\Phi(\mathbf{k})$ , referred to  $N u_0$  as origin, is

$$U(\mathbf{k}) = u'_1 + (N-1)u'_0 + S(\mathbf{k}), \quad (13)$$

where  $S(\mathbf{k})$  denotes the lattice sum of intermolecular interaction integrals, given by

$$S(\mathbf{k}) = \sum_j \exp i\mathbf{k} \cdot (\mathbf{r}^{(j)} - \mathbf{r}^{(i)}) (\Phi^{(j)} | \mathcal{W}^{(j,i)} | \Phi^{(i)}).$$

The effective vibrational Hamiltonian is the expectation value of the vibrational part of the Hamiltonian (11) with respect to any one of the electronic wave functions (12). It is

$$\sum_j \langle \mathcal{V}_\sigma^{(j)} \rangle_\sigma, \quad (14)$$

where

$$\langle \mathcal{V}_\sigma \rangle_\sigma = [\langle \mathcal{V}_\sigma \rangle_1 + (N-1)\langle \mathcal{V}_\sigma \rangle_0] / N.$$

One-molecule vibrational wave functions and energies are defined through the Schrödinger equation

$$\langle \mathcal{V}_\sigma \rangle_\sigma \chi_{\sigma m} = v_{\sigma m} \chi_{\sigma m}.$$

As we have specified that the intermolecular interaction is purely electronic—i.e. that there is no mechanical coupling of vibrations—any product of  $N$  one-molecule vibrational wave functions, one for each molecule, is an eigenfunction of the total vibrational Hamiltonian (14). Any product may be characterized by a designation of the location and degree of vibrational excitation of each vibrationally excited molecule. Consider the product representing  $d_1$  quanta of vibrational excitation of the vibrationally excited molecule whose position vector is  $\mathbf{r}^{(j)}$ ,  $d_2$  quanta of vibrational excitation of the vibrationally excited

molecule whose position vector is  $\mathbf{r}^{(j)} + \mathbf{s}_{12}$  and so on through all vibrationally excited molecules. We denote this product by

$$X_{d_1}^{(j)} s_{12} d_2 \dots . \quad (15)$$

We can write down  $N-1$  other products which differ from (15) only in the first superscript, and which thus represent an equivalent physical situation.\* To take advantage of the translational symmetry of the system, we construct linear combinations of all sets of  $N$  physically equivalent products, as follows :

$$X_{d_1} s_{12} d_2 \dots (\mathbf{l}) = N^{-1} \sum_j \exp i\mathbf{l} \cdot \mathbf{r}^{(j)} X_{d_1}^{(j)} s_{12} d_2 \dots . \quad (16)$$

Here  $\mathbf{l}$  is a vibrational wave vector analogous to the electronic wave-vector  $\mathbf{k}$ .

The vibrational wave functions, and the corresponding vibrational energies for a molecular aggregate are

$$X_{d_1} s_{12} d_2 \dots (\mathbf{l}) ; \quad V_p = (N-1)v_{c0} + v_{cp}, \quad (17)$$

where  $p = d_1 + d_2 + \dots$ . The E-V wave functions and energies are

$$\Phi(\mathbf{k}) X_{d_1} s_{12} d_2 \dots (\mathbf{l}) ; \quad U(\mathbf{k}) + V_p. \quad (18)$$

The E-V wave functions defined as above constitute an orthogonal set of functions of electronic and nuclear coordinates.

#### IV. INTERACTIONS BETWEEN E-V FUNCTIONS

The interaction integral between two E-V functions,

$$\Phi(\mathbf{k}) X_{d_1} s_{12} d_2 \dots (\mathbf{l}) \text{ and } \Phi(\mathbf{k}') X_{d'_1} s'_{12} d'_2 \dots (\mathbf{l}')$$

is

$$\langle \Phi(\mathbf{k}) X_{d_1} s_{12} d_2 \dots (\mathbf{l}) | \mathcal{H}_{\text{agg}} | \Phi(\mathbf{k}') X_{d'_1} s'_{12} d'_2 \dots (\mathbf{l}') \rangle, \quad (\mathbf{k}, \mathbf{l}) \neq (\mathbf{k}', \mathbf{l}'), \quad (19)$$

where the integration is to be carried over all electronic and nuclear coordinates. Upon integrating over the electronic coordinates, the interaction integral becomes

$$\langle X_{d_1} s_{12} d_2 \dots (\mathbf{l}) | \sum_j \langle \mathcal{V}_\sigma^{(j)} \rangle_{\text{int } \mathbf{k}\mathbf{k}'} | X_{d'_1} s'_{12} d'_2 \dots (\mathbf{l}') \rangle,$$

where

$$\langle \mathcal{V}_\sigma^{(j)} \rangle_{\text{int } \mathbf{k}\mathbf{k}'} = N^{-1} \exp i(\mathbf{k}' - \mathbf{k}) \cdot \mathbf{r}^{(j)} (\langle \mathcal{V}_\sigma^{(j)} \rangle_1 - \langle \mathcal{V}_\sigma^{(j)} \rangle_0).$$

In deriving this result, we have made use of the relationship

$$N^{-1} \sum_j \exp i(\mathbf{k} - \mathbf{k}') \cdot \mathbf{r}^{(j)} = \delta_{\mathbf{k}-\mathbf{k}'} \frac{2\pi}{a} \mathbf{b}, \quad (20)$$

where  $\mathbf{k}$  and  $\mathbf{k}'$  are two wave vectors,  $\delta$  denotes the Kronecker delta, and  $\mathbf{b}$  is any sum of primitive translation vectors in the reciprocal lattice.

\* There are certain symmetrical distributions of vibrational quanta for which there are less than  $N-1$  other products. We shall, however, ignore these possibilities except in the case of a dimer, where we note that there is only one possible product function representing two molecules vibrationally excited to the same degree.

We have the rule that the interaction integral (19) is zero unless the following condition is satisfied :

$$\mathbf{k} + \mathbf{l} = \mathbf{k} + \mathbf{l} + 2\pi\mathbf{b}. \quad (21)$$

The rule may be proved with the aid of equation (20).

The interaction integrals may be expressed in terms of the one-molecule interaction integrals

$$\langle \chi_{\sigma m} | \langle \mathcal{V}_\sigma \rangle_1 - \langle \mathcal{V}_\sigma \rangle_0 | \chi_{\sigma m'} \rangle.$$

The expansions may be carried out readily in particular cases, especially if only a few vibrational quanta are involved. We shall describe the expansions of some important interaction integrals in Section VI. By virtue of the orthogonality of the vibrational wave functions, each interaction integral may be expressed exclusively in terms of one-molecule interaction integrals for which

$$|m - m'| = |p - p'|, \quad (22)$$

where  $p'$  has a meaning analogous to  $p$ , viz.  $p' = d'_1 + d'_2 + \dots$ .

In order to obtain useful expressions for the one-molecule interaction integrals, we make use of the harmonic-oscillator property of the model, as expressed by equation (9). From the definitions of  $\mathcal{V}_\sigma$  and  $\langle \mathcal{V}_\sigma \rangle_\sigma$  (see eqns. (11) and (14)) we obtain

$$\begin{aligned} \langle \mathcal{V}_\sigma \rangle_\sigma &= \mathcal{T} + \frac{1}{2}k_\sigma R^2 - k_\sigma R_\sigma R + C_1 \\ &= \mathcal{T} + \frac{1}{2}k_\sigma(R - R_\sigma)^2 + C_2, \end{aligned}$$

where  $C_1$  and  $C_2$  are constants involving  $N$ ,  $k_1$ ,  $k_0$ ,  $R_1$ , and  $R_0$ , and

$$\begin{aligned} k_\sigma &= [k_1 + (N-1)k_0]/N, \\ R_\sigma &= [k_1 R_1 + (N-1)k_0 R_0]/Nk_\sigma. \end{aligned}$$

The eigenvalues of  $\langle \mathcal{V}_\sigma \rangle_\sigma$  are

$$v_{\sigma m} = (m + \frac{1}{2})\hbar c v_\sigma + C_2,$$

where

$$v_\sigma = \{[v_1^2 + (N-1)v_0^2]/N\}^{\frac{1}{2}}.$$

The eigenfunctions  $\chi_{\sigma m}$  of  $\langle \mathcal{V}_\sigma \rangle_\sigma$  are harmonic oscillator functions with argument  $\beta_\sigma^{\frac{1}{2}}(R - R_\sigma)$ , where

$$\beta_\sigma = 4\pi^2 \mu c v_\sigma / \hbar.$$

Again making use of the definitions of  $\mathcal{V}_\sigma$  and  $\langle \mathcal{V}_\sigma \rangle_\sigma$ , expanding in powers of  $R$  and collecting terms, we obtain

$$\langle \mathcal{V}_\sigma \rangle_1 - \langle \mathcal{V}_\sigma \rangle_0 = \frac{1}{2}(k_1 - k_0)(R - R_\sigma)^2 + (k_1 k_0/k_\sigma)(R_0 - R_1)(R - R_\sigma) + C_3,$$

where  $C_3$  is a constant similar to  $C_2$ .

With the aid of some tabulated formulas for integrals involving harmonic oscillator functions (Wilson, Decius, and Cross 1955), we obtain

$$\langle \chi_{\sigma m} | \langle \mathcal{V}_\sigma \rangle_1 - \langle \mathcal{V}_\sigma \rangle_0 | \chi_{\sigma m'} \rangle = \begin{cases} A[(m+1)(m+2)]^{\frac{1}{2}} & (m' = m+2), \\ B(m+1)^{\frac{1}{2}} & (m' = m+1), \\ 2A(m+\frac{1}{2}) + C_3 & (m' = m), \\ Bm^{\frac{1}{2}} & (m' = m-1), \\ A[(m-1)m]^{\frac{1}{2}} & (m' = m-2), \\ 0 & (m' \neq m, m' \neq m \pm 1, m' \neq m \pm 2), \end{cases} \quad (24)$$

where

$$\begin{aligned} A &= (k_1 - k_0)/4\beta_\sigma = \hbar c(v_1^2 - v_0^2)/4v_\sigma, \\ B &= k_1 k_0 (R_0 - R_1)/k_\sigma (2\beta_\sigma)^{\frac{1}{2}}. \end{aligned}$$

We note that the *A*-type integrals ( $m - m' = 0, \pm 2$ ) arise from the difference between the ground- and excited-state vibrational force constants, while the *B*-type integrals ( $m - m' = \pm 1$ ) arise from the difference between the equilibrium values of the normal coordinate—i.e. from the molecular distortion caused by electronic excitation. The constant  $C_3$  plays no part in the theory, as it always cancels out in expressions for the interaction integrals.

We have noted that the interaction integral (19) may be expressed exclusively in terms of one-molecule interaction integrals for which equation (22) holds. Referring to equation (24), we find that the interaction integral vanishes unless  $p$  and  $p'$  differ by 0, 1, or 2. This result, and the rule expressed by equation (21), may be summarized by the following statement: the interaction integral (19) vanishes unless each of the conditions,

$$\mathbf{k} + \mathbf{l} = \mathbf{k}' + \mathbf{l}' + 2\pi\mathbf{b}, \quad (25a)$$

$$p - p' = 0, \pm 1, \pm 2 \quad (25b)$$

is satisfied.

#### V. LIMITING CASES OF E-V COUPLING

Now we seek to specify the limiting conditions under which the E-V wave functions become exact\* vibronic functions of an aggregate.

A necessary condition for the steady approach of any one E-V function to an exact vibronic function is that the E-V function should not be involved in resonance interaction. This condition is satisfied for all E-V functions as long as one or other of the following inequalities are satisfied:

$$0 < \Delta U < \hbar c v_\sigma, \quad (26a)$$

$$\delta U > 2\hbar c v_\sigma, \quad (26b)$$

where  $\Delta U$  denotes the width of the band of electronic energy levels given by equation (13), and  $\delta U$  denotes the separation of the two closest-spaced levels in the band. The inequalities (26a) and (26b) were obtained by a consideration of the E-V energy levels (eqn. (18)) and the selection rules (25a) and (25b) imposed on the interaction integrals. The regions of resonance interaction are illustrated in Figure 1.

If inequality (26a) is satisfied, all of the E-V functions tend steadily to exact wave functions in the limit

$$\frac{v_1 - v_0}{R_1 - R_0} \rightarrow 0, \quad (27)$$

since the interaction integrals all vanish in that limit. If inequality (26b) is satisfied, two independent limiting conditions may be specified: they are (27) and

$$\Delta U \rightarrow \infty. \quad (28)$$

\* In this context, an "exact" wave function means exact within the limitations of the simplest form of the exciton theory (see Section II).

As the limit (28) is approached, the separations of all pairs of interacting energy levels increase indefinitely, so that the first-order corrections to the E-V wave functions tend to zero.

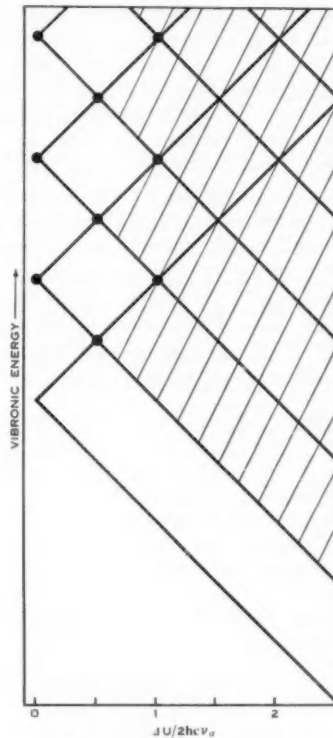


Fig. 1.—E-V levels for an electronically excited molecular aggregate, as a function of the electronic bandwidth  $\Delta U$ . At the left are the four lowest vibrational levels with spacing  $h\nu_0$ . The splitting of each such level is assumed to be symmetrical, and only the highest and lowest level of each band is shown. In the case of a dimer, resonance interaction occurs at the points marked by dots. In the case of a macroscopic aggregate, resonance interaction occurs at the points marked by dots and also in the shaded region.

As regards the totality of vibronic states of a macroscopic aggregate, the limiting condition (28) is only of academic interest, since inequality (26b) cannot be satisfied in real macroscopic systems. For the lower-energy E-V functions, however, the necessary condition of absence of resonance interaction is satisfied under less stringent conditions than indicated by the inequalities (26a) and (26b).

The extreme example is the lowest-energy E-V function, which is not involved in resonance interaction at any value of  $\Delta U$ . This wave function tends steadily to an exact wave function under either of the limiting conditions (27) or (28).

In the case of a dimer,  $\Delta U$  and  $\delta U$  are identical, and the value of  $\Delta U$  required to satisfy (26b) is of the order of magnitude of the observed splitting of electronic levels.

#### VI. RELATIONSHIP BETWEEN E-V AND ACTUAL ENERGY LEVELS FOR A SYSTEM OF NON-INTERACTING MOLECULES

The absolute E-V energy levels may be calculated by applying a second-order perturbation-theory correction to the lowest E-V level for a hypothetical system of non-interacting (i.e. infinitely separated) molecules, and identifying the corrected level with the zero-point level of the electronically excited monomer. This procedure is of course subject to the usual limitations of perturbation theory, but it should be moderately accurate in all cases in which one would choose the approach based on E-V coupling rather than m-m coupling. The use of perturbation theory may be viewed as an alternative to the procedure involving the evaluation of the eigenvalue  $u_1'$  of the Hamiltonian  $\mathcal{U}_0$ .

The second-order correction to the level  $\Phi(\mathbf{k})X$  is

$$-\sum'_{\mathbf{k}'} \sum_{\mathbf{l}} \left\{ \frac{\left| \langle X | \sum_j \langle \mathcal{V}_{\sigma}^{(j)} \rangle_{\text{int } \mathbf{k}\mathbf{k}'} | X_1(\mathbf{l}) \rangle \right|^2}{\hbar c v_{\sigma}} + \frac{\left| \langle X | \sum_j \langle \mathcal{V}_{\sigma}^{(j)} \rangle_{\text{int } \mathbf{k}\mathbf{k}'} | X_2(\mathbf{l}) \rangle \right|^2}{2\hbar c v_{\sigma}} \right\},$$

where the prime on the summation sign denotes exclusion of terms for which  $\mathbf{k}' = \mathbf{k}$ . The interaction integrals may be expressed in terms of one-molecule interaction integrals as follows :

$$\langle X | \sum_j \langle \mathcal{V}_{\sigma}^{(j)} \rangle_{\text{int } \mathbf{k}\mathbf{k}'} | X_m(\mathbf{l}) \rangle = N^{-\frac{1}{2}} (\chi_{00} | \langle \mathcal{V}_{\sigma} \rangle_1 - \langle \mathcal{V}_{\sigma} \rangle_0 | \chi_{0m}),$$

all  $\mathbf{l}$ ,  $\mathbf{k}'$  satisfying equations (25a) and (25b).

The sum consists of  $N-1$  terms. From equation (24), we obtain for the second-order correction

$$-[(N-1)/N \hbar c v_{\sigma}] [B^2 + A^2]. \quad (29)$$

The E-V levels for a system of non-interacting molecules lie on the high-energy side of the lowest monomer level, the magnitude of the displacement of the lowest E-V level being given approximately by (29). We have not considered electrostatic interactions, which if present would cause a further displacement of the entire system of energy levels.

For a system of non-interacting molecules, the electronically excited vibronic levels occur in groups of closely-spaced levels, where all levels within any one group correspond to the excitation of the same number of vibrational quanta. As a simple example we consider the group of levels corresponding to the excitation of one vibrational quantum. The group consists of two levels whose energies, referred to the zero-point level, and degeneracies (degeneracies at left) are :

$$\begin{array}{ll} N(N-1); & \hbar c v_0, \\ N; & \hbar c v_1. \end{array}$$

In the E-V description of the same system, each group of levels is represented by a single level. This artificial degeneracy is split in the first order of perturbation theory. We illustrate this with reference to the group of levels, discussed above, corresponding to the excitation of one quantum of vibration. In the E-V description this group is represented by a single level of degeneracy  $N^2$  and energy  $\hbar\omega_0$ . The energy levels correct to the first order in perturbation theory, and the corresponding wave functions, may be obtained by solution of the appropriate secular equation. The new wave functions are related to the E-V functions by the transformation

$$\Theta(\mathbf{k}, \mathbf{r}^{(e)}) = N^{-1} \sum_{\mathbf{k}'} \exp i(\mathbf{k}' - \mathbf{k}) \cdot \mathbf{r}^{(e)} \Phi(\mathbf{k}') X_1(\mathbf{k} - \mathbf{k}').$$

By expanding the right-hand side according to equations (12) and (16) it can be seen that  $\mathbf{r}^{(e)}$  represents the position vector of the site of vibrational excitation with respect to the site of electronic excitation.

The first-order perturbation treatment gives rise to two levels whose degeneracies and energies referred to the lowest E-V level are

$$N(N-1); \quad \hbar\{\omega_0 - (1/N)(\omega_1^2 - \omega_0^2)/2\omega_0\}, \quad (\mathbf{r}^{(e)} \neq 0), \\ N; \quad \hbar\{\omega_0 + [(N-1)/N](\omega_1^2 - \omega_0^2)/2\omega_0\}, \quad (\mathbf{r}^{(e)} = 0).$$

The first-order splitting and the actual level separation are equal in the approximation of neglecting the second and higher powers of  $(\omega_1 - \omega_0)/(\omega_1 + \omega_0)$ . The remaining small discrepancies between the E-V level separations and the actual level separations are presumably corrected in the second and higher orders of perturbation theory.

### VII. VIBRATIONAL OVERLAP INTEGRALS

The vibrational overlap integrals between ground-state and E-V wave functions enter into the discussion of the vibrational structure in electronic band systems. We shall take up this question in Parts II and III of this series (see pp. 345, 356).

The electronic ground-state wave functions and the corresponding energies for a molecular aggregate are given approximately by

$$\Psi X_{d_1}^{0 \quad s_{11}} d_2 \dots (l); \quad V_p^0,$$

where  $\Psi = \prod_j \psi_j^{(0)}$  and the superscript 0 denotes replacement of the subscript  $\sigma$  by 0 in symbols for one-molecule wave functions and energies.

The vibrational overlap integral between the ground-state wave function  $\Psi X_{d_1}^{0 \quad s_{11}} d_2 \dots (l)$  and the E-V function  $\Phi(\mathbf{k}) X_{d'_1}^{s'_{11}} d'_2 \dots (l')$  is

$$(X_{d_1}^{0 \quad s_{11}} d_2 \dots (l) | X_{d'_1}^{s'_{11}} d'_2 \dots (l')). \quad (30)$$

The integral (30) is zero unless the condition

$$l = l' \quad (31)$$

is satisfied.

Each non-zero integral of the type (30) may be expressed as a product of  $N$  one-molecule vibrational overlap integrals such as

$$(\chi_{0m} | \chi_{\sigma n}). \quad (32)$$

A closed expression for the overlap integral between any pair of harmonic oscillator wave functions may be obtained by a method due to Hutchisson (1930). The present notation is that of Manneback (1951). We now introduce an approximation in which the difference between the ground- and excited-state vibrational force constants is ignored—i.e. we put  $k_0 = k_\sigma = k_1$ . In this approximation, Hutchisson's expressions for the overlap integrals between the ground- and excited-state vibrational wave functions for an isolated molecule reduce to

$$(\chi_{0m} | \chi_{1n}) = I_{mn}(M),$$

where

$$I_{mn}(x) = (m! n!)^{\frac{1}{2}} \sum_q \frac{(-1)^{m-q} x^{m+n-2q}}{q (m-q)! (n-q)! q!} e^{-\frac{1}{2}x^2}, \quad (33)$$

$q$  running from zero to the smaller of the two numbers  $m$  and  $n$ , and

$$M = 2.21 \times 10^{-21} \mu^{\frac{1}{2}} (R_1 - R_0) v_\sigma \text{ (c.g.s. units).} \quad (34)$$

To obtain the corresponding expression for the one-molecule integral (32), we replace  $\chi_{1n}$  by  $\chi_{\sigma n}$ , hence  $R_1 - R_0$  by  $R_\sigma - R_0$ . Because of the approximation  $k_0 = k_\sigma = k_1$ , we have  $R_\sigma - R_0 = (R_1 - R_0)/N$ , so that  $M$  must be replaced by  $M/N$ . We thus obtain

$$(\chi_{0m} | \chi_{\sigma n}) = I_{mn}(M/N). \quad (35)$$

The condition  $k_0 = k_1$  is equivalent to that of mirror symmetry between the monomer fluorescence band and the corresponding absorption band. The fractional error introduced through the approximation in the one-molecule vibrational overlap integrals is of the order of  $(v_1 - v_0)/(v_1 + v_0)$ , which is in turn comparable with the error which might ordinarily arise through the use of the harmonic oscillator model.

#### VIH. REFERENCES

- BINGEL, W. A. (1959).—*Canad. J. Phys.* **37**: 680.
- CRAIG, D. P. (1955).—*J. Chem. Soc.* **1955**: 2302.
- CRAIG, D. P., and HOBIBBS, P. C. (1955).—*J. Chem. Soc.* **1955**: 439.
- DAVYDOV, A. S. (1948).—*J. Exptl. theor. Phys.* **18**: 210.
- GANGULY, S. C., and CHAUDHURY, N. K. (1959).—*Rev. Mod. Phys.* **31**: 990.
- HUTCHISSON, E. (1930).—*Phys. Rev.* **36**: 410.
- MCCLURE, D. S. (1958).—*Canad. J. Chem.* **36**: 59.
- MCCLURE, D. S. (1959).—*Solid State Phys.* **8**: 1.
- MCCLURE, D. S., and SCHNEPP, O. (1955).—*J. Chem. Phys.* **23**: 1575.
- MANNEBACK, C. (1951).—*Physica* **17**: 1001.
- SIMPSON, W. T., and PETERSON, D. L. (1957).—*J. Chem. Phys.* **26**: 588.
- WILSON, E. B., DECUS, J. C., and CROSS, P. C. (1955).—“Molecular Vibrations.” p. 290. (McGraw-Hill Book Co.: New York.)
- WITKOWSKI, A., and MOFFITT, W. (1960).—*J. Chem. Phys.* **33**: 872.
- WOLF, H. C. (1959).—*Solid State Phys.* **9**: 1.

## APPENDIX I

It is required to show that the special form of the present theory (M) which is obtained by putting  $N=2$  is consistent with the theory of Witkowsky and Moffitt (WM).

The models considered in M and WM are the same except in that WM retained the intermolecular distance as an explicit variable. However the terms depending on the variation of intermolecular distance did not affect their conclusions.

WM developed their theory in such a way as to reveal the Hamiltonian approximations corresponding to each of the limiting coupling cases. In particular, the case of strong (E-V) coupling was shown to correspond to the neglect of the term (WM notation; see WM eqn. (34)):

$$\frac{1}{2}[V_M(Q_A) - V_N(Q_A) - V_M(Q_B) + V_N(Q_B)]. \quad (\text{A1})$$

In M, the fragment of the Hamiltonian causing departures from E-V coupling was found by integrating over electronic coordinates in a general interaction integral between E-V functions (see M, Section IV). The resulting expectation value for a dimer ( $N=2$ ,  $\sigma=\frac{1}{2}$ ) is (M notation; see M eqn. (19) and the subsequent development):

$$\frac{1}{2}[\langle \mathcal{V}_{\frac{1}{2}}^{(1)} \rangle_1 - \langle \mathcal{V}_{\frac{1}{2}}^{(1)} \rangle_0 - \langle \mathcal{V}_{\frac{1}{2}}^{(2)} \rangle_1 + \langle \mathcal{V}_{\frac{1}{2}}^{(2)} \rangle_0]. \quad (\text{A2})$$

By means of the formulae given in the respective papers, it is easily shown that (A1) and (A2) are of the same form, and that they are in fact identical if WM's constant  $l$  is identified with (M notation)

$$k_1 k_0 (R_0 - R_1) / k_{\frac{1}{2}} - (k_1 - k_0) R_{\frac{1}{2}}$$

## APPENDIX II

It is required to show that the theory can be applied to aggregates of polyatomic molecules, as long as all modes of vibration are harmonic and only one progression of vibronic bands appears in the electronic transition to the excited state under consideration.

We assume a mode of vibration in addition to that already considered. Let  $\mathcal{V}'_a$  and  $\chi'_{am}$  respectively denote the vibrational Hamiltonian and the wave functions for the new mode, analogous to  $\mathcal{V}_a$  and  $\chi_{am}$ . In view of the harmonic oscillator property, the vibrational wave functions for the individual molecules may be written in product form, and the one-molecule interaction integrals are given by

$$\begin{aligned} & (\chi'_{am} \chi_{an} | \langle \mathcal{V}'_a \rangle_1 - \langle \mathcal{V}'_a \rangle_0 + \langle \mathcal{V}_a \rangle_1 - \langle \mathcal{V}_a \rangle_0 | \chi'_{am'} \chi_{an'}) \\ & = (\chi'_{am} | \langle \mathcal{V}'_a \rangle_1 - \langle \mathcal{V}'_a \rangle_0 | \chi'_{am'}) \delta_{nn'} + (\chi_{an} | \langle \mathcal{V}_a \rangle_1 - \langle \mathcal{V}_a \rangle_0 | \chi_{an'}) \delta_{mm'} \end{aligned}$$

In order for there to be only one vibronic progression, we must have

$$\mathcal{V}'_1 = \mathcal{V}'_0,$$

in which case the one-molecule integral vanishes unless  $m=m'$ . Consequently, the interaction integrals between E-V functions representing different degrees of excitation in the new mode all vanish. The same argument may be extended to any number of modes of vibration.

## MOLECULAR VIBRATIONS IN THE EXCITON THEORY FOR MOLECULAR AGGREGATES

### II. DIMERIC SYSTEMS

By E. G. MCRAE\*

[Manuscript received December 9, 1960]

#### *Summary*

The theory of Part I of this series (McRae 1961) is developed in detail for dimeric systems. The simplest possible theory of the exciton states for a system of two non-rigid molecules is obtained through the use of perturbation theory. The theory makes possible the prediction of electronic band structures in absorption and fluorescence spectra as functions of the theoretical Davydov splitting for two rigid molecules.

Numerical calculations are made for a dimer of a typical dye, and the results are compared with the observed absorption spectrum of the 1,1'-diethyl-2,2'-pyridocyanine iodide dimer.

### I. INTRODUCTION

The theory of the exciton states of dimers is of interest from two points of view. Firstly, a dimer is the simplest kind of molecular aggregate, and an understanding of the intermolecular interactions in a dimer is a necessary preliminary to the development of a complete theory of the exciton states of polymeric systems such as molecular crystals. Secondly, the theory may be compared with the observed spectra of dimers such as those formed in concentrated dye solutions.

The object of this paper is to study the effects of intramolecular vibrations on the electronic interaction between the two identical molecules in an electronically excited dimer, placing particular emphasis on the electronic spectra of dimeric systems. As a starting point, we adopt the set of E-V wave functions which was defined in Part I of this series (McRae 1961). We represent the dimer by a model consisting of two identical non-rigid molecules with fixed positions and orientations, and we specify that there is at least one covering operation for the whole system which interchanges the molecules. The model is a special case of the model adopted in Part I, obtained by putting  $N=2$ .

### II. INTERACTION AND VIBRATIONAL OVERLAP INTEGRALS

The notation is the same as in Part I, except for the following changes which are introduced to take advantage of the relative simplicity of dimeric systems: (i) The wave vector zero is designated by a superscript +, wave vector  $\pi b_a$  by superscript -. (ii) The general notation  $X_{d_1} \cdot \cdot \cdot d_n$  is modified by omitting the superscript, which is redundant for dimeric systems, and by

\* Division of Chemical Physics, C.S.I.R.O. Chemical Research Laboratories, Melbourne.

redefining  $d_1$  and  $d_2$  as the numbers of vibrational quanta *including zero*, excited in the respective molecules.

With the modified notation, the lattice sum of intermolecular interaction integrals reduces to

$$S^\pm = \pm (\Phi_1^{(1)} | \mathcal{W}^{(1,2)} | \Phi_1^{(2)}) = \mp \frac{1}{2} \Delta U. \quad (1)$$

Throughout the present paper, we assume that the intermolecular interaction integral is negative. For a positive integral,  $\mp$  would be replaced by  $\pm$ . The electronic and vibrational wave functions for the dimer are given, respectively, by

$$\Phi^\pm = 2^{-\frac{1}{2}} (\Phi_1^{(1)} \pm \Phi_1^{(2)}),$$

and

$$\begin{aligned} X_{mn}^\pm &= 2^{-\frac{1}{2}} (\chi_{\frac{1}{2}m}^{(1)} \chi_{\frac{1}{2}n}^{(2)} \pm \chi_{\frac{1}{2}n}^{(1)} \chi_{\frac{1}{2}m}^{(2)}), \\ X_{mn}^+ &= \chi_{\frac{1}{2}m}^{(1)} \chi_{\frac{1}{2}n}^{(2)}. \end{aligned} \quad (m \neq n),$$

To emphasize that we are dealing with molecules in a dimer, we have replaced the subscript  $\sigma$  by  $\frac{1}{2}$ . We note that the wave functions with superscript + are symmetric, and those with superscript - antisymmetric with respect to molecule interchange. The E-V functions, and the corresponding energies, are

$$\begin{aligned} \Phi^\pm X_{mn}^\pm ; & \quad u'_1 + u'_0 + v_{\frac{1}{2}m} + v_{\frac{1}{2}n} \mp \frac{1}{2} \Delta U. \\ \Phi^\pm X_{mn}^\mp ; & \end{aligned} \quad (2)$$

The interaction integral between any two E-V functions vanishes unless each of the following conditions is satisfied : the two functions are of the same overall symmetry and the vibrational subscript sums differ by two or less. These conditions are respectively equivalent to (25a) and (25b) of Part I. The interaction integrals which are not necessarily zero may be expressed in terms of one-molecule integrals as follows :

$$\begin{aligned} (X_{mn}^\pm | \langle \mathcal{V}_\frac{1}{2}^{(1)} \rangle_{int} + \langle \mathcal{V}_\frac{1}{2}^{(2)} \rangle_{int} | X_{m'n'}^\mp) &= G[(\chi_{\frac{1}{2}m} | \langle \mathcal{V}_\frac{1}{2} \rangle_1 - \langle \mathcal{V}_\frac{1}{2} \rangle_0 | \chi_{\frac{1}{2}m'}) \delta_{mn'} \\ &\quad - (\chi_{\frac{1}{2}n} | \langle \mathcal{V}_\frac{1}{2} \rangle_1 - \langle \mathcal{V}_\frac{1}{2} \rangle_0 | \chi_{\frac{1}{2}n'} \delta_{mm'} \mp (\chi_{\frac{1}{2}m} | \langle \mathcal{V}_\frac{1}{2} \rangle_1 - \langle \mathcal{V}_\frac{1}{2} \rangle_0 | \chi_{\frac{1}{2}n'} \delta_{m'n'} \\ &\quad \pm (\chi_{\frac{1}{2}n} | \langle \mathcal{V}_\frac{1}{2} \rangle_1 - \langle \mathcal{V}_\frac{1}{2} \rangle_0 | \chi_{\frac{1}{2}m'} \delta_{mn'})]. \end{aligned} \quad (3)$$

The factor  $G$  takes the value  $\frac{1}{2}$  when  $m \neq n$  and  $m' \neq n'$ , and  $2^{-3/2}$  when either  $m=n$  or  $m'=n'$ .

From the general formula for one-molecule vibrational overlap integrals, Part I, equation (35), we derive

$$| (X_{mn}^{0\pm} | X_{m'n'}^\pm) | = | (X_{m'n'}^{0\pm} | X_{mn}^+) |. \quad (4)$$

Again making use of Part I, equation (35), we obtain the following expressions for the vibrational overlap integrals required in this paper :

$$\left. \begin{aligned} | (X_{00}^{0+} | X_{mn}^+) | &= 2^{\frac{1}{2}} (m! n!)^{-\frac{1}{2}} (M/2)^{m+n} e^{-M^2/4}, \\ | (X_{00}^{0+} | X_{mm}^+) | &= (m!)^{-1} (M/2)^{2m} e^{-M^2/4}, \\ | (X_{10}^{0-} | X_{10}) | &= e^{-M^2/4}, \\ | (X_{10}^{0-} | X_{20}) | &= 2^{\frac{1}{2}} (M/2) e^{-M^2/4}. \end{aligned} \right\} \quad (5)$$

TABLE I  
SELECTED WAVE FUNCTIONS AT POINTS OF RESONANCE INTERACTION\*

$\frac{\Delta U}{2\hbar c v_{\frac{1}{2}}}$	Serial Number of Selected Wave Functions					5
	1	2	3	4		
0	$\Phi^+ X_{00}^+$	$\Phi^+ X_{00}^+$	$2^{-\frac{1}{2}}(\Phi^+ X_{01}^+ + \Phi^+ X_{01}^-)$	$2^{-\frac{1}{2}}(\Phi^+ X_{01}^+ + \Phi^+ X_{01}^-)$	$2^{-\frac{1}{2}}(\Phi^+ X_{01}^+ - \Phi^+ X_{01}^-)$	$2^{-\frac{1}{2}}(\Phi^+ X_{01}^+ - \Phi^+ X_{01}^-)$
$\frac{1}{2}$	"	$2^{-\frac{1}{2}}(\Phi^+ X_{00}^+ + \Phi^+ X_{01}^-)$	$\Phi^+ X_{01}^+$	"	$2^{-\frac{1}{2}}(\Phi^+ X_{00}^+ - \Phi^+ X_{01}^-)$	$2^{-\frac{1}{2}}(\Phi^+ X_{00}^+ + 2^{-\frac{1}{2}}(\Phi^+ X_{02}^+ - \Phi^+ X_{02}^-))$
1	"	$\Phi^+ X_{01}^-$	"	"	$2^{-\frac{1}{2}}(\Phi^+ X_{00}^+ + \Phi^+ X_{02}^-)$	$\Phi^+ X_{02}^+$
$\infty$	"	"	"	"	$\Phi^+ X_{02}^-$	"
$\frac{\Delta U}{2\hbar c v_{\frac{1}{2}}}$	8					12
	6					
0	$2^{-\frac{1}{2}}(\Phi^+ X_{01}^+ - \Phi^+ X_{02}^-)$	$2^{-\frac{1}{2}}(\Phi^+ X_{02}^+ + \Phi^+ X_{02}^-)$	$2^{-\frac{1}{2}}(\Phi^+ X_{02}^+ - \Phi^+ X_{02}^-)$			
$\frac{1}{2}$	$2^{-\frac{1}{2}}(\Phi^+ X_{01}^+ + \Phi^+ X_{02}^-)$	$2^{-\frac{1}{2}}(\Phi^+ X_{01}^+ - \Phi^+ X_{02}^-)$				$\rightarrow \dagger$
1	$2^{-\frac{1}{2}}(\Phi^+ X_{00}^+ - \Phi^+ X_{02}^-)$	$2^{-\frac{1}{2}}(\Phi^+ X_{01}^+ + 2^{-\frac{1}{2}}(3^{\frac{1}{2}}\Phi^+ X_{03}^- + \Phi^+ X_{12}^-))$	$2^{-\frac{1}{2}}(\Phi^+ X_{01}^+ - 2^{-\frac{1}{2}}(3^{\frac{1}{2}}\Phi^+ X_{03}^- + \Phi^+ X_{12}^-))$			
$\infty$	$\Phi^+ X_{03}^+$	$\Phi^+ X_{03}^-$	$\Phi^+ X_{03}^+$			

\* The wave functions are numbered in the order, for small  $\Delta U$ , of the energy levels shown in Figure 1. The signs of the mixing coefficients correspond to A and B positive.

† The wave function is of the form  $a\Phi^+ X_{03}^+ + b\Phi^+ X_{12}^+ + c\Phi^+ X_{04}^- + d\Phi^+ X_{13}^-$ . The coefficients were not calculated.

### III. METHOD OF TREATMENT

Our object in Section III is to follow the wave functions and energy levels of an electronically excited dimer as  $\Delta U$  increases from zero to a value large in comparison with a fundamental vibrational interval. As there has been no previous attempt to do this, it seems appropriate to adopt the simplest treatment which will enable us to predict absorption and fluorescence spectra as functions of  $\Delta U$ .\*

In Table 1 we have set out the zeroth-order linear combinations of E-V wave functions for the three values of  $\Delta U/2hc\nu_i$  at which the condition of resonance interaction applies (Part I, Fig. 1), together with the E-V functions which are approached as  $\Delta U$  tends to infinity. The zeroth-order mixing coefficients were obtained by solving the appropriate secular equations. The entries in Table 1 are restricted to the wave functions which are of importance in the discussion of dye dimers (Section IV). The consideration of resonance interactions between E-V functions leads to a particular correlation between vibronic levels for zero and large values of  $\Delta U$ . The correlation is illustrated in Figure 1. The splitting of the artificial degeneracies at  $\Delta U=0$  is not shown, but the extension of the correlation to the actual monomer levels is straightforward. An example is presented in Figure 2 (see Section IV).

In discussing electronic spectra, we will be concerned with relative intensities only, as the calculation of absolute intensities or quantum yields is beyond the scope of the present work. Let  $\mathcal{Q}$  denote the electronic dipole moment operator for a dimer. The electronic transition moment integrals are

$$Q^\pm = (\Psi | \mathcal{Q} | \Phi^\pm).$$

The electronic spectra for the model dimer consist of two series of vibronic bands, one with  $Q^+$  and the other with  $Q^-$  polarization. We express the intensity of each vibronic band in a given polarization as a fraction of the total intensity in that polarization.

The proposed "simplest possible" treatment of electronic spectra is as follows :

(a) *Absorption Intensities* : Construct a graph of absorption intensity  $v. \Delta U/2hc\nu_i$  ( $\Delta U/2hc\nu_i > 1$ ) and  $v. 2hc\nu_i/\Delta U$  ( $\Delta U/2hc\nu_i < 1$ ) as follows : Plot the points for  $\Delta U=0$  from the monomer spectrum, which is assumed known. Plot the points for the other three values of  $\Delta U/2hc\nu_i$  in Table 1, calculating the intensities from the tabulated wave functions and the overlap integral formulae, equation (5). Draw a smooth curve through the points, and interpolate to find the intensities at a given value of  $\Delta U/2hc$ .

(b) *Fluorescence Intensities* : Construct a graph of fluorescence intensity  $v. \Delta U/2hc\nu_i$  as follows : Plot the points for  $\Delta U=0$  from the monomer spectrum, which is assumed known. Using first-order perturbation theory, calculate the intensities at several values of  $\Delta U/2hc\nu_i$  sufficiently large for perturbation

\* McClure (1959) has given a correlation diagram linking the energy levels of dimers characterized by zero and large values of  $\Delta U$ , but no attempt was made to represent all the important states.

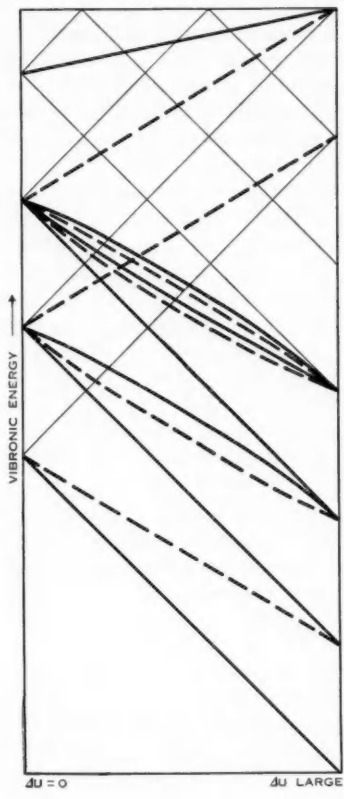


Fig. 1

Fig. 1.—Correlation between vibronic levels (thick lines) of an electronically excited dimer for zero and large values of  $\Delta U$ . Thin lines represent E-V levels.

Fig. 2.—Dependence of the vibronic levels of an electronically excited dimer on  $\Delta U/2\hbar c\nu_1$ . The molecular constants are chosen to correspond to a typical dye molecule (see text).

theory to be valid, and join the resulting curves smoothly to the points at  $\Delta U=0$ . The perturbation-theory expression for the lowest-energy exciton state is

$$D \left[ \Phi^+ X_{00}^+ + \frac{2^{-1}B}{\Delta U + \hbar c\nu_1} \Phi^- X_{10}^- + \frac{A}{\Delta U + 2\hbar c\nu_1} \Phi^- X_{20}^- \right],$$

where  $D$  is a normalization factor and  $A$  and  $B$  are the constants appearing in the one-molecule interaction integrals (Part I, eqn. (24)). The intensities may be calculated from the above wave function and the vibrational overlap integrals given in equation (5).

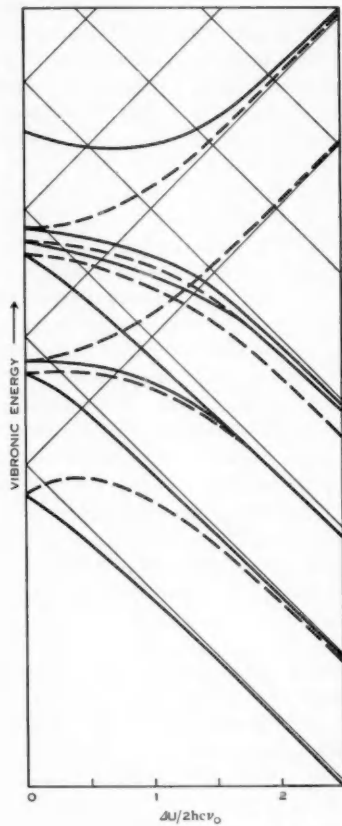


Fig. 2

(c) *Energy Levels*: Construct a graph of vibronic energy  $v.$   $\Delta U/2\hbar c\nu_1$  as follows: For  $\Delta U=0$ , calculate the displacement of the monomer levels from the E-V levels by Part I, equation (29). Using second-order perturbation theory, calculate the energy levels for values of  $\Delta U/2\hbar c\nu_1$  sufficiently large for perturbation theory to be valid, and join the resulting curves smoothly to the points at  $\Delta U=0$  in accordance with the correlation diagram, Figure 1.

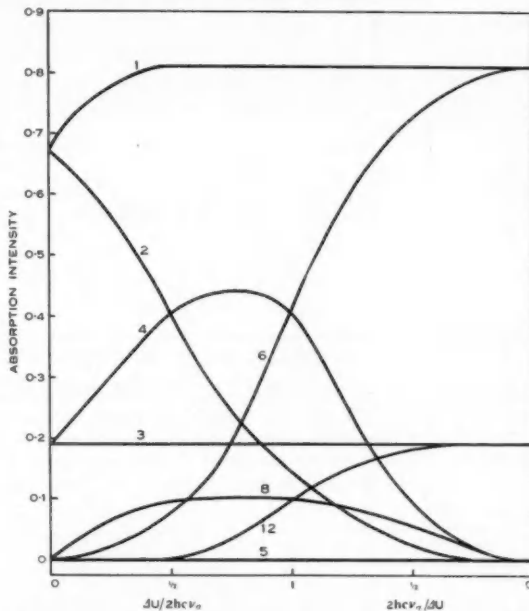


Fig. 3.—Dependence of vibronic absorption intensities on  $\Delta U$ . The numbers designate the upper states, which are numbered in order of increasing energy at small values of  $\Delta U$  (see Fig. 2). The intensity of each vibronic band is expressed as a fraction of the total intensity in the same polarization.

#### IV. APPLICATION TO DYES

##### (a) *A Hypothetical Dye*

The intense visible electronic bands of organic dyes consist typically of a single short vibronic progression with a fundamental interval in the vicinity of  $1000 \text{ cm}^{-1}$ . As an example of the application of the theory, we treat the spectrum of the dimer of a hypothetical dye characterized by the constants

$$\nu_1 = 950 \text{ cm}^{-1},$$

$$\nu_0 = 1050 \text{ cm}^{-1},$$

$$M = -\frac{1}{\sqrt{2}}.$$

The constant  $M$  is defined in Part I, equation (34). The assumed numerical value corresponds to a 2 : 1 intensity ratio for the  $0 \rightarrow 0$  and  $0 \rightarrow 1$  vibronic bands.

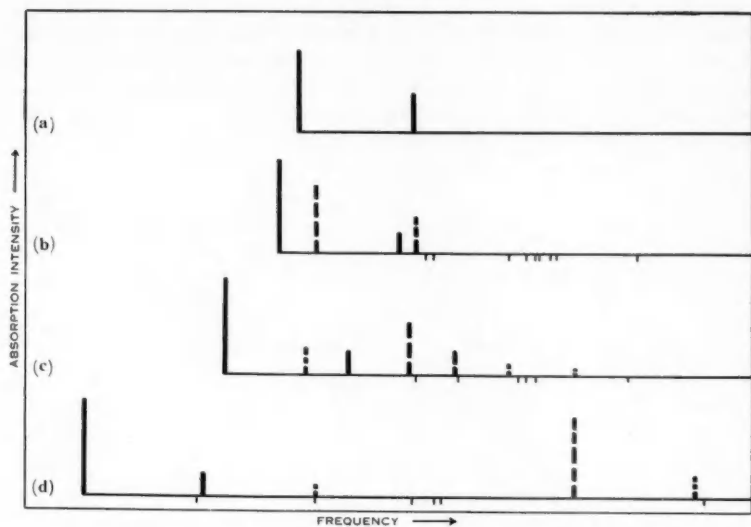


Fig. 4.—(a) Assumed monomer absorption spectrum. (b)–(d) Predicted dimer absorption spectra. Full, thick vertical lines represent  $\mathbf{Q}^+$ -polarized vibronic absorption bands, broken lines  $\mathbf{Q}^-$ -polarized bands. Thin vertical lines indicate predicted frequencies of vibronic bands less than one-tenth as strong as the strongest band. Intensities in each polarization are expressed as fractions of the total intensity in that polarization. Values of  $\Delta U/2hc\nu_{\frac{1}{2}}$ : (b)  $\frac{1}{2}$ , (c)  $\frac{3}{4}$ , (d) 2.

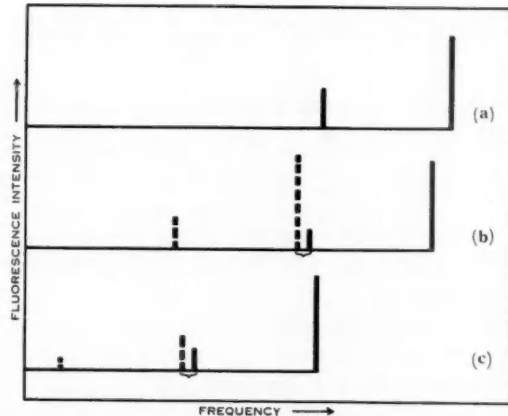


Fig. 5.—(a) Assumed monomer fluorescence spectrum. (b), (c) Predicted dimer fluorescence spectra. Full and broken vertical lines respectively represent  $\mathbf{Q}^+$  and  $\mathbf{Q}^-$  polarization. Bracketed lines represent fluorescence bands at the same frequency, but for clarity the lines are shown symmetrically separated. Relative intensities correspond to  $|\mathbf{Q}^-|^2=10|\mathbf{Q}^+|^2$ . Values of  $\Delta U/2hc\nu_{\frac{1}{2}}$ : (b)  $\frac{1}{2}$ , (c)  $\frac{3}{4}$ .

The remaining vibronic bands are assumed to have negligible intensity. From the above constants, we obtain (see Part I, eqn. (24))

$$A/\hbar c = -50 \text{ cm}^{-1}, B/\hbar c = -690 \text{ cm}^{-1}.$$

The graphs of vibronic energy and absorption intensity were drawn as described in Section III and are shown in Figures 2 and 3. Transitions to states not represented in Table 1 are predicted to have zero intensity. The graph of fluorescence intensity was not drawn, as in the present application perturbation theory is adequate for all values of  $\Delta U/2\hbar c\nu_i$ . The dimer absorption and fluorescence spectra for various values of  $\Delta U/2\hbar c\nu_i$  are shown in Figures 4 and 5. Zero-temperature populations of vibronic states were assumed throughout.

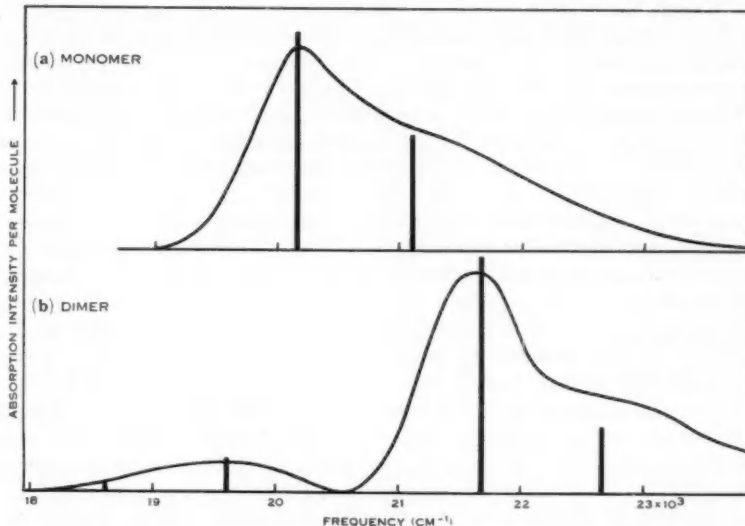


Fig. 6.—(a) Observed absorption band of monomeric pyridocyanine dye. Vertical lines represent assumed underlying vibrational structure. (b) Observed absorption band of dimer (curve) compared with the theoretical dimer spectrum. Vertical lines indicate predicted relative frequencies and intensities of vibronic bands. The absolute positions of the vertical lines on the frequency scale have been adjusted by a movement of 750 cm<sup>-1</sup> to lower frequencies.

#### (b) Comparison with Experiment

The theory of absorption spectra may be compared with the observed absorption spectrum of 1,1'-diethyl-2,2'-pyridocyanine iodide dimer. Solutions of this dye were studied experimentally by Levinson, Simpson, and Curtis (1957). Their work is of special value, because their dimer absorption spectrum is corrected for unassociated dye. The monomer absorption spectrum is reproduced in Figure 6 (a). The constants chosen for the hypothetical dye apply in this case within the limits of error in the determination of vibronic frequencies and intensities.

A consideration of the electrostatic forces between the dye molecules in the dimer (see Levinson, Simpson, and Curtis 1957) indicates that the equilibrium structure of the dimer is that in which the transition moments of the two molecules are parallel. If the intermolecular interaction potential is represented by the dipole term, and if the phase factors in the electronic wave functions are so chosen as to make the intermolecular interaction integral negative, the transition moment integral  $Q^+$  vanishes and the only allowed vibronic transitions are those between symmetric and antisymmetric states of the dimer. These transitions are polarized with the electronic transition moment vector  $Q^-$  perpendicular to the line of centres of the two molecules. The contributions of  $Q^-$ -polarized transitions to the absorption and fluorescence spectra of dimers are shown by broken lines in Figures 4 and 5.

The observed absorption band shape of the dimer is reproduced by the theory upon choosing  $\Delta U/2\hbar c\nu_1 = 2$  (Fig. 6 (b)). However, the observed absorption lies  $750 \text{ cm}^{-1}$  to the low-frequency side of the predicted position. This discrepancy is not thought to be a fundamental failure of the theory, since the displacement is in the direction and of the approximate magnitude to be expected from consideration of dispersive interactions involving higher-energy electronic states.

Levinson, Simpson, and Curtis (1957) interpreted the lowest-frequency absorption peak in the dimer spectrum as arising from a transition polarized parallel to the line of molecular centres. It was suggested that this transition could be made possible by slight, momentary departures from the parallel configuration. However, this interpretation does not account either for the observed band shape or the overall shift of the absorption to higher frequencies, whereas the present theory provides a natural explanation of these features.

Levinson, Simpson, and Curtis (1957) also studied the emission spectra of pyridocyanine iodide solutions. Only the triplet-singlet (phosphorescence) emission was observed. The results provide an example of the more general phenomenon of the enhancement of phosphorescence at the expense of fluorescence upon aggregation of dye molecules (McRae and Kasha 1958). The present theory adds little to the interpretation given by Levinson, Simpson, and Curtis, and only two points need be mentioned: according to the present theory (i) the theoretical conditions favouring the enhancement of phosphorescence apply more strongly than was previously thought, and (ii) the fact that the polarization of the emission transition is perpendicular to both the high- and low-frequency absorption transitions means only that the emission transition is polarized perpendicular to  $Q^-$ ; it is not necessarily polarized perpendicular to both  $Q^-$  and  $Q^+$  as was previously inferred by Levinson, Simpson, and Curtis. This conclusion admits the plausible interpretation that the emission is formally forbidden by the dimer selection rules but is made possible by small momentary departures from the average dimer configuration.

#### V. DISCUSSION

The patterns of vibronic bands shown in Figures 4 and 5 illustrate the changeover from m-m to E-V coupling conditions. Though the diagrams refer

specifically to dye dimers, the main features are probably common to all dimeric systems.

As  $\Delta U$  increases from zero, the distribution of intensity in the  $Q^+$ -polarized absorption remains constant except for a relative enhancement of the lowest-frequency vibronic band. The structure of the  $Q^-$ -polarized absorption depends more strongly upon  $\Delta U$ . For both small and large values of  $\Delta U$ , the structure resembles that in the monomer absorption. The effect of increasing  $\Delta U$  from an initially small value is not, however, described as a shift of an absorption of constant structure, but rather as a transfer of intensity from lower- to higher-frequency vibronic bands. At intermediate values of  $\Delta U$ , the predicted structure differs markedly from that of the monomer absorption.

We have seen that the theoretical Davydov splitting,  $\Delta U$ , for a dimer consisting of two rigid molecules also plays a most important part in the theory of the interaction between non-rigid molecules. For a dimer of a given structure,  $\Delta U$  can be calculated from the properties of the monomer. It would be desirable to calculate  $\Delta U$  from observed dimer spectra, so as to obtain an independent check of the theory. The present work shows that, in principle, a value of  $\Delta U$  may be calculated from the observed absorption spectra, this value corresponding to the value of  $\Delta U/2\hbar\nu_1$  required to fit the observed band structure. The present treatment is, however, far too crude to yield a quantitatively significant estimate of  $\Delta U$ . The theory for the model dimer could of course be made quantitative by direct solution of the appropriate secular equation.

The comparison with experiment indicates that the model dimer offers a good representation of the dimeric form of the pyridocyanine dye. The apparent success of the model in this case may perhaps be attributed to the presence of strong electrostatic forces tending to hold the two molecules rigidly in position. However, as the structure of dimers can only be guessed at, many cases will have to be studied before the model can be properly evaluated.

We point out finally that in experimental studies of dimer spectra, it is desirable, where possible, to measure both the absorption spectra and the polarized fluorescence spectra. The comparison between absorption and fluorescence spectra would provide a critical test of the theory, since they are affected in different ways by intramolecular vibrations.

#### VI. REFERENCES

LEVINSON, G. L., SIMPSON, W. T., and CURTIS, W. (1957).—*J. Amer. Chem. Soc.* **79**: 4314.  
McCLURE, D. S. (1959).—*Solid State Phys.* **8**: 1.  
MCRAE, E. G. (1961).—*Aust. J. Chem.* **14**: 329.  
MCRAE, E. G., and KASHA, M. (1958).—*J. Chem. Phys.* **28**: 721.

## MOLECULAR VIBRATIONS IN THE EXCITON THEORY FOR MOLECULAR AGGREGATES

### III. POLYMERIC SYSTEMS

By E. G. MCRAE\*

[Manuscript received December 9, 1960]

#### Summary

The theory of Part I of this series is developed for aggregates of many molecules. The low-energy exciton states are considered on the basis of perturbation theory. The conditions for applicability of perturbation theory based on E-V wave functions are examined. It is shown that perturbation theory is valid where the intermolecular interaction in the exciton state is strong and/or the vibronic progression in the monomer spectrum is short.

Expressions relating to the vibrational structure in electronic absorption and emission spectra and the vibrational inhibition of intermolecular interaction are derived. A formula connecting the polarization ratios in absorption and fluorescence is given. The formula is shown to be relatively free from uncertainties arising from the use of perturbation theory, and it offers a new method of calculating the theoretical Davydov splitting for a system of rigid molecules from experimental data.

Numerical calculations are made for a linear aggregate, and the results are compared with the observed electronic spectra of the *NN'*-diethyl- $\psi$ -cyanine dye polymer.

It is shown that the rigid-lattice model is an adequate representation of the cyanine dye polymer, but not of the anthracene crystal.

### I. INTRODUCTION

The theory of the exciton states of polymeric systems is of importance in the interpretation of electronic spectra and energy transfer in molecular crystals and macroscopic dye aggregates. The object of this paper is to develop the theory so as to obtain an understanding of the role of intramolecular vibrations in these phenomena.

As a starting-point we adopt the set of E-V wave functions which was defined in Part I of this series (McRae 1961a). There we considered the interactions between E-V functions in a model system of identical non-rigid molecules in a rigid lattice. In the present paper we retain the model and notation of Part I, but specify that  $N$  is a large number.

### II. PERTURBATION THEORY

The interaction integrals between E-V functions may be expressed in terms of one-molecule interaction integrals, which in turn depend on the quantities  $A$  and  $B$  characteristic of the individual molecules in the aggregate (see Part I, eqn. (24)). We now introduce an approximation in which the difference between

\* Division of Chemical Physics, C.S.I.R.O. Chemical Research Laboratories, Melbourne.

the ground- and excited-state vibrational force constants is ignored—i.e. we put  $k_0 = k_\sigma = k_1$ . In this approximation, we have

$$A=0; \quad B=-Mhc\nu_\sigma, \quad (1)$$

where  $M$  is as defined in Part I, equation (34).

According to Part I, equation (33),  $M^2$  is the ratio of the monomer 0→1 vibronic band intensity to that of the 0→0 band. Thus, equation (1) permits us to evaluate  $B$  by inspection of the monomer spectrum.

The neglect of the constant  $A$  is justified by exact numerical calculations of  $A$  and  $B$ , which indicate that  $B$  is ordinarily an order of magnitude greater than  $A$ . An example of such a calculation is given in Part II (McRae 1961b). The use of the simplified formula for  $B$ , equation (1) introduces a fractional error of the order of  $(\nu_1 - \nu_0)/(\nu_1 + \nu_0)$  which is probably comparable with the error arising from the use of the harmonic oscillator model.

According to first-order perturbation theory, the low-energy exciton state functions may be expressed in the form\*

$$(1 + \sum'_{\mathbf{k}'} |c_{\mathbf{kk}'}|^2)^{-1} [\Phi(\mathbf{k})X + \sum'_{\mathbf{k}'} c_{\mathbf{kk}'} \Phi(\mathbf{k}') X_1(\mathbf{k} - \mathbf{k}')], \quad (2)$$

where the prime on the summation sign indicates that the term  $\mathbf{k}' = \mathbf{k}$  is omitted. In accordance with equation (1), we have

$$c_{\mathbf{kk}'} = \frac{N^{-1} M hc\nu_\sigma}{hc\nu_\sigma + U(\mathbf{k}') - U(\mathbf{k})}. \quad (3)$$

The E-V functions entering into the expansion are limited in accordance with equation (1) and the conditions (25) of Part I.

The perturbation expansion of equations (2) and (3) represents a good approximation as long as the condition

$$\sum'_{\mathbf{k}'} |c_{\mathbf{kk}'}|^2 \ll 1 \quad (4)$$

is satisfied. We consider the most favourable case, which is that in which  $\mathbf{k} = \mathbf{k}_{\min}$ ,  $\Phi(\mathbf{k}_{\min})X$  being the lowest-energy E-V function. Let  $\rho[U(\mathbf{k}) - U(\mathbf{k}_{\min})]$  denote the energy-density of the states  $\Phi(\mathbf{k})X$ . The above inequality becomes

$$\frac{(Mhc\nu_\sigma)^2}{N} \int_0^{\Delta U} \frac{\rho(\varepsilon)d\varepsilon}{(\varepsilon + hc\nu_\sigma)^2} \ll 1.$$

For linear aggregates, the density function  $\rho$  has maxima near the highest and lowest values of the argument, whereas for two- and three-dimensional aggregates a maximum occurs nearer the median value of the argument. In order to obtain a simple expression which is approximately correct for all polymeric systems, we replace  $\rho$  by its average value,  $N/\Delta U$ . The inequality (4) becomes

$$\frac{M^2}{1 + \Delta U/hc\nu_\sigma} \ll 1. \quad (5)$$

\* The normalization of the wave function is not a part of first-order perturbation theory, since the normalization factor involves the second powers of the expansion coefficients. However, our procedure is consistent with the physical requirement that the interactions between E-V functions should not lead to any change in the total absorption intensity (Section III).

The inequality (5) may be viewed as a criterion for closeness of approach to the E-V coupling description of the low-energy exciton states. It shows that the monomer band shape, as represented by the factor  $M$ , as well as the strength of intermolecular interaction represented by  $\Delta U/2\hbar c\nu_\sigma$ , plays an important part in determining the closeness of approach to the E-V coupling limit.

The criterion (5) may be compared with that proposed by Simpson and Peterson (1957), which is

$$\Delta U/\hbar c \gg \Delta,$$

where  $\Delta$  denotes the width of the monomer electronic band system. The width of the band system may be defined as the difference between the  $0 \rightarrow 0$  band frequency and the weighted mean frequency of the vibronic bands:

$$\Delta = v_\sigma \left\{ \sum_{n=1}^{\infty} n [I_{0n}(M)]^2 \right\} / \left\{ \sum_{n=0}^{\infty} [I_{0n}(M)]^2 \right\}.$$

With the aid of Part I, equation (33), the above inequality becomes

$$\Delta U/\hbar c\nu_\sigma \gg M^2.$$

This is the same as (5) for all but unusually small values of  $M^2$ . The present theory thus supports Simpson and Peterson's more intuitive considerations.

### III. INTENSITIES IN SPECTRA

In Section III we confine our attention to the commonly-occurring case of aggregates with two molecules per unit cell. According to Davydov's (1948) theory for this case, each absorption band system consists of two components corresponding respectively to transitions to the states characterized by wave vectors  $\mathbf{k}=0$  and  $\mathbf{k}=\pi\rho$ , where if  $\mathbf{r}_{u.c.}$  denotes the translation along the line of centres of two molecules in any one unit cell,  $\pi\rho \cdot \mathbf{r}_{u.c.} = 1$ . We specify that the phase factors in the individual wave functions be so chosen as to assign  $\mathbf{k}=0$  to the lower of the two levels to which transitions are allowed. The absorption band system is shown schematically in Figure 1 (a). The intensities and polarizations of the two components may be obtained from the respective electronic transition moment integrals, for which we introduce the notation  $\mathbf{Q}(0)$  and  $\mathbf{Q}(\pi\rho)$ . The fluorescence spectrum is correspondingly described as consisting of two components with the same splitting as in absorption, but with relative intensities in accord with the Boltzmann distribution of excited-state energies.

The inclusion of intramolecular vibrations allows us to discuss the distribution of intensity among the various vibronic bands in each polarization, and, in fluorescence spectra, the polarization ratio in each vibronic band. We first consider the extreme case of E-V coupling. Referring to Part I, equations (33) and (35), we have

$$\lim_{N \rightarrow \infty} (\chi_{0m} | \chi_{0n}) = \delta_{mn}.$$

Noting also that the limiting value of the  $N$ th power of  $\exp[-\frac{1}{2}(M/N)^2]$  as  $N \rightarrow \infty$  is unity, we find that the vibrational wave functions

$$X_{d_1}^{s_{11}} d_2 \dots (1) \text{ and } X_{d_1}^0 s_{12} d_2 \dots (1)$$

become identical in the limit for large  $N$ . Therefore, (i) the intensity of a given vibronic band in  $\mathbf{Q}(\mathbf{K})$ -polarized absorption ( $\mathbf{K}=0, \pi\rho$ ) is proportional to the square of the coefficient of  $\Phi(\mathbf{K})X$  in the E-V expansion of the upper state wave function. (ii) The intensity of a given vibronic band in  $\mathbf{Q}(\mathbf{K})$ -polarized

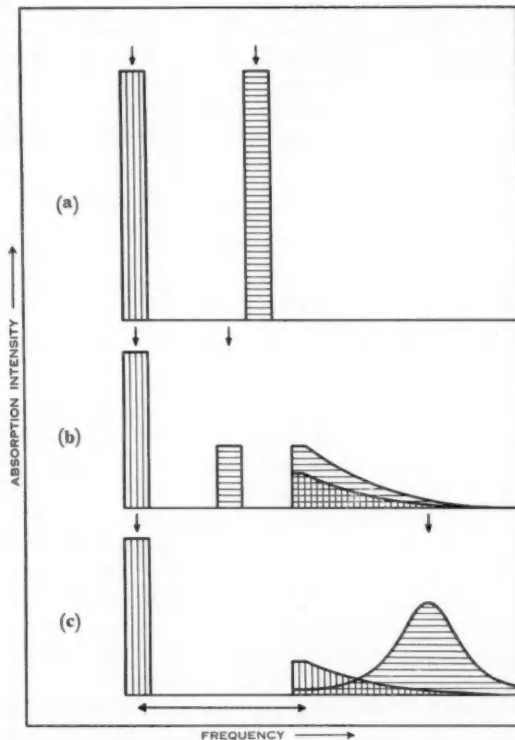


Fig. 1.—Intensity distribution in absorption spectra. Vertical shading indicates  $\mathbf{Q}(0)$  polarization, horizontal shading  $\mathbf{Q}(\pi\rho)$  polarization. Vertical arrows indicate frequencies of allowed transitions to pure E-V levels. The length of the horizontal arrow indicates one vibrational fundamental interval. No attempt has been made to represent widths of the narrow vibronic bands. (a) Extreme E-V coupling. (b) Interactions between E-V functions included,  $\Delta U < hcv_\sigma$ . (c) Interactions between E-V functions included,  $\Delta U > hcv_\sigma$ . In (b) and (c)  $\mathbf{k}_{\min} = 0$  has been assumed.

fluorescence is proportional to the product of the probability of occupation of the upper state and the square of the coefficient of  $\Phi(\mathbf{K})X$  in that state. In both of the above statements we have assumed low-temperature conditions (absence of "hot" bands) and in (ii) we have also ignored the possible dependence of radiationless transition probability on excited-state energy.

When the interactions between E-V functions are taken into account in the first order of perturbation theory, the absorption intensity in  $\mathbf{Q}(0)$  polarization is found to be shared between a narrow band at frequency  $U(0)/hc$  and a broad, diffuse absorption starting one vibrational interval to the high-frequency side of the frequency  $U(\mathbf{k}_{\min.})/hc$  (Figs. 1 (b), 1 (c)). The diffuseness of the higher-frequency band derives from the circumstance that the upper states constitute a quasi-continuum of levels, every one of which can combine with the ground state by virtue of the interactions between E-V wave functions. The lower-frequency band remains sharp because the zeroth-order wave function for the upper state has no non-vanishing interaction integral with the wave function for any neighbouring level. From the wave function (2), the fraction of  $\mathbf{Q}(0)$ -polarized absorption intensity in the narrow band is

$$I_{\text{abs}} = 1/(1 + \sum'_{\mathbf{k}'} |c_{0\mathbf{k}'}|^2). \quad (6)$$

First-order perturbation theory is not applicable to the upper states of the  $\mathbf{Q}(\pi\rho)$ -polarized transitions unless both  $M^2$  and  $\Delta U/hcv_0$  are small compared with unity. However, we can reach some general qualitative conclusions regarding these transitions. If the inequality

$$U(\pi\rho) - U(\mathbf{k}_{\min.}) < hc v_0 \quad (7)$$

is satisfied, the absorption intensity in  $\mathbf{Q}(\pi\rho)$  polarization is shared between a narrow band at frequency  $U(\pi\rho)/hc$  and a broad, diffuse absorption superposed on the diffuse  $\mathbf{Q}(0)$ -polarized absorption (Fig. 1 (b)). If the inequality (7) is not satisfied, the E-V level  $\Phi(\pi\rho)\mathbf{X}$  lies within a region of resonance interaction (Part I, Section V) and can thus interact strongly with a large number of neighbouring levels. Consequently, the  $\mathbf{Q}(\pi\rho)$ -polarized transitions give rise to a broad, diffuse absorption centred approximately at  $U(\pi\rho)/hc$  (Fig. 1 (c)).

In treating fluorescence spectra, we assume low-temperature conditions so that the onset of fluorescence lies at, or to the low-frequency side of, the onset of absorption. The important interactions between E-V functions, and the possible fluorescence transitions are shown in Figure 2. The extreme E-V description of the fluorescence spectrum is illustrated in Figure 3 (a). Only the lower-frequency component is shown (the higher-frequency component would normally be very weak). When the interactions between E-V functions are included, the fluorescence intensity in  $\mathbf{Q}(0)$  polarization is shared between a narrow band at frequency  $U(0)/hc$  and a diffuse fluorescence starting at frequency  $U(0)/hc - v_0$  and extending  $\sim kT/hc$  to higher frequencies (Fig. 3 (b);  $k$  = Boltzmann's constant,  $T$  = absolute temperature). According to first-order perturbation theory, the fraction of  $\mathbf{Q}(0)$ -polarized fluorescence intensity in the highest-frequency band is

$$I_{\text{fl}} = I_{\text{abs}} e^{-\varepsilon(0)/kT} / [I_{\text{abs}} e^{-\varepsilon(0)/kT} + \sum'_{\mathbf{k}} |c_{0\mathbf{k}}|^2 e^{-\varepsilon(\mathbf{k})/kT}], \quad (8)$$

where

$$\varepsilon(\mathbf{k}) = U(\mathbf{k}) - U(\mathbf{k}_{\min.}).$$

If  $\mathbf{k}_{\min.} = 0$ , the relative intensity of diffuse fluorescence decreases with decreasing temperature. In the low-temperature limit, the fluorescence spectrum consists

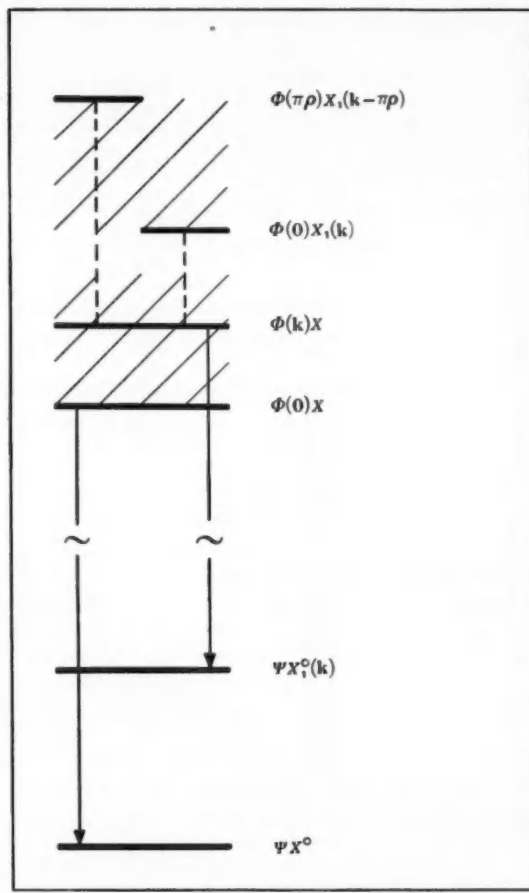


Fig. 2.—E-V states involved in fluorescence. Broken lines connect interacting levels. Arrows represent allowed transitions. Shading indicates bands of closely-spaced levels.

of a single vibronic band as shown in Figure 3 (a). If  $k_{\min} \neq 0$ , the relative fluorescence intensities do not vary monotonically with temperature, and at low temperature the theory predicts a gap of one ground-state vibrational interval between absorption and fluorescence (Fig. 3 (c)).

The interactions illustrated in Figure 2 lead to a  $Q(\pi\rho)$ -polarized component of fluorescence superposed on the diffuse  $Q(0)$ -polarized fluorescence (Fig. 3(b)).

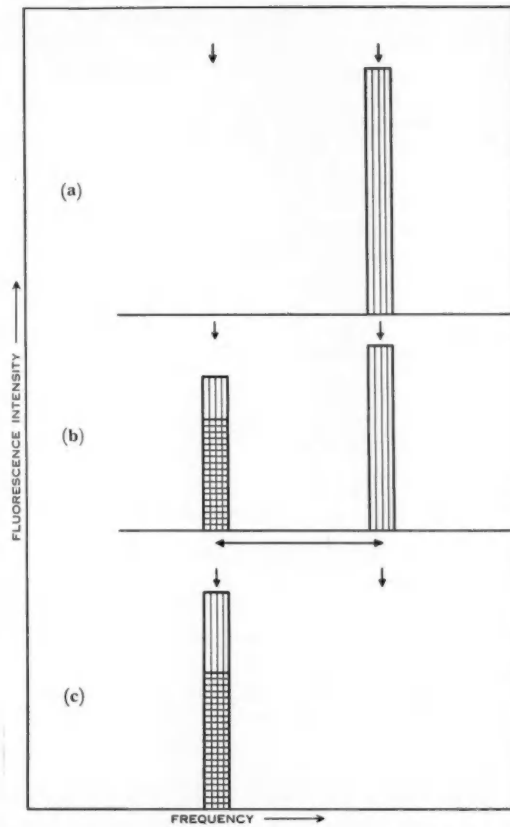


Fig. 3.—Intensity distribution in fluorescence spectra. Arrows and shading have the same meaning as in Figure 1. The high-frequency band is sharp. The lower frequency band has width  $kT/\hbar c$ , which is ordinarily too small to represent on the scale of the figure. (a) The lowest-frequency component of fluorescence according to the extreme E-V coupling description. The same diagram also represents the low-temperature limit for  $k_{\min} = 0$ , even when interactions between E-V functions are included. (b) Interactions between E-V functions included; temperature  $> 0$  °K, no restriction on  $k_{\min}$ . (c) Low-temperature limit for  $k_{\min} \neq 0$ ; interactions between E-V functions included.

The polarization ratio in the region of diffuse fluorescence is given, according to first-order perturbation theory, by \*

$$P_{fl}[Q(\pi\rho) : Q(0)] = \frac{\sum_k e^{-\epsilon(k)/kT} |c_{k\pi\rho}|^2 |Q(\pi\rho)|^2}{\sum_k e^{-\epsilon(k)/kT} |c_{k0}|^2 |Q(0)|^2}. \quad (9)$$

Equation (9) becomes exact both as the E-V coupling limit is approached and as the strength of intermolecular interaction tends to zero. In the latter limit

\* In equation (9) and the text immediately following the subscript  $\pi\rho$  refers to the vector quantity  $\pi\rho$ .

we have  $c_{\mathbf{k}0}=c_{\mathbf{k}\pi\rho}$  for all  $\mathbf{k}$ , so that the polarization ratio  $P_{\text{fl}}[Q(\pi\rho) : Q(0)]$  becomes equal to the polarization ratio in absorption. This result was presented in a preliminary report on the present work (McRae 1960), but the derivation given there was obtained from m-m coupling rather than E-V coupling. We conclude that equation (9) is relatively free from uncertainty arising from the use of perturbation theory in the evaluation of the expansion coefficients.

#### IV. INTERMOLECULAR INTERACTION INTEGRALS

The wave function (2) may be written in the alternative form

$$N^{-1} \sum_j \exp i\mathbf{k} \cdot \mathbf{r}^{(j)} \Phi^{(j)} \Xi^{(j)}, \quad (10)$$

where

$$\Xi^{(j)} = \frac{\mathbf{X} + \sum' c_{\mathbf{k}\mathbf{k}'} \exp i(\mathbf{k}' - \mathbf{k}) \cdot \mathbf{r}^{(j)} \mathbf{X}_1(\mathbf{k} - \mathbf{k}')}{(1 + \sum' |c_{\mathbf{k}\mathbf{k}'}|^2)^{\frac{1}{2}}}. \quad (11)$$

The effective intermolecular interaction integral between the  $i$ th and  $j$ th molecules is

$$(\Phi^{(j)} | \mathcal{W}^{(j,i)} | \Phi^{(i)}) F_{\mathbf{k}}(\mathbf{r}^{(i)} - \mathbf{r}^{(j)}),$$

where

$$F_{\mathbf{k}}(\mathbf{r}) = \frac{1 + \sum' |c_{\mathbf{k}\mathbf{k}'}|^2 \exp i(\mathbf{k}' - \mathbf{k}) \cdot \mathbf{r}}{1 + \sum' |c_{\mathbf{k}\mathbf{k}'}|^2}. \quad (12)$$

The factor  $F_{\mathbf{k}}(\mathbf{r})$  is always less than unity, and it represents the vibrational inhibition of intermolecular interaction between two molecules separated by  $\mathbf{r}$  when the whole system is in a stationary state characterized by the electronic wave vector  $\mathbf{k}$ .

In Part I, Section III (see Part I, eqn. (13)), we defined a lattice sum of intermolecular interaction integrals,  $S(\mathbf{k})$ . This lattice sum enters in an important way into the theory in which vibrational motions are left out of consideration. In time-independent theory,  $S(\mathbf{k})$  expresses the difference between the energy of the electronically excited monomer and the energy of the corresponding exciton state characterized by wave vector  $\mathbf{k}$ . In time-dependent theory, the group velocity  $\mathbf{G}$  of an exciton wave packet formed by superposition of elementary exciton waves with wave vectors lying within a region of  $\mathbf{k}$ -space centred at the point  $\bar{\mathbf{k}}$  is (Seitz 1940)

$$\mathbf{G} = (2\pi/\hbar) \operatorname{grad}_{\mathbf{k}} S(\mathbf{k}) |_{\bar{\mathbf{k}}}. \quad (13)$$

The group velocity of the excitation wave is generally identified with the velocity of exciton migration.

For the low-energy exciton states of a system of non-rigid molecules we define an analogous lattice sum of effective intermolecular interaction integrals as follows :

$$S_{\text{eff}}(\mathbf{k}) = \sum_j \exp i\mathbf{k} \cdot (\mathbf{r}^{(j)} - \mathbf{r}^{(i)}) (\Phi^{(j)} | \mathcal{W}^{(j,i)} | (\Phi^{(i)}) F_{\mathbf{k}}(\mathbf{r}^{(i)} - \mathbf{r}^{(j)})). \quad (14)$$

In time-independent theory,  $S_{\text{eff}}(\mathbf{k})$  expresses the difference between the energy of the wave function  $\Phi^{(j)} \Xi^{(j)}$  defined by equation (11) and the energy of the corresponding exciton state characterized by wave vector  $\mathbf{k}$ . In so far as

perturbation theory is correct, the wave function  $\Phi^{(j)}\Xi^{(j)}$  approaches a product of monomer wave functions  $\prod_i \psi_0^{(i)}\chi_{00}^{(i)}\psi_1^{(i)}\chi_{10}^{(i)}\psi_0^{(i)}\chi_{00}^{(i)}$  (for notation, see Part I, Section II) as the lattice sum decreases. We may therefore state that  $S_{\text{eff}}(\mathbf{k})$  expresses, without gross fractional error, the difference between the energy of the electronically excited monomer and the energy of the corresponding exciton state characterized by wave number  $\mathbf{k}$ . The actual errors involved here are difficult to assess, but the maximum absolute error (maximum difference between the monomer energy and the energy of the wave function  $\Phi^{(j)}\Xi^{(j)}$ ), is, from Part I, equations (29) and (1),  $M^2\text{h}ev_0$ . This error would be approached only where inequality (5) is satisfied. If we take the double inequality sign in (5) to denote difference by a factor of 10, and put  $S_{\text{eff}}(0) \approx -\Delta U/2$ , an upper limit for the fractional error is found to be 1/5.

In discussing time-dependent theory, we specify that the wave vector  $\mathbf{k}$  must correspond to a low-energy exciton state. As the expansion coefficients  $c_{\mathbf{kk}'}$  are slowly-varying functions of  $\mathbf{k}'$ , the factors  $F_{\mathbf{k}}$  for  $\mathbf{k}$ -values lying in the vicinity of  $\bar{\mathbf{k}}$  are all approximately equal to  $F_{\bar{\mathbf{k}}}$ . By an argument similar to the derivation of equation (13), we obtain for the group velocity\*

$$(2\pi/\hbar) \text{grad}_{\mathbf{k}} S_{\text{eff}}(\mathbf{k}) |_{\bar{\mathbf{k}}} = [S_{\text{eff}}(\mathbf{k})/S(\mathbf{k})] \mathbf{G}. \quad (15)$$

We have found that the stabilization of the low-energy exciton states and the velocity of exciton migration are reduced, through intramolecular vibrations, by a factor which is approximately  $S_{\text{eff}}(\mathbf{k})/S(\mathbf{k})$ . A physical interpretation of this result may be based on the proposition that the interaction between two identical molecules with variable nuclear configurations becomes stronger as the nuclear configurations become more nearly alike. Consequently, the average interaction becomes stronger as the average nuclear configurations become more nearly alike.

We now consider the instantaneous state in which the  $j$ th molecule is definitely excited. The wave function is  $\Phi^{(j)}\Xi^{(j)}$ , and the expectation value of the normal coordinate  $R^{(i)}$  of the  $i$ th molecule with respect to  $\Phi^{(j)}\Xi^{(j)}$  is to the first order in the expansion coefficients

$$\langle R^{(i)} \rangle^{(j)} = R_0 + 2N^{-1} (\chi_{00} | R | \chi_{01}) \sum'_{\mathbf{k}\mathbf{k}'} c_{\mathbf{kk}'} \cos \mathbf{k}' \cdot (\mathbf{r}^{(i)} - \mathbf{r}^{(j)}). \quad (16)$$

In the sense in which  $R_1 - R_0$  is the distortion of an isolated molecule due to its electronic excitation,  $\langle R^{(i)} \rangle^{(j)} - R_0$  is the distortion of the  $i$ th molecule in the aggregate, due to the electronic excitation of the  $j$ th molecule. As a measure of the distortion of the molecule situated at  $\mathbf{r}$ , due to the electronic excitation of a molecule at the origin, we introduce the ratio

$$D_{\mathbf{k}}(\mathbf{r}) = [R_0 - R_0 + 2N^{-1} (\chi_{00} | R | \chi_{01}) \sum'_{\mathbf{k}\mathbf{k}'} c_{\mathbf{kk}'} \cos \mathbf{k}' \cdot \mathbf{r}] / (R_1 - R_0). \quad (17)$$

Equation (17) represents a physical condition in which, at any instant, the electronically excited molecule is surrounded by a region of molecular distortion. In cases of close approach to the E-V coupling limit, the inequality (4) is satisfied

\* Merrifield (1958) has recently made an important development of time-dependent theory, affording a description of the details of the wave packet. It is not clear at present how intramolecular vibrations should be included in Merrifield's theory.

and  $D_{\mathbf{k}}(\mathbf{r})$  is a slowly-varying function. The average nuclear configuration of the electronically excited molecule differs only slightly from that of its neighbours, so that the vibrational inhibition of intermolecular interaction is slight. In cases of large departure from the E-V coupling limit, the expansion coefficients  $c_{\mathbf{k}\mathbf{k}'}$  are relatively large and vary relatively slowly with  $\mathbf{k}'$ . It can be seen from equation (17) that the molecular distortion is strongly localized in this case. The difference between the average nuclear configurations of the electronically excited molecule and its neighbours is relatively large, and the intermolecular interaction is therefore relatively strongly inhibited.

## V. APPLICATION TO LINEAR AGGREGATES

### (a) Theory

We consider a linear molecular aggregate with two molecules per unit cell, and with lattice spacing  $a$ . We neglect non-nearest neighbour interactions. The wave vector  $\mathbf{k}$  becomes a wave number  $\mathbf{x}$ ,  $\pi\rho$  becomes  $\pi\rho$ , the lattice sum  $S(\mathbf{k})$  becomes

$$S(\mathbf{x}) = -2 |W| \cos \mathbf{x}a,$$

where  $W$  is the nearest-neighbour intermolecular interaction integral, and  $\Delta U$  becomes  $4 |W|$ .

We set out now to obtain explicit expressions for the right-hand sides of equations (6), (8), (9), (12), and (17) for the linear aggregate. For this purpose we require to evaluate the various sums occurring in these equations. To simplify the notation we express intermolecular distances by  $\eta a$ , where  $\eta$  is an integer or zero. Upon adopting the perturbation-theory expressions (3) for the expansion coefficients  $c_{\mathbf{x}\mathbf{x}'}$ , and replacing summation over  $\mathbf{x}'$  (omitting the term  $\mathbf{x}'=\mathbf{x}$ ) by integration over the complete range of  $\mathbf{x}$  from  $-\pi/a$  to  $\pi/a$ , we get

$$\begin{aligned} \sum'_{\mathbf{x}'} c_{0\mathbf{x}'} \cos \mathbf{x}'\eta a &= \frac{N^{-\frac{1}{2}} M}{2\pi} \int_{-\pi}^{\pi} \frac{\cos \eta a dx}{1 + (1 - \cos x)/(\gamma - 1)} \\ &= N^{\frac{1}{2}} M [\gamma - (\gamma^2 - 1)^{\frac{1}{2}}]^{\eta} [(\gamma - 1)/(\gamma + 1)]^{\frac{1}{2}}, \end{aligned} \quad (18)$$

$$\begin{aligned} \sum'_{\mathbf{x}'} |c_{0\mathbf{x}'}|^2 \exp i\mathbf{x}'\eta a &= \frac{M^2}{2\pi} \int_{-\pi}^{\pi} \frac{e^{i\eta a} dx}{[1 + (1 - \cos x)/(\gamma - 1)]^2} \\ &= [M^2/(\gamma + 1)][\gamma + \eta(\gamma^2 - 1)^{\frac{1}{2}}] \\ &\quad \times [\gamma - (\gamma^2 - 1)^{\frac{1}{2}}]^{\eta} [(\gamma - 1)/(\gamma + 1)]^{\frac{1}{2}}, \end{aligned} \quad (19)$$

$$\begin{aligned} \sum'_{\mathbf{x}'} |c_{\mathbf{x}\mathbf{x}'}|^2 e^{-\varepsilon(\mathbf{x})/kT} &= \frac{M^2}{2\pi} \int_{-\pi}^{\pi} \frac{e^{-\Delta U(1 - \cos x)/2kT} dx}{[1 + (\cos x - 1)/(\gamma - 1)]^2} \\ &= \frac{M^2}{(2\pi)^{\frac{1}{2}} (\Delta U/2kT)^{\frac{1}{2}}} \left[ 1 + \left( 1 + \frac{8}{\gamma - 1} \right) \frac{1}{8(\Delta U/2kT)} + \dots \right], \end{aligned} \quad (20)$$

$(\Delta U/2kT \gg 1)$ ,

$$\begin{aligned} \sum'_{\mathbf{x}} |c_{x\pi\rho}|^2 e^{-\varepsilon(\mathbf{x})/kT} &= \frac{M^2}{2\pi} \int_{-\pi}^{\pi} \frac{e^{-\Delta U(1 - \cos x)/2kT} dx}{[1 + (\cos x + 1)/(\gamma - 1)]^2} \\ &= \left( \frac{\gamma - 1}{\gamma + 1} \right)^2 \frac{M^2}{(2\pi)^{\frac{1}{2}} (\Delta U/2kT)^{\frac{1}{2}}} \left[ 1 + \left( 1 + \frac{8}{\gamma - 1} \right) \frac{1}{8(\Delta U/2kT)} + \dots \right], \end{aligned} \quad (21)$$

$(\Delta U/2kT \gg 1)$ , where

$$\gamma = (hc\nu_0 + \frac{1}{2}\Delta U)/\frac{1}{2}\Delta U.$$

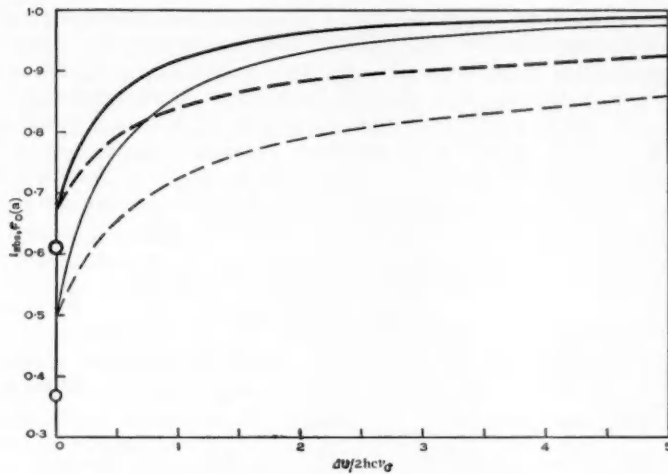


Fig. 4.—The variation of relative absorption intensity  $I_{\text{abs}}$  (broken lines) and vibrational inhibition factor  $F_0(a) = S_{\text{eff}}(0)/S(0)$  (full lines) with  $\Delta U / 2hcv_0$  according to equations (6') and (12') for a linear aggregate. Thick lines,  $M^2 = 0.5$ ; thin lines  $M^2 = 1$ . Circles indicate exact values for  $\Delta U = 0$  (eqn. (22)).

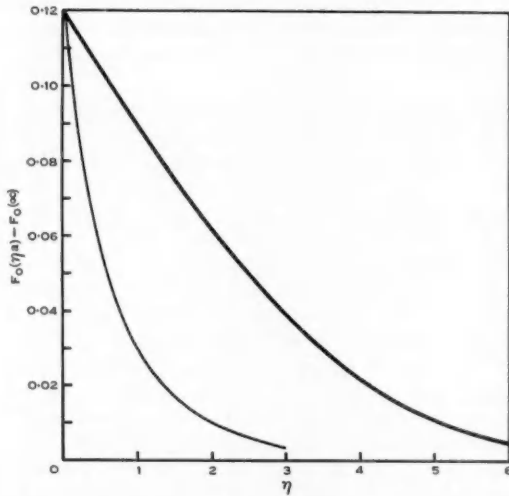


Fig. 5.—The variation of vibrational inhibition factor  $F(\eta a)$  with  $\eta$ , according to equation (12') for a linear aggregate. Thick line,  $\Delta U / 2hcv_0 = 5$ ; thin line,  $\Delta U / 2hcv_0 = 0.5$ .  $M^2 = 1$  for both curves.

The integrals in (18) and (19) were converted into elementary contour integrals through the substitution  $z=e^{ixa}$ . The integral in (20) was evaluated through the substitution  $y=\cos x$ , followed by Taylor series expansion of the factor  $[1+(y-1)/(y+1)]^{-2}$  about the point  $y=1$  and term-by-term integration. The first term is a tabulated integral (Gröbner and Hofreiter 1958) and successive terms were obtained by differentiating the first term with respect to  $\Delta U/2kT$ . The individual terms were expanded in inverse powers of  $\Delta U/2kT$  according to an asymptotic formula for large values of  $\Delta U/2kT$ . The integral in equation (21) was treated in a similar way.

Upon substituting equation (19) in equations (6) and (12), we get

$$I_{\text{abs}} = 1/\{1 + M^2 \gamma [(\gamma - 1)/(\gamma + 1)]^{1/2}/(\gamma + 1)\}, \quad (6')$$

$$F_0(\eta a) = \frac{1 + [M^2/(\gamma + 1)][\gamma + \eta(\gamma^2 - 1)^{1/2}][\gamma - (\gamma^2 - 1)]^\eta[(\gamma - 1)/(\gamma + 1)]^{1/2}}{1 + [M^2/(\gamma + 1)][(\gamma - 1)/(\gamma + 1)]^{1/2}\gamma}. \quad (12')$$

Because of the nearest-neighbour approximation, we have  $S_{\text{eff}}(0) = S(0)F_0(a)$ . In Figure 4, the expressions (6') and (12') for  $I_{\text{abs}}$  and  $F_0(a)$  are plotted against  $\Delta U/2hc\nu_o$  for two values of  $M$ . Since the derivations depend on perturbation theory, the curves become increasingly inaccurate as  $\Delta U$  tends to zero. The results at  $\Delta U=0$  may be compared with the exact results for a system of non-interacting molecules conforming to the present model:

$$I_{\text{abs}} = I_{\text{fl}} = F_0(a) = |\langle \chi_{00} | \chi_{10} \rangle|^2 = e^{-M^2}. \quad (22)$$

This comparison (Fig. 4) indicates that perturbation theory is actually a good approximation over a wider range of  $M$  and  $\Delta U$  than is indicated by the inequality (5).

Figure 5 shows the variation of  $F_0(\eta a)$  with  $\eta$  for two values of  $\Delta U/2hc\nu_o$  and  $M^2=1$ , calculated from equation (12'). The calculation shows that the lattice sums of intermolecular interaction integrals for low-energy exciton states are more strongly convergent than would be expected if intramolecular vibrations were left out of consideration.

Upon substituting the first two terms from equation (20) into (8) and noting that in the present case we have  $\kappa_{\min}=0$ , we get after rearrangement

$$I_{\text{fl}} = I_{\text{abs}} / \left\{ I_{\text{abs}} + M^2(\gamma - 1)^{1/2}(kT/hc\nu_o)^{1/2} \left[ 1 + \left( 1 + \frac{8}{\gamma - 1} \right) \frac{kT}{hc\nu_o} \frac{\gamma - 1}{8} \right] / (2\pi)^{1/2} \right\}. \quad (8')$$

In Figure 6 the expression (8') is plotted against  $\Delta U/2hc\nu_o$  for  $T=300$  °K and  $T=4$  °K ( $\nu_o=1000$  cm<sup>-1</sup>). The strong temperature dependence of  $I_{\text{fl}}$  may be attributed almost entirely to the term in  $T^{1/2}$  in the denominator of the expression (8').

An expression for the polarization ratio of the diffuse fluorescence may be obtained by substituting from equations (20) and (21) into equation (9). Upon expanding the resulting expression in powers of  $T$ , we obtain

$$P[\mathbf{Q}(\pi\rho) : \mathbf{Q}(0)] = \left( \frac{\gamma - 1}{\gamma + 1} \right)^2 \frac{|\mathbf{Q}(\pi\rho)|^2}{|\mathbf{Q}(0)|^2} \left( 1 - \frac{2}{(\gamma + 1)} \frac{kT}{hc\nu_o} + \dots \right). \quad (9')$$

The polarization ratio in the vicinity of one vibrational interval from the onset of fluorescence is thus independent of  $M$  and, since the factor  $2/(\gamma+1)$  cannot exceed unity, it is almost independent of temperature.

As is illustrated in Figure 7, the polarization ratio depends strongly on  $\Delta U$ . For systems conforming to the present model, the ratio of  $P[Q(\pi\varphi) : Q(0)]$  to the polarization ratio in absorption is a measure of the theoretical Davydov splitting,  $\Delta U$ .

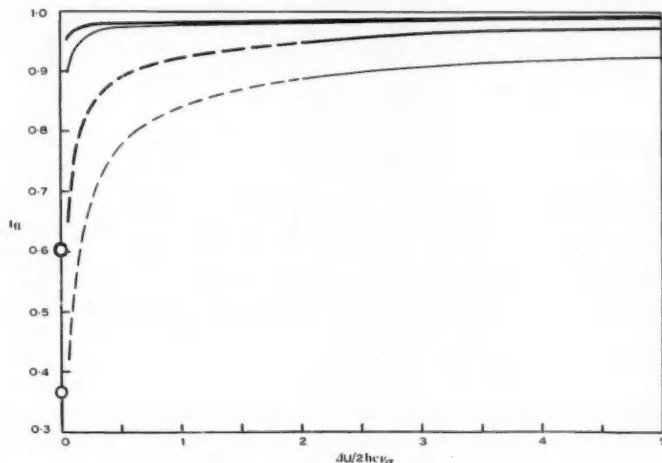


Fig. 6.—The variation of relative fluorescence intensity  $I_f$  with  $\Delta U/2h\nu_0$  according to equation (8') for a linear aggregate. Thick lines,  $M^2=0.5$ ; thin lines,  $M^2=1$ . The two top lines refer to  $T=4$  °K and the two bottom lines to  $T=300$  °K, where  $\nu_0=1000$  cm<sup>-1</sup> in both cases. Full lines represent the results of calculations with  $\Delta U/2kT>10$ , under which condition the asymptotic expansion (see text) is valid. Broken lines,  $\Delta U/2kT<10$ . Circles denote exact values for  $\Delta U=0$  (eqn. (22)).

Finally, an expression for the relative molecular distortion,  $D(\eta a)$ , may be obtained by substituting equation (18) into equation (17). Making use of the properties of the harmonic oscillator, we have

$$(\chi_{\sigma 0} | R | \chi_{\sigma 1}) = (2\beta_\sigma)^{-\frac{1}{2}}, \\ k_\sigma/\beta_\sigma = \hbar c \nu_\sigma.$$

Also,  $R_\sigma \approx R_0$ . Hence

$$D(\eta a) = [\gamma - (\gamma^2 - 1)]^\eta [(\gamma - 1)/(\gamma + 1)]^{\frac{1}{2}}. \quad (17')$$

The expression (17') is plotted in Figure 8 as a function of  $\eta$  for a large and a small value of  $\Delta U/2h\nu_0$ . It may be seen that there is appreciable delocalization of molecular distortion for values of  $\Delta U$  normally encountered in molecular aggregates.

#### (b) Comparison with Experiment

The theory may be tested by a comparison with the visible absorption and fluorescence spectra of the cationic dye *NN'*-diethyl- $\psi$ -cyanine. In concentrated

aqueous solutions, the dye associates to form thread-like polymers.\* The absorption spectra at various concentrations have been measured by Zimmermann and Scheibe (1956), and the spectrum observed with the most concentrated solution studied by them is reproduced in Figure 9 in comparison with the monomer spectrum. The spectrum obtained with the concentration solution

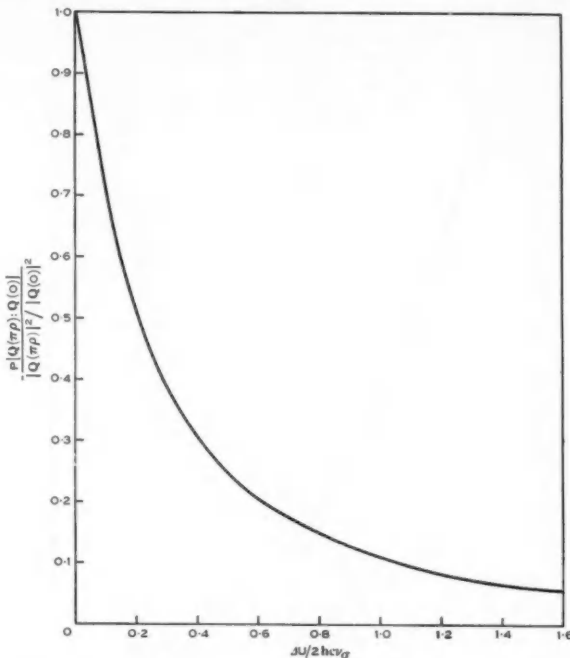


Fig. 7.—The variation of fluorescence polarization factor  
 $P[Q(\pi\rho) : Q(0)] / [ |Q(\pi\rho)|^2 / |Q(0)|^2 ]$   
with  $\Delta U/2hc\nu_0$  according to equation (9') for a linear aggregate.  
The curves for  $T=4^\circ\text{K}$  and  $T=300^\circ\text{K}$  cannot be distinguished on  
the scale of the diagram.

probably contains a significant contribution from the absorption of monomeric and dimeric species, but the three absorption maxima are thought by the present writer to be real features of the polymer spectrum.

The polarized absorption spectrum of the polymer is not available, but the lowest-frequency vibronic band, which is called the J band, is known to be polarized with the electric vector parallel to the length of the polymer. The

\* The formation and properties of the dye polymers have been described in a review by Bayliss (1951), where references to the older literature are given. The P band referred to in Bayliss' review is here called the J band.

rest of the spectrum has been shown by an indirect method to be at least partly perpendicularly polarized, but it is not known to what extent.

The fluorescence spectrum of the polymer apparently consists of a single band, also called the J band, at the same frequency as the J band in absorption.

The observed absorption spectrum corresponds qualitatively to the theoretical expectation for an aggregate with two molecules per unit cell and with  $\Delta U > \hbar c v_0$  (see Figs. 9 and 1 (c) for a comparison of observed and predicted absorption band

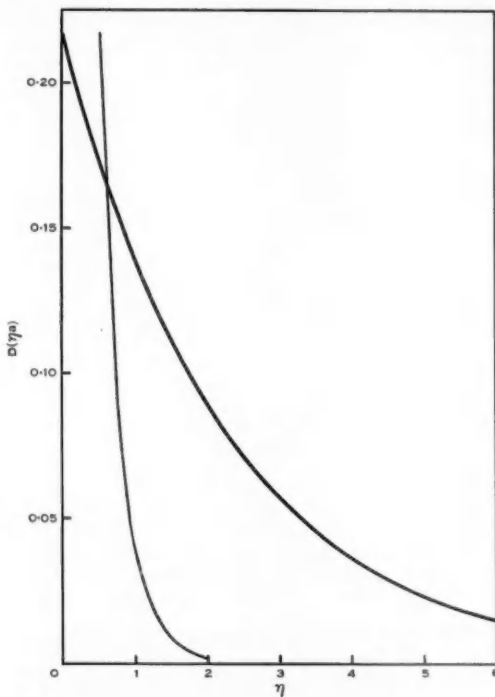


Fig. 8.—The variation of molecular distortion  $D(\eta a)$  with  $\eta$ , according to equation (17') for a linear aggregate. Thick line,  $\Delta U/2\hbar c v_0 = 10$ ; thin line,  $\Delta U/2\hbar c v_0 = 0.1$ .

shapes). The separation of the highest- and lowest-frequency absorption maxima ( $2800 \text{ cm}^{-1}$ ) may be regarded as a rough approximation to  $\Delta U/\hbar c$ . Also, from the monomer spectrum (Fig. 9) we have  $M^2 \approx 0.7$ ,  $v_0 \approx 1200 \text{ cm}^{-1}$ . From these numerical values we get

$$M^2/(1 + \Delta U/\hbar c v_0) \approx 0.2.$$

According to our criterion (5), the polymer spectrum presents a case of moderately close approach to the E-V coupling limit.

The theory furnishes a prediction of the fractional contributions of the J bands to the intensities of the parallel-polarized components of absorption and fluorescence.

(i) *The J Band in Absorption.*—According to Figure 4, for

$$\Delta U/2\hbar c\nu_0 \approx 2800/2400,$$

the J band should contribute  $\sim 80\%$  of the total parallel-polarized absorption, leaving  $\sim 20\%$  for the parallel-polarized absorption starting one vibrational interval to higher frequencies. Referring to the observed spectrum (Fig. 9), we see that the middle absorption maximum lies at  $18,800 \text{ cm}^{-1}$ , which is

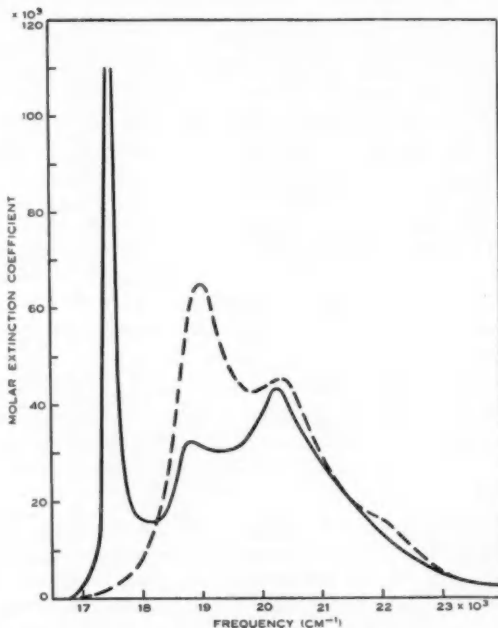


Fig. 9.—Absorption spectra of *NN'*-diethyl- $\beta$ -cyanine iodide in water according to Zimmermann and Scheibe (1956). Broken line, concentration  $10^{-5}\text{M}$ . Full line, concentration  $3 \times 10^{-6}\text{M}$ .

$1300 \text{ cm}^{-1}$  to the high-frequency side of the J band. When allowance is made for the overlap of neighbouring bands and the J-band intensity present but not shown in Figure 9, the integrated intensity of the absorption near  $18,800 \text{ cm}^{-1}$  is found to be less than half that of the J band. This fraction would be reduced by correction for the absorption due to unassociated dye. The theoretical result is consistent with the observed spectrum, but as the polarized spectrum is not available, and because of the possible incompleteness of association, a more detailed comparison is not possible at present.

(ii) *The J Band in Fluorescence.*—According to Figure 6 the J band in the room-temperature fluorescence should contribute  $\sim 90\%$  of the total parallel-polarized intensity. The remaining intensity ( $\sim 10\%$  of the total) should be present in a diffuse fluorescence band of width  $\sim 200 \text{ cm}^{-1}$  lying one vibrational interval ( $\sim 1200 \text{ cm}^{-1}$ ) to the low-frequency side of the J band. According to Figure 7 the diffuse fluorescence should be predominantly parallel-polarized. At lower temperatures, the diffuse fluorescence band should become narrower and weaker. There do not seem to be any experimental results with which to compare these theoretical predictions, other than that the J band is the dominant feature of the fluorescence spectrum.

## VI. DISCUSSION

The theory given in this and the preceding Parts I and II of this series refers to a model system consisting of an array of non-rigid molecules in a rigid lattice. We shall discuss firstly the theory for this model, and secondly the accuracy with which the model represents real molecular aggregates.

### (a) Theory for the Model

The low-energy exciton states may be described by perturbation theory if a suitable choice is made between the m-m and E-V sets of zeroth-order wave functions. For small values of  $M(M^2 < 1/2)$  there is a considerable overlap between the respective ranges of  $\Delta U/2\hbar c\nu_0$  within which the m-m and E-V expansions are useful. The theory for the low-energy states is thus in a fairly satisfactory condition.

The higher-energy exciton states are less tractable. However, for a dimer these states could be studied, on the basis of either m-m or E-V wave functions, through the direct solution of a secular equation. The properties of dimers might serve as a guide in the treatment of the more difficult problem presented by polymeric systems.

As a consequence of the difficulty of treating the higher-energy exciton states, it is not possible at present accurately to relate the theoretical Davydov splitting ( $|U(\pi\rho) - U(0)|/\hbar c$  in aggregates with two molecules per unit cell) to observed absorption band frequencies in the spectrum of an aggregate. The theory does, however, provide a relationship between the theoretical Davydov splitting and the polarization ratios in absorption and fluorescence. This relationship is implicit in equation (9) and is given explicitly in (9') for a case in which the theoretical Davydov splitting is identical with  $\Delta U$ . A more complete discussion of the relationship will be given in another publication.

### (b) Validity of the Model

The accuracy with which the model represents a molecular aggregate may be judged by comparison between theory and experiment in cases in which the theory for the model may be expected to hold accurately.

The comparison between theory and experiment in Section IV indicates that the cyanine dye polymer is accurately represented by the model. However,

for the intense ultraviolet absorption band system of the anthracene crystal (Lyons and Morris 1959) we calculate\*

$$I_{\text{abs}} \approx 1 - \frac{M^2}{1 + \Delta U/hc\nu_0} \gtrsim 0.8,$$

which may be compared with the observed value,  $\sim 0.5$ . The pronounced difference between the theoretical and experimental values of  $I_{\text{abs}}$  cannot be explained as resulting from a breakdown of perturbation theory, as inequality (5) is satisfied. We must therefore conclude that the model is at fault. The success of the model in the case of the cyanide dye polymer may perhaps be attributed to strong electrostatic forces tending to keep the dye molecules rigidly locked in their equilibrium positions. It seems likely that where electrostatic binding forces are absent, as in the anthracene crystal, lattice vibrations and lattice defects should not be left out of consideration.

### VII. ACKNOWLEDGMENTS

I am pleased to acknowledge that my interest in the subject treated in this series of papers was first aroused through an association with Professor M. Kasha. I wish to thank Dr. J. Ferguson for some helpful discussions of the experimental aspects, Dr. V. W. Maslen for help with some of the mathematical derivations, and Dr. I. G. Ross for reading the manuscript before publication.

### VIII. REFERENCES

BAYLISS, N. S. (1951).—*Rev. Pure & Appl. Chem.* **1**: 64.  
 DAVYDOV, A. S. (1948).—*J. Expt. Theor. Phys. (U.S.S.R.)* **18**: 210.  
 GRÖBNER, W., and HOFREITER, N. (1958).—“Integraltafel II.” 2nd Ed. p. 63. (Springer-Verlag: Vienna and Innsbruck.)  
 LYONS, L. E., and MORRIS, G. C. (1959).—*J. Chem. Soc.* **1959**: 1551.  
 LYONS, L. E., and MORRIS, G. C. (1960).—*J. Mol. Spectroscopy* **4**: 480.  
 MCRAE, E. G. (1960).—*J. Chem. Phys.* **33**: 932.  
 MCRAE, E. G. (1961a).—*Aust. J. Chem.* **14**: 329.  
 MCRAE, E. G. (1961b).—*Aust. J. Chem.* **14**: 344.  
 MERRIFIELD, R. E. (1958).—*J. Chem. Phys.* **28**: 647.  
 SEITZ, F. (1940).—“The Modern Theory of Solids.” 1st Ed. p. 417. (McGraw-Hill Book Co.: New York.)  
 SIMPSON, W. T., and PETERSON, D. L. (1957).—*J. Chem. Phys.* **26**: 588.  
 ZIMMERMANN, H., and SCHEIBE, G. (1956).—*Z. Elektrochem.* **60**: 566.

\* From equation (6) we have

$$I_{\text{abs}} = 1 - \sum'_{\mathbf{k}'} |c_{0\mathbf{k}'}|^2,$$

when inequality (4) is satisfied. By the argument leading to inequality (5), we have

$$\sum'_{\mathbf{k}'} |c_{0\mathbf{k}'}|^2 \approx M^2 / (1 + \Delta U/hc\nu_0).$$

From the observed spectrum,  $\Delta U/hc \geq 8000 \text{ cm}^{-1}$ ,  $\nu_0 \approx 1300 \text{ cm}^{-1}$ ,  $M^2 \approx 1.5$ . The values assigned to  $\nu_0$  and  $M^2$  are rough estimates based on the integrated intensity and mean frequency of the vibronic bands contributing to the shoulder in the solution spectrum. There are actually several short, totally-symmetric progressions in the vapour spectrum (Lyons and Morris 1960), and we have in effect lumped these together into a single progression of fundamental interval  $1300 \text{ cm}^{-1}$ .

## SOME PROPERTIES OF COMPRESSIONAL WAVES IN LENNARD-JONES AND DEVONSHIRE LIQUIDS

### II. SHOCK WAVES

By H. G. DAVID† and S. D. HAMANN‡

[Manuscript received February 14, 1961]

#### *Summary*

This paper describes some theoretical calculations of the thermodynamic changes which occur when a condensed substance is compressed by a shock wave from an explosion. It is assumed that the material is a simple molecular fluid (or a plastic solid) obeying Lennard-Jones and Devonshire's equation of state.

The calculations have been applied to single and colliding shock waves, to shocks generated in a precompressed material, and to the adiabatic expansion of a material from a shocked state. The results are in good qualitative agreement with the experimental data where these exist. In addition they suggest possible ways of extending the scope and usefulness of shock wave experiments.

### I. INTRODUCTION

In Part I of this series (David and Hamann 1961) we computed the speed of sound in liquids obeying Lennard-Jones and Devonshire's (1937) equation of state. The present paper describes similar calculations of the properties of strong shock waves.

The purpose of the work has been to predict the kinds of conditions which may exist in compressional waves launched by explosions. It is known that if a high explosive is detonated in contact with an inert solid or liquid it drives a steep-fronted shock wave into the material and that the pressure behind the shock front may be as great as a million atmospheres for a few millionths of a second. It is possible to measure the pressure, the density, and even some of the chemical properties of shocked materials (see, for instance, Hamann 1960a). But no means has yet been devised for measuring the transient temperature. Instead this is estimated by combining a postulated equation of state with the Rankine-Hugoniot shock relations (see, for instance, Hirschfelder, Curtiss, and Bird 1954; Hamann 1960a). In the present calculations we have employed Lennard-Jones and Devonshire's (LJD) equation of state in this way. We have used it to calculate (i) the properties of plane shock waves in classical monatomic liquids; (ii) the corresponding properties in a "quantal" liquid; (iii) the conditions after adiabatic expansion from a shocked state; (iv) the conditions

† Division of Physical Chemistry, C.S.I.R.O. High Pressure Laboratory, 338 Blaxland Road, Ryde, N.S.W.

‡ Division of Physical Chemistry, C.S.I.R.O. High Pressure Laboratory; present address: Chemical Research Laboratories, C.S.I.R.O., Melbourne.

at the head-on collision of two plane shocks; (v) the initial shock conditions for liquid argon in contact with the explosive 60/40 RDX/TNT; (vi) shock conditions in precompressed liquids.

Since we began this work, Fickett and Wood (1960) have published the results of some LJD calculations of shock properties in liquid argon. Their method was rather more empirical than ours because it made use of the experimental density and energy of unperturbed argon. They employed the LJD theory at high pressures where they believed it right and the experimental data at low pressures where it appeared to be wrong.<sup>†</sup> For their particular purpose this was a justifiable procedure, but here we have preferred to be consistent and use the theoretical LJD equation throughout.

## II. DEFINITIONS OF SYMBOLS USED

Most of the following symbols have been defined more fully in earlier papers (Hamann 1960b; David and Hamann 1961).

The subscript zero denotes properties characteristic of the molecules. Asterisks indicate quantities expressed in molecular units.

- $N$ , Avogadro's number,
- $k$ , Boltzmann's constant,
- $h$ , Planck's constant,
- $\epsilon_0$ , depth of the energy well in the Lennard-Jones 12:6 intermolecular potential,
- $r_0$ , radius of the energy well,
- $m$ , molecular mass,
- $M$ , molar mass ( $=Nm$ ),
- $\Lambda^*$ , de Boer's (1948) quantal parameter ( $=2^{1/6}h/r_0(m\epsilon_0)^{1/2}$ ),
- $C_V$ , specific heat per mole at constant volume,
- $C_V^*$ ,  $C_V/Nk$ ,
- $E$ , internal energy per mole,
- $\hat{E}$ , internal energy per unit mass,
- $E^*$ ,  $E/N\epsilon_0$ ,
- $P$ , pressure,
- $P_0$ ,  $2^{1/2}\epsilon_0/r_0^3$ ,
- $P^*$ ,  $P/P_0$ ,
- $S$ , entropy per mole,
- $S^*$ ,  $S/Nk$ ,
- $T$ , absolute temperature,
- $T_0$ ,  $\epsilon_0/k$ ,
- $T^*$ ,  $T/T_0$ ,
- $u$ , velocity of sound,
- $u_0$ ,  $(\epsilon_0/m)^{1/2} = (N\epsilon_0/M)^{1/2}$ ,
- $u^*$ ,  $u/u_0$ ,

<sup>†</sup> During the course of our calculations it has become increasingly apparent that the LJD theory is really more appropriate to the solid state than to the liquid. Barker's (1960, 1961a) "tunnel" model is a much better one for liquids, and we hope to apply it later in some shock calculations.

$U$ , shock velocity,  
 $U^*$ ,  $U/u_0$ ,  
 $V$ , volume per mole,  
 $\hat{V}$ , volume per unit mass,  
 $V_0$ ,  $Nr_0^3/2^{1/2}$ ,  
 $V^*$ ,  $V/V_0$ ,  
 $w$ , flow velocity,  
 $w^*$ ,  $w/w_0$ .

The following subscripts are applied to shock properties :

no subscript, indicates the initial conditions ahead of a shock wave,  
 subscript 1, denotes the conditions behind a single shock,  
 subscript 2, denotes the conditions after the interaction of one shock with  
 another, or with a rarefaction wave.

### III. DETAILS OF THE CALCULATIONS

#### (a) General

A shock wave is a steep-fronted compression wave which causes very abrupt changes in the pressure, density, and temperature of the material through which it passes. The existence of extreme gradients in these properties through the shock front means that the compression is thermodynamically irreversible and non-adiabatic. Nevertheless there exist some rigorous relations between the conditions ahead of and behind the shock front. They are based on the principles of conservation of mass, momentum, and energy, and they are usually known as the Rankine-Hugoniot relations† (Rankine 1870; Hugoniot 1887, 1889). If the fluid ahead of the shock wave is stationary, the relations are

$$U_1 = \hat{V}[(P_1 - P)/(\hat{V} - \hat{V}_1)]^{1/2} \quad (1)$$

$$w_1 = [(P_1 - P)(\hat{V} - \hat{V}_1)]^{1/2}, \quad (2)$$

$$\hat{E}_1 - \hat{E} = \frac{1}{2}(P_1 + P)(\hat{V} - \hat{V}_1), \quad (3)$$

where  $P$ ,  $\hat{V}$ , and  $\hat{E}$  are the pressure, volume per unit mass, and internal energy per unit mass in the initial state, and  $P_1$ ,  $\hat{V}_1$ ,  $\hat{E}_1$  are the corresponding properties of the shocked fluid.  $U_1$  denotes the velocity of the shock front and  $w_1$  the velocity of flow of the material behind the front. In the limit of low amplitude shock waves  $P_1 - P$ ,  $\hat{V} - \hat{V}_1$ ,  $w_1$ , and  $\hat{E}_1 - \hat{E}$  all approach zero and  $U_1$  approaches the normal velocity of sound,  $u = \hat{V}(-\partial P/\partial \hat{V})_S^{1/2}$ .

For a Lennard-Jones and Devonshire liquid the Rankine-Hugoniot relations can be rewritten in molecular units (defined in Section II) thus

$$U_1^* = V^*[(P_1^* - P^*)/(V^* - V_1^*)]^{1/2}, \quad (4)$$

$$w_1^* = [(P_1^* - P^*)(V^* - V_1^*)]^{1/2}, \quad (5)$$

$$E_1^* - E^* = \frac{1}{2}(P_1^* + P^*)(V^* - V_1^*). \quad (6)$$

† This title is misleading : formulae equivalent to (1) and (2) were first derived by Stokes (1848).

The last of these formulae is particularly important because it defines all the possible  $P_1^*$ ,  $V_1^*$ , points which can be reached in a single shock compression from the initial conditions  $P^*$ ,  $V^*$ . This follows from the fact that  $E_1^* - E^*$  is related to  $P_1^*$ ,  $V_1^*$  by the LJD equation of state as well as by the Rankine-Hugoniot relation. It is therefore possible to eliminate  $E_1^* - E^*$  and obtain a specific relationship between  $P_1^*$  and  $V_1^*$  provided that  $P^*$  and  $V^*$  are specified. The locus of points obtained in this way will be referred to as a "Hugoniot" compression curve, and  $P^*$ ,  $V^*$  will be called the "starting point".

(b) *Single Shock Compression of a Classical Liquid from  $P^* \approx 0$*

We shall consider first a set of starting points corresponding to an LJD liquid which is either at atmospheric pressure or under its own vapour pressure. In these circumstances  $P^*$  is very small and can be considered to be zero. The LJD theory then gives a unique relationship, which we have already derived (David and Hamann 1961), between  $V^*$  and the reduced temperature  $T^*$ .

We can trace the Hugoniot curve from any particular starting point in the following way. We first suppose the fluid to be compressed isothermally from  $V^*$  to a smaller volume  $V_1^*$ . This generally raises its internal energy, although not sufficiently to satisfy equation (6). We then imagine the fluid to be heated at constant volume until it reaches a temperature  $T_1^*$  at which the LJD energy does equal the Hugoniot energy. This point  $(P_1^*, V_1^*, T_1^*)$  must lie on the Hugoniot curve starting at  $(P^* = 0, V^*, T^*)$ . By repeating the operation for a range of final volumes we can find the general form of the Hugoniot curve.

In principle the calculations can be performed automatically on a computer, but in our work we have used the existing LJD compilations of Wentorf *et al.* (1950), together with suitable interpolation formulae.† We have calculated Hugoniot curves from seven starting temperatures in the range  $T^* = 0.7$  to  $1.0$ , and, for comparison, worked out the corresponding isothermal and adiabatic compression curves from the same starting points. We have also estimated some of the thermodynamic properties of the fluid along the Hugoniot curve, again by interpolation in the tables of Wentorf *et al.* (1950).

(c) *Shock Compression of a Quantal Liquid from  $P^* \approx 0$*

Lennard-Jones and Devonshire's theory is based on classical statistical mechanics, which are known to be inadequate for light liquids such as helium, hydrogen, and neon. For these it is necessary to use a more general equation of state involving de Boer's (1948) quantal parameter  $\Lambda^*$ . In earlier papers (Hamann 1952, 1957; David and Hamann 1953) we have derived an equation of this kind by applying a quantum correction to the classical theory. We have now used this equation to compute a single Hugoniot curve for a quantal liquid ( $\Lambda^* = 1$ ) starting from  $P^* = 0$ ,  $T^* = 0.75$ .

† Dr. W. Fickett and Dr. W. W. Wood of the Los Alamos Scientific Laboratory have recently confirmed our results for liquid argon (Fig. 2) by automatic calculations on the IBM 704 computer (personal communication).

(d) *Conditions after Adiabatic Expansion from a Shocked State*

After the passage of a shock wave through a material the substance expands into its surroundings. This expansion occurs adiabatically because shock waves of rarefaction are forbidden by thermodynamics (Hirschfelder, Curtiss, and Bird 1954, p. 789). We can therefore follow the course of the expansion of a shocked LJD fluid by tracing points of constant entropy starting from a Hugoniot point ( $P_1^*$ ,  $V_1^*$ ,  $T_1^*$ ,  $S_1^*$ ) and moving to a series of points of lower pressure and larger volume ( $P_2^*$ ,  $V_2^*$ ,  $T_2^*$ ,  $S_2^* = S_1^*$ ). In this way we have traced adiabats from several points on the Hugoniot based on the starting point  $P^* = 0$ ,  $T^* = 0.75$ .

For reasons to be discussed in the next paragraph, it is sometimes important to know the contribution which the expansion makes to the forward flow velocity of the material. This is given by the Riemann integral

$$\dot{w_2} = \int_{P_1^*}^{P_2^*} \left( -\frac{\partial V^*}{\partial P^*} \right)_S^{\frac{1}{2}} dP^*, \quad (7)$$

where the integration is carried out along the expansion adiabat (see, for instance, Rice, McQueen, and Walsh 1958). The total flow velocity in the direction of the original shock is then  $\dot{w_1} + \dot{w_2}$ . In evaluating (7) we have found it convenient to fit the adiabat to an empirical equation of the form used by Tait (1900), and then perform the integration numerically by means of Simpson's rule.

If the material expands into a vacuum, then the final pressure is zero and the corresponding value of  $\dot{w_1} + \dot{w_2}$  is the velocity, in molecular units, of the free surface of the material after shock acceleration. If on the other hand the material expands into another substance, say air, it generates a shock wave in the second substance and the boundary conditions require that the absolute pressure  $P_2$  and velocity  $\dot{w_1} + \dot{w_2}$  at the interface must lie on the pressure/flow-velocity curve for the second material. If this Hugoniot relation is known, as it is for ideal gases, then the interfacial conditions can be worked out. These conditions are important because they determine whether or not the original material will vaporize after the passage of a shock wave. In the present calculations we have considered the expansion of a shocked LJD fluid into air, which we have assumed to obey the ideal gas relationship

$$\dot{w_1} = (P_1 - P) \left( \frac{5\hat{V}}{P + 6P_1} \right)^{\frac{1}{2}}. \quad (8)$$

(e) *Conditions at the Head-on Collision of Two Plane Shocks*

It is worthwhile to consider the conditions which exist after the head-on collision of two plane shock waves in an LJD fluid. We shall designate these conditions by the subscript 2, and the conditions in one of the initial shocks by the subscript 1. The Rankine-Hugoniot relations (4)-(6) can then be rewritten

$$U_2^* = -V_1^*[(P_2^* - P_1^*)/(V_1^* - V_2^*)]^{\frac{1}{2}}, \quad (9)$$

$$\dot{w}_2^* = -[(P_2^* - P_1^*)(V_1^* - V_2^*)]^{\frac{1}{2}}, \quad (10)$$

$$E_2^* - E_1^* = \frac{1}{2}(P_2^* + P_1^*)(V_1^* - V_2^*), \quad (11)$$

where  $U_2^*$  and  $w_2^*$  are velocities relative to the velocity of flow in the original shock 1. The absolute shock and flow velocities after collision are thus  $w_1 + U_1^*$  and  $w_1 + w_2^*$ . Formula (11) can be applied in the same way as (6) to trace the course of the final compression curve from the starting point  $(P_1^*, V_1^*, T_1^*)$ . In the present work we have calculated the properties of secondary shocks based on three starting points, all on the primary Hugoniot centred on the unperturbed state  $P^*=0$ ,  $V^*=1.0503$ ,  $T^*=0.75$ .

An interaction of special interest is the head-on collision of two equal shock waves, which is mathematically equivalent to the total reflection of a single shock at a rigid boundary. Such a collision must reduce the absolute flow velocity to zero and the final conditions can be found by imposing the restriction

$$w_2^* = -w_1^*. \quad (12)$$

Interactions of this kind will be discussed in Section IV (d).

*(f) Shock Conditions for Liquid Argon in Contact with the Explosive 60/40 RDX/TNT*

In Section III (c) we considered the transmission of a shock wave from an LJD fluid into another material. We shall now examine the converse process of transmitting a shock from a high explosive into an LJD fluid. Again the boundary conditions require that the pressure and flow velocity be continuous across the interface. These conditions can be satisfied by the reflection of either a compressive shock or a rarefaction wave back into the explosive products.

It is, of course, necessary to match the absolute pressures  $P$  and flow velocities  $w$  at the interface, not the reduced quantities  $P^*$  and  $w^*$ . This means that we must sacrifice generality and specify the materials of the explosive and the fluid. We have selected the explosive 60/40 RDX/TNT both because it is widely used in experimental work and because Deal (1958) has made a thorough experimental study of the propagation characteristics of shock waves and rarefaction waves in its products of explosion. We have chosen argon as the LJD liquid and transformed our theoretical LJD results into absolute units by means of the following factors derived from the second virial coefficient of gaseous argon (Hamann 1960b).

$$\begin{aligned} P &= P^* \times P_0 & P_0 &= 415 \text{ atm}, \\ V &= V^* \times V_0 & V_0 &= 24.0 \text{ cm}^3/\text{mole}, \\ T &= T^* \times T_0 & T_0 &= 120 \text{ }^\circ\text{K}, \\ U &= U^* \times u_0 \\ w &= w^* \times u_0 \end{aligned}$$

$$u_0 = 158 \text{ m/sec.}$$

The conditions at the interface are given by the point of intersection on a  $P/w$  diagram of the Hugoniot curve for forward-going shocks in argon and the curve for backward-going shocks and rarefactions in the explosive products (cf. Fig. 5).

*(g) Shock Conditions in Precompressed Liquids*

It is not difficult to repeat the calculations of Section III (b), starting not from pressures near zero but from quite high pressures. We have made a few calculations of this kind in order to determine the effects of precompression on

the final shock conditions in LJD fluids. In particular, we have estimated the shock properties of precompressed argon in contact with 60/40 RDX/TNT (cf. Section III (f)).

#### IV. RESULTS AND DISCUSSION

##### (a) The Properties of Plane Shock Waves in Classical LJD Liquids

Figure 1 illustrates the results of some of our calculations of Hugoniot curves for classical LJD liquids. It will be seen that the pressure rises much more rapidly with decreasing volume than it does under isothermal or adiabatic conditions. This is a reflection of the fact that a shock wave always increases the entropy of the material through which it is travelling (Hirschfelder, Curtiss, and Bird 1954, p. 789) and so raises its temperature above the value that would be reached in adiabatic (isentropic) compression over the same volume interval.

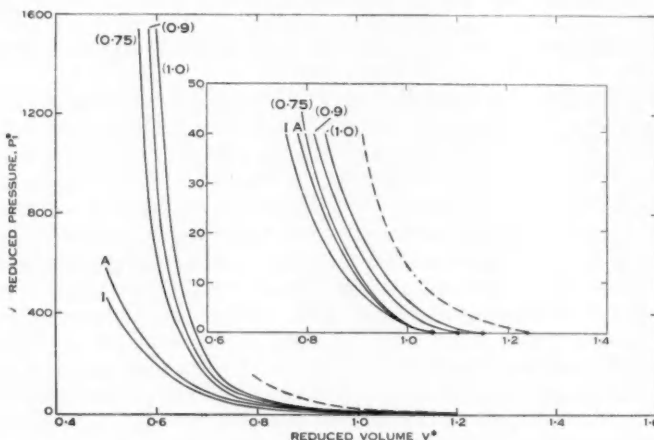


Fig. 1.—Calculated shock Hugoniot curves for LJD fluids. The compressions start at  $P^*=0$  and at values of  $T^*$  indicated by the numbers in brackets. The curves labelled *I* and *A* are the isotherm and adiabat based on the starting point  $P^*=0$ ,  $T^*=0.75$ . The dotted curve is the Hugoniot for a quantal liquid ( $\Lambda^*=1$ ) starting from  $P^*=0$ ,  $T^*=0.75$ .

Table 1 lists some of the thermodynamic properties of an LJD liquid along the Hugoniot based on the starting point  $P^*=0$ ,  $T^*=0.75$ .

Several points emerge from these results. First, the relationship between the increase in temperature and the shock pressure is accurately described by the simple formula

$$T_1^* - T^* = 0.0198(P_1^*)^{1.21}, \quad (13)$$

which is close to being a linear function. In this connection it is significant that Rice and Walsh (1957) concluded from explosive shock experiments on water that the temperature was "almost linear in pressure". For an ideal gas it would be exactly linear, in the limit of very strong shocks.

TABLE I

THERMODYNAMIC PROPERTIES OF A CLASSICAL LJD FLUID UNDER SHOCK COMPRESSION, STARTING FROM THE LIQUID STATE AT  $P^*=0$ ,  $T^*=0.75$ ,  $V^*=1.0503$

The symbols are defined in Section II

Pressure	$P_1^*$	0	3.007	22.32	123.7	371	1546
Volume	$V_1^*$	1.0503 ( $= V^*$ )	0.9899	0.8485	0.7071	0.6364	0.5657
Temperature	$T_1^*$	0.750	0.881†	1.605	7.202	26.31	144.9
Energy	$E_1^*$	-6.063	-5.972	-3.811	+15.16	+70.5	+368
Specific heat	$(C_V)_1$	2.577	2.653	2.710	2.724	2.499	2.248
Entropy	$S_1^* \ddagger$	0	0.00	0.50	3.35	5.95	9.33
Shock velocity	$U_1^*$	6.47	7.41	11.04	19.94	31.44	59.3
Flow velocity	$w_1^*$	0	0.426	2.122	6.51	12.39	27.4
Velocity of sound	$u_1^*$	6.47	8.73	11.71	21.8	29.7	58.3

† All the temperatures to the right of this point are above the critical temperature for the liquid state ( $T_c^*=1.3$ ).

‡ The listed values are relative to those at the starting point.

Secondly, there is a nearly linear relationship between the flow velocity and the shock velocity. This agrees with McQueen and Marsh's (1960) conclusions from measurements of these velocities in explosively shocked metals, and with Rice and Walsh's (1957) data for water.† The relationship would be exactly linear for very strong shock waves in a perfect gas.

Thirdly, the speed of sound  $u$  always exceeds the flow velocity  $w$ , which means that the flow is subsonic over the range of compressions considered. On the other hand, although the speed of sound is slightly greater than the shock velocity  $U$  at low pressures, it becomes less than  $U$  at high pressures. This is exactly the behaviour which Rice and Walsh (1957) have found in experiments on water and which McQueen and Marsh (1960) have observed in some shocked metals. In an ideal gas  $u$  may be either less or greater than  $w$ , and it is always less than  $U$ .

It seems from these comparisons that the LJD theory gives at least a qualitative description of the properties of shock waves in condensed materials. It is more difficult to test the theory quantitatively because of the paucity of good experimental data for liquids simple enough to conform to the LJD model. The theory assumes that the molecules of the material are non-polar and effectively spherical, and it is thus most appropriate to the condensed inert gases. Of these, only argon has been studied under shock conditions. Dapoigny, Kieffer, and Vodar (1955) have made a few X-ray determinations of the density of argon at shock pressures up to 72 000 atm. There are reasons for believing that their results may be suspect (Rice, McQueen, and Walsh 1958, p. 28) but in the absence of any other data it is worthwhile to compare them with the corresponding

† A plot of  $U$  against  $w$  from Rice and Walsh's data actually shows two straight lines, joined at about 120 000 atm. Altshuler, Bakanov, and Trunin (1958) believe that the discontinuity arises from the partial freezing of water at that pressure.

theoretical LJD Hugoniot curve. This comparison is made in Figure 2, where it will be seen that the agreement between the LJD curve and the experiments is not remarkably good: the LJD model consistently underestimates the specific volume. However, we should emphasize that our entire calculations involve only one experimental quantity, the second virial coefficient of gaseous argon used to derive the molecular units listed in Section II. The comparison in Figure 2 is therefore a very severe test of a long chain of reasoning linking the

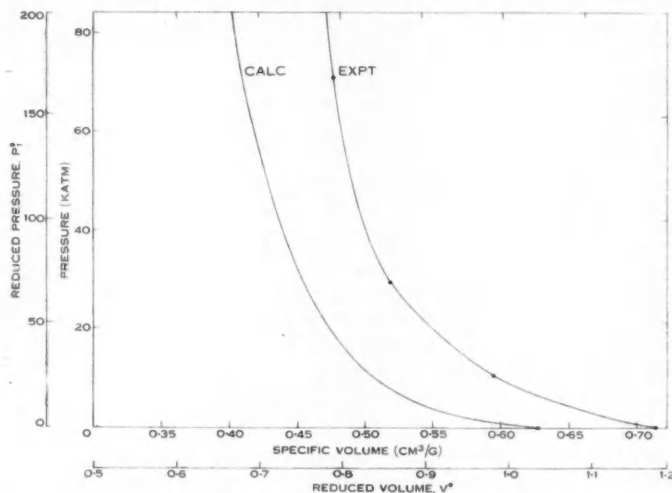


Fig. 2.—A comparison of the calculated LJD Hugoniot curve for liquid argon, initially at 1 atm and  $87.2^{\circ}\text{K}$  ( $P^* \approx 0$ ,  $T^* = 0.727$ ), with the experimental points of Dapoigny, Kieffer, and Vodar (1955). The calculated (LJD) temperature at the highest experimental point is  $1230^{\circ}\text{K}$ .

properties of a highly compressed state with those of a dilute gas. We could undoubtedly improve the agreement by incorporating the experimental volume of liquid argon at  $P \approx 0$ , as was done by Fickett and Wood (1960). But this would be unrealistic, since at that volume the LJD theory predicts a metastable state with a negative pressure of about  $P^* = -1.7$ . A more justifiable procedure is to calculate the ratio  $\hat{V}_1/\hat{V}$  of the volume of the shocked fluid to that of the original liquid. If we do this we find that the LJD values of the ratio are very close to the experimental ones.

#### (b) The Behaviour of a "Quantal" LJD Liquid

The dotted curve in Figure 1 describes the Hugoniot compression of a quantal liquid ( $\Lambda^* = 1$ ) calculated by the method outlined in Section III (c). It is displaced to volumes larger than those of the classical liquids.

Table 2 lists some thermodynamic properties of the fluid along the Hugoniot curve. Comparing these data with those in Table 1, we find that at any particular

pressure the temperature of the quantal fluid is greater than that of the classical fluid. On the other hand its relative volume  $V_1^*/V^*$  is always less, indicating that the compression " squeezes out " some of the quantal inflation of the volume. Unfortunately there are no experimental data to test these conclusions. Some measurements on, say, helium, neon, and argon would be highly desirable.

TABLE 2

THERMODYNAMIC PROPERTIES OF A QUANTAL LJD FLUID ( $\Lambda^*=1$ ) UNDER SHOCK COMPRESSION, STARTING FROM  $P^*=0$ ,  $T^*=0\cdot75$ ,  $V^*=1\cdot245$

The symbols are defined in Section II

Pressure	$P_1^*$	0	2.964	7.023	15.12
Volume	$V_1^*$	1.245 (= $V^*$ )	1.1314	1.0607	0.9899
Temperature	$T_1^*$	0.75	0.979	1.221	1.671
Energy	$E_1^*$	-4.115	-3.946	-3.468	-2.185
Specific heat	$(C_V)_1$	2.480	2.589	2.650	2.689
Shock velocity	$U_1^*$	4.58	6.36	7.68	9.58
Flow velocity	$w_1^*$	0	0.581	1.138	1.964
Velocity of sound	$u_1^*$	4.58	6.85	8.26	11.51

(c) *Conditions after Adiabatic Expansion from a Shocked State*

Section III (d) described a method for arriving at conditions during the adiabatic expansion of a shock-compressed material. Our results for LJD fluids are shown as dotted curves in a  $P^*/V^*$  plot in Figure 3 and in a  $P^*/w^*$  plot in Figure 4. We have worked out a number of thermodynamic properties along the adiabats but there is no need to give the results here. It is sufficient to point out that the adiabats in Figure 3 intersect the zero-pressure line at considerably larger volumes and at higher temperatures than those at which the shock compression began. The highest adiabat only approaches the line at very large volumes, indicating that the liquid is partially vaporized in the final state.

In Figure 4 the adiabats are represented by the right-hand sections of the dotted curves crossing the original Hugoniot. It will be seen that the adiabatic expansion of a shocked fluid from  $P_1^*=123.7$  to  $P_2^*=0$  increases the flow velocity from  $w_1^*=6.51$  to  $w_1^*+w_2^*=13.69$ .

Of course expansion into a vacuum ( $P_2^*=0$ ) seldom occurs in practice: in most experimental work the shocked material expands into the surrounding air. We can determine the surface conditions here by the method outlined in the last paragraph of Section III (d). If we suppose that the LJD liquid is argon and assume that it is (hypothetically) thermally insulated from air at 25 °C and 1 atm, we find that the conditions of the argon at the starting point in Figure 4 are  $P \approx 1$  atm,  $\hat{V} = 0.633$  cm<sup>3</sup>/g,  $T = 90$  °K and in the shocked state at the point A are  $P_1 = 51\,000$  atm,  $\hat{V}_1 = 0.425$  cm<sup>3</sup>/g,  $T_1 = 860$  °K,  $w_1 = 1029$  m/sec. The final conditions, given by the point of intersection of the expansion adiabat with the compression Hugoniot for air are  $P_2 = 69$  atm,  $\hat{V}_2 = 0.926$  cm<sup>3</sup>/g,  $T_2 = 144$  °K,

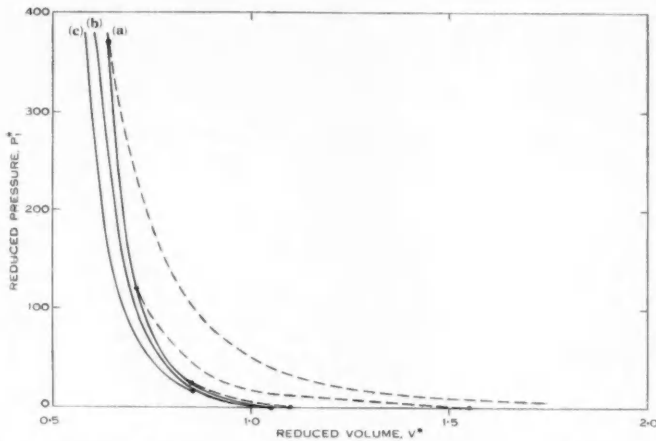


Fig. 3.—Hugoniot curves for normal and precompressed LJD liquids starting from  $T^*=0.75$ . The starting pressures are (a)  $P^*=0$ ; (b)  $P^*=2.041$ ; (c)  $P^*=15.15$ . The dotted curves are those for adiabatic expansion from shocked states on the Hugoniot curve (a).

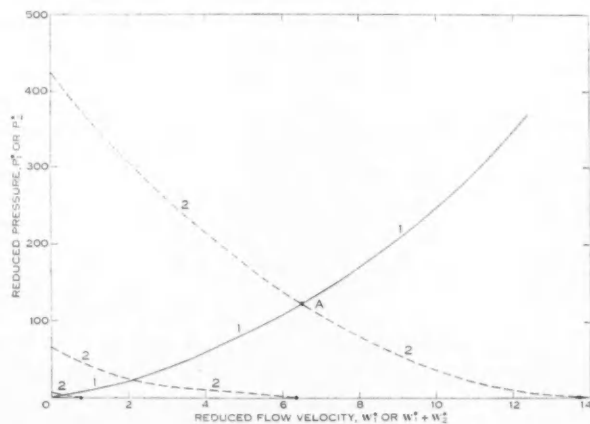


Fig. 4.—A pressure/flow-velocity diagram illustrating the interaction of forward-going shock waves 1 with backward-going shocks or rarefactions 2. The primary shocks 1 are based on the starting point  $P^*=0$ ,  $T^*=0.75$ .

$w_1 + w_2 = 2160$  m/sec. In this example the final pressure is sufficiently high to prevent the argon from boiling at the interface. The final flow velocity (that is, the "free" surface velocity) is slightly more than twice  $w_1$ , in agreement with some experimental results for water (Rice and Walsh 1957). It would be exactly  $2w_1$  in the limit of very weak shocks.

(d) *Conditions at the Head-on Collision of Two Plane Shock Waves*

The left-hand sections of the dotted curves in Figure 4 trace the changes in pressure and flow velocity which occur when secondary shock waves are driven back into the original shock. They were calculated by the method described in Section III (e). It is particularly interesting to consider the conditions which exist after the collision of two equal shocks (which is equivalent to the total reflection of a single shock). Such a collision reduces the absolute flow velocity  $w_1 + w_2$  to zero, and the final state is therefore given by the point of intersection of the secondary Hugoniot curve with the pressure axis in Figure 4. The conditions corresponding to three values of the primary shock pressure are given in Table 3.

TABLE 3  
CONDITIONS BEFORE AND AFTER THE HEAD-ON COLLISION OF TWO PLANE SHOCK WAVES  
Unshocked conditions :  $P^* = 0$ ,  $V^* = 1.0503$ ,  $T^* = 0.75$

Before Collision			After Collision		
Pressure $P_1^*$	Temperature $T_1^*$	Compression $V^*/V_1^*$	Pressure $P_2^*$	Temperature $T_2^*$	Compression $V^*/V_2^*$
3.007	0.881	1.061	7.0	0.99	1.115
22.32	1.605	1.238	63.0	2.40	1.431
123.7	7.202	1.485	424	14.88	1.849

It is known that the total reflection of weak (sound) waves doubles the wave pressure at the boundary. But in shock waves the pressure ratio is always greater than this, and in an ideal monatomic gas it approaches the limiting value of 6 in very strong shocks. The LJD results in Table 3 show a similar increase from the low pressure ratio of 2 to a ratio of 3.4 in the strongest shock considered.

It should be noted that the temperature in the doubly-shocked material is considerably lower than it would have been had the liquid been compressed to the same total pressure by a *single* shock wave (cf. Table 1).† This effect could be exploited experimentally as a means of varying the temperature independently of the pressure, which it is impossible to do in a single shock compression from a given starting point.

† The reason for this is that step-wise compression is closer to being adiabatic than is single shock compression. In fact, true adiabatic compression could be imagined to occur by the superposition of an infinite number of infinitesimal shocks.

(e) Shock Conditions for Liquid Argon in Contact with the Explosive 60/40 RDX/TNT

By the method outlined in Section III (f) we have estimated that the explosion of a charge of 60/40 RDX/TNT ("Composition B") in contact with argon at 90 °K ( $T^*=0.75$ ) and at atmospheric pressure ( $P^*\approx 0$ ) would launch a shock wave in which the pressure would be 236 000 atm and temperature 5240 °K. These are the conditions at the point of intersection of the Hugoniot curve (a) in Figure 5 with the shock and rarefaction loci for the products of explosion.

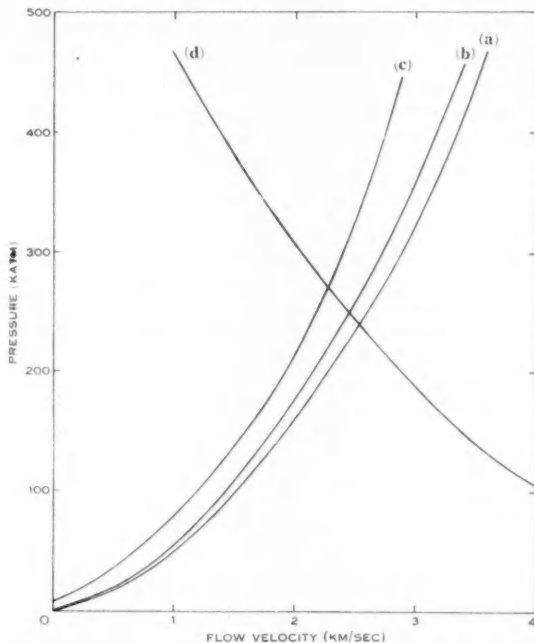


Fig. 5.—A pressure/flow-velocity diagram showing the effects of precompression on the initial shock pressure of liquid argon in contact with the explosive 60/40 RDX/TNT. The curves (a), (b), and (c) are Hugoniot curves based on the starting pressures  $P \approx 1$  atm,  $P = 850$  atm,  $P = 6300$  atm, respectively, and the starting temperature 90 °K. The curve (d) is the locus of reflected shocks and rarefactions in the explosive products (Deal 1958).

(f) Shock Conditions in Precompressed Liquids

We have calculated Hugoniot curves from two finite starting pressures on the isotherm for  $T^*=0.75$ . The results are listed in Table 4 and plotted in Figure 3. At a given volume the pressure and temperature are always less than for the uncompressed liquid, and at a given pressure the volume and temperature are also less. Precompression therefore provides an additional means of varying

TABLE 4

CALCULATED HUGONIOT COMPRESSIONS FOR NORMAL AND PRECOMPRESSED LJD LIQUIDS, STARTING FROM  $T^* = 0.75$

The symbols are defined in Section II

Starting Pressure	$V_1^*$ :	1.0503	0.9899	0.8485	0.7071	0.6364	0.5657
$P^* = 0$	$P_1^*$	0	3.007	22.32	123.7	371	1546
	$T_1^*$	0.750	0.881	1.605	7.202	26.31	144.9
	$U_1^*$	6.47	7.41	11.04	19.94	31.44	59.3
	$w_1$	0	0.426	2.122	6.51	12.39	27.4
$P^* = 2.042$	$P_1^*$		2.042	19.30	101.0	267	964
	$T_1^*$		0.750	1.238	4.57	14.75	72.0
	$U_1^*$		7.64	10.93	18.25	27.1	49.5
	$w_1$		0	1.562	5.29	9.68	20.2
$P^* = 15.15$	$P_1^*$			15.15	72.8	167	446
	$T_1^*$			0.750	1.594	4.07	16.20
	$U_1^*$			N.D.	17.13	22.7	34.3
	$w_1$			0	2.855	5.67	11.42

the shock temperature independently of the pressure (cf. Section IV (d)). In practice the experiments would be difficult, although not impossible. We have considered it worthwhile to attempt to predict the effects of precompression on the properties of shock waves generated in argon by the explosion of a charge of 60/40 RDX/TNT. Because the behaviour of this explosive is known only under normal conditions, we are forced to consider a hypothetical experiment in which the explosive remains at normal temperature and pressure although it is in

TABLE 5

CALCULATED PROPERTIES OF SHOCK WAVES IN PRECOMPRESSED ARGON IN CONTACT WITH 60/40 RDX/TNT

Initial temperature : 90 °K

Initial Conditions			Shock Conditions		
Pressure, $P$ (atm)	Volume, $\hat{V}$ (cm³/g)	Temperature, $T$ (°K)	Pressure, $P_1$ (atm)	Volume, $\hat{V}_1$ (cm³/g)	Temperature, $T_1$ (°K)
0	0.633	90	236 000	0.368	5240
850†	0.597	90	247 000	0.356	4150
6300†	0.512	90	270 000	0.331	3300

† Argon is actually solid at these pressures at 90 °K (Robinson 1954). But the results are still significant because the LJD model is a good one for solids (Barker 1961b).

contact with cold argon at a high pressure. However, our calculations should have some bearing on more realistic experiments.

The curves (b) and (c) in Figure 5 are the  $P/w$  relations for argon, precompressed to 850 and 6500 atm, respectively, at 90 °K. Their points of intersection with the  $P/w$  curve for the explosive products correspond to the conditions listed in Table 5. It will be seen that the precompression has a much greater effect on the shock temperature than on the pressure and volume. It could be a useful way of altering experimental shock conditions and so obtaining more extensive information about the equations of state of real substances.

#### V. CONCLUSIONS

We regard the results of these calculations as being qualitatively correct. But it is too soon to judge how well they describe the quantitative properties of shock waves in real materials. Perhaps the main value of the calculations lies in the fact that they have enabled us to predict some effects which have not been studied experimentally, and which could be useful in extending the scope of shock-wave techniques.

#### VI. REFERENCES

- ALTSHULER, L. V., BAKANOV, A. A., and TRUNIN, R. F. (1958).—*Dokl. Akad. Nauk.* **121**: 67.
- BARKER, J. A. (1960).—*Aust. J. Chem.* **13**: 187.
- BARKER, J. A. (1961a).—*Proc. Roy. Soc. A* **259**: 442.
- BARKER, J. A. (1961b).—“Lattice Theories of the Liquid State.” (Pergamon Press: London.) (in press).
- BOER, J. DE (1948).—*Physica 'sGrav.* **14**: 139.
- DAPOIGNY, J., KIEFFER, J., and VODAR, B. (1955).—*J. Rech.* **31**: 260.
- DAVID, H. G., and HAMANN, S. D. (1953).—*Trans. Faraday Soc.* **49**: 711.
- DAVID, H. G., and HAMANN, S. D. (1961).—*Aust. J. Chem.* **14**: 1.
- DEAL, W. E. (1958).—*Phys. Fluids* **1**: 523.
- FICKETT, W., and WOOD, W. W. (1960).—*Phys. Fluids* **3**: 204.
- HAMANN, S. D. (1952).—*Trans. Faraday Soc.* **48**: 303.
- HAMANN, S. D. (1957).—*Aust. J. Chem.* **10**: 373.
- HAMANN, S. D. (1960a).—*Rev. Pure Appl. Chem.* **10**: 139.
- HAMANN, S. D. (1960b).—*Aust. J. Chem.* **13**: 325.
- HIRSCHFELDER, J. O., CURTISS, C. F., and BIRD, R. B. (1954).—“Molecular Theory of Gases and Liquids.” (John Wiley & Sons: New York.)
- HUGONIOT, H. (1887).—*J. Éc. polyt. Paris* **57**: 1.
- HUGONIOT, H. (1889).—*J. Éc. polyt. Paris* **58**: 1.
- LENNARD-JONES, J. E., and DEVONSHIRE, A. F. (1937).—*Proc. Roy. Soc. A* **163**: 53.
- MCQUEEN, R. G., and MARSH, S. P. (1960).—*J. Appl. Phys.* **31**: 1253.
- RANKINE, W. J. M. (1870).—*Phil. Trans.* **160**: 277.
- RICE, M. H., MCQUEEN, R. G., and WALSH, J. M. (1958).—“Solid State Physics.” Vol. 6. (Academic Press Inc.: New York.)
- RICE, M. H., and WALSH, J. M. (1957).—*J. Chem. Phys.* **26**: 824.
- ROBINSON, D. W. (1954).—*Proc. Roy. Soc. A* **225**: 393.
- STOKES, G. G. (1848).—*Phil. Mag. (Ser. 3)* **33**: 349.
- TAIT, P. G. (1900).—“Scientific Papers.” Vol. 2. Nos. 61 and 107. (Cambridge Univ. Press.)
- WENTORF, R. H., BUEHLER, R. J., HIRSCHFELDER, J. O., and CURTISS, C. F. (1950).—*J. Chem. Phys.* **18**: 1484.

## HEATS OF MIXING

### IV. SYSTEMS OF n-ALCOHOLS WITH BENZENE AT 25, 35, AND 45 °C

By I. BROWN\* and W. FOCK\*

[Manuscript received February 17, 1961]

#### Summary

A new apparatus has been made for the precise measurement of heats of mixing of liquids. With this apparatus measurements can be made in the absence of air, vapour, or mercury for systems which have volume changes on mixing of up to 1 ml per mol of mixture.

The apparatus has been used to measure the heats of mixing of ethanol, 1-propanol, and 1-butanol with benzene at 45 °C for comparison with previous measurements. New measurements have also been made over the concentration range for heats of mixing of ethanol, 1-propanol, and 1-butanol with benzene at 25 and 35 °C and for methanol, 1-hexanol, and 1-octanol with benzene and ethanol with toluene at 35 °C.

For these systems the heat of mixing per mol of mixture has a maximum at a mole fraction of alcohol from 0·30 to 0·35. The results show that the heats of mixing at a mole fraction of alcohol of 0·30 increase linearly with increase in temperature and at a given temperature they increase with the molecular weight of the alcohol but at a lower rate for the higher alcohols.

#### I. INTRODUCTION

A new cell has been designed to eliminate various undesirable features of the cell used previously (Brown and Fock 1955). This had one basic defect in design ; the heater was on the outside of the cell and the temperature measuring device was on the inside. This has been found to lead to errors in the measured values of heats of mixing due to uncertainty in the amount of heat exchange between the cell with its contents and the surroundings, particularly when appreciable changes in temperature occur during heating and mixing. It was also difficult to fill with the correct amount of liquid and the use of mercury as the separating medium was undesirable due to its possible catalytic effect on some mixtures and appreciable heat capacity.

The optimum design of such cells has been discussed in detail by McGlashan (1961), who showed that the ideal design is one in which there are no air or vapour spaces and no pressure changes due to volume changes on mixing.

In the design of a cell in which vapour or air spaces are not permissible it is necessary to allow for expansion of the liquids on heating from room temperature to the temperature of operation and for expansion due to changes in volume on mixing. In the new cell described below, thin corrugated diaphragms are used to reconcile these changes in volume with the minimum pressure change.

\* Division of Physical Chemistry, C.S.I.R.O. Chemical Research Laboratories, Melbourne.

## II. APPARATUS

The cell, which has a total capacity of 30 ml, is shown diagrammatically in Figure 1. The brass body is in two parts *A* and *B* bolted together with six small bolts. The liquids in the two parts of the cell are separated by a 0.0005 in. brass diaphragm *C* held in place between two machined Teflon gaskets *D*. Side *A* contains a manganin heater *E* wound on a Teflon cylinder with leads soldered to glass-metal seals *F* fixed to the walls. The side *B* contains a strong coiled spring *G* held in compression by the catch *H* engaged on pin *I* which is triggered off by an external electromagnet that attracts the iron trigger *J*.

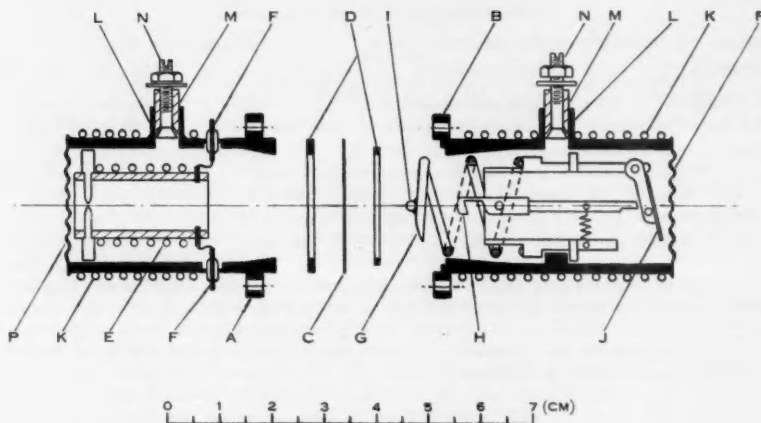


Fig. 1.—Heat of mixing cell.

A nickel resistance thermometer *K* of  $140\ \Omega$  of 0.002 in. diameter wire is wound on both parts of the cell and insulated by a thin film of Araldite. Leads from the thermometer are connected to a Wheatstone bridge which automatically records the resistance-time curve. This recorder has a range of  $150\ \Omega$  and a span of  $1.00\ \Omega$ . An electrically driven decade box automatically changes the range as the pen reaches the top or bottom of the scale.

Each side has a filling opening *L* closed by a Teflon plug *M* which is expanded by a conical stainless steel bolt *N*. The assembled cell is mounted on a Polythene carriage in the vacuum box described previously by Brown and Fock (1955) and mixing is done by rocking the whole cell which contains a stainless-steel ball to help mixing.

The ends of the cell are corrugated diaphragms made from 0.003 in. beryllium-copper to allow for the expansion of the liquids on heating the cell to thermostat temperature and the volume change on mixing.

A microscope cover glass was also tried as the dividing diaphragm, but this required a modified breaking device and softer gaskets of Neoprene which adsorb some of the components used. The use of flexible metal bellows to allow

for expansion leads to incomplete mixing in the convolutions and prevents the removal of trapped air bubbles on "filling."

It was found that these diaphragms could be used repeatedly if the total volume change due to expansion on mixing and expansion on heating from the charging temperature of 20 °C to the operating temperature was less than 0.5 ml. The life of the diaphragms was limited when the mixing was carried out at 45 °C due to the volume change of about 1 ml on heating to the higher working temperature.

For the systems studied here, the heats of mixing were high and the error due to leaving an air space of 0.5 ml in each side of the cell was only about 0.1%. Measurements at 25 °C were done with the cell completely filled but those at 35 and 45 °C were made with an air space adjusted to give 0.5 ml on each side of the cell at thermostat temperature.

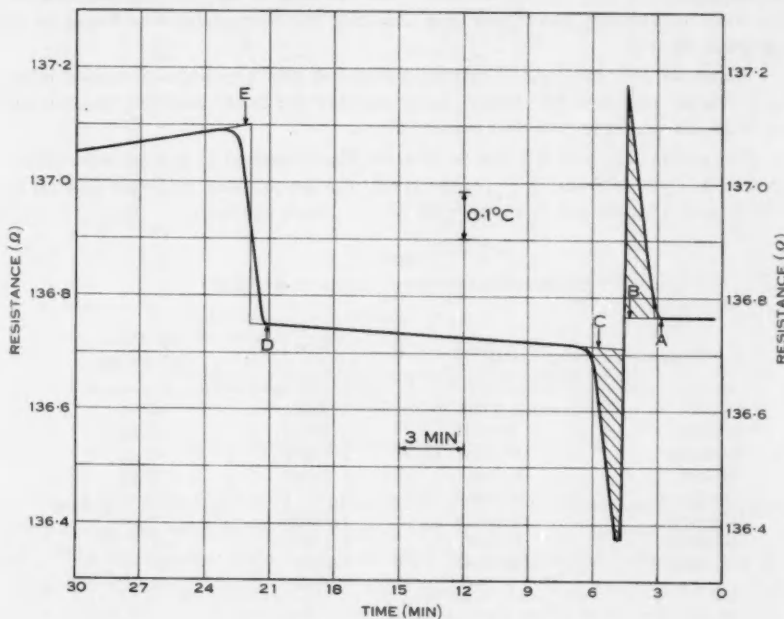


Fig. 2.—Typical resistance-time curve.

### III. EXPERIMENTAL PROCEDURE

The spring was cocked and the cell assembled with its brass diaphragm, each side was completely filled, and the closed cell weighed to  $\pm 1$  mg after each filling. The electrical leads were soldered on and the cell mounted in the carriage in the vacuum box. After evacuation the cell was left overnight to reach thermostat temperature.

Mixtures with a mole fraction of alcohol  $x_1$  from about 0·4 to 0·6 were obtained by mixing pure liquids, mixtures of higher or lower mole fraction were made with one side of the cell filled with a mixture whose heat of mixing was known from a previous run.

The measured heating of the cell was done at the same time as the mixing as described previously by Brown and Fock (1956). A typical recorder chart is reproduced in Figure 2. During the measured heating period *A* to *C* an amount of electrical energy approximately equal to the heat of mixing was dissipated in the heater. Mixing was made at time *B* chosen to make the shaded areas under the curve approximately equal. The second heating period from *D* to *E* provided a calibration for inexact compensation of the heat of mixing. Electrical energy measurements followed Brown and Fock's (1955) method. The changes in resistance recorded on the chart were proportional to the change in temperature of the resistance winding for the small range of temperature used. The heat of releasing the spring and breaking the diaphragm was found to be negligible (0·2 j).

Values of  $H^M$ , the heat of mixing per mol of mixture, were calculated using the methods described by Ruiter (1955) to allow for heat exchange between the cell with its contents and the surroundings.

The errors in  $x_1$  and  $H^M$  due to errors in the measured quantities were calculated to be  $\pm 0\cdot0008$  and 0·8% respectively for the primary mixtures and up to 0·0018 and 2% for mixtures of high or low mole fraction.

TABLE I  
THE PHYSICAL PROPERTIES OF THE COMPONENTS

Compound	$d_4^{25\text{-}00}$	$n_D^{25\text{-}00}$	Boiling Point (°C/760 mmHg)
Benzene . . .	0·87365	1·49801	80·07
Toluene . . .	0·86224	1·49406	110·60
Methanol . . .	0·78683	1·32662	64·54
Ethanol . . .	0·78511	1·35926	78·29
1-Propanol . . .	0·79959	1·38314	97·08
1-Butanol . . .	0·80578	1·39731	117·52
1-Hexanol . . .	0·81531	1·41607	157·5
1-Octanol . . .	0·82247	1·42741	195·2

#### IV. PURIFICATION AND PHYSICAL PROPERTIES OF COMPONENTS

Benzene, 1-propanol, and 1-butanol were purified by the methods of Brown and Smith (1959), ethanol by the method of Barker, Brown, and Smith (1953), and toluene by that of Brown, Fock, and Smith (1956). Methanol was distilled from sulphuric acid, fractionally distilled and dried over magnesium. 1-Hexanol and 1-octanol were fractionally distilled and the fractions showing a single peak on a gas chromatogram were used. The physical properties of the components are given in Table 1.

## V. RESULTS

First, new measurements were made of the heats of mixing of ethanol, 1-propanol, and 1-butanol with benzene at 45 °C to test the performance of the cell and for comparison with those from the former cell. These results are presented in Tables 2(c), 3(c), and 4(c).

The present values obtained for ethanol + benzene are compared in Figure 3 with the recent results of Williamson and Scott (1960) measured at 45·0 °C in an apparatus similar to that described by Adcock and McGlashan (1954). The comparison is made between values of  $H^M/x_1x_2$ , where  $H^M$  is the heat of mixing in absolute joules per mole of mixture,  $x_1$  is the mole fraction of ethanol, and  $x_2$  that of benzene. The agreement is excellent.

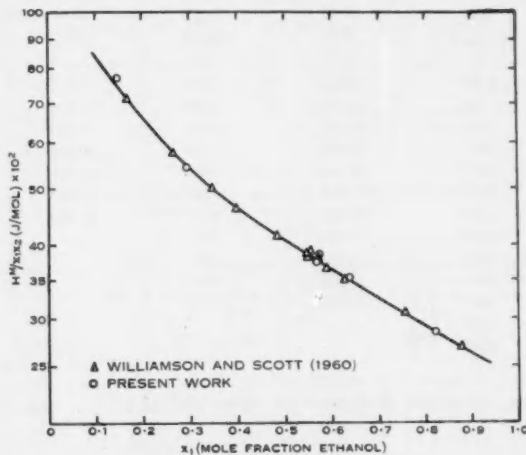


Fig. 3.—Heats of mixing ethanol + benzene 45·0 °C.

The heat of mixing data for this system at 45 °C obtained using Brown and Fock's (1955) cell were found to be about 13% higher than the new values given here. The old values were measured with the temperature changes due to mixing and measured heating taking place separately. This led to errors in the extrapolation of the temperature-time curves as well as those inherent in having an external heater and an internal temperature measuring device.

All subsequent measurements using the former cell (Brown and Fock 1956, 1957; Brown, Fock, and Smith 1956) were made with the mixing and heating done simultaneously to minimize temperature changes in the cell. The data obtained with this cell in 1957 for the systems 1-propanol + benzene and 1-butanol + benzene at 45 °C are approximately 2% and 1% respectively higher than the new values given in Tables 3 (c) and 4 (c). From these comparisons and those made with new measurements on other systems it appears that the measure-

ments made with the 1955 cell with simultaneous heating and mixing are in agreement with values measured in the new cell for  $H^M$  below about 1000 j/mol and are about 2% high for values of  $H^M$  from about 1300 to 1400 j/mol.

Measurements were then made of a number of n-alcohol + benzene systems at 25 and 35 °C; the results are shown in Tables 2 to 5.

TABLE 2  
HEATS OF MIXING ETHANOL + BENZENE

(a) 25·0 °C		(b) 35·0 °C		(c) 45·0 °C	
$x_1$	$H^M$ (j/mol)	$x_1$	$H^M$ (j/mol)	$x_1$	$H^M$ (j/mol)
0·057	510*	0·162	905*	0·146	970
0·130	715*	0·164	880*	0·294	1130
0·130	725*	0·297	1005	0·567	925
0·269	845*	0·335	1005*	0·569	930
0·278	855*	0·343	995*	0·571	945
0·335	870	0·552	820*	0·637	815
0·541	710*	0·552	810*	0·822	420
0·560	690*	0·571	800		
0·596	635	0·636	705		
0·609	630	0·649	680*		
0·658	555*	0·859	295*		
0·660	540*				
0·865	220*				

\* These measurements were made with the former cell.

TABLE 3  
HEATS OF MIXING 1-PROPANOL + BENZENE

(a) 25·0 °C		(b) 35·0 °C		(c) 45·0 °C	
$x_1$	$H^M$ (j/mol)	$x_1$	$H^M$ (j/mol)	$x_1$	$H^M$ (j/mol)
0·141	855	0·249	1145	0·326	1330
0·278	1035	0·250	1145	0·510	1205
0·289	1040	0·321	1180	0·585	1090
0·538	900	0·322	1175		
0·548	885	0·511	1070		
0·785	450	0·512	1060		
		0·575	955		
		0·577	955		
		0·783	540		

TABLE 4  
HEATS OF MIXING 1-BUTANOL+BENZENE

(a) 25·0 °C		(b) 35·0 °C		(c) 45·0 °C	
$x_1$	$H^M$ (j/mol)	$x_1$	$H^M$ (j/mol)	$x_1$	$H^M$ (j/mol)
0·118	830	0·213	1160	0·213	1270
0·239	1070	0·280	1245	0·243	1310
0·251	1090	0·453	1220	0·459	1350
0·487	1050	0·460	1215	0·461	1340
0·487	1030	0·488	1195	0·483	1340
0·496	1035	0·498	1180		
0·500	1035	0·526	1140		
0·740	600	0·528	1130		
		0·706	745		
		0·777	605		

TABLE 5  
HEATS OF MIXING OF ALCOHOL SYSTEMS AT 35·0 °C

(a) Methanol+Benzene		(b) 1-Hexanol+Benzene		(c) 1-Octanol+Benzene		(d) Ethanol+Toluene	
$x_1$	$H^M$ (j/mol)	$x_1$	$H^M$ (j/mol)	$x_1$	$H^M$ (j/mol)	$x_1$	$H^M$ (j/mol)
0·381	800	0·089	835	0·158	1155	0·204	925
0·658	545	0·187	1150	0·353	1370	0·337	975
0·659	545	0·187	1145	0·356	1370	0·370	970
		0·410	1285			0·388	955
		0·422	1285			0·614	715
		0·688	855			0·614	720
						0·641	680
						0·654	650
						0·674	625

## VI. DISCUSSION

The variation of the heats of mixing with temperature for mixtures of normal alcohols with benzene is shown in Figure 4 and the variation of  $H^M$  with the size of the alcohol molecule is shown in Figure 5. The values shown in these figures are for mixtures containing 0·30 mole fraction of alcohol and were estimated from the experimental data by interpolation on plots of  $H^M/x_1x_2$  against  $x_1$ . It can be seen that the variation is linear with temperature. Our data for the methanol and ethanol systems are in excellent agreement with those of Williamson and Scott (1960). Figure 4 enables a comparison to be made between present data and published data measured at other temperatures.

For the system methanol + benzene the data at 25 °C of Thacker and Rowlinson (1954) are in good agreement with our data. The values of Tsao and Smith (1957) at 25 °C, Scatchard *et al.* (1952) at 20 °C, and Schmidt (1926) at 15 °C are slightly higher. The data of Pahlke (1935) at 20 °C are about 13% higher, and those of Williams, Rosenberg, and Rothenberg (1948) at 25 °C and of Washburn and Lightbody (1930) at 23 °C are about 7% lower than our values.

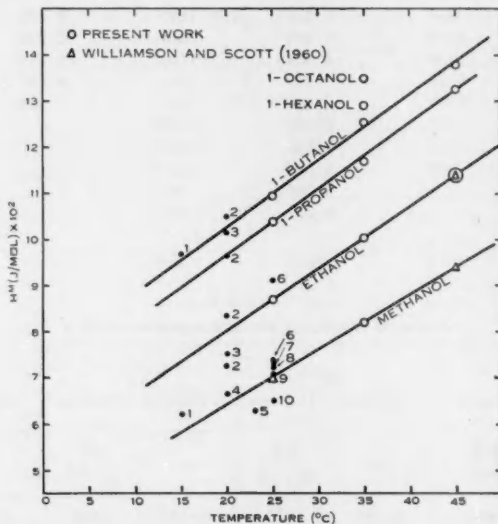


Fig. 4.—Heats of mixing of normal alcohols with benzene at  $x_1=0.30$ .  
 1, Schmidt (1926); 2, Pahlke (1935); 3, Perrakis (1925); 4, Scatchard *et al.* (1952); 5, Washburn and Lightbody (1930); 6, Schnaible, Van Ness, and Smith (1957); 7, Tsao and Smith (1953); 8, Murti and van Winkle (1958); 9, Thacker and Rowlinson (1954); 10, Williams, Rosenberg, and Rothenberg (1948).

For the system ethanol + benzene the values of Schnaible, Van Ness,\* and Smith (1953) at 25 °C and Pahlke (1935) at 20 °C are about 5% higher than our values and those of Perrakis (1925) at 20 °C about 6% lower. The data of Vialla (1914) at 20 °C and Winkelmann (1873) at 0, 5, and 15 °C are about 30% lower.

For the system 1-propanol + benzene the data of Pahlke (1935) at 20 °C are in agreement with our values, but the values of Schmidt (1926) at 15 °C are about 8% higher. For 1-butanol + benzene the values of Pahlke at 20 °C are slightly higher and those of Perrakis at 20 °C slightly lower than our data.

\* A recent personal communication has been received by the authors from Professor H. C. Van Ness, Rensselaer Polytechnic Institute, New York, giving heats of mixing data at 25, 35, and 45 °C for a number of the systems studied in this paper. His results are slightly higher but in substantial agreement with the present data.

The values of Chalela, Steinhauser, and Hougen (1957) for the system 1-pentanol + benzene at 20 °C appear to be appreciably low in comparison with our data on the other systems.

Values of heats of mixing for n-alcohol + benzene systems calculated from an extensive correlation of activity coefficients by Black (1959) give values which are about 6% higher than ours for methanol + benzene from 20 to 55 °C, but the values calculated at 55 °C for the systems containing ethanol to pentanol are too low by up to 50% and show a decrease with increase in molecular weight of the alcohol instead of an increase.

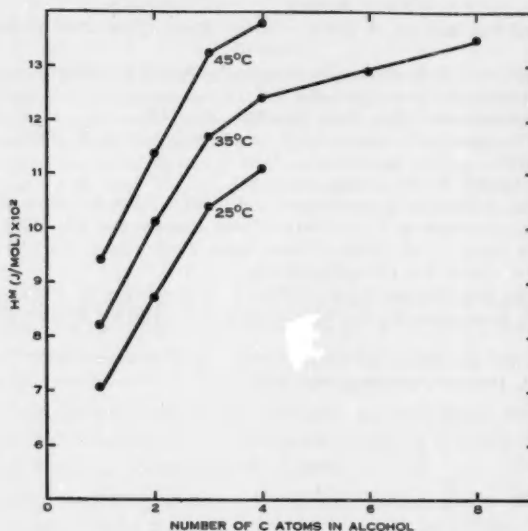


Fig. 5.—Heats of mixing of normal alcohols with benzene at  $x_1 = 0.30$ .

The data given here show the changes in the values of  $H^M$  of benzene solutions of normal alcohols with changes in temperature and size of the alcohol molecule more accurately than those given previously by Brown and Fock (1957). A more detailed study of the behaviour of benzene solutions of alcohols will be possible when values of the excess free energies, heats of mixing, and volume changes on mixing for systems containing branched alcohols become available. These measurements are in progress.

#### VII. ACKNOWLEDGMENTS

The authors wish to thank Professor R. L. Scott and Dr. A. G. Williamson for sending their data before publication and for their valuable discussions; also Professor H. C. Van Ness for his data.

## VIII. REFERENCES

ADCOCK, D. S., and McGlashan, M. L. (1954).—*Proc. Roy. Soc. A* **226** : 266.  
 BARKER, J. A., BROWN, I., and SMITH, F. (1953).—*Disc. Faraday Soc.* **15** : 142.  
 BLACK, C. (1959).—*Amer. Inst. Chem. Engng. J.* **5** : 249.  
 BROWN, I., and FOCK, W. (1955).—*Aust. J. Chem.* **8** : 361.  
 BROWN, I., and FOCK, W. (1956).—*Aust. J. Chem.* **9** : 180.  
 BROWN, I., and FOCK, W. (1957).—*Aust. J. Chem.* **10** : 417.  
 BROWN, I., FOCK, W., and SMITH, F. (1956).—*Aust. J. Chem.* **9** : 364.  
 BROWN, I., and SMITH, F. (1959).—*Aust. J. Chem.* **12** : 407.  
 CHALELA, D. A., STEINHAUSER, H. H., and HOUGEN, J. O. (1957).—*Industr. Engng. Chem. Chem. & Engng. Data Series* **2** : 66.  
 McGLASHAN, M. L. (1961).—“Experimental Thermochemistry.” Vol. 2. I.U.P.A.C. (Butterworths Scientific Publications : London.)  
 MURTI, P. S., and VAN WINKLE, M. (1958).—*Industr. Engng. Chem. Chem. & Engng. Data Series* **3** : 65.  
 PAHLKE, H. (1935).—“Landolt-Börnstein Tabellen.” (Springer : Berlin.)  
 PERRAKIS, N. (1925).—*J. Chim. Phys.* **22** : 296.  
 RUITER, L. H. (1955).—*Rec. Trav. chim. Pays-Bas.* **74** : 1131.  
 SCATCHARD, G., TICKNOR, L. B., GOATES, J. R., and McCARTNEY, E. R. (1952).—*J. Amer. Chem. Soc.* **74** : 3721.  
 SCHMIDT, G. C. (1926).—*Z. Phys. Chem.* **121** : 221.  
 SCHNAIBLE, H. W., VAN NESS, H. C., and SMITH, J. M. (1957).—*Amer. Inst. Chem. Engng. J.* **3** : 147.  
 THACKER, R., and ROWLINSON, J. S. (1954).—*Trans. Faraday Soc.* **50** : 1036.  
 TSAO, C. C., and SMITH, J. M. (1953).—*Chem. Engng. Progr. (Symp. Ser.)* **50** : 1036.  
 VIALLA, E. (1914).—*Bull. Soc. Chim. Fr.* **15** : 5.  
 WASHBURN, E. R., and LIGHTBODY, A. (1930).—*J. Phys. Chem.* **34** : 2701.  
 WILLIAMS, G. C., ROSENBERG, S., and ROTHENBERG, H. A. (1948).—*Industr. Engng. Chem.* **40** : 1273.  
 WILLIAMSON, A. G., and SCOTT, R. L. (1960).—*J. Phys. Chem.* **64** : 440.  
 WINKELMANN, A. (1873).—*Ann. Phys.* **30** : 592.

## SURFACE PROPERTIES OF LIQUID SODIUM AND SODIUM-POTASSIUM ALLOYS IN CONTACT WITH METAL OXIDE SURFACES

By D. H. BRADHURST\* and A. S. BUCHANAN\*

[Manuscript received February 15, 1961]

### Summary

Dissolved oxygen was shown to be surface active in liquid sodium from measurements of surface tension and of contact angle of the liquid on various oxide surfaces. When sufficient oxygen was present wetting of  $\text{UO}_3$  by liquid sodium could be brought about at temperatures above approximately 300 °C. Observations on the wetting of several solid oxides by sodium gave some support to the hypothesis that wetting was more effective on those oxides with larger cations. Sodium-potassium alloys showed non-wetting contact angles when relatively free of oxygen but wetting occurred when the oxygen content of the liquid was increased.

### I. INTRODUCTION

The ability of a liquid metal to wet an oxide surface has recently become of interest in nuclear reactor technology, where the production of a stable suspension of nuclear fuel uranium dioxide in a medium of high thermal conductivity such as a liquid metal could form the basis of a homogeneous reactor.

As a preliminary approach to the problem the wetting of uranium dioxide by lead was studied (Bradhurst and Buchanan 1959a) by a sessile-drop technique similar to that used by Humenik and Kingery (1953).

It was found that oxygen had a significant surface active effect in molten lead, and the present study is an extension of this work to include molten sodium and sodium-potassium alloy. The dependence of the surface tension and contact angle of these liquid metals on such variables as the liquid constitution, nature of the solid oxide, type of atmosphere, and temperature has been investigated.

### II. EXPERIMENTAL

Measurements of surface tension by the sessile-drop technique were carried out by focusing a magnified image of the liquid metal drop (on a prepared oxide plaque) on to a photographic plate. An f4·5 8-in. focal length lens was used in conjunction with a microscopic eyepiece and bellows mounted on an optical bench. Using an exposure of 60 sec at f23 very sharp images were obtained. Measurements of drop dimensions and contact angle were made on traced enlargements (magnification 30 times) of these plates, and using Dorsey's (1928) method of calculation surface tensions could be reproducibly determined to within  $\pm 4\text{--}5\%$ . Contact angles were determined to within  $\pm 2^\circ$ .

\*Chemistry Department, University of Melbourne.

The measurements required for calculating surface tension are independent of the overall drop height and its angle of contact with the oxide surface. The equation used was

$$T = gdr^2(0.05200/f - 0.1227 + 0.0481f), \quad (1)$$

where  $T$  = surface tension ( $\text{dyne cm}^{-1}$ ),

$$f = y/r - 0.4142,$$

$y$  = acceleration due to gravity ( $\text{cm sec}^{-2}$ ),

$d$  = density of the liquid metal ( $\text{g cm}^{-3}$ ),

$r$  = drop radius (cm),

$y$  = distance from the drop apex to the point of intersection of the two  $45^\circ$  tangents.

The alkali metals studied (sodium and sodium-potassium alloy) were handled by two different techniques.

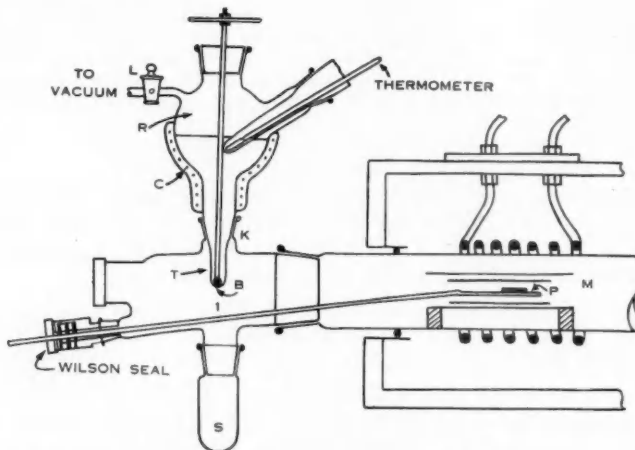


Fig. 1.—The sessile-drop apparatus for measuring surface tension and contact angle with liquid alkali metals.

#### (a) Dynamic Vacuum Technique

The apparatus consisted of a 6 by 1 in. diameter molybdenum tube furnace, heated by induction and enclosed within a water-cooled Pyrex glass tube. This tube is shown in Figure 1, together with the apparatus for introduction of the liquid alkali metals.

A vacuum line was connected to the furnace tube, and evacuated by a mercury diffusion pump, cold trap, and backing pump, giving a pressure of about  $5 \times 10^{-6}$  mmHg. Purified argon, hydrogen, or carbon monoxide atmospheres could be introduced through a purification line consisting of a liquid air trap, a column of heated magnesium turnings, and two  $\text{P}_2\text{O}_5$  drying columns.

The reservoir,  $R$ , and the furnace tube containing the sliding platform,  $P$ , were evacuated to the limit of the pumping system and the susceptor and oxide

plaque were thoroughly degassed by heating in vacuum to 700 °C. The platform containing the plaque was then moved to a position just below  $T$ , and by means of the heating coils,  $C$ , on the alkali metal reservoir the temperature was raised sufficiently to ensure that the metal was molten down to the introduction tip,  $T$  (120–130 °C for sodium). A Teflon sleeve was used at  $K$ , lightly lubricated with Silicone vacuum grease, and proved satisfactory at the temperatures used.

By means of the ball valve,  $B$ , liquid metal was allowed to pass into the sampling tube,  $S$ , until a steady and controllable dropping rate was obtained. A single drop was then allowed to fall on the prepared oxide surface.

The platform was then moved carefully into the centre of the furnace, and levelled with the aid of a cathetometer focused on the image of the drop on the glass screen of the camera. A series of photographs of plaque and drop was then taken at different temperatures.

The liquid metal contained dissolved oxide approximately equal to the saturation concentration at the temperature of introduction. Excess oxide remained in the reservoir as a skin on the surface of the metal and the drops drawn off from the dropping tip beneath were always bright and free of bulk oxide.

The brightness of the metal surface was found to be a sensitive indicator of the presence of oxygen, and at pressures greater than  $10^{-3}$  mmHg (McLeod gauge) perceptible dulling of the surface of liquid sodium occurred. This was undoubtedly due to small quantities of desorbed oxygen from the cold walls of the furnace tube and the susceptor itself, which although not affecting the total pressure of the system appreciably were sufficient to form a significant amount of oxide on the surface of the comparatively small sample. Providing a vacuum of  $10^{-5}$  mmHg or better could be maintained in the furnace tube, the metal surface remained bright indefinitely (a period of greater than 28 hr was recorded for Na-K alloy) and no difficulty was experienced in making measurements.

Figure 5 (b) shows a series of photographs of molten sodium, on stoichiometric uranium dioxide, achieved by this method.

#### (b) Sealed-Tube Technique

It was found necessary to use sealed-tube techniques in order to study contact angles at temperatures greater than approximately 250 °C, as volatilization of the molten sodium was too rapid *in vacuo* above this temperature and clear photographs could not be taken. Furthermore, even in a purified argon atmosphere (argon passed through heated Mg turnings) there was sufficient residual oxygen in the system, either from the argon itself, or from outgassing of the cooled Pyrex walls of the furnace tube, to form appreciable amounts of oxide on the surface of the molten metal, which itself acted as an extremely efficient oxygen getter above 250 °C.

This problem was overcome by using the apparatus shown in Figure 2. It consisted of a simple Pyrex tube with a bulb blown at one end, and a side arm into which was sealed a metal oxide plaque. A sample of B.D.H. commercial sodium was cut from the centre of a block, introduced into the bulb, and the

tube quickly evacuated to  $10^{-5}$  mmHg. The tube was flame heated to degas the walls, and, if necessary (as in the case of  $\text{UO}_2$ ) the oxide surface was heated in hydrogen to approximately 500 °C to remove the oxygen in excess. The sodium was then melted and distilled carefully under vacuum by flame heating until a sample of clean bright sodium rested on the glass wall at position C. During the distillation, a vacuum of  $10^{-5}$  mmHg or better was maintained, and heating was controlled very carefully to ensure that the temperature did not reach values at which discoloration of the walls occurs due to reaction of sodium and the Pyrex glass.

After admitting argon, sealing, and drawing off the tube at A and D, a drop of sodium was rolled into E, and by means of flame heating and tilting the tube the drop could be manoeuvred onto the prepared plaque. The residual amount of sodium at C was then strongly heated to act as an oxygen getter. The tube was resealed and drawn off at F, to allow the sample to be placed in an electrically heated cruciform furnace. The sample was observed and photographed using the same optical system as used for the induction heated furnace.

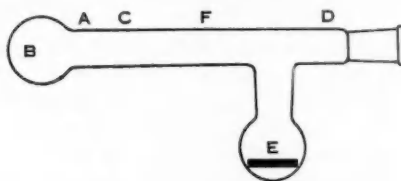


Fig. 2.—The sealed tube apparatus for observation on sessile drops of alkali metals at elevated temperatures.

The quality of the image produced through the curved wall of the sealed tube was, of course, inferior to that obtainable with the optical flats of the larger furnace tube, but the contact angle could still be determined to within  $\pm 2^\circ$  in many cases. Surface tension values were less accurate and were probably not more reliable than  $\pm 10\%$ . However, a series of photographs on the one system gave reliable comparisons. An error in calculation of up to  $\pm 5\%$  was caused in some cases by reduction of the factor  $f$  in equation (1) due to the combined effects of small drop radius and the low density of sodium which reduces the "flatness" of the drop.

Analysis for oxygen was carried out on samples collected in method (a) by the butyl bromide method (White 1954; Smythe and de Bruin 1958). At the conclusion of each run butyl bromide was distilled into the sample tube, S (Fig. 1), from a prefrozen sample tube attached to the main vacuum line. After reaction had occurred with the sodium sample, the mixture was leached with water and the alkali produced was titrated potentiometrically with standard  $\text{HNO}_3$  to pH 7. The sample size was then determined by a Mohr estimation of the total bromide.

Oxide plaques were prepared by cold pressing the powdered oxide at 100,000 p.s.i. and sintering either in air or in a controlled atmosphere. In the case of  $\text{UO}_2$ , a weighed sample of  $\text{UO}_{2-00}$  was heated in air for 10 min at 200 °C, during which time the composition was altered to  $\text{UO}_{2-13}$ . This non-stoichiometric oxide sinters more readily than  $\text{UO}_{2-00}$  (Murray, Rodgers, and Williams 1952), and plaques of density 8.5 to 9.3 were obtained by cold pressing and sintering at 1500 °C in dynamic vacuum of approximately  $10^{-3}$  mm. The plaque surfaces were ground flat and polished on a silicon carbide stone, then reduced to stoichiometric  $\text{UO}_2$  prior to each run as described above.

### III. RESULTS AND DISCUSSION

Considerable evidence was found for surface activity of dissolved oxygen in molten sodium. Figure 3 shows the lowering of surface tension, as measured by the sessile-drop technique (*a*).

The sodium which contained oxygen possessed sufficient (0.034 wt. %) to give approximate saturation in the temperature range 100 to 250 °C, but not enough to form a coherent solid oxide film on the liquid sodium surface since the surface remained bright during all measurements.

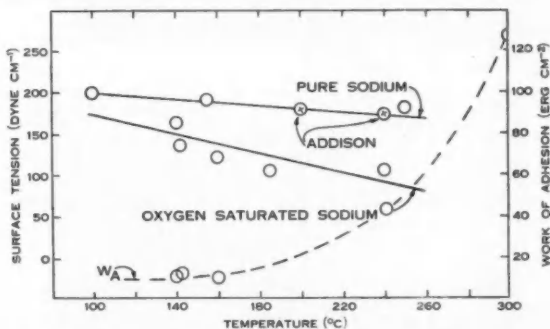


Fig. 3.—Variation with temperature of surface tension of liquid sodium and work of adhesion of liquid sodium on uranium dioxide.

It may be seen from Figure 3 that the lowering in surface tension obtained was proportional to the temperature. An increase in the effect is to be expected since increase in temperature will increase the solubility of oxygen as oxide. The curve for oxygen-free sodium is also shown, and was considerably above that for sodium in the presence of oxygen. In the latter case the extrapolated value of surface tension at the melting point is not far below that of pure sodium, which is again to be expected since the solubility of oxygen in sodium at 100 °C is very small (USAEC 1955) and very little lowering of surface tension should occur at this temperature.

The values obtained for the work of adhesion shown in Figure 3 were calculated from the "oxygen saturated" values for the contact angle, shown as curve *A* in Figure 4. It is interesting to note that the contact angle did not fall

below 90° until the temperature was increased to greater than 300 °C, even though sufficient oxide was present to allow saturation at all temperatures up to 300 °C.

It may be seen from Figure 3 that the decrease in surface tension obtained was accompanied by an increase in the wetting of uranium dioxide by molten sodium, as indicated by the increased work of adhesion. Furthermore, this wetting was found to be irreversible, as in all other cases studied, low values of contact angle being maintained on cooling to the melting point.

The curves *A* and *C* in Figure 4 represent the extremes in the contact angle values obtained in the presence of saturation and minimum oxygen concentrations respectively. It is possible that curve *C* would have been even higher if a more thorough oxygen "gettering" technique could have been employed, but it is

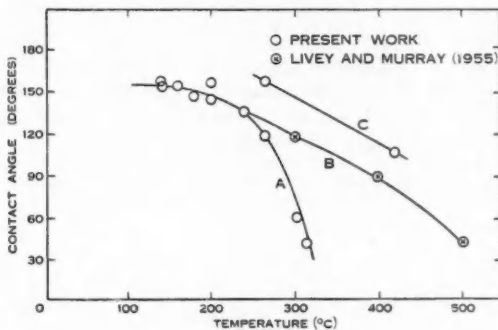


Fig. 4.—Variation with temperature of the contact angle on uranium dioxide of liquid sodium (containing various amounts of oxygen as solute).

*A*, O<sub>2</sub>-saturated Na; *B*, Na+some O<sub>2</sub>; *C*, oxygen-free Na.

significant that the values obtained were higher than those of Livey and Murray (1955), and Taylor and Ford (1955), indicating that insufficient attention has been paid in the past to the effect of traces of oxygen on the surface tension of metals.

Further evidence in support of the surface activity of oxygen in sodium was provided by the occurrence of "spreading wetting" (Osterhoff and Bartell 1927) of sodium on oxide surfaces. A drop of sodium on a calcium oxide surface was allowed to evaporate progressively *in vacuo*, thus increasing the concentration of residual oxygen and causing a decrease in contact angle. Eventually the surface tension decreased sufficiently to cause spreading of the molten sodium, which is shown in Figure 5. The spreading is indicated by an approach of the drop towards the wall of the Pyrex glass tube through which the photographs were taken.

A second series of photographs (Fig. 6) shows the reduction of contact angle with increase in oxygen concentration, but spreading wetting did not occur at this low temperature, due to the relatively small saturation concentration of oxygen.

As in the work with lead and lead oxide, the process of solution of sodium oxide in molten sodium was accompanied by random motion of the solid oxide particles (Bradhurst and Buchanan 1959b) on the liquid surface, after which reduction of contact angle invariably occurred. Furthermore the high contact angle values obtained in curve C (Fig. 4) for sodium on uranium dioxide were only possible when the uranium dioxide was in its stoichiometric form,  $\text{UO}_{2\cdot00}$ , any higher oxides yielding the excess oxygen to the molten sodium, with conse-

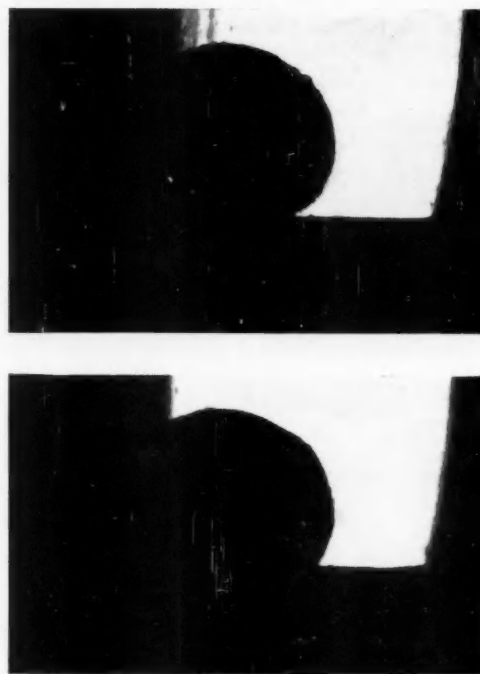


Fig. 5.—Spreading of liquid sodium on calcium oxide due to increased solution of oxygen in the sodium.

quent reduction of surface tension and contact angle. This behaviour is similar to that of lead. When a plaque of  $\text{U}_3\text{O}_8$  ( $\text{UO}_{2\cdot67}$ ) was used in conjunction with sodium already containing a small amount of oxygen, reaction occurred with sufficient rapidity at 250 °C to disintegrate the plaque, possibly with the formation of a sodium uranate.

The relative lowering of surface tension of sodium by dissolved oxygen was greater than that obtained for lead (Table 1). This may be due to the greater difficulty of accommodating the large oxygen anion in the liquid consisting of small sodium ions, and hence a greater surface excess of oxide is established.

The more pronounced ionic character of the solid oxides of sodium would tend to favour the existence of independent ions in molten sodium rather than any molecular species which may exist in molten lead (Bradhurst and Buchanan 1959a).

(a) *Dependence of the Contact Angle on the Radius Ratio of the Solid Oxide* [ $M^{++} : O^-$ ]

Livey and Murray (1955), in a recent study of wetting of oxides by liquid metals, suggested that the non-wetting behaviour of most metals was due to mutual repulsion between oxygen anions on the oxide surface (which occupy the greater proportion of the surface) and the electron "cloud" of the liquid metal.

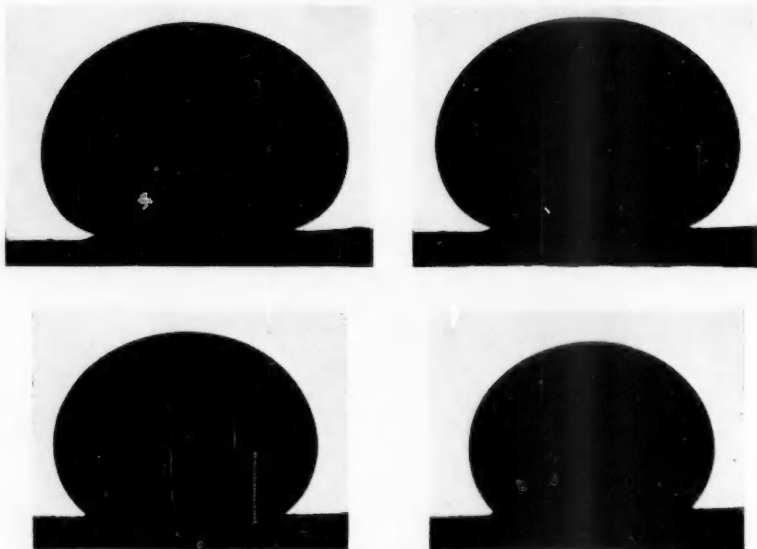


Fig. 6.—Reduction of contact angle of sodium on uranium dioxide as concentration of dissolved oxygen increases in the sodium, the concentration increasing in the drops from left to right.

The present measurements with liquid sodium offered an opportunity to test this hypothesis using MgO, CaO, and BaO as the solid phases. A reduction of contact angle should occur as a result of the increasing proportion of the surface occupied by the positively charged alkaline earth cations in this series.

The results obtained are shown in Table 2, and graphically in Figure 7. Sealed tube techniques were used and the oxygen concentration was probably small and reasonably constant as shown by the high contact angle values obtained at temperatures up to 500 °C. Assuming this was so, the results appear to lend some support to the views of Livey and Murray, although the effects are relatively small and may be open to other interpretations.

In general terms, however, it is probably true to say that, the more metallic the surface, the greater will be the wetting by a liquid metal (Taylor and Ford 1955).

TABLE I  
RELATIVE LOWERING OF SURFACE TENSIONS OF LIQUID SODIUM  
AND LEAD BY DISSOLVED OXYGEN

Species	Ionic Radius (Å)	Max. Lowering of Surface Tension* (%)
Pb <sup>++</sup>	1.2	22
Na <sup>+</sup>	0.95	36
O <sup>=</sup>	1.4	—

\* By dissolved oxygen.

(b) *Studies on Sodium-Potassium Alloy in Contact with UO<sub>2-00</sub>*

The sodium-potassium eutectic alloy has been used as a heat transfer medium in nuclear reactor technology, and many of its physical properties are known (USAEC 1955).

A brief study of the contact angle with uranium dioxide was carried out by Abrahams, Carlson, and Flotow (1957) and a number of less fundamental studies have been performed on sodium-potassium alloy-uranium dioxide slurries (Furman 1957; Bromberg and Tarpley 1958).

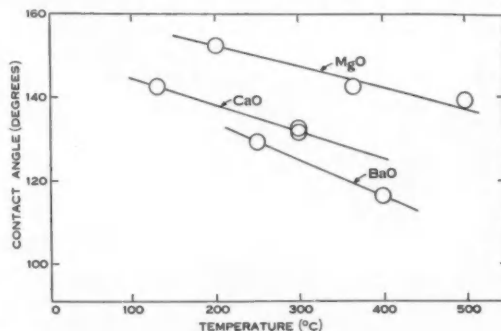


Fig. 7.—The contact angle of liquid sodium on magnesium, calcium, and barium oxides.

Sodium-potassium alloys are dangerous to handle, being pyrophoric in air to the point of explosion if vibrated. They may be handled safely under argon or *in vacuo*, however, and a series of four measurements was carried out on an alloy of approximately 60 wt. % sodium using technique (a) described in Section II. Throughout the determinations, which were performed with a vacuum of

better than  $10^{-5}$  mmHg, the surface brightness of the alloy did not decrease. The oxygen concentration was not known, but as the manipulation was done at 25–30 °C, and no solid oxide was visible, it was probably not greater than the saturation concentration at 30 °C (approx. 0.001 wt. % O) (Bogard and Williams 1951).

TABLE 2  
CONTACT ANGLE OF LIQUID SODIUM ON ALKALINE EARTH OXIDES

Solid Surface	Radius Ratio $M^{++} : O^-$	Contact Angle (degrees at 400 °C)
MgO	0.460	$142 \pm 3$
CaO	0.708	$125 \pm 3$
BaO	0.965	$116 \pm 2$

Figure 8 shows the decrease in the advancing contact angle obtained at a temperature of 250 °C in a vacuum. Non-wetting values were obtained at first under these conditions but showed a progressive decrease culminating in a rapid fall to a wetting value of 60°. The sudden decrease shown in Figure 8 was

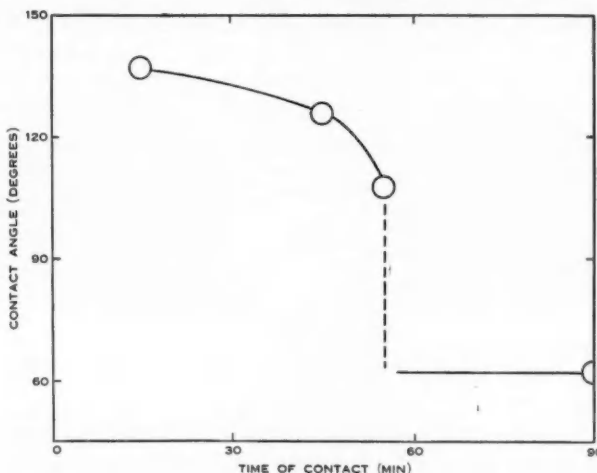


Fig. 8.—Change with time of contact angle of liquid sodium-potassium alloy on uranium dioxide.

induced by vibration. In the light of previous experience on the surface activity of dissolved oxide and bearing in mind the very strong affinity of the sodium-potassium alloy for oxygen, it is possible that this decrease in contact angle is associated with increasing concentration of dissolved oxygen, the latter possibly derived from degassing of the walls. In this connection it is interesting to note

TABLE 3  
VARIATION OF WORK OF ADHESION OF LIQUID SODIUM-POTASSIUM EUTECTIC ALLOY TO  $\text{UO}_2$  WITH TIME OF CONTACT

Temperature (°C)	Time of Contact (min)	Pressure (mmHg)	Surface Tension (dyne cm <sup>-1</sup> )	Contact Angle with $\text{UO}_{2-00}$	Work of Adhesion (erg cm <sup>-2</sup> )
30	15	$5 \times 10^{-6}$	$133 \pm 6$	$137 \pm 2$	42
200	45	"	$124 \pm 7$	$126 \pm 2$	55
250	55	"	$116 \pm 7$	$107 \pm 2$	52
$\mp 100$	90	"	—	$62 \pm 2$	189

that Abrahams, Carlson, and Flotow (1957) claimed that the sodium-potassium eutectic wet  $\text{UO}_{2-00}$  but not  $\text{UO}_{2-02}$  at 25 °C. This result is difficult to interpret unless in the second case the alloy reacted with sufficient oxygen from the oxygen excess  $\text{UO}_2$  to give an impervious skin on the surface of the metal, a condition which will give rise to non-wetting behaviour.

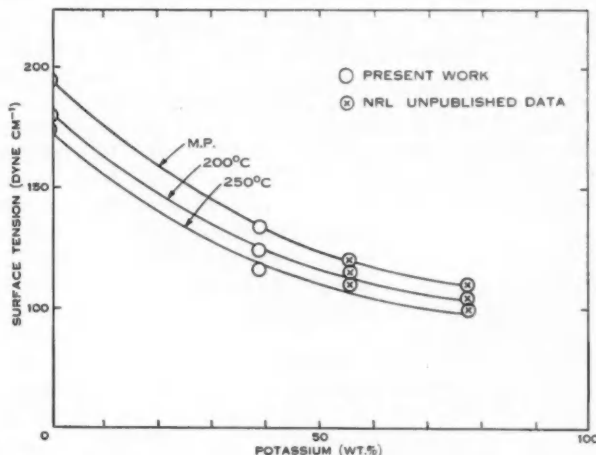


Fig. 9.—The surface tension isotherms of sodium-potassium alloys at several temperatures.

The surface tensions corresponding to the contact angles of Figure 8 are shown in Table 3.

Surface tension data from the United States Naval Research Laboratories (USAEC 1955) were given as 110–100 dyne cm<sup>-1</sup> from the melting point to 250 °C for the 78 wt. % potassium alloy, and 120–110 dyne cm<sup>-1</sup> over the same temperature range for the 56 wt. % potassium alloy. A summary of all these results is shown in the surface tension *v.* composition isotherms in Figure 9, and

it may be seen that the results obtained here agree well with the NRL values. The isotherms are non-linear, indicating that the surface layer in sodium-potassium alloys is potassium rich, and that the system is not ideal. This is supported by recent vapour pressure measurements (Kistiakowsky 1955) on sodium-potassium alloys where non-ideal behaviour was found and attributed to polymeric species in the vapour phase.

#### IV. ACKNOWLEDGMENT

This work was supported by a grant from the Australian Atomic Energy Commission and forms part of a programme of work on the surface chemistry of liquid metals.

#### V. REFERENCES

ABRAHAMS, B. M., CARLSON, R. D., and FLOTOW, H. E. (1957).—USAEC Rep. NESC-104.  
BOGARD, A. D., and WILLIAMS, D. D. (1951).—USAEC Rep. NRL-3865.  
BRADHURST, D. H., and BUCHANAN, A. S. (1959a).—*J. Phys. Chem.* **63**: 1486-88.  
BRADHURST, D. H., and BUCHANAN, A. S. (1959b).—*Aust. J. Chem.* **12**: 523.  
BROMBERG, L., and TARPLEY, W. B. (1958).—USAEC Rep. NYO-7929.  
DORSEY, N. E. (1928).—*J. Wash. Acad. Sci.* **18**: 505.  
FURMAN, S. C. (1957).—USAEC Rep. KAPL-1648.  
HUMENIK, M., and KINGERY, W. D. (1953).—*J. Phys. Chem.* **57**: 359.  
KISTIAKOWSKY (1955).—USAEC Rep. NRL-P-2958.  
LIVEY, D. J., and MURRAY, P. (1955).—*Plansee Proc.* **1955**: 375.  
MURRAY, P., RODGERS, E. P., and WILLIAMS, A. E. (1952).—AERE Rep. M/R 893.  
OSTERHOFF, H. J., and BARTLETT, F. E. (1927).—5th Colloid Symp. Monogr.  
SMYTHE, L. E., and DE BRUIN, H. J. (1958).—*Analyst* **83**: 242.  
TAYLOR, J. W., and FORD, T. D. (1955).—UKAERE Rep. M/R 1729.  
USAEC (1955).—"The Liquid Metals Handbook." Sodium and Sodium-Potassium Supplement.  
TID-5277, pp. 7-8, 32-44. (USAEC: Washington, D.C.)  
WHITE, J. C. (1954).—*Analyst. Chem.* **26**: 210.

## SURFACE PROPERTIES OF MOLTEN BISMUTH-BISMUTH CHLORIDE IN CONTACT WITH URANIUM DIOXIDE

By D. H. BRADHURST and A. S. BUCHANAN\*

[Manuscript received February 15, 1961]

### Summary

The wetting of uranium dioxide by liquid bismuth has been investigated by means of measurements of surface tension of the liquid and contact angle of the liquid on the solid. Bismuth chloride in low concentration was found to be a very effective surface active agent in improving the wetting of the solid by the metal.

### I. INTRODUCTION

In general pure liquid metals and alloys do not wet oxide surfaces. On the other hand, appreciably improved wetting can be achieved by the solution of certain non-metallic elements in the metal phase. Oxygen has proved to be one of the more effective surface active solutes in this respect and contact angles of less than 90° can be attained in certain cases. Whilst this phenomenon is of some assistance in securing a stable dispersion of an oxide in a liquid metal, the effects are frequently of insufficient magnitude and other more effective non-metallic solutes were therefore sought. Recent work on the miscibility of metal-molten salts (Cubicciotti 1953; Bredig 1955, 1956; Grjotheim, Gronvold, and Krogh-Moe 1955; Corbett 1957; Ohlberg 1958) indicated that certain of these systems might be suitable. The bismuth-bismuth chloride system was investigated from the point of view of its surface tension and contact angle on oxide surfaces and hence of its ability to wet these surfaces. Bismuth trichloride shows appreciable solubility (a fraction of 1 mole %) in metallic bismuth at temperatures above the melting point of the latter (271 °C). As the temperature is increased the range of solubility increases and is of the order of several mole % at 500 °C. At higher concentrations of bismuth trichloride there is an extensive range of composition in which two mutually saturated liquid phases exist and complete solution is only attained at a temperature of the order of 800 °C (Yosini *et al.* 1959).

### II. EXPERIMENTAL

#### (a) Preparation of Bismuth-Bismuth Trichloride Sample

Dehydration of bismuth chloride was achieved by repeatedly melting bismuth chloride (B.D.H.) under vacuum in a round-bottomed distillation flask equipped with a side arm and sample tube constricted at the inlet. Part of the material was then distilled into the sample tube under approximately 40 cm pressure of dried argon. The tube was sealed and samples obtained were subsequently handled in a dry box. The bismuth chloride prepared in this way had a melting point of approximately 235 °C and was of satisfactory purity for the

\* Chemistry Department, University of Melbourne.

surface tension measurements which were made using the maximum bubble pressure method.

The bismuth–bismuth chloride samples used in the contact angle measurements were prepared by introducing a sample of bismuth chloride into a pre-weighed silica sample tube containing a weighed amount of pure bismuth and the weighed solid specimen of uranium dioxide and then sealing under argon using an oxy-gas torch. Check analyses for chloride showed that the amount of hydrolysis which occurred during the sealing process was negligible.

(b) *Measurements of Surface Tension and Contact Angle*

Surface tensions at the bismuth chloride end of the system were measured by the maximum bubble pressure technique. The apparatus consisted of a Pyrex vessel containing the Bi–BiCl<sub>3</sub> mixture immersed in a bath of molten sodium nitrate–potassium nitrate. A Pyrex capillary tube passed through the stopper and the tube could be raised or lowered precisely by means of a brass stop and micrometer screw gauge firmly clamped to a steel vacuum frame. The vessel was connected to the vacuum and gas purification line. Bismuth trichloride was first distilled into this vessel as described above, and argon was admitted to atmospheric pressure. The stopper containing the capillary assembly was then inserted, the lower half of the tube placed in the molten-salt bath, and the vessel evacuated, and refilled with argon. When the temperature was steady at the value required for measurement, the capillary tip was lowered into the surface and argon or nitrogen was passed through at a rate corresponding to the formation of one bubble per 6–7 sec. The maximum pressure  $p_m$  just before the "breakaway" point was measured with a *m*-xylene (density 0·859 g cm<sup>-3</sup>) manometer having a mirror-backed scale. The optimum depth of immersion of the capillary tip proved to be about 0·02 cm.

The surface tension was calculated from the formula

$$\gamma = \frac{1}{2}r(h_2\rho_{2g} - h_1\rho_{1g}),$$

where  $r$ =average radius (cm) of the capillary (measured by a travelling microscope),

$h_1$ =depth of tip below liquid surface (cm),

$\rho_1$ =density of liquid (g cm<sup>-3</sup>),

$h_2$ =difference in manometer liquid heights (cm),

$\rho_2$ =density of manometer liquid (g cm<sup>-3</sup>).

The capillaries were prepared by drawing out Pyrex tubing in an oxy-gas flame, scratching the surface with a file, and snapping the capillary. After several attempts, a tip could be prepared which was perpendicular to the bore of the tube. Tips prepared in this way, as others have found (Boardman, Palmer, and Heymann 1948), have a sharper circumference than ground tips, and give a cleaner, more definite "breakaway" point.

Measurements of contact angle were carried out by taking photographs of a plate of uranium dioxide dipping into the liquid phase of a bismuth–bismuth trichloride melt, enclosed in either a Pyrex glass or silica tube. The tubes were sealed under approximately 1 atm of argon, as described above.

These tubes were heated in a cruciform tube furnace, permitting observation at elevated temperatures. Photographs were taken using an f4·5 anastigmatic lens, and quarter-plate camera mounted on an optical bench. Photographs of the profile of the  $\text{UO}_2$  plaque in the liquid were taken at 300 and 800 °C for a series of bismuth–bismuth trichloride mixtures ranging in composition from 0–100% bismuth.

### III. RESULTS

The values obtained for the maximum bubble pressure in molten bismuth trichloride showed a gradual increase for any one set of readings (Table 1). However, replacement of the cleaned and dried capillary tip gave the original values, suggesting that the rise was probably due to constriction of the capillary by deposited material. The Pyrex glass was wetted by the molten bismuth trichloride, and appreciable capillary rise was observed when the capillary tip first touched the liquid surface. The minimum pressure was therefore taken to be the most reliable and the results shown in Table 1 compared favourably with previous values (Jaeger and Kahn 1916).

TABLE I  
CALIBRATION OF CAPILLARY FOR MAXIMUM BUBBLE PRESSURE MEASUREMENTS OF SURFACE TENSION

Substance	Maximum Bubble Pressure (cm <i>m</i> -xylene)	Temperature (°C)	$\gamma$ (dyne $\text{cm}^{-1}$ )	Time (min)
$\text{BiCl}_3$	4·21	286	$66\cdot9 \pm 0\cdot3$	3
	4·21	288	$66\cdot9$	5
	4·75	286	$74\cdot9$	10
	4·19	285	$66\cdot1 \pm 0\cdot3$	3
	4·19	289	$66\cdot1$	5
	4·47	290	$70\cdot4$	9
$\text{H}_2\text{O}$	4·68	15	$73\cdot3 \pm 0\cdot3$	—
	4·70	15	$73\cdot5 \pm 0\cdot3$	—

This method was used for bismuth–bismuth trichloride mixtures at 300 °C and, as shown in Table 2, there was little change in surface tensions up to 24 mole % bismuth.

At the bismuth-rich end of the phase diagram, maximum bubble pressure measurements were carried out at temperatures up to 320 °C but a slightly more elaborate purification procedure was required in order to prevent oxidation of the molten bismuth. The cylinder nitrogen used in these experiments was dried by passing it through a liquid air trap and phosphorus pentoxide column.

Oxygen was then removed by a second column containing magnesium turnings, electrically heated to 400 °C. This procedure ensured the maintenance of a bright metal surface during measurements and individual readings remained

constant indefinitely. The surface tension *v.* concentration isotherm obtained at 300 °C is shown in Figure 1. Due to the large miscibility gap which exists at this temperature no measurements could be performed in the range 40–98 mole % bismuth.

TABLE 2  
SURFACE TENSION OF BISMUTH-BISMUTH TRICHLORIDE MIXTURES

Bismuth (mole %)	Surface Tension (dyne cm <sup>-1</sup> )	Temperature (°C)
0	66.1 ± 0.3	272
10.0	66.3 ± 0.3	283
24.4	66.9 ± 0.3	272

The 300 °C isotherm was used to estimate the surface excess concentration of solute, and the area per molecule by the application of the Gibbs adsorption isotherm (see Fig. 2).

Bismuth trichloride proved a very effective solute in reducing the contact angle of molten bismuth on UO<sub>2</sub>. The contact angle was reduced to zero on addition of about 5 mole % of bismuth trichloride, and the wetting was irreversible

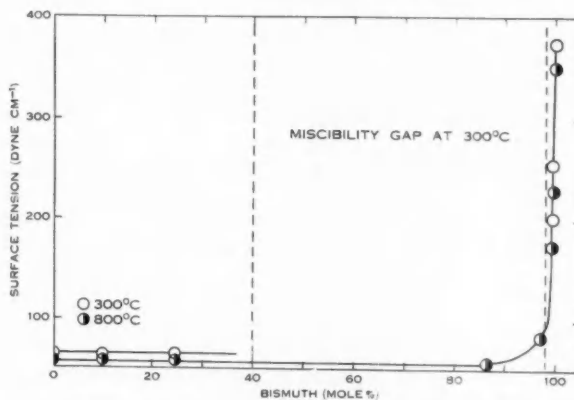


Fig. 1.—Surface tension isotherms for bismuth-bismuth trichloride at 300 and 800 °C.

as has been observed in other systems studied (Bradhurst 1960). Figure 3 shows three photographs of the contact angle between UO<sub>2</sub> and different Bi-BiCl<sub>3</sub> melts, illustrating wetting and non-wetting values, and Figure 4 shows the isotherms obtained for contact angle *v.* composition, at 300 and 800 °C respectively.

Above 300 °C the mixtures consisted of a two-phase liquid with bright metallic bismuth at the bottom and a dark salt-rich phase at the top. For

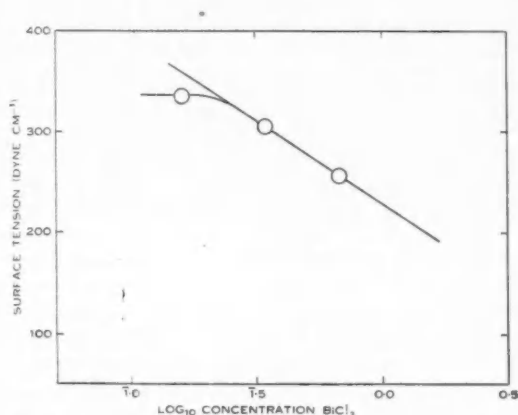


Fig. 2.—Gibbs adsorption isotherm for bismuth–bismuth trichloride at 300 °C. Slope =  $-164$ ;  $\Gamma = 9 \cdot 1 \times 10^{14}$  molecules  $\text{cm}^{-2}$ .

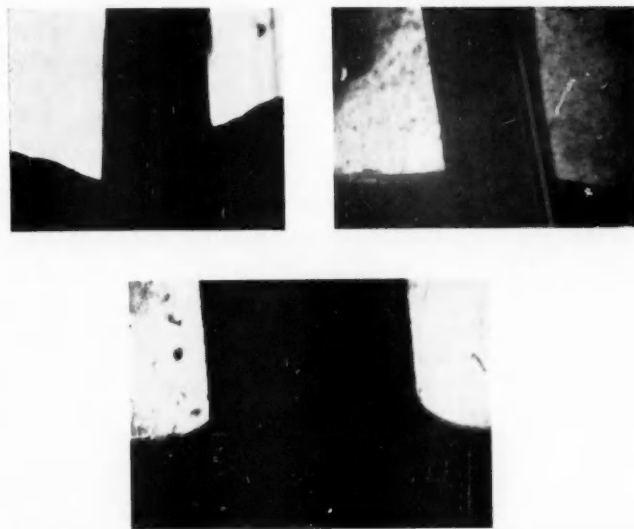


Fig. 3.—Photographs of the contact angle of bismuth–bismuth trichloride on uranium (in the form of compressed plates inserted in the melt). Reduction in contact angle is shown with increasing bismuth trichloride concentration from top to bottom on photographs.

metal-rich mixtures the whole liquid became bright and metallic as the miscibility gap was passed on heating. The dark salt-rich phase reappeared on cooling and the observation of this transitional point was used by Yosini to construct the phase diagram for the system.

During each determination, the silica tube walls remained very clean, showing that there must have been very little of the mixture existing in the vapour phase, as the partial pressure due to argon alone was approximately 4 atm at 800 °C. Some difficulty was experienced with optical distortion due to the slightly striated silica tube walls, but the contact angle could still be determined in the better photographs to within  $\pm 2^\circ$ .

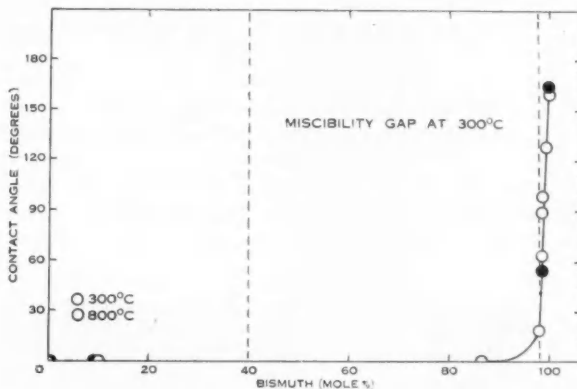


Fig. 4.—Isotherms for the contact angle of bismuth–bismuth trichloride melts on uranium dioxide at 300 and 800 °C.

#### IV. DISCUSSION

A considerable amount of work has been done in recent years on bismuth–bismuth halide systems (Corbett 1958a, 1958b; Cubicciotti 1958; Cubicciotti and Keneshea 1958; Yosini *et al.* 1959), but very little has been done on metal-rich mixtures, or at temperatures above 400 °C, apart from phase studies alone. In other systems which we have studied, such as metal–metal oxides, surface activity was definitely present (Addison 1954; Livey and Murray 1955; Bradhurst and Buchanan 1959) but the oxide was usually so insoluble that the metal was saturated before appreciable reduction in surface tension or contact angle had occurred. On the other hand in the bismuth–bismuth trichloride–uranium dioxide system complete wetting by pure bismuth trichloride was replaced by almost complete non-wetting for pure bismuth, as the composition changed from 0–100% bismuth, and from the isotherms of Figures 1 and 4 it is apparent that bismuth trichloride must be strongly surface active when dissolved in molten bismuth.

Wetting of  $\text{UO}_2$  by liquid bismuth trichloride is not surprising in view of its relatively low surface tension ( $66 \text{ dyne cm}^{-1}$ ) and its surface activity in

molten bismuth will be due to the great difference in surface tensions of the two substances (surface tension of bismuth is 380 dyne cm<sup>-1</sup> at 300 °C). In the mixed liquid the surface is probably almost entirely composed of bismuth trichloride and, in effect, a non-metallic chloride surface is presented to the UO<sub>2</sub> which itself probably has a surface composed largely of oxide ions (Livey and Murray 1955).

Vapour pressure and partial molal volume measurements (Cubicciotti 1958; Cubicciotti and Keneshea 1958) on bismuth trichloride–bismuth systems have shown that marked positive deviations from Raoult's law occur at 400 °C as bismuth is added to molten bismuth trichloride and that the volume of the system decreases initially when Bi is added to BiCl<sub>3</sub>. Early work on conductivities by Aten (1909) showed that the conductivity of bismuth trichloride increased initially with the addition of metallic bismuth. It is also known (Corbett 1958a, 1958b) that salt-rich solutions are diamagnetic. The two main schools of thought on the nature of the species existing in these solutions have been due to Corbett (1958a, 1958b), whose work supports polymers of the type (BiCl)<sub>n</sub>, and Cubicciotti (1958), who has postulated the existence of Bi<sub>n</sub><sup>+m</sup> polymers. This second postulate is supported by the conductivity, magnetic, and volume measurements. The species Bi<sub>2</sub> has been identified in the gaseous phase (Bracket and Brewer 1954, USAEC report), and dissolved in lead (Kelley 1936). On the other hand, stoichiometric BiCl has been identified as a component of bismuth trichloride–bismuth melts below 327 °C, and the polymeric form Bi<sub>2</sub>Cl<sub>4</sub> has been used (Corbett 1958a, 1958b) to explain the positive deviations from Raoult's law observed by Cubicciotti.

Recent measurements (Cubicciotti 1958) of partial molal volumes of bismuth and bismuth trichloride have led to postulates of a chloride "quasi-lattice" (again at temperatures less than 400 °C) which can incorporate added bismuth in "octahedral holes". Using calculated values of ionic radii it has been shown that this model may be adapted to explain the changes in partial molal volume of bismuth in bismuth trichloride for limited ranges of temperature and concentration. In the metal-rich miscible range at 300 °C added chloride ion would likewise be fitted into octahedral holes with only a small expansion in the liquid bismuth "quasi-lattice".

The pronounced surface activity of chloride found in the present work indicates that this ion is not easily accommodated within the liquid metal "lattice", and expansion at elevated temperatures is required for this purpose. However, in the work on liquid lead (Bradhurst and Buchanan 1959) and the solutes O, S, Se, and Te it was observed that the least readily accommodated species, oxygen (having the greatest non-metallic character) was the solute exhibiting the most pronounced surface activity. The lack of metallic character would appear to be of considerable importance in the present case also since both chloride ions and chlorine atoms could be readily accommodated in the bismuth lattice with very little expansion, and hence size of the species concerned cannot be the only criterion of miscibility (Table 3).

Application of the Gibbs adsorption isotherm to the measurements on the reduction in surface tension with increase of bismuth chloride concentration at

300 °C (Fig. 2) in the 98–100% bismuth region gives an area per surface molecule of about  $11 \text{ \AA}^2$ . The area for the chloride ion is about  $10 \cdot 3 \text{ \AA}^2$ . This procedure is very approximate but provides some support for the view that the surface species may be chloride ions or oriented  $\text{BiCl}$  ion pairs in view of the other evidence for entities of this kind.

TABLE 3  
RADII OF POSSIBLE SPECIES IN BISMUTH-BISMUTH TRICHLORIDE

Species . . . .	Bi	$\text{Cl}^-$	Cl
Radius (Å) (Bragg 1937) . .	1.78	1.81	0.99

The high electronegativity of chlorine (3.0 on Pauling's scale) gives something of a measure of its non-metallic character and inability to yield electrons to the conduction bands of the molten bismuth and hence become easily assimilated in the metallic medium. Oxygen on the same scale has an even higher electronegativity (3.5) and displays surface activity in liquid metals although limited by its quite low solubility in this respect.

#### V. REFERENCES

ADDISON, C. C. (1954).—*J. Chem. Soc.* **1954**: 2861.  
 ADDISON, C. C. (1955).—*J. Chem. Soc.* **1955**: 2262.  
 ATEN, A. (1909).—*Z. Phys. Chem.* **66**: 641.  
 BOARDMAN, N. K., PALMER, A. R., and HEYMANN, E. (1948).—*Trans. Faraday Soc.* **51**: 259.  
 BRACKET, E., and BREWER, L. (1954).—USAEC Rep. UCRL 3712.  
 BRADHURST, D. H. (1960).—M.Sc. Thesis, Melbourne.  
 BRADHURST, D. H., and BUCHANAN, A. S. (1959).—*J. Phys. Chem.* **63**: 1486.  
 BRAGG, W. L. (1937).—“Atomic Structure of Minerals.” (Oxford Univ. Press.)  
 BREDIG, M. A. (1955).—*J. Amer. Chem. Soc.* **77**: 1454.  
 BREDIG, M. A. (1956).—Proc. 3rd Symp. High Temperature, Berkeley.  
 CORBETT, J. D. (1957).—*J. Amer. Chem. Soc.* **79**: 3020.  
 CORBETT, J. D. (1958a).—*J. Amer. Chem. Soc.* **80**: 4757.  
 CORBETT, J. D. (1958b).—*J. Phys. Chem.* **62**: 1149.  
 CUBICCIOTTI, D. (1953).—USAEC Rep. AECD 3623.  
 CUBICCIOTTI, D. (1958).—*J. Phys. Chem.* **62**: 843.  
 CUBICCIOTTI, D., and KENESHEA, F. J. (1958).—*J. Phys. Chem.* **62**: 463.  
 GROTHEIM, K., GRONVOLD, F., and KROGH-MOE, F. (1955).—*J. Amer. Chem. Soc.* **77**: 5824.  
 JAEGER, F. M., and KAHN, J. (1916).—*Proc. Acad. Sci. Amst.* **19**: 381–97.  
 KELLEY, K. K. (1936).—Bull. U.S. Bur. Min. No. 393.  
 LIVEY, D. J., and MURRAY, P. (1955).—*Planssee Proc.* **1955**: 375–404.  
 OHLBERG, S. M. (1958).—USAEC Rep. NAA-SR-2939.  
 YOSINI, T. J. ET AL. (1959).—*J. Phys. Chem.* **63**: 230.

## SURFACE PROPERTIES OF LIQUID METALS: BISMUTH, LEAD-BISMUTH, TIN

By D. H. BRADHURST\* and A. S. BUCHANAN\*

[Manuscript received February 15, 1961]

### Summary

Dissolved oxygen was shown to have inappreciable surface activity in liquid bismuth up to 700 °C. Introduction of lead as a third solute in the liquid bismuth however increased the surface activity of oxygen. The solutes oxygen, sulphur, selenium, and tellurium showed the same order of surface activity in liquid tin as in liquid lead.

### I. INTRODUCTION

The preceding papers of this series have recorded the wetting behaviour of liquid metals such as lead (Bradhurst and Buchanan 1959a, 1959b), sodium and sodium-potassium mixtures (Bradhurst and Buchanan 1961a), and bismuth (Bradhurst and Buchanan 1961b) towards oxide surfaces. In general, pure liquid metals show marked non-wetting characteristics on all oxide surfaces up to quite high temperatures. On the other hand introduction of certain non-metallic solutes such as oxygen and the halogens may greatly improve the wetting even in quite low concentrations. Such surface active solutes must clearly accumulate at the surface of the liquid metal and in this way reduce its metallic character. In the present paper further studies are recorded on surface activity in bismuth, bismuth-lead mixtures, and tin.

### II. EXPERIMENTAL

The sessile-drop technique for measuring surface tensions and contact angles of the liquid on a solid surface has been described previously (Bradhurst and Buchanan 1959, 1961a).

Pure specimens of the metals to be investigated were obtained from the Metallurgy Department, University of Melbourne. Cylindrical pellets ( $3.5 \times 6.5$  mm) were prepared using a stainless steel punch and the weighed solutes were confined before melting in small holes drilled in the tops of the pellets. The lead-bismuth eutectic alloy was prepared in a graphite container in the evacuated furnace.

### III. RESULTS

#### (a) Surface Activity of Oxygen in Liquid Bismuth

Weighed amounts of  $\text{Bi}_2\text{O}_3$  were added to molten bismuth and surface tension and contact angle on  $\text{UO}_2$  determined (Table 1).

The concentrations of oxygen shown in column 1 are in fact in excess of the saturation value of 0.00695 mole %  $\text{Bi}_2\text{O}_3$  (Hansen 1958) and excess solid

\* Chemistry Department, University of Melbourne.

$\text{Bi}_2\text{O}_3$  was present on the surface of the drop throughout the experiment. Furthermore there was no evidence, on microscopic observation, of recrystallization of the oxide from the liquid metal on cooling the drop to room temperature.

TABLE 1  
SURFACE ACTIVITY OF OXYGEN IN MOLTEN BISMUTH

$\text{Bi}_2\text{O}_3$ (mole %)	Surface Tension at 700 °C (dyne cm <sup>-1</sup> )	Contact Angle (degrees)
0	$350 \pm 7$	$156 \pm 2$
0.063	$346 \pm 7$	$149 \pm 2$
0.318	$345 \pm 7$	$150 \pm 2$

TABLE 2  
SURFACE ACTIVITY OF OXYGEN IN LEAD-BISMUTH EUTECTIC

PbO (mole %)	Surface Tension at 700 °C (dyne cm <sup>-1</sup> )	Contact Angle (degrees)	Work of Adhesion (dyne cm <sup>-1</sup> )
0	$388 \pm 7$	152	45.4
0.369	$374 \pm 7$	130	133
0.786	$370 \pm 7$	120	185

TABLE 3  
COMPARISON OF SURFACE ACTIVITY IN TIN AND LEAD AT  
800 °C

Solute	Maximum Reduction in Surface Tension (% at 800 °C)	
	Sn	Pb
Oxygen	20.4	22.0
Sulphur	15.8	7.0
Selenium	12.0	5.0
Tellurium	2.0	2.5

### (b) The Lead-Bismuth Eutectic Mixture

Oxygen, when dissolved in the lead-bismuth eutectic, displayed significant surface activity although the effects were rather less than for pure lead (Table 2). The largest value for the work of adhesion to  $\text{UO}_2$  corresponds approximately with that obtained for lead with oxygen as solute (198 dyne cm<sup>-1</sup>).

*(c) Surface Activity in Liquid Tin*

This metal was studied over the temperature range 250–800 °C and solutes used were oxygen, sulphur, selenium, and tellurium. Saturation concentration was achieved for the first two, which are the least soluble. The results at 800 °C are compared with a similar set obtained for liquid lead (Table 3).

**IV. DISCUSSION**

The surface activity of oxygen in liquid bismuth is clearly very slight (Table 1) and in fact is scarcely significant. This may be associated with the quite low solubility of oxygen in liquid bismuth, although on the other hand experience in the case of lead (Bradhurst and Buchanan 1959a) indicated that the least soluble and least metallic of the solutes, oxygen, was the most surface active. In this connection introduction of lead into the bismuth (to give the eutectic composition) significantly improved the surface activity of oxygen as a third solute (Table 2). The contact angle on  $\text{UO}_2$  was decreased quite significantly although the surface tension was less definitely influenced. It is evident that the presence of lead as part of the liquid phase permits dissolved oxygen to accumulate in the surface either as oriented  $\text{PbO}$  molecules or ion pairs. Further studies on other solutes in bismuth (e.g. S, Se) would probably give some indication of the reason for the lack of surface activity (up to 700 °C) of oxygen in this metal.

Surface activity of the solutes oxygen, sulphur, selenium and tellurium in liquid tin show the same order of effectiveness as in liquid lead (Table 3). It is again evident that the important factor in determining whether a surface excess of solute will be established is the metallic character and compatibility of the solute with the liquid metal. In this connection the greater surface activity of sulphur and selenium in tin as compared with lead may be due to lower solubility and reduced compatibility of these elements with the metal.

The conclusions reached in this work may have consequences in interpreting liquid metal behaviour. Soft solder, for example, should flow and wet an oxidized metal surface more readily if the solder has already been subject to oxidizing conditions and contains a significant amount of dissolved oxygen. Naturally, flow will occur most readily on a clean non-oxidized solid metal surface. The role of a flux is probably to limit oxidation of the solid metal which is being soldered or welded. It could in certain circumstances provide non-metallic surface active solutes for the liquid metal and hence increase its ability to wet a partially oxidized solid metal surface.

**V. REFERENCES**

BRADHURST, D. H., and BUCHANAN, A. S. (1959a).—*J. Phys. Chem.* **63**: 1486.  
BRADHURST, D. H., and BUCHANAN, A. S. (1959b).—*Aust. J. Chem.* **12**: 523.  
BRADHURST, D. H., and BUCHANAN, A. S. (1961a).—*Aust. J. Chem.* **14**: 397.  
BRADHURST, D. H., and BUCHANAN, A. S. (1961b).—*Aust. J. Chem.* **14**: 409.  
HANSEN, M. (1958).—"Constitution of Binary Alloys." 2nd Ed. (McGraw-Hill Book Co.: New York.)

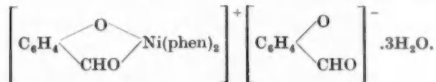
## A CHEMICAL AND MAGNETIC STUDY OF SOME BIVALENT NICKEL COMPLEXES

By C. M. HARRIS,\* S. L. LENZER,\* and R. L. MARTIN†

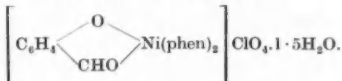
[Manuscript received April 4, 1961]

### Summary

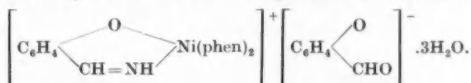
Diamagnetic and square-coordinated nickel(II) complexes of nitrogen substituted salicylaldimines,  $[\text{Ni}(\text{N}-\text{R salicylaldimine})_2]$  ( $\text{R}=\text{CH}_3$ ,  $\text{C}_2\text{H}_5$ , and  $\text{C}_6\text{H}_5$ ), readily react with 1,10-phenanthroline (phen) in benzene and form paramagnetic ( $\mu \sim 3.2$  B.M.) six-covalent complexes of the type  $[\text{Ni}(\text{phen})(\text{N}-\text{R salicylaldimine})_2]$ . Similar paramagnetic monophenanthroline adducts are formed by the diamagnetic  $[\text{Ni}(o\text{-hydroxyacetophenoxime})_2]$  and  $[\text{Ni}(N\text{-methyl-}o\text{-hydroxyacetophenimine})_2]$  complexes. The paramagnetic ( $\mu \sim 3.2$  B.M.) nickel-salicylaldehyde complex,  $[\text{Ni}(\text{salicylaldehyde})_2(\text{H}_2\text{O})_2]$ , reacts with 2 moles of the ligand forming the paramagnetic ( $\mu \sim 3.2$  B.M.) derivative,  $\text{Ni}(\text{phen})_2(\text{salicylaldehyde})_2 \cdot 3\text{H}_2\text{O}$ . This is an electrolyte in nitrobenzene and possesses the structure



The complex cation was isolated as its perchlorate,



The diamagnetic aldimine derivative  $[\text{Ni}(\text{salicylaldimine})_2]$  also reacts with 2 moles of 1,10-phenanthroline, with partial hydrolysis of the imine, and forms the unusual compound:  $\text{Ni}(\text{phen})_2(\text{salicylaldimine})(\text{salicylaldehyde}) \cdot 3\text{H}_2\text{O}$ . This paramagnetic compound is also an electrolyte in nitrobenzene and possesses the structure



The following diamagnetic compounds,  $[\text{Ni}(o\text{-hydroxyacetophenimine})_2]$ ,  $[\text{Ni}(o\text{-hydroxyacetophenoxime})_2]$ , and  $[\text{Ni}(N\text{-methyl-}o\text{-hydroxyacetophenimine})_2]$ , are converted by heat to paramagnetic forms which exhibit an unusual temperature variation of their magnetic moments. They revert to their original diamagnetic forms on recrystallization from chloroform.

### I. INTRODUCTION

The paramagnetism developed by certain diamagnetic four-coordinated complexes of nickel(II) when dissolved in organic solvents of vastly differing donor properties such as chloroform, benzene, dioxane, or ethanol has excited much interest during the past decade. Paramagnetic triplet ground states can

\* Department of Inorganic Chemistry, School of Chemistry, The University of New South Wales, Broadway, N.S.W.

† Central Research Laboratories, I.C.I.A.N.Z. Ltd., Melbourne.

theoretically arise for all three established stereochemical configurations for bivalent nickel (shown in Table 1), so that explanations of the above phenomenon have been couched in terms of an equilibrium between the diamagnetic square form and one of these three paramagnetic forms.

Willis and Mellor (1947) were the first to observe that some square-coordinated diamagnetic complexes of salicylaldehyde derivatives developed paramagnetism when dissolved in various organic solvents, and attributed the development of this partial paramagnetism in solution to an equilibrium between

TABLE I  
POSSIBLE ELECTRONIC CONFIGURATIONS AND STEREOCHEMISTRY FOR PARAMAGNETIC NICKEL(II)  
COMPOUNDS

Stereochemistry	Electronic Configuration																																				
	Non-bonding Electrons		Bonding Electrons																																		
	3d	4s	4p																																		
Tetrahedral*	<table border="1" style="margin-left: auto; margin-right: auto;"> <tr><td>↑</td><td>↓</td><td>↑</td><td>↓</td><td>↑</td><td>↓</td><td>↑</td></tr> <tr><td>↓</td><td>↑</td><td>↑</td><td>↑</td><td>↑</td><td>↑</td><td>↑</td></tr> <tr><td>(3d<sub>z</sub><sup>4</sup> 3d<sub>y</sub><sup>4</sup>)</td><td></td><td></td><td></td><td></td><td></td><td></td></tr> </table>	↑	↓	↑	↓	↑	↓	↑	↓	↑	↑	↑	↑	↑	↑	(3d <sub>z</sub> <sup>4</sup> 3d <sub>y</sub> <sup>4</sup> )							<table border="1" style="margin-left: auto; margin-right: auto;"> <tr><td>↑</td><td>↓</td></tr> <tr><td>↓</td><td>↑</td></tr> <tr><td>↑</td><td>↓</td></tr> <tr><td>↑</td><td>↓</td></tr> </table>	↑	↓	↓	↑	↑	↓	↑	↓	4s4p <sup>3</sup>					
↑	↓	↑	↓	↑	↓	↑																															
↓	↑	↑	↑	↑	↑	↑																															
(3d <sub>z</sub> <sup>4</sup> 3d <sub>y</sub> <sup>4</sup> )																																					
↑	↓																																				
↓	↑																																				
↑	↓																																				
↑	↓																																				
Octahedral† . .	<table border="1" style="margin-left: auto; margin-right: auto;"> <tr><td>↑</td><td>↓</td><td>↑</td><td>↓</td><td>↑</td><td>↓</td></tr> <tr><td>↓</td><td>↑</td><td>↑</td><td>↑</td><td>↑</td><td>↑</td></tr> <tr><td>(3d<sub>x</sub><sup>6</sup> 3d<sub>y</sub><sup>2</sup>)</td><td></td><td></td><td></td><td></td><td></td><td></td></tr> </table>	↑	↓	↑	↓	↑	↓	↓	↑	↑	↑	↑	↑	(3d <sub>x</sub> <sup>6</sup> 3d <sub>y</sub> <sup>2</sup> )							<table border="1" style="margin-left: auto; margin-right: auto;"> <tr><td>↑</td><td>↓</td></tr> <tr><td>↓</td><td>↑</td></tr> <tr><td>↑</td><td>↓</td></tr> <tr><td>↑</td><td>↓</td></tr> <tr><td>↑</td><td>↓</td></tr> <tr><td>↑</td><td>↓</td></tr> </table>	↑	↓	↓	↑	↑	↓	↑	↓	↑	↓	↑	↓	4s4p <sup>3</sup> 4d <sup>2</sup>	4d		
↑	↓	↑	↓	↑	↓																																
↓	↑	↑	↑	↑	↑																																
(3d <sub>x</sub> <sup>6</sup> 3d <sub>y</sub> <sup>2</sup> )																																					
↑	↓																																				
↓	↑																																				
↑	↓																																				
↑	↓																																				
↑	↓																																				
↑	↓																																				
Square‡ . .	<table border="1" style="margin-left: auto; margin-right: auto;"> <tr><td>↑</td><td>↓</td><td>↑</td><td>↓</td><td>↑</td><td>↓</td></tr> <tr><td>↓</td><td>↑</td><td>↑</td><td>↑</td><td>↑</td><td>↑</td></tr> <tr><td>(3d<sub>x</sub><sup>6</sup> 3d<sub>y</sub><sup>2</sup>)</td><td></td><td></td><td></td><td></td><td></td><td></td></tr> </table>	↑	↓	↑	↓	↑	↓	↓	↑	↑	↑	↑	↑	(3d <sub>x</sub> <sup>6</sup> 3d <sub>y</sub> <sup>2</sup> )							<table border="1" style="margin-left: auto; margin-right: auto;"> <tr><td>↑</td><td>↓</td></tr> <tr><td>↓</td><td>↑</td></tr> <tr><td>↑</td><td>↓</td></tr> <tr><td>↑</td><td>↓</td></tr> </table>	↑	↓	↓	↑	↑	↓	↑	↓	4s4p <sup>3</sup> 4d	4d						
↑	↓	↑	↓	↑	↓																																
↓	↑	↑	↑	↑	↑																																
(3d <sub>x</sub> <sup>6</sup> 3d <sub>y</sub> <sup>2</sup> )																																					
↑	↓																																				
↓	↑																																				
↑	↓																																				
↑	↓																																				

\* Only recently has strong evidence for the rare occurrence of tetrahedral nickel(II) complexes been presented (see Venanzi 1958; Gill and Nyholm 1959).

† Paramagnetic six-covalent nickel(II) is well established (see Nyholm 1953, and references therein). Recently evidence has been presented (Harris, Nyholm, and Phillips 1960) for the occurrence of diamagnetic nickel(II) complexes exhibiting a coordination number greater than four.

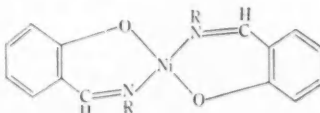
‡ The existence of diamagnetic square nickel(II) complexes is well established by X-ray structural determinations. There has not been to the author's knowledge any convincing evidence offered for the existence of square coordinated nickel(II) complexes which are paramagnetic.

square and tetrahedral forms. Clark and Odell (1955) extended their work by measuring the magnetic susceptibility of bis(*N*-methylsalicylaldimine)nickel(II) in chloroform, benzene, toluene, and *m*-xylene over a range of temperature, and used their data to calculate equilibrium constants, heats of reaction, free energy, and entropy changes, assuming a square tetrahedral conformational equilibrium.

The existence or non-existence of tetrahedrally coordinated bivalent nickel has recently provided the basis for many claims and counter-claims in the literature. The apparent non-existence of such compounds has been claimed to be in agreement with the predictions of crystal field theory (Bjerrum and

Jorgensen 1956), but in 1958 Venanzi claims that complexes of the type  $[(\text{Ph}_3\text{P})_2\text{Ni}(\text{hal})_2]$  provide examples of sterically forced nickel(II) complexes which are paramagnetic with a distorted tetrahedral arrangement about the central nickel atom. Since then, Gill and Nyholm (1959) have shown that bivalent nickel forms tetrahedral complexes of the type  $[\text{Ni}(\text{hal})_4]^{2-}$  possessing magnetic moments ( $3.5-3.9$  B.M.) which are much higher than those normally observed ( $2.9-3.2$  B.M.) for "high spin" nickel complexes. A more recent claim by Cotton *et al.* (1959) that triphenylphosphine oxide forms a sterically forced tetrahedral nickel(II) complex  $[\text{Ni}(\text{Ph}_3\text{PO})_4](\text{ClO}_4)_2$  with a magnetic moment of  $3.51$  B.M. has now been retracted by Cotton and Bannister (1960) in favour of a square-coordinated structure. However, their published analysis\* for this compound fits closely a six-covalent diaquo-complex  $[\text{Ni}(\text{Ph}_3\text{PO})_4(\text{H}_2\text{O})_2](\text{ClO}_4)_2$  and this would appear to us to be more compatible with the observed magnetism.

Willis and Mellor's proposal implies that the diamagnetic square-coordinated configuration is stabilized by crystal forces in the solid, but that in solution with solvents of low donor properties the tetrahedral and square forms have similar energies. On the other hand, it is known that strong donor solvents will interact with these complexes, and Clark and Odell (1955) have shown that pyridine solutions of bis(salic<sub>1</sub>alldoxime)nickel(II) and also of bis(*N*-methylsalicylaldimine)nickel(II) behaved as though they contained octahedral bispyridine adducts in which the paramagnetism was fully developed. These pyridine adducts have been isolated and characterized in the solid state (see also Basolo and Matoush 1953). However, it is significant that certain compounds such as bis(salicylaldimine)nickel(II) exhibit temperature-dependent equilibria between diamagnetic and paramagnetic forms even in pyridine solution. Clark and Odell regard these forms as being planar (diamagnetic) and octahedral (paramagnetic) respectively, and have since confirmed this hypothesis by studies of absorption spectra (Clark and Odell 1956). However, they were unable to interpret their results in weak donor solvents, such as chloroform and aromatic hydrocarbons, in this manner.

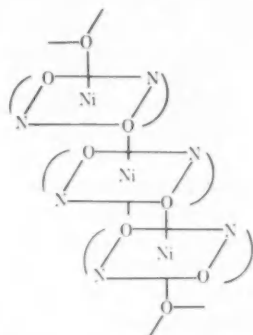


(I)

Undoubtedly, square-coordinated nickel can possess a strong tendency to become six-coordinated by interaction with ligands at right angles to the plane of the parent molecule, and it is therefore of interest, in connection with the solution paramagnetism of bis(*N*-methylsalicylaldimine)nickel(II), that the present authors (Harris, Lenzer, and Martin 1958) recently succeeded in transforming the diamagnetic parent (I; R=CH<sub>3</sub>) into a paramagnetic isomer

\* Found : C, 61.6; H, 4.8; Ni, 4.19%. Calc. for  $[\text{Ni}((\text{C}_6\text{H}_5)_3\text{PO})_4(\text{H}_2\text{O})_2](\text{ClO}_4)_2$  : C, 61.5%; H, 4.6%; Ni, 4.2%. The anhydrous compound requires C, 63.1; H, 4.4; Ni, 4.3%.

( $\mu = 3.2$  B.M.). This was also achieved independently by Sacconi, Paoletti, and Cini (1958). The diamagnetic-paramagnetic transformation can be achieved by heating the diamagnetic form either in biphenyl solution or in the solid state to temperatures in the range 150–200 °C. The resulting buff coloured compound has the same analysis as the green diamagnetic form. Its magnetic susceptibility obeys a Curie-Weiss law (with  $\theta = 20$  °C) between 115 and 350 °K, so that its magnetic moment is nearly independent of temperature. Unlike the diamagnetic isomer, the paramagnetic form displays a marked insolubility in polar and non-polar solvents. These characteristics are best understood by formulating the paramagnetic isomer as a polymeric six-covalent structure involving the use of  $4s4p^34d^2$ -bonding orbitals by the central nickel atom. Such a structure can arise, for example, by a phase change in the solid at 150–200 °C, leading to a polymerized arrangement of the type shown in structure (II).



(II)

Sacconi, Paoletti, and Del Re (1957) favour an interpretation of the phenomenon of solution paramagnetism based on a square-coordinated "high-spin" isomer as the species contributing to paramagnetism in solution. Dielectric polarization data for a series of bis(*N*-alkylsalicylaldimine)nickel(II) complexes (where alkyl =  $\text{CH}_3$ ,  $\text{C}_2\text{H}_5$ ,  $\text{C}_3\text{H}_7$ ,  $\text{C}_4\text{H}_9$ , and  $\text{C}_5\text{H}_{11}$ ), together with magnetic moments in the range 0.3–2.2 B.M. in chloroform, benzene, and dioxane solutions, were taken to indicate that both the diamagnetic and the paramagnetic species possessed a planar structure. The dipole moment data do not necessarily eliminate *trans*-disolvated structures for these complexes. Furthermore, it might be expected that this postulated electron-configurational equilibrium between square forms should probably be observable in the solid state, whereas Harris, Lenzer, and Martin (1958) found that  $\text{Ni}(\text{N-methylsalicylaldimine})_2$  is uniformly diamagnetic in the solid state between 102 and 291 °K. The possibility of the solvent promoting an equilibrium between two square forms of different electronic energy states was ignored by Sacconi, Paoletti, and Del Re (1957).

Clearly, the solvent plays the vital role in promoting the phenomenon of solution paramagnetism, and it must be remembered that excellent evidence is available to prove that even aromatic molecules such as benzene can function as donor molecules and hence could interact with nickel in octahedral sites. Maki (1958) and subsequently Ballhausen and Liehr (1959) have attempted to clarify the problem by interpretations of the electronic absorption spectra of these solutions in terms of the ligand field theory. According to Maki, closely lying singlet and triplet states are to be expected for all the established configurations of bivalent nickel and in the case of square nickel(II) complexes the energy of the lowest lying triplet state is decreased relative to the energy of the lowest singlet state by weak axial ( $z$ -axis) perturbation by solvent molecules. Ballhausen and Liehr support this view, and also include the effect of the changes in bond lengths and bond angles on the relative energies of the electronic states. Maki's analysis agrees with the fact that the magnetic moments of such solutions decrease with increasing temperature (see Clark and Odell 1955) since such an increase should effectively increase both the average intermolecular distance and orientational disorder of the solvent molecules. She was also able to assign the spectrum of the solid diamagnetic *N*-methylsalicylaldimine nickel(II) complex in four-coordinated *trans*-planar symmetry in keeping with its known structure (Frasson and Sacconi 1957).

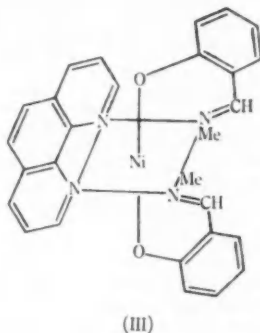
If the energy gap between low lying singlet and triplet levels becomes comparable with thermal energy ( $kT \approx 200 \text{ cm}^{-1}$  at room temperature), the molecules will distribute between the states according to a Maxwell-Boltzmann law, the compound becoming paramagnetic with a moment lying between 0·3–2 B.M. Recently, Saeconi *et al.* (1960) have investigated the magnetic properties of *N*-alkyl(salicylaldimine)nickel(II) complexes in the molten state over the temperature range 150–200 °C, and have found that these substances also acquire paramagnetism on melting with moments which vary in a complicated way between 0·8–1·2 B.M. They conclude that the mechanism of this transition is substantially the same as in solution and that it involves an equilibrium between planar molecules in singlet and triplet states separated by about 770–1100  $\text{cm}^{-1}$ .

Another possible explanation for the development of solution paramagnetism by diamagnetic nickel(II) salicylaldimine derivatives in solvents such as benzene and chloroform could be one involving association of the complex. A recent note by Holm and McKinney (1960) reports that the *N*-isopropyl, *N*-cyclopentyl, and *N*-s-butylsalicylaldimine derivatives have moments in the range 2·1–2·6 B.M. in benzene solution and that the molecular complexity of these complexes in freezing benzene lies in the range 1·2–1·5. These workers have suggested that this may be due to association via weak Ni...O interactions between adjacent molecules.

The present work is concerned with further attempts to transform other related diamagnetic nickel(II) complexes into paramagnetic isomers as well as with a study of their reactions with the bidentate chelate group 1,10-phenanthroline.

## II. DISCUSSION

The tendency for diamagnetic bis(*N*-methylsalicylaldimine)nickel(II) to develop paramagnetism both in solution and the solid state is further reflected in its ready reaction with 1,10-phenanthroline in benzene solution to form the paramagnetic ( $\mu \sim 3.2$  B.M.) monophenanthroline complex,  $[\text{Ni}(\text{phen})(N\text{-methylsalicylaldimine})_2]$ . This compound is virtually a non-electrolyte in nitrobenzene solution (see Table 2), and, since the occurrence of "high spin" square-nickel(II) complexes has not been substantiated, its paramagnetism implies an octahedral environment for the central nickel atom. Clearly, the *N*-methylsalicylaldimine chelate no longer occupies a square-planar arrangement about the nickel due to the 1,10-phenanthroline occupying *cis*-octahedral positions as in (III).



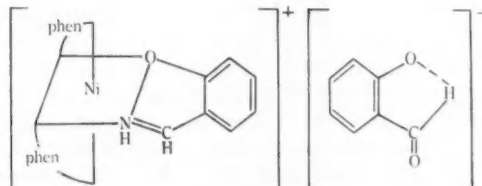
Attempts to convert the diamagnetic *N*-ethyl- and *N*-phenylsalicylaldimine-nickel(II) complexes to paramagnetic forms by heating, either in the solid state or in boiling biphenyl, have been unsuccessful. However, both these compounds react with 1,10-phenanthroline forming the paramagnetic ( $\mu \sim 3.2$  B.M.) complexes  $[\text{Ni}(\text{phen})(N\text{-ethylsalicylaldimine})_2]$  and  $[\text{Ni}(\text{phen})(N\text{-phenylsalicylaldimine})_2]$ . Thus, although both these square diamagnetic nickel complexes react readily with 1,10-phenanthroline to form octahedral adducts with molecular structures of the type shown in (III), they will not rearrange on heating to form paramagnetic isomers. The larger molecular volumes of the ethyl and phenyl groups compared with the methyl group, presumably offer serious steric hindrance to a molecular stacking in the solid state of the type envisaged in (II), so that polymeric, paramagnetic isomers cannot be isolated. In this connection it is interesting to note that Sacconi, Paoletti, and Del Re (1957) have recently shown that the diamagnetic *N*-ethyl compound develops some paramagnetism in chloroform, benzene, and in dioxane solution and that hence, although the ethyl group is sufficiently large to sterically hinder the formation of a polymeric structure, it is not large enough to prevent nickel-solvent interaction in the vacant octahedral sites.

The behaviour of the parent diamagnetic complex  $[\text{Ni}(\text{salicylaldimine})_2]$  is in marked contrast to that of its *N*-methyl analogue. Various heating pro-

TABLE 2  
MOLECULAR CONDUCTIVITIES OF NICKEL(II) COMPLEXES IN  $10^{-5}$ M NITROBENZENE SOLUTION AT 25 °C

Compound	Conductivity (in mho)
$\left[ \text{C}_6\text{H}_4 \begin{array}{c} \text{O} \\ \diagdown \\ \text{CHO} \end{array} \text{Ni}(\text{phen})_2 \right] \left[ \text{C}_6\text{H}_4 \begin{array}{c} \text{O} \\ \diagdown \\ \text{C} \\ \parallel \\ \text{O} \end{array} \text{H} \right] \cdot 3\text{H}_2\text{O}$	19.0
$\left[ \text{C}_6\text{H}_4 \begin{array}{c} \text{O} \\ \diagdown \\ \text{CH}=\text{NH} \end{array} \text{Ni}(\text{phen})_2 \right] \left[ \text{C}_6\text{H}_4 \begin{array}{c} \text{O} \\ \diagdown \\ \text{C} \\ \parallel \\ \text{O} \end{array} \text{H} \right] \cdot 3\text{H}_2\text{O}$	18.6
$\left[ \text{C}_6\text{H}_4 \begin{array}{c} \text{O} \\ \diagdown \\ \text{CHO} \end{array} \text{Ni}(\text{phen})_2 \right] \text{ClO}_4 \cdot 1.5\text{H}_2\text{O}$	29.0
$\left[ \left( \text{C}_6\text{H}_4 \begin{array}{c} \text{O} \\ \diagdown \\ \text{CH}=\text{NR} \end{array} \right)_2 \text{Ni}(\text{phen}) \right] (\text{R}=\text{H or CH}_3)$	<2

cedures designed to induce a phase change always failed and yielded only the original material. The diamagnetic salicylaldoxime compound  $[\text{Ni}(\text{salicylaldoxime})_2]$ , also could not be converted into a paramagnetic form. Clearly, steric factors are not involved in these two cases, for both the OH group and the hydrogen atom have smaller volumes than the methyl group. It seems most likely that the paramagnetic tendency of these types of compounds is greatly



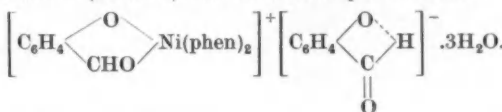
(IV)

influenced by small changes in the donor properties of the nitrogen atom which of course will be modified by its substituents. Also in this connection it is of interest to note that the magnetic moment (1.1 B.M.) of  $[\text{Ni}(\text{salicylaldoxime})_2]$  in chloroform is much less than that of  $[\text{Ni}(N\text{-methylsalicylaldoxime})_2]$  ( $\mu=2.3$  B.M.).

Treatment of bis(salicylaldoxime)nickel(II) with 1,10-phenanthroline in benzene failed to yield a mono-complex. However, in boiling 98% ethanol the imine dissolved on the addition of 2 moles of phenanthroline and on crystal-

lizing the mixture the unusual complex  $\text{Ni}(\text{phen})_2(\text{salicylaldimine})(\text{salicylaldehyde}) \cdot 3\text{H}_2\text{O}$  was obtained. This substance is paramagnetic with  $\mu = 3.25$  B.M./Ni atom and since 1,10-phenanthroline does not function as a monodentate group it follows that either the salicylaldimine and salicylaldehyde groups must be functioning as monodentates or the substance is ionized possessing a salt formulation. The conductivity of this compound in nitrobenzene (see Table 2) supports the salt-like structure (IV).

The paramagnetic ( $\mu \sim 3.2$  B.M.) bis-salicylaldehyde complex  $[\text{Ni}(\text{H}_2\text{O})_2(\text{salicylaldehyde})_2]$  also gives a bis(1,10-phenanthroline) complex,  $\text{Ni}(\text{phen})_2(\text{salicylaldehyde})_2 \cdot 3\text{H}_2\text{O}$ , when treated with the ligand in 98% ethanol. This paramagnetic compound ( $\mu \sim 3.2$  B.M.) also functions as an electrolyte in nitrobenzene solution (Table 2) and undoubtedly is the salt

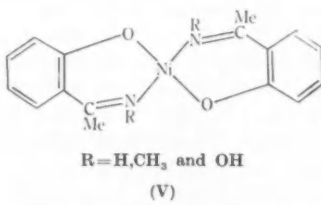


Unlike the monophenanthroline complexes discussed previously, this compound readily dissolves in warm water to form a yellow solution from which the perchlorate,  $\left[ \text{C}_6\text{H}_4 \begin{array}{c} \text{O} \\ \diagdown \\ \text{CHO} \end{array} \text{Ni}(\text{phen})_2 \right] \text{ClO}_4 \cdot 1.5\text{H}_2\text{O}$  precipitates on the addition of sodium perchlorate. Aqueous solutions of the  $\left[ \text{C}_6\text{H}_4 \begin{array}{c} \text{O} \\ \diagup \\ \text{CH}=\text{NH} \end{array} \text{Ni}(\text{phen})_2 \right]^+$  ion undergo hydrolysis and the addition of perchlorate ions to such solutions gives an impure precipitate of the above perchlorate.

The low conductivities ( $\sim 20$  mho) of the two bis(1,10-phenanthroline) derivatives in Table 2, compared to the value of 29 mho for the perchlorate, may reflect some association between the anion and cation through H-bonding or possibly an equilibrium of the type



This has not been further investigated.



Compounds of the type (V), in which the non-aromatic carbon atom is methyl substituted, were also studied during this investigation. These three compounds are diamagnetic and the compounds, in which  $\text{R} = \text{CH}_3$  and OH readily formed paramagnetic ( $\mu \sim 3.2$  B.M.) mono(1,10-phenanthroline) adducts from benzene solution. An attempt was also made to convert compounds of type (V) into paramagnetic forms and, although the compounds of type (I) (where  $\text{R} = \text{H}$

and OH) have not been obtained in paramagnetic forms, these three compounds yielded rather unexpected results. Thus we have found that the diamagnetic compounds, bis(*N*-methyl-*o*-hydroxyacetophenimine)nickel(II), bis(*o*-hydroxyacetophenimine)nickel(II), and bis(*o*-hydroxyacetophenoimine)nickel(II), can be converted into paramagnetic forms by refluxing them in biphenyl and quenching the boiling mixtures. The excess biphenyl is easily extracted from the quenched mixtures with light petroleum. The extent of the paramagnetism induced by this treatment varies with the concentration of the compound in the biphenyl solution. It was found that compounds possessing room temperature moments in the range 2.4–2.8 B.M. per nickel atom were obtained from 2% solutions

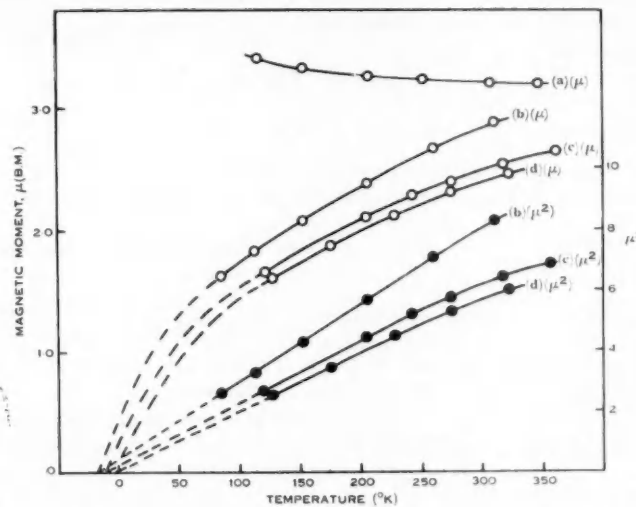


Fig. 1.—Variation of magnetic moments ( $\mu$  and  $\mu^2$ ) with temperature ( $^{\circ}$ K) for paramagnetic isomers of (a) bis(*N*-methylsalicylaldiminine)nickel(II); (b) bis(*o*-hydroxyacetophenoimine)nickel(II); (c) bis(*N*-methyl-*o*-hydroxyacetophenimine)nickel(II); (d) bis(*o*-hydroxyacetophenimine)nickel(II).

(see Section III). At higher concentrations substances with lower moments were obtained. The above moments are rather lower than the fully developed moment ( $\mu \sim 3.2$  B.M.) previously found for the paramagnetic isomer of bis(*N*-methylsalicylaldiminine)nickel(II). Also, these three paramagnetic substances are readily soluble in chloroform from which they can be recrystallized in their original diamagnetic forms. This ready solubility would seem to eliminate the possibility of a polymeric structure of type (II) for these compounds.

The magnetic behaviour of these three paramagnetic forms is of a type not previously observed for bivalent nickel compounds for their magnetic moments exhibit a striking variation with temperature and decrease steadily from their room temperature values, quoted above, to 1.3–1.6 B.M. in the vicinity of

80 °K (see Fig. 1). These moments also rise with increasing temperature and reach values of 2.5–3.0 B.M. at 350 °K. It is even more instructive to plot  $\mu^2$  against temperature for the plots are linear below 250 °K with  $\mu^2$  approaching zero at 0 °K (see Fig. 1). This suggests that the three compounds may be diamagnetic in the region of absolute zero, but they become increasingly paramagnetic and approach a limiting value at higher temperatures.

At first sight it would appear that the observed magnetic behaviour of these compounds may arise from the existence of a lower singlet state ( $S=0$ ) and an upper triplet state ( $S=1$ ) separated by an energy interval of  $\sim 300 \text{ cm}^{-1}$ . This behaviour would be analogous to the type of solvent perturbations recently discussed by Maki (1958) and Ballhausen and Liehr (1959) and would lead to the expression

$$\mu^2 = 8[1 + \frac{1}{2} \exp(E/kT)]^{-1},$$

where  $E$  represents the energy separation between a diamagnetic ground state and a low-lying excited paramagnetic triplet. This equation reproduces the magnetic behaviour of the binuclear copper(II) alkanoates, in which singlet and

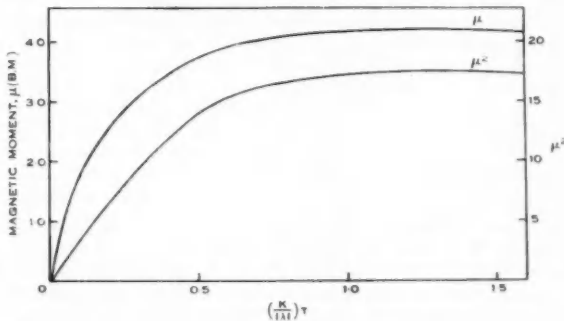


Fig. 2.—Variation of magnetic moment ( $\mu$  and  $\mu^2$ ) for tetrahedral nickel(II) in weak field.

triplet states are separated by some  $300 \text{ cm}^{-1}$  (see Figgis and Martin 1956; Martin and Waterman 1957). It does not, however, reproduce in correct detail the nearly linear variation with temperature of  $\mu^2$  observed here.

Yet another hypothesis which may be invoked to explain the anomalous magnetism of these compounds is the possibility that they have been thermally excited from the square to a tetrahedral conformation which is then maintained in a metastable condition by rapid quenching in the solid state. In this connection the unusual temperature dependence of their magnetic moments requires comment. Thus Figgis (1958) has recently discussed the magnetism of tetrahedral nickel(II) for the case in which the nickel(II) ion is surrounded by four identical ligands generating a weak field. He concludes that the magnetic moment for such an arrangement is given by the expression

$$\mu^2 = \frac{3[0.625x + 6.80 + (0.125x + 4.09) \exp(-3x) - 10.89 \exp(-9x/2)]}{x[5 + 3 \exp(-3x) + \exp(-9x/2)]},$$

where  $x = \lambda/kT$ ,  $\lambda$  representing the spin-orbit coupling constant for the free ion. Thus, at temperatures above c.  $0.3 |\lambda|/k$ , the magnetic moment is predicted to lie between 3.1 and 4.2 B.M. and at temperatures below this value, the moment should fall rapidly to zero as  $(k/|\lambda|)T \rightarrow 0$ , and in particular  $\mu^2$  should decrease nearly linearly to zero (see Fig. 2). The above three paramagnetic isomers approximate to this general type of magnetic behaviour. Their somewhat lower moments may be due to the presence of some of the original diamagnetic forms. In this connection it is of interest to report that the *N*-methyl-*o*-hydroxyacetophenimine complex was obtained in a paramagnetic form, with  $\mu$  varying from 3.7–4.6 B.M. by heating the diamagnetic compound at temperatures in the range 210–230 °C for 4–5 hr. Unfortunately, this procedure causes some decomposition with losses of a small percentage in weight. However, a plot of

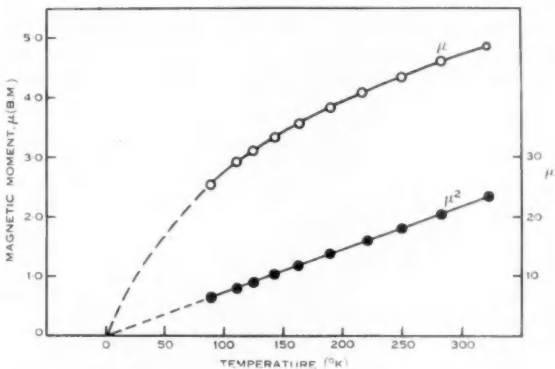


Fig. 3.—Variation of magnetic moment ( $\mu$  and  $\mu^2$ ) with temperature (°K) for paramagnetic isomer of bis(*N*-methyl-*o*-hydroxyacetophenimine)nickel(II) prepared by heating in the solid state.

$\mu$  v. temperature for a specimen obtained by heating at 230 °C for 4 hr and with a room temperature moment of  $\mu = 4.6$  B.M. per nickel atom is shown in Figure 3. This curve is strikingly similar to the previous curves in Figure 1 and seems to confirm the suggestion that quenching from boiling biphenyl produces paramagnetic forms still partly contaminated with diamagnetic starting material.

Unfortunately, the present anomalous magnetic behaviour does not provide a sufficiently critical criterion for distinguishing between a metastable tetrahedral nickel(II) complex and a tetragonal nickel(II) complex with closely lying singlet and triplet levels. It is apparent that a structural investigation of the paramagnetic compounds of type (V) is needed before any complete explanation of their magnetic properties can be forthcoming.

### III. EXPERIMENTAL

I. *Bis(salicylaldimine)nickel(II)*.—This compound was prepared by the method of Tyson and Adams (1940) and dried at 105 °C for 1 hr (Found: C, 56.4; H, 4.0; N, 9.3%. Calc. for  $C_{14}H_{12}O_2N_2Ni$ : C, 56.2; H, 4.1; N, 9.4%).

**II. Bis(N-methylesalicylaldimine)nickel(II).**—The dark green complex was prepared by the method of Klemm and Raddatz (1942). It was purified by recrystallization from chloroform and dried under vacuum over phosphoric oxide (Found : C, 58.7; H, 4.8; N, 8.7%. Calc. for  $C_{16}H_{16}O_4N_2Ni$  : C, 58.8; H, 4.9; N, 8.6%).

**III. Bis(N-ethylsalicylaldimine)nickel(II).**—This compound was prepared by the method of Sacconi, Paoletti, and del Re (1957) and purified by recrystallization from ethanol. The dark green crystals were dried at 105 °C for 1 hr (Found : C, 60.1; H, 5.5; N, 7.9%. Calc. for  $C_{17}H_{18}O_2N_2Ni$  : C, 59.9; H, 5.3; N, 8.2%).

**IV. Bis(N-phenylsalicylaldimine)nickel(II).**—This compound was prepared by a modification of the method used by Baeolo and Matoush (1953). A mixture of bis(salicylaldehyde)nickel(II) dihydrate (3 g), ethanol (5 ml), and aniline (2.5 ml) was refluxed for some time on the water-bath until the light green starting material was converted to olive green crystals of the required compound ; yield 2.37 g. The compound was recrystallized by dissolving it in chloroform and adding acetone to incipient turbidity (Found : C, 69.5; H, 4.5; N, 6.1%. Calc. for  $C_{28}H_{30}O_2N_2Ni$  : C, 69.2; H, 4.5; N, 6.2%). The compound is soluble in chloroform and benzene and insoluble in alcohol and acetone.

**V. Bis(salicylaldehyde)nickel(II) Dihydrate.**—The compound was prepared by the method of Tyson and Adams (1940), and dried *in vacuo* over phosphoric oxide (Found : C, 49.5; H, 4.1%. Calc. for  $C_{14}H_{16}O_4Ni \cdot 2H_2O$  : C, 49.9; H, 4.2%). The water of crystallization was held very firmly and only 1 mole of water was lost on heating the compound for 2 hr at 200 °C.

**VI. Bis(o-hydroxyacetophenimine)nickel(II).**—This compound was prepared by a modification of the method used by Pfeiffer, Buchholz, and Bauer (1931). A mixture of nickel(II) acetate tetrahydrate (0.88 g) dissolved in water (10 ml) and *o*-hydroxyacetophenone (1.84 g) dissolved in ethanol (15 ml) was refluxed for 10 min on the water-bath. Ammonium hydroxide (5 ml) was then added until the solution was alkaline followed by 5 ml in excess. The red precipitate was filtered, washed with water, ethanol, and ether ; yield, 1.1 g. The substance was recrystallized from chloroform and dried at 110 °C for 1 hr (Found : C, 59.0; H, 4.8; N, 8.7%. Calc. for  $C_{18}H_{16}O_2N_2Ni$  : C, 58.8; H, 4.9; N, 8.6%). The compound is sparingly soluble in chloroform, slightly soluble in benzene, and practically insoluble in ethanol and acetone.

**VII. Bis(N-methyl-o-hydroxyacetophenimine)nickel(II).**—Nickel(II) acetate tetrahydrate (0.88 g) was dissolved in water (10 ml) and filtered. A solution of *o*-hydroxyacetophenone (1.84 g) in 95% ethanol (10 ml) was added and the mixture refluxed for  $\frac{1}{2}$  hr on the water-bath when a bright green solution was obtained. To this solution was added a 33% solution of methylamine in ethanol (7 ml). The solution turned dark olive green and refluxing was continued for 2-3 hr until reddish brown crystals deposited. The compound was washed with ethanol and ether ; yield 0.89 g. It was recrystallized by dissolving it in chloroform and adding light petroleum to incipient turbidity. The reddish brown crystals were dried for 1 hr at 105 °C (Found : C, 60.8; H, 5.5; N, 7.8%. Calc. for  $C_{18}H_{20}O_2N_2Ni$  : C, 60.9; H, 5.7; N, 7.9%). The compound is soluble in chloroform, slightly soluble in benzene, and very slightly soluble in ethanol and acetone.

**VIII. Bis(o-hydroxyacetophenoxime)nickel(II).**—Hydroxylamine hydrochloride (5 g) was dissolved in water (20 ml) and 10% NaOH solution (7 ml) added. To the above solution *o*-hydroxyacetophenone (1.84 g) in ethanol (25 ml) was added and the mixture was refluxed for 15 min, cooled, and a solution of nickel(II) acetate tetrahydrate (0.88 g) in water (10 ml) added slowly with shaking. On diluting the reaction mixture with water to 150 ml a light green flocculent precipitate was formed. This was filtered, washed with water and ethanol, and dried ; yield 1.29 g. The compound was recrystallized from chloroform and dried for 1 hr at 105 °C (Found : C, 53.5; H, 4.2; N, 7.9%. Calc. for  $C_{18}H_{16}O_4N_2Ni$  : C, 53.5; H, 4.5; N, 7.8%). This substance is very soluble in chloroform, soluble in benzene, slightly soluble in acetone and light petroleum, and insoluble in ethanol.

**IX. The Reaction of Bis(salicylaldimine)nickel(II) with 1,10-Phenanthroline.**—A mixture of bis(salicylaldimine)nickel(II) (0.75 g; 0.0025M) and 1,10-phenanthroline (1.0 g; 0.005M) was heated under reflux with ethanol (25 ml) for about 30 min. The deep red solution was filtered and orange-yellow crystals were precipitated by the addition of ether ; yield 1.65 g. The compound was recrystallized by dissolving in ethanol and adding ether to incipient crystallization.

The crystals were filtered, washed with ether, and dried at 105 °C for 1 hr (Found : C, 64·5; H, 4·3; N, 9·7; Ni, 8·1%). Calc. for  $C_{38}H_{26}O_3N_4Ni \cdot 3H_2O$  : C, 64·0; H, 4·5; N, 9·8; Ni, 8·2%). The compound is soluble in chloroform and ethanol and insoluble in ether and light petroleum.

X. *Bis(1,10-Phenanthroline)-bis(salicylaldehyde)nickel(II) Trihydrate*.—A mixture of bis(salicylaldehyde)nickel(II) dihydrate (0·64 g; 0·002M), 1,10-phenanthroline (0·80 g; 0·004M) and ethanol (20 ml) was refluxed on the water-bath for a short time. The resulting greenish brown solution was filtered and on the addition of ether reddish brown crystals were formed. The compound was recrystallized by dissolving it in ethanol and adding ether to incipient crystallization and dried at 110 °C (Found : C, 64·1; H, 4·3; N, 8·0; Ni, 8·2%). Calc. for  $C_{38}H_{26}O_4N_4Ni \cdot 3H_2O$  : C, 63·8; H, 4·5; N, 7·8; Ni, 8·2%). The compound dissolves in warm water forming a yellow solution.

TABLE 3  
MAGNETIC SUSCEPTIBILITIES

Compound	Temp. (°K)	$10^6 \times \chi_s$	$10^6 \times \Delta$	$10^6 \times \chi_M$	$\mu$ (B.M.)
I	297	-0·067			0
II	293	-0·079			0
III	296	-0·042			0
IV	297	-0·0016			0
V	298	12·48	-161	4366	3·23
VI	296	-0·257			0
VII	296	-0·338			0
VIII	294	-0·326			0
IX	297	5·595	-436	4427	3·25
X	296	5·464	-430	4338	3·22
XI	292	5·786	-376	4235	3·16
XII	293	7·231	-297	4095	3·11
XIII	297	7·652	-320	4417	3·25
XIV	301	5·927	-358	4099	3·16
XV	299	7·003	-314	4126	3·15
XVI	302	7·375	-290	4267	3·23

XI. *Preparation of the Monoperchlorate from Compound (x).*—Bis(1,10-phenanthroline)bis(salicylaldehyde)nickel(II) trihydrate (0·8 g) was dissolved in water (300 ml) at 70–80 °C with continuous stirring. The greenish yellow solution was filtered hot and treated dropwise with sodium perchlorate (5 g) solution (10 ml) at 70 °C. The greenish yellow perchlorate was filtered off at 40 °C, washed several times with cold water followed by ether, and dried in a vacuum over  $P_2O_5$ . Yield 0·76 g (Found : C, 55·6; H, 3·3; N, 8·7; Ni, 8·8%). Calc. for  $C_{31}H_{21}O_6N_4Ni \cdot 1 \cdot 5H_2O$  : C, 55·9; H, 3·6; N, 8·4; Ni, 8·8%). This compound is very soluble in ethanol.

XII. *1,10-Phenanthroline-bis(N-methylsalicylaldimine)nickel(II) Monohydrate*.—A solution of bis(N-methylsalicylaldimine)nickel(II) (0·8 g) in hot benzene (100 ml) was treated with a benzene solution (10 ml) of 1,10-phenanthroline (0·8 g). The compound precipitated in the form of small buff coloured crystals which were washed with acetone and dried in a vacuum over  $P_2O_5$ . Yield 1·0 g (Found : C, 64·1; H, 5·1; N, 10·9%). Calc. for  $C_{38}H_{24}O_2N_4Ni \cdot H_2O$  : C, 64·0; H, 5·0; N, 10·7%). The compound lost its water of crystallization on heating to 130–140 °C for 1 hr (Found : C, 66·6; H, 4·7%). Calc. for  $C_{28}H_{24}O_2N_4Ni$  : C, 66·3; H, 4·8%).

XIII. *1,10-Phenanthroline-bis(N-ethylsalicylaldimine)nickel(II) Monohydrate*.—Bis(N-ethylsalicylaldimine)nickel(II) (0·71 g) was dissolved in benzene (5 ml) and a benzene solution (5 ml)

of 1,10-phenanthroline (0.36 g) was added. The compound precipitated in the form of a pale greenish buff microcrystalline powder and was washed with ethanol and ether; yield 0.75 g. The substance was recrystallized from ethanol and dried for 1 hr at 105 °C (Found : C, 65.1 ; H, 5.8 ; N, 10.0%). Calc. for  $C_{30}H_{28}O_2N_4Ni\cdot H_2O$  : C, 65.1 ; H, 5.5 ; N, 10.1%.

XIV. *1,10-Phenanthroline-bis(N-phenylsalicylaldimine)nickel(II)*.—Bis(*N*-phenylsalicylaldimine)nickel(II) (0.45 g) was dissolved in hot benzene (15 ml) and a solution of 1,10-phenanthroline (0.18 g) in benzene (5 ml) added. Light green, shiny crystals precipitated immediately; yield 0.38 g. The compound was recrystallized by dissolving in chloroform and adding ethanol to incipient crystallization (Found : C, 71.7 ; H, 4.3 ; N, 8.8%). Calc. for  $C_{38}H_{36}O_2N_4Ni$  : C, 72.3 ; H, 4.5 ; N, 8.9%). The compound is insoluble in benzene.

XV. *1,10-Phenanthroline-bis(N-methyl-o-hydroxyacetophenimine)nickel(II) Hemihydrate*.—Bis(*N*-methyl-o-hydroxyacetophenimine)nickel(II) (0.35 g) suspended in hot benzene (20 ml) was treated with a benzene solution (15 ml) of 1,10-phenanthroline (0.198 g). The mixture was stirred without further heating until the reddish brown crystals of the original compound dissolved

TABLE 4  
ROOM TEMPERATURE MAGNETIC MOMENTS OF PARAMAGNETIC ISOMERS  
OBTAINED FROM BIPHENYL SOLUTIONS

Compound	Conc. of Compound in Biphenyl (%)	Temp. (°K)	$\mu$ (B.M.)
VI	$\begin{cases} 3.8 \\ 2.0 \\ 1.9 \end{cases}$	291	1.64
		289	2.05
		291	2.35*
VII	$\begin{cases} 7.0 \\ 4.7 \\ 2.0 \end{cases}$	290	1.39
		293	2.51
		289	2.45*
VIII	$\begin{cases} 2.5 \\ 2.0 \end{cases}$	292	1.75
		294	2.80*

\* These preparations were used for the magnetic measurements at various temperatures in Table 5.

and a red solution formed. On cooling yellow needle-shaped crystals precipitated. They were filtered and washed with benzene; yield 0.43 g. The compound was not recrystallized because it readily decomposed even on slight heating. It was dried in a vacuum over  $P_2O_5$ . It crystallizes as the hemihydrate (Found : C, 66.2 ; H, 5.4 ; N, 10.4%). Calc. for  $C_{30}H_{28}O_2N_4Ni\cdot 0.5H_2O$  : C, 66.2 ; H, 5.4 ; N, 10.3%). An attempt to remove the water of crystallization at 56 °C in a vacuum over  $P_2O_5$  caused partial decomposition of the compound.

XVI. *1,10-Phenanthroline-bis(o-hydroxyacetophenimine)nickel(II)*.—Bis(*o*-hydroxyacetophenimine)nickel(II) (0.718 g) was dissolved in boiling benzene (30 ml) and a solution of 1,10-phenanthroline (0.396 g) dissolved in benzene (15 ml) added to it. The green coloured solution turned reddish brown and on cooling and adding acetone bluish green crystals were deposited. The compound was washed with acetone (yield 0.5 g) and recrystallized from chloroform by adding acetone to incipient precipitation. The recrystallized compound was dried in a vacuum over  $P_2O_5$  at 100 °C for 1 hr (Found : C, 62.1 ; H, 4.6 ; N, 10.2%). Calc. for  $C_{28}H_{24}O_4N_4Ni$  : C, 62.3 ; H, 4.5 ; N, 10.4%).

*Preparation of Paramagnetic Isomers*

Paramagnetic isomers were prepared from compounds VI, VII, and VIII by using the same general method : the compound was ground with biphenyl in a mortar, using a pestle, and transferred into a large Pyrex tube ; the tube was then heated on a sand-bath to the boiling point of the biphenyl and refluxed for about 10 min to dissolve the substance completely. The solution was rapidly cooled by pouring it into a cold silica dish, pulverized and extracted in a Soxhlet apparatus with light petroleum until the substance was free of biphenyl. It was observed that

TABLE 5  
VARIATION OF THE MAGNETIC MOMENTS OF THE PARAMAGNETIC ISOMERS WITH TEMPERATURE

Compound	Temp. (°K)	$10^6 \times \gamma_g$	$10^6 \times \gamma_M$ (corr.)	$\mu$ (B.M.)	$\mu^a$
VI (from biphenyl)	127.5	7.14	2486	1.60	2.56
	176.5	6.99	2438	1.86	3.46
	229.0	6.88	2402	2.11	4.45
	275.0	6.80	2375	2.30	5.29
	323.0	6.57	2301	2.45	6.00
VII (from biphenyl)	120.5	7.41	2790	1.65	2.72
	205.0	7.04	2660	2.10	4.41
	243.0	7.04	2660	2.28	5.20
	275.0	6.80	2574	2.39	5.71
	319.0	6.55	2485	2.53	6.40
	357.0	6.20	2361	2.61	6.81
VIII (from biphenyl)	85.0	10.22	3828	1.62	2.62
	114.0	9.61	3608	1.82	3.31
	153.5	9.20	3462	2.07	4.29
	205.5	9.11	3430	2.38	5.66
	260.0	8.94	3368	2.66	7.08
	311.0	8.70	3282	2.87	8.24
VII (by heating in the solid state)	87.0			2.58	6.66
	110.0			2.92	8.53
	123.0			3.09	9.55
	143.0			3.34	11.16
	162.0			3.53	12.46
	190.0			3.80	14.44
	220.0			4.10	16.81
	249.0			4.35	18.92
	282.0			4.59	21.07
	321.0			4.87	23.72

if the concentration of the compound in biphenyl is higher than 2% smaller moments are obtained (see Table 4). The colour of the paramagnetic compounds is similar to the original diamagnetic ones but lighter in shade.

Compound VI was obtained as a light red microcrystalline powder (Found : C, 58.2 ; H, 4.7 ; N, 8.7%. Calculated for  $C_{16}H_{16}O_2N_2Ni$  : C, 58.7 ; H, 4.9 ; N, 8.6%).

Compound VII was obtained as a fine light brown powder (Found : C, 60.4 ; H, 5.4 ; N, 7.7%. Calc. for  $C_{18}H_{20}O_2N_2Ni$  : C, 60.9 ; H, 5.7 ; N, 7.9%).

Compound VIII was obtained as a fine pale green powder. It was found that, in this case, the biphenyl had to be removed by several extractions using cold light petroleum, because the

compound was very soluble in a hot mixture of biphenyl and light petroleum even though it was only sparingly soluble in light petroleum alone (Found : C, 53.4 ; H, 4.3 ; N, 7.6%. Calc. for  $C_{18}H_{18}O_4N_2Ni$  : C, 53.5 ; H, 4.5 ; N, 7.8%).

#### *Magnetic Measurements*

These were made by the Gouy method. The gram susceptibility  $\chi_g$ , the molar susceptibility  $\chi_M$  (corrected for the underlying diamagnetism of all atoms,  $\Delta$ ) and the magnetic moment  $\mu$  are set out in Table 3. The measurements for the paramagnetic isomers of compounds VI, VII, and VIII are summarized in Tables 4 and 5.

#### IV. ACKNOWLEDGMENT

The authors wish to thank Dr. E. Challen, The University of New South Wales, for the microanalytical determination of carbon, hydrogen, and nitrogen.

#### V. REFERENCES

- BALLHAUSEN, C. J., and LIEHR, A. D. (1959).—*J. Amer. Chem. Soc.* **81** : 538.
- BASOLO, F., and MATOUSH, W. R. (1953).—*J. Amer. Chem. Soc.* **75** : 5663.
- BJERRUM, J., and JORGENSEN, C. K. (1956).—*Rec. Trav. Chim. Pays-Bas* **75** : 658.
- CLARK, H. C., and ODELL, A. L. (1955).—*J. Chem. Soc.* **1955** : 3431.
- CLARK, H. C., and ODELL, A. L. (1956).—*J. Chem. Soc.* **1956** : 520.
- COTTON, F. A., and BANNISTER, E. (1960).—*J. Chem. Soc.* **1960** : 1873.
- COTTON, F. A., BANNISTER, E., BARNES, R., and HOLM, R. H. (1959).—*Proc. Chem. Soc.* **1959** : 158.
- FIGGIS, B. N. (1958).—*Nature* **182** : 1568.
- FIGGIS, B. N., and MARTIN, R. L. (1956).—*J. Chem. Soc.* **1956** : 3837.
- FRASSON, E., and SACCONI, L. (1958).—“Chemistry of the Coordination Compounds—A Symposium.” p. 443. (Pergamon Press : London and New York.)
- GILL, N. S., and NYHOLM, R. S. (1959).—*J. Chem. Soc.* **1959** : 3977.
- GILL, N. S., NYHOLM, R. S., and PAULING, P. (1958).—*Nature* **182** : 168.
- HARRIS, C. M., LENZER, S. L., and MARTIN, R. L. (1958).—*Aust. J. Chem.* **11** : 331.
- HARRIS, C. M., NYHOLM, R. S., and PHILLIPS, D. J. (1960).—*J. Chem. Soc.* **1960** : 4379.
- HOLM, R. H., and MCKINNEY, T. M. (1960).—*J. Amer. Chem. Soc.* **82** : 5506.
- KLEMM, W., and RADDATZ, R. R. (1942).—*Z. anorg. Chem.* **250** : 121-228.
- MAKI, G. (1958).—*J. Chem. Phys.* **29** : 1129.
- MARTIN, R. L., and WATERMAN, H. (1957).—*J. Chem. Soc.* **1957** : 2545.
- NYHOLM, R. S. (1953).—*Chem. Rev.* **53** : 263.
- PFEIFFER, P., BUCHHOLZ, E., and BAUER, O. (1931).—*J. prakt. Chem.* **129** : 172.
- SACCONI, L., CINI, R., CAMPOLINI, M., and MAGGIO, F. (1960).—*J. Amer. Chem. Soc.* **82** : 3487.
- SACCONI, L., PAOLETTI, P., and CINI, R. (1958).—“Chemistry of the Coordination Compounds—A Symposium.” p. 492. (Pergamon Press : London and New York.) (See also *J. Amer. Chem. Soc.* **80** : 3583 (1958).)
- SACCONI, L., PAOLETTI, P., and DEL RE, G. (1957).—*J. Amer. Chem. Soc.* **79** : 4062.
- TYSON, G. N., and ADAMS, S. C. (1940).—*J. Amer. Chem. Soc.* **62** : 1228.
- VENANZI, L. M. (1958).—*J. Chem. Soc.* **1958** : 719 (see also Powell, H. M., and Venanzi, L. M. (1956).—*Proc. Chem. Soc.* **1956** : 6).
- WILLIS, J. B., and MELLOR, D. P. (1947).—*J. Amer. Chem. Soc.* **69** : 1237.

## SYNTHESIS OF SOME DERIVATIVES OF ISOTHIOCYANIC ACID CONTAINING SULPHUR-35

By C. J. MOYE\*

[Manuscript received March 7, 1961]

### Summary

Phenylisothiocyanate-<sup>35</sup>S and n-dodecylisothiocyanate-<sup>35</sup>S have been synthesized and a number of thiourea derivatives of phenylisothiocyanate-<sup>35</sup>S have been prepared. n-Dodecylisothiocyanate-<sup>35</sup>S has been converted routinely into 1-n-dodecylthiourea for the evaluation of sulphur exchange kinetics.

### I. INTRODUCTION

The translocation of a series of radioactive compounds containing substituent groups of varying polarity was to be studied in bean plants by autoradiographic and paper chromatographic methods. A thiourea series was chosen for various reasons and it was hoped to correlate the "relative rates" of movement of these compounds with physical properties such as their oil-water partition. It was appreciated that only gross differences in the transport rate would be detected in this way, but it was anticipated that this work would indicate the direction future investigations should take.

Chin-Tzu Peng (1958)† reported the synthesis of phenylisothiocyanate-<sup>35</sup>S by sulphur exchange without giving experimental details. Previously three <sup>35</sup>S-labelled thioureas had been prepared and no satisfactory synthesis of phenylisothiocyanate-<sup>35</sup>S had been reported. Thiourea-<sup>35</sup>S had been synthesized by treating cyanamide with hydrogen sulphide-<sup>35</sup>S (Murphy and Williams 1958) while 1-phenylthiourea-<sup>35</sup>S and 1,3-diphenylthiourea-<sup>35</sup>S had been prepared by sulphur exchange reactions (Guryanova 1954). Phenylisothiocyanate-<sup>35</sup>S had been prepared in 10% yield by the reaction of phenylisothiocyanate with ammonium hydrogen sulphide-<sup>35</sup>S and decomposition of the resulting ammonium phenyldithiocarbamate-<sup>35</sup>S (Wieland, Merz, and Rennecke 1958).

Phenylisothiocyanate is normally prepared by the reaction of lead ions on ammonium phenyldithiocarbamate but the reported macroscale yield could not be realized on the microscale. Other unsuccessful approaches involved the direct synthesis of 1-phenylthiourea by heating ammonium phenyldithiocarbamate in concentrated ammonia solution (when 1,3-diphenylthiourea was formed) and in copper tetrammine sulphate solution. In the last case the yield of impure product never exceeded 50%. Further utilization of the 1-phenylthiourea following the method of Cymerman-Craig *et al.* (1954) would have resulted in the simul-

\* I.C.I.A.N.Z. Central Research Laboratories, Ascot Vale, Victoria; present address: C.S.R. Research Laboratories, Pyrmont, N.S.W.

† This book appeared as the present work neared completion.

taneous preparation of phenylisothiocyanate and 1,3-diphenylthiourea. The method finally chosen was the reaction of ethyl chloroformate with the triethylamine salt of phenyldithiocarbamic- $^{35}\text{S}$  acid to give the ethoxycarbonyl ester which spontaneously decomposed to the isothiocyanate in a yield of 75% based on carbon disulphide- $^{35}\text{S}$ .

Ethyl chloroformate reacted smoothly with the triethylamine salt of phenyldithiocarbamic acid on the semi-microscale and the reaction was readily adaptable to gas-line work. Caking of the triethylamine hydrochloride produced in the reaction occasionally interfered with the distillation of the phenylisothiocyanate; nevertheless yields approaching 80% were usually obtained. Six thioureas were prepared from the phenylisothiocyanate- $^{35}\text{S}$  by reaction with various amines. These condensations were effected in moderate to good yields on the semi-microscale, and where possible, the purity of the product was determined by paper chromatography (Kjaer and Rubenstein 1953; and Table 1 present paper).

TABLE I  
THIOUREA CHARACTERIZATION

Compound	Melting Point (°C uncorr.)	$R_F$ Values (Kjaer and Rubenstein 1953)
I 1-Phenyl-3-(2'-hydroxyethyl)thiourea (Knorr and Roessler 1903)	138	0·65
II 1-Phenyl-3-(2'-hydroxyethyl)thiourea .. ..	96-97	0·49
III 1-Phenyl-3-(2'-ethylhexyl)thiourea .. ..	48-50	1·00
IV 1-Phenyl-3-cyclohexylthiourea (Skita and Rolfs 1920)	150-151	1·00
V 1,3-Diphenylthiourea .. .. .. ..	154-155	1·00
VI N-(N'-phenyl)thiocarbamoylmorpholine (Henry and Dehn 1950)	130·5	0·93

Translocation experiments were carried out with these thioureas but they proved to be unsatisfactory compounds for this purpose due to the lability of the sulphur. It was not possible to recover compounds 1 and 2 (Table 1) from macerated plant tissue. Subsequent unpublished work has supported our finding that compounds containing sulphur doubly bonded to carbon should be used with caution in biological experiments.

n-Dodecylisothiocyanate- $^{35}\text{S}$  was prepared by a sulphur exchange reaction, in the absence of solvent at a temperature of approximately 165 °C. The kinetics of the exchange were first investigated in the normal way and the preparative run was performed on the basis of these results. Activated copper prepared by the method of Blumer (1957) proved to be an excellent scavenger of inorganic sulphur, which would otherwise have interfered with the counting of the thiourea derivative of n-dodecylisothiocyanate- $^{35}\text{S}$ . The exchange samples were placed directly onto a column of activated copper and eluted with ethanol. The thiourea was prepared "in situ" in the eluate by the addition of aqueous ammonia and

warming. The exchange reaction obeyed zero-order kinetics but was considered to be of pseudo-zero order, as special conditions existed wherein the chemical concentration of all the reactants remained constant (Kirk and Othmer 1953).

## II. EXPERIMENTAL

Melting points are uncorrected. Light petroleum has b.p. 40–70 °C. Radioactive assays were carried out at infinite thickness in a 1 cm<sup>2</sup> planchette (Popjak 1950). Activated copper was prepared by the method of Blumer (1957). Microanalyses were carried out by Dr. K. W. Zimmerman and associates, C.S.I.R.O. and University of Melbourne Microanalytical Laboratory; and chromatography of thioureas by Kjaer and Rubenstein's (1953) method.

(a) *Phenylisothiocyanate-<sup>35</sup>S*.—Triethylamine (222 mg; 2.2 mmoles), aniline (186 mg; 2 mmoles), and absolute ethanol (approx. 4 ml) were added to the reaction vessel (Fig. 1). The carbon disulphide-<sup>35</sup>S (152 mg; 20·60 mc) was contained in two breakseal vessels which were attached to the vacuum system at A and C. The carbon disulphide-<sup>35</sup>S was distilled into the

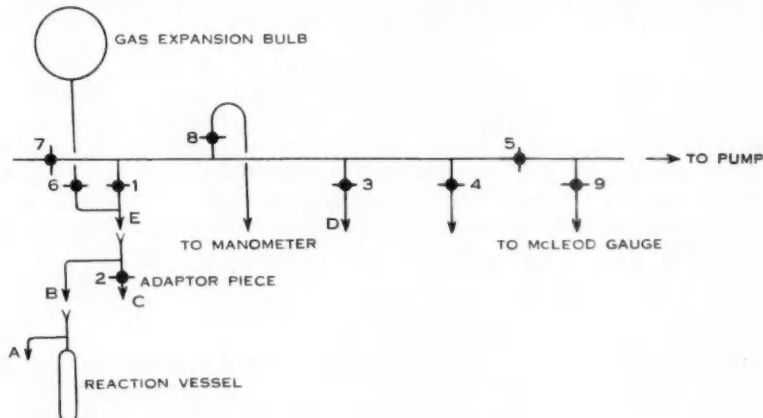


Fig. 1.—Vacuum line arrangement.

reaction vessel in the usual way, and after a lapse of 30 min the two carbon disulphide containers were sealed off, the vacuum released, and the reaction vessel (with the breakseal cap still in place) removed and securely stoppered. The reactants, with occasional shaking, were allowed to warm up and stand at room temperature for 2 hr. A copious precipitate formed during this time. The contents of the reaction vessel were refrozen, the cap on A replaced by the tared container which was to receive the phenylisothiocyanate, and the whole replaced on B. The cap on C was also replaced by a "Quickfit" test tube with a constricted neck. After evacuating, the ethanol, triethylamine in excess, and unreacted carbon disulphide-<sup>35</sup>S were distilled into the vessel on C, which was sealed off for disposal. The cap on C was replaced by another identical constricted neck test tube and ethyl chloroformate (5 ml) was transferred to the reaction vessel in the usual way. With tap 1 closed and tap 6 open (to guard against excessive pressure developing in the system) the ethyl chloroformate was allowed to react with the triethylamine salt overnight. The carbon oxysulphide, ethanol, and unreacted ethyl chloroformate were then distilled into the container on C which was sealed off for disposal. The distillation was carried out slowly and

\* The synthesis was carried out in a well-ventilated hood, and every effort was made to keep mercury vapour out of the line.

carefully over a period of 2 hr to prevent bumping. The remaining material was now refrozen and evacuated to  $10^{-5}$  to  $10^{-6}$  mm pressure. The phenylisothiocyanate distilled over slowly on warming at 70–80 °C. It was found necessary to refreeze and re-evacuate on occasions to aid the distillation. The phenylisothiocyanate was purified by passage in light petroleum through a short column of deactivated alumina (B.D.H. laboratory grade containing 5% by weight of 10% acetic acid) using 3 g alumina per 200 mg of compound, and recovered after elution, by evaporation. The compound travelled with the solvent front. The reaction vessel was left standing for 48 hr with inactive phenylisothiocyanate (320 mg) in light petroleum (10 ml). Recovery of the light petroleum and passage through deactivated alumina yielded a further active product (307 mg) which was compared with the distilled product by a comparative assay of derived thioureas. The dilution factor was calculated to be 1 : 5.67. The diluted product was therefore equivalent to 56 mg of the more active material. The total yield was 202 mg (75%).

(b) *1-Phenyl-3-(2'-hydroxyethyl)thiourea- $^{35}\text{S}$ .*—Phenylisothiocyanate- $^{35}\text{S}$  (36.4 mg) in light petroleum (2 ml) was treated with ethanalamine (16.5 mg) in ethanol (1 ml). The mixture was warmed for 1 min at 60–70 °C and allowed to stand. After several minutes, fine colourless crystals separated out. These were recrystallized once from ethanol to yield chromatographically pure thiourea (21 mg). All the mother liquors were mixed and the total activity recovered by successive dilutions and recrystallizations. In this way a number of specimens of the one thiourea with varying activities was obtained.

(c) *1-Phenyl-3-di(2'-hydroxyethyl)thiourea- $^{35}\text{S}$ .*—Diethanalamine (28.4 mg) in a mixture of ethyl acetate/benzene (3 : 1, 1 ml) was added to phenylisothiocyanate- $^{35}\text{S}$  (36.4 mg) in light petroleum (2 ml) and the solution was warmed until most of the petrol had evaporated. The solution was seeded, and deposited clumpy colourless needles of the thiourea, which were recrystallized from the ethyl acetate/benzene mixture to yield a chromatographically pure compound (12.0 mg) (Found : C, 55.0%; H, 6.8%. Calc. for  $\text{C}_{11}\text{H}_{14}\text{N}_2\text{O}_2\text{S}$  : C, 55.0%; H, 6.6%). The remaining activity was recovered by the dilution method as above.

(d) *1-Phenyl-3-(2'-ethylhexyl)thiourea- $^{35}\text{S}$ .*—2-Ethylhexylamine (34.8 mg) was treated directly with phenylisothiocyanate- $^{35}\text{S}$  (36.4 mg) in light petroleum (4 ml) and the mixture warmed for several minutes. The product repeatedly separated as an oil. Eventually a small amount of solid was obtained and was recrystallized from light petroleum to give a microcrystalline colourless solid (6.0 mg). Successive dilutions with pure inactive thiourea gave more readily crystallizable material (Found : C, 68.3%; H, 9.1%. Calc. for  $\text{C}_{15}\text{H}_{24}\text{N}_2\text{S}$  : C, 68.2%; H, 9.1%). (In practice runs little difficulty was experienced with this compound.)

(e) *1-Phenyl-3-cyclohexylthiourea- $^{35}\text{S}$*  (*Skita and Rolfs 1920*).—Phenylisothiocyanate- $^{35}\text{S}$  (50 mg) in light petroleum (2 ml) was warmed for 2 min with cyclohexylamine (36.7 mg) in ethanol (1 ml). The thiourea separated in large cubes on standing and was recrystallized from ethanol to give a pure product (49.0 mg). The remainder of the activity was recovered by dilution techniques.

(f) *1,3-Diphenylthiourea- $^{35}\text{S}$ .*—Phenylisothiocyanate- $^{35}\text{S}$  (50 mg) was treated with aniline (34.4 mg) in ethanol (1 ml) and the mixture warmed and allowed to stand. The product was recrystallized from ethanol to yield colourless plates (47.0 mg) and the remaining activity was also recovered from the mother liquors by the dilution method.

(g) *N-(N'-phenyl)thiocarbamoylmorpholine- $^{35}\text{S}$*  (*Henry and Dehn 1950*).—Morpholine (32.2 mg) in ethanol (1 c.c.) was added to phenylisothiocyanate- $^{35}\text{S}$  (50 mg) and an immediate precipitate formed. Recrystallization from ethanol gave chromatographically pure colourless needles (41 mg). Isotopic dilution recovered the remainder of the activity.

(h) *Kinetic Studies.*—A tube containing n-dodecylisotiocyanate (4.34 g) was heated in a boiling mesitylene vapour-bath for 15 min. A platinum boat containing radioactive sulphur dissolved in o-xylene (3.60 mg solution containing 0.0173 mg  $^{35}\text{S}$  = 0.053 mc) was added quickly to the n-dodecylisothiocyanate and the solution mixed by removing the reaction vessel, shaking rapidly, and replacing. Samples (250–300 mg) were taken at various time intervals and added directly to a column of activated copper packed in ethanol. Each sample was washed into the column with ethanol and eluted by ethanol after a residence time of approximately 15 min. In the initial run the thiourea derivative was prepared "in situ" in the eluted solution by the addition

of ammonia solution ( $d=0.880$ ) with warming. In the final run the n-dodecylisothiocyanate- $^{35}\text{S}$  was distilled before the derivative was prepared.

(i) *Derivative Preparation*.—The n-dodecylisothiocyanate- $^{35}\text{S}$  eluate (approx. 30 ml containing 250–300 mg isothiocyanate- $^{35}\text{S}$ ) was treated with  $\text{NH}_3$  soln. (3–4 ml;  $d=0.880$ ), and warmed until all cloudiness disappeared. The solution was then set aside to crystallize. Ethyl acetate and aqueous ethanol were used successively as recrystallizing solvents until the derivative had a constant specific radioactivity (i.e. the count rate of the sample did not vary by more than  $\pm 1\%$  ( $1\sigma$ ) between each of three successive recrystallizations).

(j) *n-Dodecylisothiocyanate -  $^{35}\text{S}$* .—n-Dodecylisothiocyanate (2.75 g) was heated at  $163.5 \pm 0.5^\circ\text{C}$  with a solution of  $^{35}\text{S}_8$  in *o*-xylene (0.43 g solution  $\equiv 3.97$  mc  $^{35}\text{S}_8$ ) for 4 hr. The product in ethanol was passed through a copper column and distilled (b.p. 0.01 mm =  $98$ – $104^\circ\text{C}$ ).

### III. ACKNOWLEDGMENTS

I wish to thank Mr. D. Fieldhouse and Mr. K. Napier for technical assistance, and the Directors of I.C.I.A.N.Z. for permission to publish this work.

### IV. REFERENCES

BLUMER, M. (1957).—*Analyt. Chem.* **29**: 1039.  
CHIN-TZU, P. (1958).—“Liquid Scintillation Counting.” 1st Ed. p. 198. (Pergamon Press: London.)  
CYMERMAN-CRAIG, J. ET AL. (1954).—*Chem. & Ind.* **27**: 785.  
GURYANOVA, E. W. (1954).—*J. Phys. Chem. U.S.S.R.* **28**: 67.  
HENRY, R. A., and DEHN, W. M. (1950).—*J. Amer. Chem. Soc.* **72**: 2806.  
KIRK, R. E., and OTHMER, D. F. (1953).—“Encyclopedia of Chemical Technology.” Vol. 11, p. 576. (Interscience Publishers Inc.: New York.)  
KJAER, A., and RUBENSTEIN, K. (1953).—*Acta Chem. Scand.* **7**: 528.  
KNORR, L., and ROESSLER, P. (1903).—*Chem. Ber.* **36**: 1280.  
MURRAY, A., and WILLIAMS, D. (1958).—“Organic Syntheses with Isotopes.” 1st Ed. Pt. II, p. 1942. (Interscience Publishers Inc.: New York.)  
POPJAK, J. (1950).—*Biochem. J.* **46**: 560.  
SKITA, A., and ROLFES, H. (1920).—*Chem. Ber.* **53**: 1247.  
WIELAND, T., MERZ, H., and RENNECKE, A. (1958).—*Chem. Ber.* **91**: 683.

## DEUTERIUM EXCHANGE REACTIONS WITH SUBSTITUTED AROMATICS

### II. THE MONOHALOGENATED BENZENES AND NAPHTHALENES

By J. L. GARNETT\* and W. A. SOLLICH\*

[Manuscript received December 2, 1960]

#### Summary

The platinum-catalysed exchange between heavy water and the monohalogenated benzenes and naphthalenes has been studied at 130–180 °C. Rate of exchange is found to decrease with increasing size of halogen substituent. Naphthalene derivatives exchange more slowly than the corresponding members of the benzene series. Rate of exchange increases with increasing ionization potential. From this correlation it is postulated that chemisorption of aromatic molecules on active platinum occurs through  $\pi$ -complex formation. In the benzene series, exchange in the *ortho*-position is slower than in the *meta*- or *para*-positions which react at approximately the same speed. *ortho*-Exchange increases with increasing size of halogen substituent. This deuteration technique is applicable to tritium labelling especially for aromatics since radiochemical by-product formation is minimized.

#### I. INTRODUCTION

In a previous paper of this series (Brown and Garnett 1958a, 1958b) the transition-metal catalysed exchange of aromatic hydrogens in substituted benzenes with deuterium oxide has been reported. Confirmatory evidence of the technique using benzoic acid as an example has also been published (Le Noble and Wheland 1958).

During an investigation designed to study some aspects of the mechanism of the reaction, a series of heterogeneous exchange experiments has been performed on the monohalogenated benzenes and naphthalenes. The results are reported in the present paper.

Previous work in this field, which involved a study of the fundamental aspects of heterogeneous catalysis, has been essentially confined to hydrocarbons. Two theories which differ in the nature of the proposed bond in chemisorption have been developed. These bonds are exemplified by the dissociative mechanism of Farkas and Farkas (1933) and the associative mechanism of Horuiti and Polanyi (1934). More recently modified versions of the above mechanisms have been proposed (Twigg 1939; Twigg and Rideal 1939; Beek 1945; Jenkins and Rideal 1955). The dissociative mechanism postulates an attachment via a ruptured C–H bond, while the associative mechanism visualizes chemisorption as occurring through the opening of a double bond. It is generally accepted that exchange of saturated hydrocarbons proceeds via the dissociative mechanism; however, no agreement has been reached on exchange involving unsaturated hydrocarbons (Taylor 1957). The difficulty associated with a satisfactory inter-

\* Department of Physical Chemistry, The University of New South Wales, Broadway, N.S.W.

TABLE I  
EXCHANGE REACTIONS OF MONOHALOGENATED BENZENES AND NAPHTHALENES

Run	Exchange Time (hr)	Temperature (°C)	Weight of $\text{PbO}_2$ (mg)	Quantity of $\text{D}_2\text{O}$ ( $\text{mole} \times 10^{-2}$ )	Compound Benzene	Quantity of Compound ( $\text{mole} \times 10^{-2}$ )	Theoretical Equilibrium Deuterium Content (%)	Reaction Completion (%)
1	46.5	130	100	2.5	Fluoro-Chloro-Bromo-Iodo-	1.0 1.0 1.0 1.0	50 50 50 50	82 66 2-4 0.0
2	47.0	130	100	7.5	Fluoro-Chloro-Bromo-Iodo-	3.0 3.0 3.0 3.0	50 50 50 50	86 74 2-4 0.0
3	22.0	130	100	7.5	Fluoro-Chloro-	1.5 1.5	66 66	90 24
4	3.5	130	100	7.5	Fluoro-Benzene	3.0 3.0	50 40	56 75
5	4.5	180	100	7.5	Bromo-Iodo-	1.5 1.5	66 66	8 1-2
6	7.2	130	100	7.0	Naphthalene Chloronaphthalene Bromonaphthalene	1.0 1.0 1.0	65 69 69	15 22 6

pretation of our results using either theory, has led us to consider the possibility that chemisorption of unsaturated hydrocarbons on a platinum catalyst occurs via non-integral bond formation, similar to that found in  $\pi$ -complexes.

## II. EXPERIMENTAL

Exchange reactions were carried out at 130 °C, or higher temperatures, by shaking evacuated tubes containing platinum catalyst (prereduced with deuterium gas), deuterium oxide, and the organic substrate. Deuterium oxide was used in preference to deuterium gas since the latter by simultaneous hydrogenation of the species complicates the identification of the deuterated products.\*

A quantitative estimation of exchange was obtained from infrared spectrometry of the organic compounds. In this respect the 700–900 and the 2200–3100  $\text{cm}^{-1}$  regions are of particular interest. It has been shown (Whiffen and Thompson 1945) that three absorption bands characteristic of *ortho*-, *meta*-, and *para*-substituted benzenes appear at 750–780, 790–810, and 820–850  $\text{cm}^{-1}$ , respectively. These bands are very intense, and of approximately equal intensity (Choptin and Nance 1951). Thus a ready method is available for the detection of low deuterium concentrations as well as possible differences in exchange rates of the various ring positions. However, in most cases the reaction had progressed sufficiently to enable quantitative estimations to be made from the less intense C—H or C—D stretching frequencies in the 2200–3100  $\text{cm}^{-1}$  regions.

## III. RESULTS AND DISCUSSION

Two general phenomena were observed in our study of exchange reactions. The first of these concerns the trend in overall reactivity of the molecule, while the second, which is discussed in Section III (c), refers to the relative reactivity of the various ring positions within the molecule.

From data in Table 1, it is evident that there are marked differences in the exchange rates between individual members of each series. In the halogenated benzenes, the reactivity decreases towards the iodo-derivative. A similar trend is also observed for monohalogenated naphthalenes where the reactivity is very much lower than in the corresponding benzene series. The observed trend in exchange rates may be attributed to several factors which include steric effects, catalyst poisoning, or relative bond strength in chemisorption. To distinguish between these possibilities, additional exchange reactions were performed and the results reported in Table 2.

### (a) Steric Effects and Catalyst Poisoning

If, during the process of chemisorption, the adsorbed molecule is assumed to lie on the catalyst surface in a horizontal position, then the observed trend in reactivities could be attributed to steric hindrance by a bulky substituent.

\* The procedure also offers a convenient one-step synthesis of tritiated aromatic compounds when heavy water is replaced with tritiated water. In the case of  $\text{T}_2\text{O}$  the method has the added advantage that the labelled material is obtained with a minimum of radiochemical by-products and hence under certain conditions this method is preferable to conventional techniques such as recoil labelling (Brown and Garnett 1958, 1959; and references therein) and tritium gas irradiation (Wilzbach 1957).

Iodobenzene should then be least strongly chemisorbed in the monohalogenated benzenes. However, the fact that the exchange of chlorobenzene is completely stopped when carried out in the presence of iodobenzene (run 9, Table 2) is inconsistent with weak chemisorption. An explanation involving steric hindrance is also difficult to accept in view of the reported results for toluene (Tiers 1956), aniline (Lauer and Errede 1954), and sodium benzoate (Brown and Garnett 1958a, 1958b), all of which possess large substituents but exchange readily.

The possibility should also be considered that the observed exchange trend occurs via a simultaneous side reaction which poisons the catalyst. Autocatalytic poisoning, i.e. poisoning due to stronger chemisorption of one of the reactants, is discussed in Section III (b).

TABLE 2  
MISCELLANEOUS EXCHANGE REACTIONS\*

Purpose of Investigation	Run	Reagents				$x^{\dagger}$
		Reference Mixture	Quantity (moles)	Test Mixture	Quantity (moles)	
Catalyst poisoning	7	Deuterium oxide Chlorobenzene	$7 \cdot 5 \times 10^{-2}$ $1 \cdot 5 \times 10^{-2}$	Deuterium oxide Chlorobenzene Iodine	$7 \cdot 5 \times 10^{-2}$ $1 \cdot 5 \times 10^{-2}$ $1 \cdot 2 \times 10^{-4}$	1.0
	8	Deuterium oxide Chlorobenzene	$7 \cdot 5 \times 10^{-2}$ $1 \cdot 5 \times 10^{-2}$	Deuterium oxide Chlorobenzene Biphenyl	$7 \cdot 5 \times 10^{-2}$ $1 \cdot 5 \times 10^{-2}$ $6 \cdot 5 \times 10^{-4}$	
Mixed exchange	9	Deuterium oxide Chlorobenzene	$7 \cdot 5 \times 10^{-2}$ $7 \cdot 5 \times 10^{-2}$	Deuterium oxide Chlorobenzene Iodobenzene	$3 \cdot 75 \times 10^{-2}$ $1 \cdot 5 \times 10^{-2}$ $1 \cdot 5 \times 10^{-2}$	0.0

\* All reactions were performed for 48 hr, at 130 °C with 100 mg of reduced PtO<sub>2</sub>.

†  $x = \frac{\text{deuterium content in test chlorobenzene}}{\text{deuterium content in reference chlorobenzene}}$ .

The first side reaction investigated was the formation of molecular or atomic halogen (X) from C—X bond rupture, since considerable quantities of iodine were detected during the exchange of iodobenzene. Tendency to poison the catalyst in this way would be expected to increase with decreasing C—X bond strength. Similarly, poisoning could occur through biphenyl formation. Significant quantities of this compound have been detected in the relatively high temperature exchange (150 °C) of benzene (Dixon and Schiessler 1954). These two possibilities were investigated by performing exchange reactions in the presence of these substances. Results are compared with reference mixtures containing none of the suspected poisons. It is evident from Table 2 that no

significant change in the exchange rate of the test samples was observed. Hence neither biphenyl nor molecular halogen are catalyst poisons when present in relatively low concentrations.

(b) *Relative Bond Strength in Chemisorption*

Present evidence suggests that the observed trend in exchange may be attributed to different strengths of chemisorption, so that the more strongly an aromatic compound is adsorbed, the more slowly it will exchange with deuterium. In terms of results in Table 1, iodobenzene would then be the most strongly chemisorbed member of the halogenated benzene series, and fluorobenzene the least. From Farkas' results, which indicate that exchange between deuterium gas and water was not significantly slowed down by the presence of benzene, it may be concluded that benzene is chemisorbed on specific sites, which constitute only a small fraction of the catalyst surface. Thus it is possible to distinguish between two effects as the bond strength increases in chemisorption. Firstly, locational specificity may be maintained, but desorption may become the rate-determining step. Alternatively, loss of specificity may occur resulting in the displacement of all chemisorbed water, and the onset of autocatalytic poisoning. The excessive sluggishness of the bromo- and iodo-derivatives would favour the latter explanation. The validity of these mechanisms is emphasized by the increased reaction rate obtained at higher temperatures (run 5, Table 1).

In terms of the conventional dissociative mechanism, which envisages chemisorption of aromatic molecules to occur via their  $\sigma$ -electrons, our observed trend is difficult to explain since any variation in the carbon-metal bond strength must be attributed to the influence of the halogen substituent. However, since the effect on  $\sigma$ -electrons by substituents is insignificant when compared with that on  $\pi$ -electrons, it is difficult to visualize how such a mechanism can explain the strengthening of the carbon catalyst bond.

A mechanism which postulates participation of the halogen atom in chemisorption by a donation of electrons towards the catalyst is also difficult to accept since such a bond would be of even greater importance in the case of aniline. The relatively greater strength in chemisorption of naphthalene compared with that of benzene would also remain unexplained.

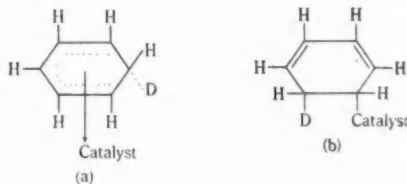
The objection to the associative mechanism arises from the postulate of  $\pi$ -electron localization with the resultant loss of resonance energy. Chemisorption of this kind would be characterized by a high activation energy and in all probability be endothermic. Both of these features, however, are contrary to results encountered in catalysis.

A more satisfactory method of explaining the observed reactivity is to postulate that chemisorption of aromatic molecules on active platinum (and possibly other transition metals) occurs through the formation of a  $\pi$ -complex type of bond. Complexes of this type have already been shown to exist between such inorganic ions as silver, chromium, and platinum and organic substrates such as benzene and its monohalogenated derivatives (Keefer and Andrews 1950, 1951). Fluorobenzene, possessing the highest ionization potential of the mono-halogenated benzenes, is able to donate  $\pi$ -electrons less readily and consequently

is found to form the least stable  $\pi$ -complexes, whereas iodobenzene, with the lowest ionization potential, forms the complex of greatest stability. This trend in stability in the monohalogenated benzene complexes agrees with the observed exchange rates and may be taken as evidence for the proposed  $\pi$ -bonding theory. Additional evidence in support of the  $\pi$ -complex bond hypothesis is found in the work of Selwood (1957). His investigation of changes in paramagnetism during the chemisorption of hydrogen, ethylene, and benzene shows that benzene, during bond formation, donates three times as many electrons to the catalyst as does ethylene. Selwood concludes that benzene is held to the metal surface via a six point attachment. A similar argument can also be used to account for the relative reactivity of the halogenated naphthalene derivatives. The fact that naphthalenes exchange more slowly than corresponding members of the benzene series can also be explained by the postulated bond, since this trend is consistent with ionization potential data (benzene, 9.24 eV; naphthalene, 8.30 eV).

However, a detailed mechanism of exchange reactions cannot be given on the basis of our results alone. From the data reported by other investigators, it is apparent that heavy water furnishes chemisorbed deuterium atoms which then exchange with the chemisorbed aromatic hydrocarbon. Although the exact mechanism of the final step is not yet clear, this could well occur through the formation of a transient hydrocarbon radical from carbon-hydrogen bond rupture, or via a conventional substitution mechanism with chemisorbed hydrogen as the attacking radical. The nature of such an attacking species is in doubt, since chemisorbed hydrogen is known to be strongly polarized. It is emphasized, however, that a dissociative type of mechanism is closely linked to the proposed  $\pi$ -complex bonding in that such bonding aids the dissociation process.

Chemisorption then would be responsible for the formation of most radicals, and not the converse as implied by the conventional dissociative theory. In the case of the alternative mechanism (i.e. radical substitution) it is of interest to observe that the transition state (a) closely resembles the "half hydrogenated" state of the conventional associative mechanism (b).



### (c) Orientation Effects in Exchange

An interesting fact emerges from the monohalogenated benzene series of exchange reactions, namely, that hydrogen in the *ortho*-position exchanges at a slower rate than those in the *meta*- or *para*-positions, which react at approximately the same speed. This phenomenon was observed from infrared bands in the 700–900 cm<sup>-1</sup> region. Orientation effects have already been reported during

the exchange of aniline (Lauer and Errede 1954) and sodium benzoate (Brown and Garnett 1958a, 1958b) where the *ortho*-positions exchange much faster than the *meta*- and *para*-. Lauer and Errede explain the result for aniline by postulating that the molecule is adsorbed at the catalyst through its lone-pair of electrons thereby placing the *ortho*-positions favourably. A similar argument was applied to sodium benzoate.

Unfortunately, an explanation for *ortho*-deactivation, as observed in our experiments, cannot be derived from any of these preceding arguments. The situation is also complicated by two additional factors; firstly, our lack in precise knowledge of the exchange mechanism and, secondly, the uncertainty involved in ascribing properties to chemisorbed reagents which were originally derived from molecular orbital, or valence bond theory of these molecules in their free state. As a consequence, *ortho*-deactivation may mean that a radical

TABLE 3  
ORIENTATION EFFECT IN MONOHALOGENATED BENZENES

Compound	Band Type	Relative Band Intensity	Compound	Band Type	Relative Band Intensity	Compound	Band Type	Relative Band Intensity
Chloro-benzene	<i>ortho</i> - <i>meta</i> - <i>para</i> -	1·0 6·0 6·0	Bromo-benzene	<i>ortho</i> - <i>meta</i> - <i>para</i> -	1·0 5·0 5·0	Iodo-benzene	<i>ortho</i> - <i>meta</i> - <i>para</i> -	1·0 1·7 1·7

is less readily formed in the *ortho*-position, or that the position is deactivated towards the hydrogen radical attack. It is also difficult to establish whether in the latter case attack is purely homolytic in nature, since chemisorbed hydrogen is known to be strongly polarized. A steric hindrance argument cannot be applied since *ortho*-deactivation decreases with increasing size of the substituent (Table 3). This observation is of considerable interest as it shows that *ortho*-deactivation is related to the electronegativity of the substituent. It would appear, therefore, that deactivation of the *ortho*-position occurs when the inductive effect acts out of the ring, while activation takes place when this effect acts in the reverse direction.

#### IV. REFERENCES

BEEK, O. (1945).—*Rev. Mod. Phys.* **17**: 61.  
 BROWN, W. G., and GARNETT, J. L. (1958a).—*J. Amer. Chem. Soc.* **80**: 5272.  
 BROWN, W. G., and GARNETT, J. L. (1958b).—Proc. symp. peaceful uses of atomic energy in Australia. p. 575.  
 BROWN, W. G., and GARNETT, J. L. (1959).—*Int. J. Appl. Rad. Isotopes* **5**: 114.  
 CHOPTIN, A. R., and NANCE, O. A. (1951).—"A Spectral Study of Some Mono-Substituted Derivatives of Deuterobenzenes." NR-055-083. (Louisiana State Univ. Press.)  
 DIXON, J., and SCHISSLER, R. W. (1954).—*J. Amer. Chem. Soc.* **76**: 2197.  
 FARKAS, A., and FARKAS, L. (1933).—*Nature* **132**: 894.  
 HORUJITI, J., and POLANYI, M. (1934).—*Trans. Faraday Soc.* **30**: 1164.  
 JENKINS, G. I., and RIDEAL, E. K. (1955).—*J. Chem. Soc.* **1955**: 2490.  
 KEEFER, R. M., and ANDREWS, L. T. (1950).—*J. Amer. Chem. Soc.* **72**: 4677, 5034, 5170.

KEEFER, R. M., and ANDREWS, L. T. (1951).—*J. Amer. Chem. Soc.* **73**: 4169.  
LAUER, W. M., and ERREDE, L. A. (1954).—*J. Amer. Chem. Soc.* **76**: 516.  
LE NOBLE, W. J., and WHELAND, G. W. (1958).—*J. Amer. Chem. Soc.* **80**: 5401.  
SELWOOD, P. W. (1957).—*J. Amer. Chem. Soc.* **79**: 3346, 4637, 5391.  
TAYLOR, T. L. (1957).—“Catalysis.” Vol. 5. pp. 257–400. (Reinhold Publishing Corp.: New York.)  
TIERS, G. V. D. (1956).—Ph.D. Thesis, University of Chicago.  
TWIGG, G. H. (1939).—*Trans. Faraday Soc.* **35**: 934.  
TWIGG, G. H., and RIDEAL, E. K. (1939).—*Proc. Roy. Soc. A* **171**: 55.  
WHIFFEN, D. H., and THOMPSON, H. W. (1945).—*J. Chem. Soc.* **1945**: 268.  
WILZBACH, K. E. (1957).—*J. Amer. Chem. Soc.* **79**: 1013.

## THE CARDIAC GLYCOSIDES PRESENT IN MISTLETOES GROWING ON *NERIUM OLEANDER*

By C. BOONSONG\* and S. E. WRIGHT\*

[Manuscript received December 22, 1960]

### Summary

Three species of mistletoe growing on *Nerium oleander* have been shown to extract selectively cardiac glycosides from the host plant. The substances selected were the three most polar glycosides present in the leaves of *N. oleander* and have been identified as strospeside, neritaloside, and odoroside H. These glycosides had been previously isolated from the seeds of *N. oleander*.

### I. INTRODUCTION

Mistletoes growing on *Nerium oleander* have a bitter taste and, as Trautner (1952) has shown that mistletoes growing on *Duboisia myoporoides* contain some of the alkaloids of the host plant, it was thought likely that the parasite might also extract cardiac glycosides from *N. oleander*. Accordingly three species of mistletoe were investigated for the presence of cardiac glycosides. These were *Phrygilanthus celastroides* (from Sydney), *Dendrophthoe falcata* (from Brisbane and Newcastle), and *Amyema congener* (from Queensland).

### II. PROCEDURE

A preliminary investigation by paper chromatography of each mistletoe collected showed the presence of the same three glycosides as indicated by the  $R_F$  values measured using three solvent systems. Furthermore the  $R_F$  values of these three glycosides corresponded with those of the three most polar glycosides present in the leaves of *N. oleander* plants on which the parasites were growing. These glycosides were provisionally named glycosides A, B, and C (Fig. 1).

A mixture of these three glycosides was obtained by extraction of *D. falcata* and chromatographed on neutral alumina. The glycosides separated into three main groups (Fig. 2) from which glycoside A and glycoside C were ultimately separated in a pure condition by fractional crystallization. Glycoside B, however, could not be separated from glycoside C by this method.

#### (a) Glycoside A

This substance (m.p. 252–255 °C) was identified as strospeside (I) (Rittel, Hunger, and Reichstein 1952) by the preparation of its tribenzoate and by the formation of 14,16-dianhydrogitoxigenin (IV) (Fig. 3) after hydrolysis with hydrochloric acid in acetone (Schindler and Reichstein 1952). The glycoside

\* Department of Pharmacy, University of Sydney.

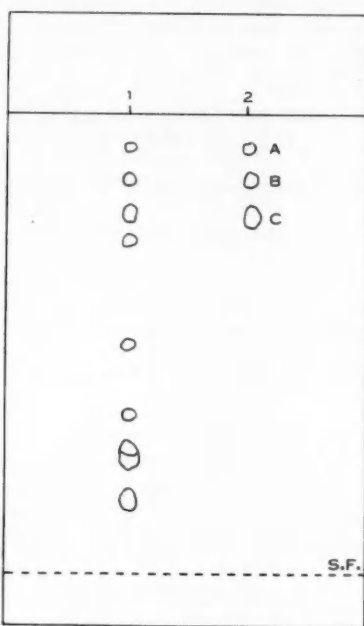


Fig. 1.—Paper chromatogram of leaf extracts of  
1, *Nerium oleander*; 2, *Dendrophthoe falcata*.  
S.F., solvent front,  $3\frac{1}{2}$  hr, downward. Solvent system,  
methyl isobutyl ketone-isopropyl ether (4 : 1) sat.  
formamide (system II).

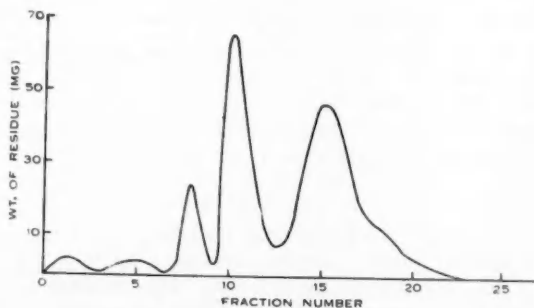
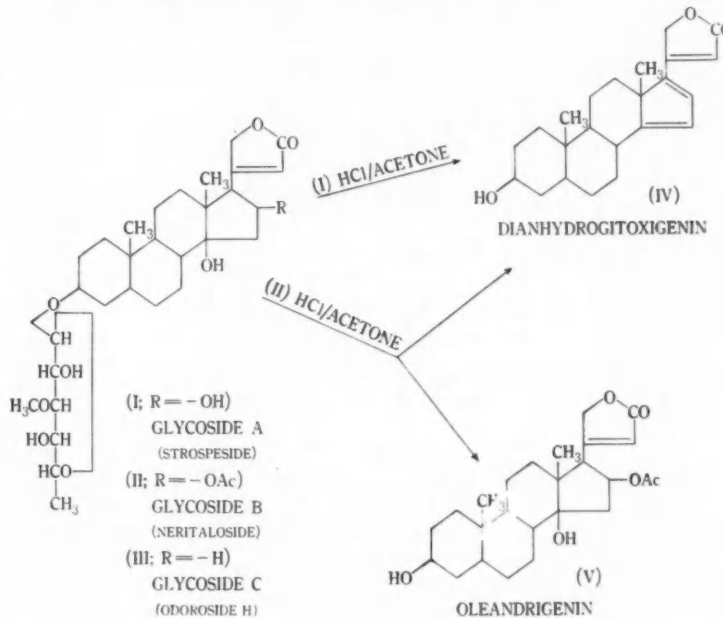


Fig. 2.—Alumina chromatography of mixed glycosides A, B,  
and C obtained from *Dendrophthoe falcata*.

could not be separated from strospeside on paper chromatograms (Fig. 4) and colour reactions with sulphuric acid were similar. Strospeside has been isolated from the seeds of *N. oleander* by Jäger, Schindler, and Reichstein (1959).

(b) *Glycoside C*

This glycoside (m.p. 233–235 °C) had the same constants, melting point, and mixed melting point as odoroside H (III) (Rheiner, Hunger, and Reichstein 1952). It could not be separated from odoroside H on paper chromatograms (Fig. 4) and gave a diacetate corresponding to odoroside H diacetate (Mohr, Schindler, and Reichstein 1954). Odoroside H was isolated from seeds of *N. oleander* by Jäger, Schindler, and Reichstein (1959).



(c) *Glycoside B*

This substance could not be separated from glycoside C by fractional crystallization, alumina chromatography, or partition chromatography on silica gel, but separation was finally achieved by preparative paper chromatography. The glycoside was amorphous but was crystallized as a dioxane complex and had the same melting point and mixed melting point (135–140 °C) as the dioxane complex of neritaloside (II) first isolated by Jäger, Schindler, and Reichstein (1959) from the seeds of *N. oleander* and crystallized in the same way. It could not be separated from neritaloside on paper chromatograms (Fig. 4). The ultraviolet spectra of glycoside B in concentrated sulphuric acid (Brown and

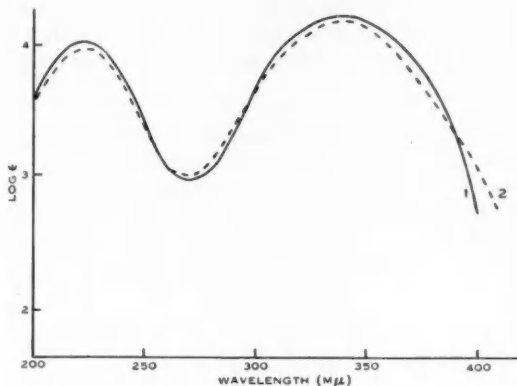


Fig. 3.—Ultraviolet absorption spectra in ethanol.  
 1, Genin from hydrolysis of substance A:  $\lambda_{\text{max}}$ . 224 m $\mu$   
 $\log \epsilon=4.03$ ; 337-338 m $\mu$   $\log \epsilon=4.32$ .  
 2, 14,16-Dianhydrogitoxigenin (Schindler and Reichstein 1952);  
 $\lambda_{\text{max}}$ . 222.5 m $\mu$   $\log \epsilon=4.02$ ; 337.5 m $\mu$   $\log \epsilon=4.31$ .

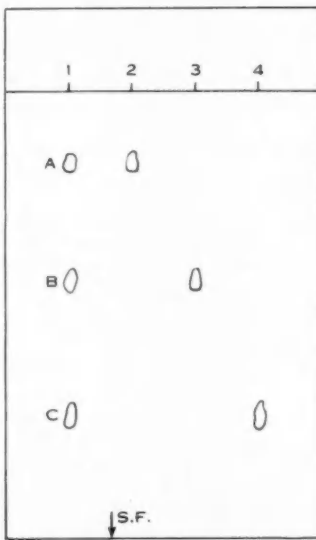


Fig. 4.—Paper chromatogram of mistletoe glycosides (*D. falcata*).  
 1, Mixed glycosides A, B, and C; 2, strospeside; 3, neritaloside; 4, odoroside H. Development 12 hr, downwards (system II).

Wright 1960) was similar to that of oleandrin in the same solvent (Fig. 5) and when treated with methanolic potassium bicarbonate it gave a product which could not be separated from strospeside on paper chromatograms. Strospeside was also isolated from a mixture of glycoside B and glycoside C (odoroside H) after saponification with methanolic potassium bicarbonate. Hydrolysis of glycoside B with hydrochloric acid in acetone gave a mixture of oleandrigenin (V) 14,16-dianhydrogitoxigenin (IV) and only one sugar identified as digitalose. These reactions confirm the structure of neritaloside as 16-acetylstrospeside (digitaloside of oleandrigenin).

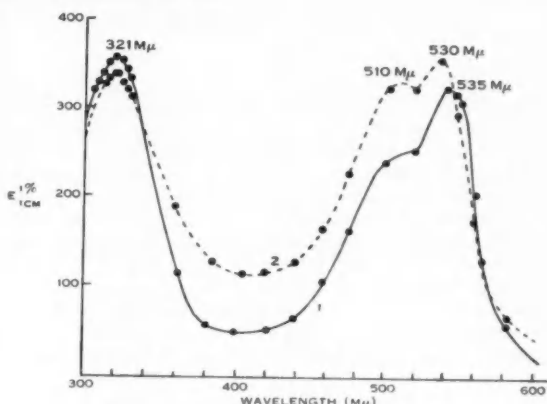


Fig. 5.—Ultraviolet absorption spectra in sulphuric acid.  
1, Glycoside B; 2, oleandrin.

### III. DISCUSSION

Although paper chromatograms of extracts of the leaves of *N. oleander* reveal at least 12 glycosides, the mistletoes select only three of them. The glycosides selected by the mistletoe are all digitalosides and the differences in polarity are due entirely to the presence of substituents at position 16 in the aglycone. The least polar, odoroside H, has no substituent group at C<sub>16</sub>, and the most polar of the three, strospeside, has a hydroxyl at C<sub>16</sub>. Intermediate in order of polarity is neritaloside with an acetoxy group at C<sub>16</sub>.

The selection of the three glycosides by the mistletoe could be due to the fact that only the polar glycosides present in the leaves are translocated in the oleander. However, as the seeds of *N. oleander* have been shown to contain at least 15 glycosides and aglycones (Jäger, Schindler, and Reichstein 1959) they must be translocated in the plant and hence it would appear that the haustoria of the mistletoe select the polar glycosides preferentially.

### IV. EXPERIMENTAL

Melting points were determined on a Kofler-block type apparatus and are corrected. Elemental analyses were carried out by Dr. K. W. Zimmerman, C.S.I.R.O. Microanalytical Laboratory, Melbourne.

## (a) Paper Chromatography

For the separations of glycosides and aglycones the following systems were used on formamide-impregnated Whatman No. 1 paper based on the methods of Zaffaroni, Burton, and Keutmann (1951), Schindler and Reichstein (1951), Gisvold and Wright (1956), and Kaiser (1955).

*System I*: Chloroform-benzene-butanol (78 : 12 : 6) saturated with formamide.

*System II*: Methyl isobutyl ketone-isopropyl ether (4 : 1) saturated with formamide.

*System III*: Benzene saturated with formamide.

*System IV*: Benzene-chloroform (9 : 1) saturated with formamide.

*System V*: Tetrahydrofuran-chloroform (1 : 1) saturated with formamide.

The glycosides or aglycones were detected on the paper by immersion in a mixture of 1% methanolic solution of 3,5-dinitrobenzoic acid (40 ml) and 20% aqueous NaOH solution (10 ml) (Kedde reagent).

## (b) Extraction of Plant Material

Ground leaves (3.85 kg) of *Dendrophthoe falcata* (which was most readily available in quantity) were extracted by successive macerations with 20% ethanol in water until no further reaction was given for glycosides with alkaline m-dinitrobenzene (Raymond reagent). The ethanolic extract was treated with a concentrated solution of lead acetate, until no further precipitation occurred, and filtered. The filtrate was concentrated under reduced pressure to about 1 l. and then extracted with three portions of 500 ml of chloroform. Each chloroform extract was washed three times with 10% NaHCO<sub>3</sub> solution and then with water. After drying over anhydrous Na<sub>2</sub>SO<sub>4</sub>, the chloroform extract was evaporated to dryness in a vacuum. Yield, 2.29 g of crude glycosides (equiv. to 0.059% of the dried leaf).

Extracts prepared in the same way from small amounts of *Phrygilanthus celastroides* and *Amyema congener* were chromatographed on paper for comparison with the glycosides isolated from *D. falcata*. The R<sub>F</sub> values of the glycosides present in the three plants studied are compared in Table 1.

TABLE I  
R<sub>F</sub> VALUES OF MISTLETOE GLYCOSIDES A, B, AND C

Systems :	I			II			III		
	A	B	C	A	B	C	A	B	C
Glycosides :									
Mistletoe									
<i>P. celastroides</i> ..	0.76	0.73	0.68	0.22	0.29	0.38	0.69	0.58	0.54
<i>A. congener</i> ..	0.76	0.72	0.67	0.21	0.29	0.38	0.68	0.57	0.54
<i>D. falcata</i> ..	0.76	0.73	0.68	0.22	0.29	0.38	0.69	0.58	0.53

## (c) Alumina Chromatography

Crude glycoside (0.5 g) dissolved in 20 ml of chloroform was diluted to 60 ml with benzene. This solution was applied to an alumina column packed with benzene-chloroform (2 : 1) and eluted with 50 ml portions of solvent. The results of a typical chromatogram are shown in Table 2 (see also Fig. 2).

(i) Fractions 7-9 were combined and the material obtained from them recrystallized several times from acetone-ether, yield 28 mg of pure glycoside C.

(ii) Fractions 10-13 contained a mixture of glycosides B and C and these were reserved for separation by preparative paper chromatography.

(iii) Fractions 14-21 contained mainly glycoside A which was recrystallized from methanol-water, yield 150 mg of crystalline glycoside A.

## (d) Separation of Glycosides B and C by Preparative Paper Chromatography

Mixed glycosides B and C (160 mg) were dissolved in 16 ml methanol and 1 ml of the solution applied to the starting line of each of 16 pieces of Whatman No. 3 filter paper (9 by 22 in.) previously impregnated with formamide by drawing through a 25% solution of formamide in acetone. The chromatograms were developed using system II by the descending method for 11 hr. The chromatograms were then dried in air for 1 hr at room temperature, narrow longitudinal strips cut from each edge, and the glycoside was located with Kedde reagent. The glycoside areas were eluted with chloroform and the chloroform layers washed with three successive quantities of water, dried with anhydrous  $\text{Na}_2\text{SO}_4$ , and evaporated in a vacuum to yield 75 mg of glycoside B and 69 mg of glycoside C. Glycoside C (69 mg) was chromatographed on neutral alumina packed with benzene-chloroform (1 : 1). From the pure chloroform fractions 44.2 mg of crystalline glycoside C, m.p. 233–235 °C, was recovered after recrystallization from acetone-ether.

TABLE 2  
CHROMATOGRAPHY OF MIXED GLYCOSIDES OF D. FALCATA ON NEUTRAL ALUMINA

Fraction	Eluting Solvent	Residue (mg)	Raymond Reaction
1–3	Benzene : chloroform (2 : 1)	8.18	—ve
4–6	Benzene : chloroform (1 : 1)	3.97	—ve
7	Chloroform	1.10	+ve
8	Chloroform	25.74	+ve
9	Chloroform	5.21	+ve
10	Methanol : chloroform (0.5 : 99.5)	66.0	+ve
11	Methanol : chloroform (0.5 : 99.5)	45.42	+ve
12	Methanol : chloroform (0.5 : 99.5)	9.13	+ve
13	Methanol : chloroform (0.5 : 99.5)	11.81	+ve
14	Methanol : chloroform (1 : 99)	36.17	+ve
15–21	Methanol : chloroform (1 : 99)	130.91	+ve
22–25	2% Methanol in chloroform	4.53	—ve

The amorphous glycoside B recovered from the paper (75 mg) was chromatographed on neutral alumina. The chloroform-methanol (95.5) fractions yielded 50 mg of colourless amorphous material, which crystallized from dioxane-ether (Jäger, Schindler, and Reichstein 1959).

(i) *Glycoside A*.—From methanol-water, colourless needles, m.p. 253–255 °C; mixed melting points with an authentic sample from *Strophanthus speciosus* 251–255 °C,  $[\alpha]_D^{20} +15.7 \pm 2^\circ$  (c, 1.27 in chloroform) (Found: C, 64.9; H, 8.3; —OCH<sub>3</sub>, 5.66%. Calc. for  $C_{20}H_{16}O_5$ : C, 65.4; H, 8.4; —OCH<sub>3</sub>, 5.6%). Colour reaction with 84%  $H_2SO_4$  (time in min) 0 yellow, 30 orange, 60 reddish brown, 120 brown, 240 green; u.v. spectra; max. 217 m $\mu$ , log ε 4.14.

(1) *Benzoylation of Glycoside A* (Rittel, Hunger, and Reichstein 1953). Glycoside A (43 mg; m.p. 253–255 °C) dissolved in 1 ml dry pyridine and 0.4 ml purified benzoyl chloride added at 0 °C. The reaction mixture was allowed to stand at 0 °C for 1 hr and then at room temperature (23 °C)

for 20 hr. Methanol (0.2 ml) was then added and allowed to stand for 2 hr. The methyl benzoate was removed by distillation under vacuum (0.02 mmHg) at 50 °C for 2 hr. Yield 73 mg of non-crystalline material. This was dissolved in 10 ml light petroleum-benzene (40 : 60) and chromatographed on a column of 2 g of silica gel. The fraction benzene-chloroform (4 : 1) gave 33 mg of colourless crystals of the tribenzoate from light petroleum-acetone, m.p. 254–256 °C,  $[\alpha]_D^{20} +58.9 \pm 2^\circ$  (c, 0.98 in chloroform) (Found : C, 70.4 ; H, 6.8%. Calc. for  $C_{51}H_{58}O_{12}$  : C, 71.0 ; H, 6.7%).

(2) *Hydrolysis of Glycoside A (Mannich).* Glycoside A (187 mg) was added to 100 ml of dry acetone and heated to boiling to dissolve, cooled rapidly to room temperature (20 °C), and 0.7 ml conc. HCl added. The solution was allowed to stand at room temperature for 14 days. The acetone was then removed under reduced pressure, 25 ml of water being added gradually as acetone was removed; 20 ml of methanol was added and the solution refluxed for 30 min. The methanol was removed in a vacuum and 20 ml water added. The aqueous solution was extracted with  $3 \times 25$  ml of chloroform and the chloroform extracts washed with water,  $NaHCO_3$  and water. The chloroform solution was dried over anhydrous  $Na_2SO_4$  and then evaporated *in vacuo*. A yellow oily residue (131 mg) was obtained. This was dissolved in light petroleum-benzene (1 : 1) and chromatographed on neutral alumina (5 g, activity III). The pure benzene fraction contained aglycone and yielded 44 mg of colourless crystals of 14,16-dianhydrogitoxigenin recrystallized from methanol-water, m.p. 203–206 °C,  $[\alpha]_D^{20} +619$  (c, 0.61 in methanol) (Found : C, 77.4 ; H, 8.6%. Calc. for  $C_{28}H_{30}O_8$  : C, 77.9 ; H, 8.5%). Reaction with tetraniromethane strongly positive; u.v. spectra shown in Figure 3.

(ii) *Glycoside C.*—From acetone-ether colourless needles, m.p. 233–235 °C, mixed melting point with a sample of odoroside H 230–235 °C,  $[\alpha]_D^{20} +8.46 \pm 2^\circ$  (c, 1.06 in methanol) (Found : C, 67.0 ; H, 8.8%. Calc. for  $C_{30}H_{46}O_8$  : C, 67.3 ; H, 8.7%). Colour reaction with 84%  $H_2SO_4$  (time in min) 0 yellow, 30 orange, 60 purple, 120 purple, 270 colourless; u.v. spectra, max. 217 m $\mu$ , log  $\varepsilon = 4.22$ .

(1) *Acetylation of Glycoside C (Mohr, Schindler, and Reichstein 1954).* Glycoside C (68 mg; m.p. 233–235 °C) dissolved in 1 ml dry pyridine and 1 ml acetic anhydride was added. The solution was kept at room temperature (22 °C) for 2 days. The solution was then diluted with 10 ml water (0 °C) and extracted with  $4 \times 10$  ml chloroform. The chloroform solution was washed with dil.  $H_2SO_4$  ( $2 \times 5$  ml) then with 10%  $NaHCO_3$  ( $2 \times 5$  ml), and finally with water ( $3 \times 5$  ml). The chloroform solution was dried over anhydrous sodium sulphate and evaporated to yield 90 mg of colourless foam which, on recrystallization from methanol-water, yielded 68 mg of colourless needles of the diacetate, m.p. 228–235 °C,  $[\alpha]_D^{21} +10.9 \pm 2^\circ$  (c, 0.85 in chloroform) (Found : C, 65.2 ; H, 8.2%. Calc. for  $C_{34}H_{50}O_{10}$  : C, 66.0 ; H, 8.2%. U.v. spectra : max. 217 m $\mu$ , log  $\varepsilon = 4.15$ .

(iii) *Glycoside B.*—This was obtained by separation from glycoside C by preparative chromatography and crystallized from dioxane-ether, m.p. 135–140 °C. Mixed melting point with an authentic sample of neritaloside-dioxane complex 135–140 °C. U.v. spectra in cone.  $H_2SO_4$  (Fig. 5). Colour reactions with 84%  $H_2SO_4$  (time in min) 0 yellow, 3 orange, 15 reddish orange, 30 reddish orange, 60 reddish brown, 120 yellow-brown, 24 (hr) yellow-brown.

(1) *Hydrolysis of Glycoside B (Mannich).* Amorphous glycoside B (30 mg) obtained from paper chromatograms was dissolved in dry acetone and 0.1 ml conc. HCl added. The solution was allowed to stand at room temperature (20–24 °C) for 14 days and then treated as for glycoside A. Paper chromatograms on systems III and IV showed two substances. The faster running substance could not be separated from 14,16-dianhydrogitoxigenin and the more polar substance could not be separated from oleandrenogenin on either system.

The acid phase was concentrated to 15 ml *in vacuo* and treated according to the methods of Schindler and Reichstein (1952) for the isolation of sugars. The sugar residue obtained after distillation at 0.02 mm at 100–120 °C was identified as digitalose by comparison with an authentic sample by paper chromatography using the system butanol-acetic acid-water (Partridge 1948) and ethyl acetate-pyridine-water (Tschesche and Grimmer 1954).

(2) *Deacetylation of Glycoside B.* Amorphous glycoside B (12 mg) obtained from paper chromatograms was dissolved in 2.5 ml methanol and 0.25 ml of 5% solution of  $\text{KHCO}_3$  added and allowed to stand at room temperature ( $24^\circ\text{C}$ ) for 10 days and evaporated at  $50^\circ\text{C}$  *in vacuo*. The residue was extracted three times with chloroform (1 ml) and centrifuged. The chloroform solution was evaporated and used for paper chromatography on systems I and II. No separation from stroseside occurred. The reaction was repeated with 200 mg of a mixture of glycosides B and C. Paper chromatography of the products of the reaction showed some unchanged B and C and a larger amount of stroseside. The reaction products (139 mg) dissolved in 12 ml of benzene-chloroform (2 : 1) were chromatographed on 6 g of neutral alumina. The fraction 0.5% methanol in chloroform gave 34 mg of a substance crystallized from acetone-ether, m.p.  $249\text{--}250^\circ\text{C}$ ,  $[\alpha]_D^{20} +16.4 \pm 2^\circ$  (c, 0.48 in chloroform) which gave no melting point depressions with stroseside.

#### V. ACKNOWLEDGMENTS

The authors wish to thank Dr. L. J. Webb, Division of Plant Industry, C.S.I.R.O., for suggesting this problem and for the provision of Queensland plant material, and Professor T. Reichstein, Organic Chemistry Institute, University of Basel, Switzerland, for reference samples of odoroside H, stroseside, and digitalose. Dr. J. Russell, Organic Chemistry Section, C.S.I.R.O., kindly supplied us with a sample of neritaloside.

#### VI. REFERENCES

BROWN, B. T., and WRIGHT, S. E. (1960).—*J. Amer. Pharm. Ass. Sci. Ed.* **49**: 777.  
GISVOLD, O., and WRIGHT, S. E. (1956).—*J. Amer. Pharm. Ass. Sci. Ed.* **46**: 535.  
JÄGER, H., SCHINDLER, O., and REICHSTEIN, T. (1959).—*Helv. Chim. Acta* **42**: 977.  
KAISER, F. (1955).—*Chem. Ber.* **88**: 558.  
MOHR, K., SCHINDLER, O., and REICHSTEIN, T. (1954).—*Helv. Chim. Acta* **37**: 462.  
PARTRIDGE, S. M. (1948).—*Biochem. J.* **42**: 238.  
RHEINER, A., HUNGER, A., and REICHSTEIN, T. (1952).—*Helv. Chim. Acta* **35**: 687.  
RITTEL, W., HUNGER, A., and REICHSTEIN, T. (1952).—*Helv. Chim. Acta* **35**: 434.  
RITTEL, W., HUNGER, A., and REICHSTEIN, T. (1953).—*Helv. Chim. Acta* **36**: 434.  
SCHINDLER, O., and REICHSTEIN, T. (1951).—*Helv. Chim. Acta* **34**: 108.  
SCHINDLER, O., and REICHSTEIN, T. (1952).—*Helv. Chim. Acta* **35**: 442.  
TRAUTNER, E. M. (1952).—*Aust. J. Sci.* **15**: 98.  
TSCHESCHE, R., and GRIMMER, G. (1954).—*Chem. Ber.* **87**: 418.  
ZAFFARONI, A., BURTON, R. B., and KEUTMANN, E. H. (1951).—*J. Biol. Chem.* **188**: 763.

## SHORT COMMUNICATIONS

### FARADAIC ADMITTANCE OF ELECTROCHEMICAL PROCESSES\*

By S. K. RANGARAJAN† and K. S. G. DOSS†

Ershler (1947) and Randles (1947) showed that the behaviour of micro-electrodes under the action of a small alternating potential gives a powerful tool for measuring the rates of fast electrode reactions. It was shown that :

- (i) The change in the concentration of the oxidant lags behind the anodic faradaic current by  $\frac{1}{2}\pi$ .
- (ii) The phase angle  $\varphi$  between the alternating components of the voltage and the faradaic current is given by the relation

$$\cot \varphi = 1 + \frac{1}{K_s} \sqrt{\left(\frac{1}{2}\omega D\right)}, \quad (1)$$

so that  $\varphi$  is always  $< \frac{1}{4}\pi$ .

Breyer, Bauer, and Hacobian (1955) have derived an expression for the phase angle between the concentration of the oxidant and the alternating voltage which leads to the relation

$$\cot \varphi = 1 - \frac{1}{K_s} \sqrt{\left(\frac{1}{2}\omega D\right)}. \quad (2)$$

This obviously differs from equation (1). Bauer, Smith, and Elving (1960) have pointed out that "the reported experimental results have on occasion appeared to support equation (1) (Randles 1947; Randles and Somerton 1952; Rosenthal and Ershler 1948) and at other times equation (2) (Buchanan and Werner 1954; Breyer, Bauer, and Hacobian 1955; Bauer and Elving 1958)". It seems (Bauer and Elving 1960) that either of the two equations can be used depending on whether  $\varphi \leq \frac{1}{4}\pi$ . The derivation of Breyer, Bauer, and Hacobian (1955) has been examined and it will be shown in the present paper that equations (1) and (2) become identical on correcting an error due to inconsistency of sign conventions, which has crept into the derivation of the latter equation.

The relation

$$\Delta i_{(E)} = nFAD \frac{\partial(\Delta c_{(0,\pi,E)})}{\partial x_{x \rightarrow 0}}$$

(Breyer and Hacobian 1954) implies that  $\Delta i_{(E)}$  is to be considered positive when  $\partial \Delta c_{(0,\pi,E)} / \partial x_{x \rightarrow 0}$  is negative, i.e. when the concentration gradient of the oxidant is negative in the immediate vicinity of the electrode. In other words, the net

\* Manuscript received March 14, 1961.

† Central Electrochemical Research Institute, Karaikudi-3, South India.

current is termed positive when it is anodic in character. Hence Breyer and Hacobian's (1954) equation

$$\Delta i_{(E)} = nFA\Delta c_{0(0, E)} \sqrt{(\omega D)} \cos(\omega\tau + \theta' + \frac{1}{4}\pi) \quad (3)$$

conveys that the *anodic* current *leads* the concentration polarization of the oxidant by  $\frac{1}{4}\pi$ . (This is perfectly true and is equivalent to the statement: "the concentration of the oxidant leads the *cathodic* current by  $\frac{3}{4}\pi$ .) While developing the derivation in the latter paper, Breyer, Bauer, and Hacobian (1955) have started with the rate equation,

$$i_{(E_s)} = nFA [K_f c_{0, \tau, E_s}^{0x} e^{-(\alpha nFe)/RT} - K_b c_{0, \tau, E_s}^{\text{Red}} e^{(1-\alpha)(nFe)/RT}]. \quad (4)$$

Obviously,  $\Delta i_{(E_s)}$  as defined above is "net cathodic" current. They have further put

$$i_{(E_s)} = i_{(E_s)} + \Delta i_{(E_s)}, \quad (5)$$

here,  $\Delta i_{(E_s)}$  is the contribution of the a.c. towards the total current (the contribution being taken as positive when it is cathodic), and

$$i_{(E_s)} = nFA (K_f \frac{1}{2} v_B - K_b \frac{1}{2} v_B).$$

It is thus seen that the sign conventions used in equations (3) and (5) as regards  $\Delta i_{(E_s)}$  are not consistent. It can be appreciated that  $\Delta i_{(E_s)}$  (of eqn. (5)) =  $-\Delta i_{(E_s)}$  (of eqn. (3)). On making the correction,  $\cot \theta'$  turns out to be

$$\cot \theta' = -2K_e Z - 1 \text{ and } \cot \varphi = -\cot(\theta' + \frac{1}{4}\pi) = -\left(1 + \frac{1}{K_e} Z\right),$$

$\varphi$  being the phase angle between the voltage and the current and  $Z = \sqrt{(2/\omega D)}$  which is identical with equation (1) if one takes into account the different sign conventions used for the potential.

This difference can be explained by the fact that Randles in his derivation considers the phase difference between the current and the potential of the solution whereas in the present derivation, the phase angle considered is between the current and potential of the electrode. The two phase angles naturally would differ by  $\pi$ . It is to be further pointed out that since  $\varphi$  here represents the phase angle by which the potential of the *electrode leads* the cathodic current whereas the corresponding quantity of Randles (say  $\varphi_R$ ) represents the phase angle by which the cathodic current *leads* the potential of the *solution*, the relation between  $\varphi_R$  and  $\varphi$  is given by  $\varphi_R = -\varphi + \pi$ , whence we get  $-\cot \varphi_R = \cot \varphi$ .

#### References

- BAUER, H. H., SMITH, D. L., and ELVING, P. J. (1960).—*J. Amer. Chem. Soc.* **82**: 2091, 2094.
- BAUER, H. H., and ELVING, P. J. (1958).—*Analyt. Chem.* **30**: 334.
- BREYER, B., BAUER, H. H., and HACOBIAN, S. (1955).—*Aust. J. Chem.* **8**: 322.
- BREYER, B., and HACOBIAN, S. (1954).—*Aust. J. Chem.* **7**: 225.
- BUCHANAN, G. S., and WERNER, R. L. (1954).—*Aust. J. Chem.* **7**: 230.
- ERSHLER, B. (1947).—*Disc. Faraday Soc.* **1**: 269.
- RANDLES, J. E. B. (1947).—*Disc. Faraday Soc.* **1**: 11.
- RANDLES, J. E. B., and SOMERTON, K. W. (1952).—*Trans. Faraday Soc.* **48**: 937, 951.
- ROSENTHAL, K., and ERSHLER, B. (1948).—*Zh. fiz. khim.* **22**: 1344.

## TEMPERATURE EFFECTS IN ALTERNATING CURRENT POLAROGRAPHY\*

By H. H. BAUER† and P. B. GOODWIN†

Little published data are available on the temperature coefficients of the heights of a.c. polarographic waves. With reversibly and nearly reversibly reduced, unadsorbed, depolarizers, it is expected on theoretical grounds (Breyer and Bauer 1960) that the temperature coefficient of the a.c. wave-height will be about 0·3% per degC less than that of the corresponding d.c. step-height; this expectation is qualitatively confirmed by Breyer, Gutmann, and Hacobian's (1950) data on zinc(II) and cadmium(II) (a.c. temperature coefficient = 0·4% per degC between 20 and 40 °C), by that of Yasumori and Eguchi (1960) on chloride in 10M sulphuric acid (a.c. temperature coefficient = 0·6% per degC at 30 °C), and by that of Itsuki and Suzuki (1959) on copper(II) and zinc(II) in ammoniacal solutions; for lead(II) (Yasumori and Nishimura 1960) the a.c. wave-height changed with time at temperatures above 20 °C.

With only partly reversible (i.e. slow) electrochemical processes, the temperature coefficient of the a.c. wave depends on the temperature-dependence of the electrochemical rate constant (Breyer and Bauer 1960), and would be expected to be larger than for a reversible process. In addition, the change in rate constant with temperature will result in different temperature coefficients of the a.c. wave-height when different frequencies of the superposed alternating voltage are used. Randles and Somerton (1952) have measured the activation energies of several reactions from determination by a.c. measurements, at different temperatures, of the rate constant; however, a modified a.c. bridge technique was used which did not provide data on the temperature coefficients of the a.c. wave-heights.

In the case of adsorbed depolarizers, Breyer and Bauer (1955) found that the temperature coefficient of the a.c. wave-height varied with concentration of the depolarizer, in accordance with the expected lowering of the extent of adsorption with increasing temperature.

It is apparent that investigation of the effect of temperature on a.c. waves can provide a useful tool in the study of the nature and mechanism of electrode processes. In this communication, we report results obtained with a number of inorganic depolarizers.

The results presented in Table 1 were obtained with alternating voltages of 60 c/s and 10 mV r.m.s., and were corrected for series resistance effects; measure-

\* Manuscript received April 12, 1961.

† Faculty of Agriculture, The University of Sydney.

ments were carried out at 20, 40, 60, and 80 °C. The temperature coefficients were calculated from the formula

$$i_2 = i_1 (1 + x/100)^{(T_2 - T_1)},$$

where  $i_2$ ,  $i_1$  are the currents at temperatures  $T_2$  and  $T_1$ , and  $x$  the temperature coefficient in % per degC. Coefficients calculated in this way are more constant with temperature than those calculated by means of the formula

$$\frac{(i_2/i_1) - 1}{T_2 - T_1} \times 100.$$

The temperature coefficients of the d.c. steps are, with the exception of that for the reduction of tin, all of the expected order of magnitude for diffusion-controlled processes, and therefore do not provide any other indication of the mechanisms of the reductions. The a.c. temperature coefficients are about 0·5%

TABLE I  
TEMPERATURE COEFFICIENTS OF INORGANIC DEPOLARIZERS

System Studied	Temperature a.c. Wave- Height (% per degC)	Coefficient of d.c. Step- Height (% per degC)
10 <sup>-3</sup> M Cd(II) in 1M KCl+0·1M HCl	0·6	1·1
10 <sup>-3</sup> M Tl(I) in 0·5M H <sub>2</sub> SO <sub>4</sub>	0·4	1·0
2 × 10 <sup>-4</sup> M Sb(III) in 0·5M HCl	0·4–0·9*	1·1
10 <sup>-3</sup> M Cu(II) in 0·5M H <sub>2</sub> SO <sub>4</sub>	1·5–0·7†	1·3
10 <sup>-3</sup> M In(III) in 1M KCl+0·1M HCl	1·6–0·8†	1·5–0·8†
10 <sup>-3</sup> M Pb(II) in 1M KCl+0·1M HCl	—‡	1·0
2 × 10 <sup>-4</sup> M Sn(II) in 0·5M HCl	1·7	3·2
10 <sup>-3</sup> M Zn(II) in 0·1M KCl+10 <sup>-3</sup> M HCl	2·5–1·0†	1·4–0·9†

\* Increases with temperature.

† Decreases with temperature.

‡ a.c. wave-height decreases between 20 and 60 °C and then increases to 80 °C.

per degC less than the d.c. values for cadmium(II), thallium(I), and antimony(III), in qualitative accordance with the expected behaviour (above) of reversible processes; with copper(II) and indium(III), the a.c. and d.c. values are virtually the same, perhaps indicating that the a.c. process is partly kinetically controlled; in the case of tin(II), even the d.c. values alone indicate some unusual type of reaction.

From the present point of view, lead(II) and zinc(II) are interesting because the a.c., but not the d.c., temperature coefficients indicate that the processes are not simple, reversible ones; thus is it immediately evident that the further study of these systems is likely to be rewarded by insight into the nature of other than the simplest type of electrochemical reaction.

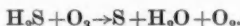
*References*

BREYER, B., and BAUER, H. H. (1955).—*Aust. J. Chem.* **8**: 467, 472.  
 BREYER, B., and BAUER, H. H. (1960).—*Rev. Polarography (Japan)* **8**: 157.  
 BREYER, B., GUTMANN, F., and HACOBIAN, S. (1950).—*Aust. J. Sci. Res. A* **3**: 567.  
 ITSUKI, K., and SUZUKI, F. (1959).—*Japan. Analyst* **8**: 89.  
 RANDLES, J. E. B., and SOMERTON, K. W. (1952).—*Trans. Faraday Soc.* **48**: 937, 951.  
 YASUMORI, Y., and EGUCHI, T. (1960).—*Japan. Analyst* **9**: 680.  
 YASUMORI, Y., and NISHIMURA, T. (1960).—*Japan. Analyst* **9**: 37.

### THE REACTION BETWEEN OZONIZED OXYGEN AND HYDROGEN SULPHIDE IN THE GASEOUS PHASE\*

By I. K. GREGOR† and R. L. MARTIN‡

The reaction between hydrogen sulphide and ozone (usually diluted with air or oxygen) is believed (Mellor 1930) to yield sulphur and water according to the equation



If this is so the reaction might well provide the basis of a useful method for removal of traces of hydrogen sulphide from polluted air; with water, oxygen, and a precipitate of sulphur being the only reaction products.

A detailed examination of the literature reveals that the experimental basis for this reaction is obscure and, in fact, very little is known about the reaction. Bresciani (1915) showed that ozonized oxygen reacts with hydrogen sulphide in the presence of water vapour at c. 120 °C and demonstrated that sulphuric acid was a product of the reaction; however, only 5% of the hydrogen sulphide was oxidized. The only other relevant contribution to the gaseous reaction is a qualitative observation of Schwarz and Munchmeyer (1913), who observed that the rate of reaction between hydrogen sulphide and ozonized air was determined by the concentration of ozone present. Accordingly, the present preliminary investigation was undertaken in a static system to establish the nature of reaction products and the overall stoichiometry of the reaction.

#### *Experimental*

##### (a) Preparation of Materials

(i) Hydrogen sulphide was prepared by treating iron(II) sulphide with HCl and condensing the gas at -78 °C. The gas was purified by recycling it through distilled water and baryta solutions at 0 °C and drying over P<sub>2</sub>O<sub>5</sub>. Final purification was effected by repeated high vacuum

\* Manuscript received January 25, 1961.

† School of Chemistry, The University of New South Wales, Broadway, N.S.W.

‡ School of Chemistry, The University of New South Wales; present address: Central Research Laboratories, I.C.I.A.N.Z. Ltd., Ascot Vale, Victoria.

trap-to-trap distillation through a trap maintained at  $-135^{\circ}\text{C}$ . The vapour pressure of the retained fraction matched the accurate data of Clark, Cocket, and Eisner (1951) in the temperature range  $-111$  to  $-86.4^{\circ}\text{C}$ .

(ii) Sulphur dioxide from a cylinder was dried over  $\text{P}_2\text{O}_5$ , washed with conc.  $\text{H}_2\text{SO}_4$ , and purified by high vacuum trap-to-trap fractionation. Final purification was effected by condensing the gas in a Le Roy (1950) still, and using the fraction having a vapour pressure of c. 1 mmHg at  $-95^{\circ}\text{C}$ .

(iii) Ozonized oxygen was prepared by passing high purity "dry-breathing" oxygen (99.5%) through a silent discharge in a Towers model laboratory ozonizer, of the type described in detail by Vogel (1952). Carbon dioxide and water were first removed from the oxygen stream by passing the gas through two towers containing B.D.H. "Carbosorb" and  $\text{P}_2\text{O}_5$  suspended on powdered asbestos (Pennington 1949). The emergent gas required further drying over  $\text{P}_2\text{O}_5$  to remove traces of water formed during ozonolysis.

#### *(b) Analysis of Ozone/Oxygen Mixtures*

Because of the possibility of ozone decomposing catalytically on glass surfaces, it was necessary to devise a sampling procedure which would provide two nearly identical samples of ozonized oxygen, one for reaction with hydrogen sulphide and one for analysis. This was performed using twin reaction vessels joined through a T-piece as shown in Figure 1. Ozonized oxygen was admitted into vessel A of known volume (c. 2.5 l.) to a pressure of 1 atm. It was then expanded

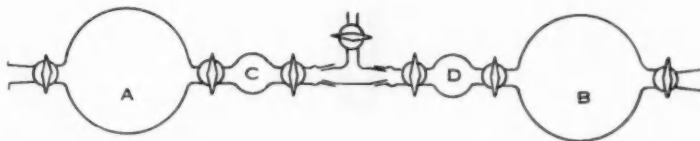


Fig. 1.—Twin reaction and analysis vessels.

via a T-piece into the evacuated vessel B, and the pressure inside the two reaction vessels measured. The small metering bulb D (c. 75 ml) of vessel B was then evacuated and hydrogen sulphide subsequently expanded in at a known temperature and pressure (usually c. 10 mmHg).

The ozone content of the twin reaction vessel A was determined simultaneously, by filling the evacuated metering bulb C with an excess of 7% KI solution and then admitting the solution to the larger bulb A containing ozonized oxygen at c. 380 mm pressure. The iodine-iodide solution was washed from the vessel, acidified with 2N  $\text{H}_2\text{SO}_4$ , and titrated with standard  $\text{Na}_2\text{S}_2\text{O}_3$  solution. This procedure required 15–20 min, and repeated analyses confirmed that no detectable decomposition of ozone occurred within this period. Ozone concentrations in oxygen were generally close to 4% by volume.

#### *(c) Experimental Procedures*

(i) *Reaction between Hydrogen Sulphide and Ozone.*—Known quantities of hydrogen sulphide were treated in the vessels D and B (Fig. 1) at ambient temperatures and illumination using conventional high-vacuum techniques. A white cloud or mist rapidly formed in the larger vessel as hydrogen sulphide diffused in from the metering bulb. Normally, the vessels were allowed to stand for c. 16 hr to ensure complete reaction and, during this period, the cloud dispersed and very small droplets of liquid condensed onto the walls of the vessels. The volatile materials in the vessels, together with diluent oxygen, were pumped extremely slowly through four U-traps in series, maintained at temperatures  $-78$ ,  $-183$ ,  $-183$ , and  $-183^{\circ}\text{C}$ . The need to condense any unreacted ozone in excess at these temperatures was avoided both by employing the 16 hr standing period, long enough for decomposition to occur of the ozone in excess, and by always

choosing  $O_3 : H_2S$  ratios below c. 20 : 1. The most satisfactory stopcock lubricant resistant to ozone was found to be a mixture of Hooker Electrochemical Co. "Fluorolube LG" and colloidal silica.

(ii) *Water Analysis*.—During a typical reaction about 2 mg of a colourless liquid with a vapour pressure of c. 20 mmHg at 20 °C was retained in the first trap at —78 °C. The liquid failed to oxidize a 5% dichromate solution in amyl alcohol to blue perchromic acid, confirming the absence of hydrogen peroxide. Infrared spectra in the 2–15  $\mu$  region of both the liquid and the vapour confirmed that the material trapped at —78 °C was water. The quantity produced was conveniently estimated by condensing it into a calibrated volume with a manometer attached as in Figure 2. The vapour pressure of water was measured with a cathetometer (reading to 0·02 mm) and the total mass calculated assuming the ideal gas equation to be applicable.

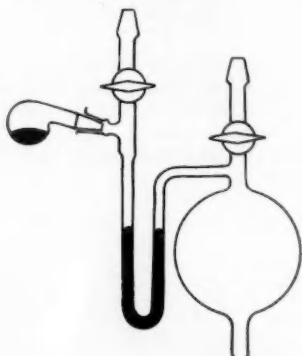


Fig. 2.—Apparatus for water analysis.

(iii) *Sulphur Dioxide Analysis*.—The contents of the three traps maintained at —183 °C were combined and condensed into a 10 cm path length infrared gas cell. The resulting spectrum was characterized by strong absorption at 1350  $\text{cm}^{-1}$  and left no doubt that sulphur dioxide was the principal component. Excess unreacted hydrogen sulphide was also retained at —183 °C and the problem of separating milligram quantities of sulphur dioxide and hydrogen sulphide was solved by fractionating the condensate using a still of the type described by Le Roy (1950). This ingenious device for fractionating millilitre quantities of polycomponent gas samples enabled a complete fractionation of hydrogen sulphide and sulphur dioxide to be readily made. The efficiency of separations by this technique may be gauged from the data given by Gregor and Martin (1959).

The shape of the temperature-pressure profile during operation of the column confirmed that no third sulphur-containing component was present in the condensate retained in traps at —183 °C.

(iv) *Sulphuric Acid Analysis*.—The non-volatile film deposited on the walls of the reaction vessels after mixing hydrogen sulphide and ozonized oxygen was readily soluble in water. Tests for hydrogen and sulphate ions were positive and indicated that either sulphur trioxide,  $H_2SO_4$ , or perhaps one of the peroxy acids such as peroxymonosulphuric acid or peroxydisulphuric acid had been formed. The aqueous solution prepared under a nitrogen atmosphere failed to oxidize iodide to iodine, indicating that peroxy acids of sulphur were absent. Hydrogen ion was estimated by standard alkali titrations and sulphate ion was determined gravimetrically as barium sulphate. The  $H^+/\text{SO}_4^{2-}$  ratio was always close to two confirming that  $H_2SO_4$  (or sulphur trioxide and water) was an end-product of the reaction. Typical figures are quoted in Table 1. No evidence for elemental sulphur was obtained in any of 40 reactions carried out.

(v) *Reaction of Hydrogen Sulphide and Oxygen.*—It was important to establish whether hydrogen sulphide could react with diluent oxygen. In a duplicate experiment, in which the ozone/oxygen mixture was replaced by oxygen, it was found that the initial quantity of hydrogen sulphide was recovered unchanged after the reactants had stood for 16 hr. Thus 0.229 mm of hydrogen sulphide was mixed with oxygen and after 16 hr 0.225 mm was recovered. The slight loss, if experimentally significant, would be attributed to adsorption of hydrogen sulphide on the walls, and particularly on the stopcock lubricant, of the vacuum apparatus.

(vi) *The Problem of Carbon Dioxide Contamination.*—Many of the earlier runs (up to run 28) were partly vitiated because the apparent yield of sulphur in reaction products (sulphur dioxide, hydrogen sulphide, and  $H_2SO_4$ ) exceeded the sulphur content of the hydrogen sulphide initially used. It was estimated that as little as 0.02% by volume of a gas of similar volatility to hydrogen sulphide could cause these spurious results, since it would be condensed together with hydrogen sulphide in the traps at  $-183^{\circ}C$ . Furthermore, if of closely similar volatility, the Le Roy column would fail to separate it from hydrogen sulphide.

TABLE I  
ANALYSES FOR HYDROGEN AND SULPHATE ION

Run	$H^+$ (g-ion)	$SO_4^{=}$ (g-ion)	$H^+/SO_4^{=}$ Ratio
20	$0.82 \times 10^{-4}$	$0.45 \times 10^{-4}$	1.82
26	$0.98 \times 10^{-4}$	$0.51 \times 10^{-4}$	1.92
11	$7.08 \times 10^{-5}$	$3.68 \times 10^{-5}$	1.92

The troublesome impurity was eventually demonstrated to be carbon dioxide present in extremely small amounts in the ozonized oxygen, and presumably arising from reaction between ozone and carbon containing impurities in the  $P_2O_5$  (c. 98%  $P_2O_5$ ) drying tower. The traces of carbon dioxide could not be removed chemically without causing decomposition of the ozone, and it was therefore decided to separate the residual hydrogen sulphide/carbon dioxide mixture quantitatively by making use of the liquid phase reaction between hydrogen sulphide and sulphur dioxide recently described by Gregor and Martin (1959). By this method the exact amount of unreacted hydrogen sulphide was estimated and more accurate mass balances were then obtained (see Table 3).

#### Discussion

The present work demonstrates that when hydrogen sulphide and ozonized oxygen are mixed under initially anhydrous conditions, reaction occurs with water, sulphur dioxide and sulphuric acid being formed as end-products. No evidence for the formation of either peroxy compounds or elemental sulphur was obtained.

Several interesting trends emerge from an evaluation of the data accumulated from some 40 reactions. For example, it is apparent from Figure 3 and Table 2, that under the present reaction conditions, the percentage of hydrogen sulphide actually oxidized steadily increases with increase in the ozone : hydrogen sulphide ratio, and complete oxidation of hydrogen sulphide only occurs at ozone : hydrogen sulphide ratios in excess of c. 9 : 1. This, of course, only places an upper limit on the ozone required to react under the present conditions with a given quantity of hydrogen sulphide and reflects the competitive degradation of ozone in other ways (see for example, Axworthy and Benson 1959).

TABLE 2  
REACTION BETWEEN OZONE AND HYDROGEN SULPHIDE—YIELDS AND CONVERSIONS

Reaction No.	Initial O <sub>3</sub> : H <sub>2</sub> S	Percentage Initial H <sub>2</sub> S Oxidized	Percentage Initial H <sub>2</sub> S converted to :		Percentage Oxidized H <sub>2</sub> S converted to :	
			SO <sub>2</sub>	H <sub>2</sub> SO <sub>4</sub>	SO <sub>2</sub>	H <sub>2</sub> SO <sub>4</sub>
22	0.44	13	—	0	100	0
33	0.65	13	12	0.5	93	4.1
21	0.67	—	13	0	100	0
31	0.86	19	17	0.6	92	3.4
32	0.99	29	26	1.4	88	4.9
24	1.0	(19)	18	0.28	(96)	(1.5)
30	1.7	38	34	1.6	90	4.3
28	2.4	(43)*	39	3.7	(92)	(8.8)
25	2.6	(43)	39	6.0	(90)	(14)
29	2.6	56	46	6.3	83	11.4
26	3.0	—			(74)	(31.2)
20	3.3	(57)	47	10.2	(84)	(18)
27	3.4	(70)	54	9.2	(89)	(15)
23	3.6	(53)	50	6.9	(94)	(13)
36	4.0	67	50	13.5	75	20.3
37	4.9	79	61	18.2	77	23
35	6.4	91	56	31	62	35
39	9.5	100	49	52	49	* 52
40	20.0	100	Nil	96	0	96

\* The values in brackets are calculated by mass balancing reactants and products for hydrogen and sulphur. These runs were partly initiated by the presence of c. 0.02% CO<sub>2</sub> impurity.

A feature of the oxidation is the unvarying production of water and sulphur dioxide in equimolar quantities. Data taken from some 13 reactions are listed in Table 3, whence it is seen that the mean sulphur dioxide : water ratio is close to unity. It is possible that sulphurous acid is formed as an unstable intermediate reaction product, which spontaneously decomposes to yield water and sulphur dioxide in the observed ratio.

The quantity of sulphuric acid produced in the reaction increases steadily with increasing initial ozone : hydrogen sulphide ratio, until at a ratio of c. 18 : 1 the oxidation of all the initial hydrogen sulphide to sulphuric acid is virtually complete (cf. Fig. 3, Table 2). For ratios below c. 9 : 1, sulphur dioxide is the principal product, but in this region, a cross-over occurs and sulphuric acid becomes the predominant product. The maximum in the curve (Fig. 3) representing the sulphur dioxide produced is not theoretically significant, and simply reflects the increasing percentage of both hydrogen sulphide and sulphur dioxide oxidized with increasing ozone : hydrogen sulphide ratio. Thus when the yields of sulphur dioxide and sulphuric acid are replotted in terms of the hydrogen sulphide actually oxidized, it is seen (Fig. 4) that at very low ozone : hydrogen sulphide ratios, sulphur dioxide is the only reaction product, but as the ratio

TABLE 3  
REACTION DATA

Reaction No.	Reactants (g-mol) $\times 10^4$		Initial O <sub>3</sub> : H <sub>2</sub> S	Products (g-mol) $\times 10^4$			Percentage Deficiency		Ratio SO <sub>2</sub> : H <sub>2</sub> O
	Initial O <sub>3</sub>	Initial H <sub>2</sub> S		H <sub>2</sub> S Oxidized	SO <sub>2</sub> Formed	H <sub>2</sub> O Formed	H <sub>2</sub> SO <sub>4</sub> Formed	CO <sub>2</sub> Impurity	
23	17.7	4.96	(2.63)*	3.6	2.46	2.12	0.34	(0.69)	—
24	3.61	3.61	(0.68)	1.0	0.66	0.69	0.01	(0.12)	1.16 0.96
25	8.7	3.36	(1.44)	2.6	1.30	1.18	0.20	(0.25)	1.10
26	5.8	1.93	(1.57)	3.0	1.16	0.97	0.49	(1.24)	1.26
27	7.3	2.18	(1.32)	3.4	1.17	1.07	0.20	(0.20)	1.09
28	4.6	1.90	(0.80)	2.4	0.74	0.72	0.07	—	1.03
29	5.4	2.05	1.14	2.6	0.95	0.89	0.13	0.29	5.3 1.07
30	3.24	1.86	0.70	1.7	0.63	0.68	0.03	0.32	6.0 —1.4
31	2.69	3.13	0.59	0.86	0.54	0.58	0.02	0.16	5.1 —1.7
32	2.78	2.81	0.82	0.99	0.72	0.76	0.04	0.18	4.9 2.4
33	3.72	5.74	0.74	0.65	0.69	—	0.03	0.13	2.7 —
35	25.5	3.98	3.61	6.4	2.24	—	1.25	0.59	3.3 —
36	15.6	3.86	2.57	4.0	1.93	1.80	0.52	0.34	4.7 1.07
37	12.1	2.47	1.95	4.9	1.51	1.47	0.45	0.23	—0.5 1.03
39	10.4	1.10	1.10	9.5	0.53	0.57	0.66	0.9	0 1.02
40	32.4	1.62	1.62	20.0	Nil	1.56	—	3.7	3.7 —

\* The values in brackets are calculated by mass balancing reactants and products for hydrogen and sulphur. These runs were partly vitiated by the presence of c. 0.02% CO<sub>2</sub> impurity.

is increased, the production of sulphuric acid increases linearly at the expense of the quantity of sulphur dioxide which decreases linearly over the whole of the concentration range studied.

Although the experimental points display some scatter, they serve to confirm that water, sulphur dioxide, and sulphuric acid are almost certainly the only reaction end-products. In eight of the reactions carried out, it was possible to analyse for all products and reactants. The data are given in Table 3 and it is seen that sulphur and hydrogen mass balances are usually obtained to within

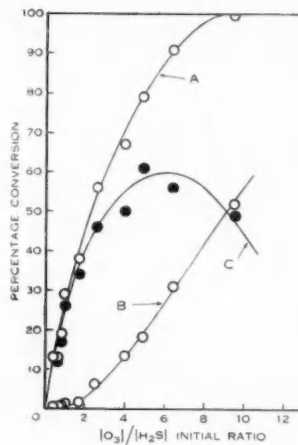


Fig. 3

Fig. 3.—Conversion of initial H<sub>2</sub>S to SO<sub>2</sub> and H<sub>2</sub>SO<sub>4</sub>.  
*A*, Initial H<sub>2</sub>S oxidized (%).  
*B*, Initial H<sub>2</sub>S converted to H<sub>2</sub>SO<sub>4</sub> (%).  
*C*, Initial H<sub>2</sub>S converted to SO<sub>2</sub> (%).

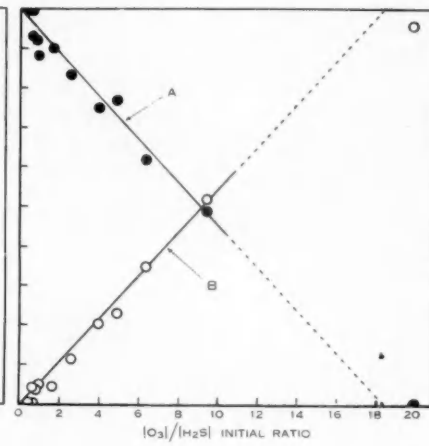


Fig. 4

Fig. 4.—Conversion of oxidized H<sub>2</sub>S to SO<sub>2</sub> and H<sub>2</sub>SO<sub>4</sub>.  
*A*, Oxidized H<sub>2</sub>S converted to SO<sub>2</sub>.  
*B*, Oxidized H<sub>2</sub>S converted to H<sub>2</sub>SO<sub>4</sub>.

about  $\pm 5\%$ , which is not an unreasonable scatter when one considers that considerably less than millimolar quantities are being handled and fractionated under high vacuum conditions. The overall stoichiometry of the reaction can, under the present conditions, therefore be conveniently represented by an equation of the form



where  $0 < x < 1$  and  $x \rightarrow 0$  as the initial ratio  $[\text{O}_3]/[\text{H}_2\text{S}] \rightarrow 18$  or greater. It was impossible in the present work to perform mass balances for oxygen, because of the apparent photochemical and catalytic decomposition of ozone, the extent of which was unknown under the present reaction conditions.

The authors thank the Metropolitan Water, Sewerage and Drainage Board of Sydney for financial assistance with this project. They are also grateful to the Hooker Electrochemical Co., U.S.A., and the Monsanto Chemical Co., U.S.A., for their respective gifts of "Fluorolube" stopcock lubricant and colloidal silica.

### References

AXWORTHY, A. E., and BENSON, S. W. (1959).—"Ozone Chemistry and Technology." p. 388. (Amer. Chem. Soc.: Easton, Pa.)

BRESCIANI, U. (1915).—*Ann. Chim. appl.* **4**: 343.

CLARK, A. M., COCKET, A. H., and EISNER, H. S. (1951).—*Proc. Roy. Soc. A* **209**: 408.

GREGOR, I. K., and MARTIN, R. L. (1959).—*Aust. J. Chem.* **12**: 424.

LEROUY, D. J. (1950).—*Canad. J. Res. B* **28**: 492.

MELLOR, J. W. (1930).—"A Comprehensive Treatise on Inorganic and Theoretical Chemistry." Vol. 10. p. 130. (Longman's: London.)

PENNINGTON, W. A. (1949).—*Analyt. Chem.* **21**: 766.

SCHWARZ, L., and MUNCHMEYER, G. (1913).—*Z. Hyg. InfektKr.* **75**: 81.

VOGEL, A. I. (1952).—"Text Book of Practical Organic Chemistry." p. 819. (Longman's: London.)

## THE CHEMICAL CONSTITUENTS OF AUSTRALIAN *FLINDERSIA* SPECIES\*

### XIV. THE CONSTITUENTS OF *FLINDERSIA ACUMINATA* C. T. WHITE

By E. RITCHIE,† W. C. TAYLOR,† and STEPHANIE T. K. VAUTIN†

*Flindersia acuminata* C. T. White, also commonly known as silver silkwood, Putt's pine, Paddy King's beech, and icewood, is a large tree occurring in the rain-forests of the Johnstone River and Atherton Tableland of north Queensland. The timber, which is light, soft, and silver-white, is used in cabinet-making.

Systematic extractions of the bark, leaves, and wood have been carried out and a number of constituents isolated and identified. From the bark, dictamnine (0·0003%), maculine (0·0003%), and hesperidin (0·085%) were obtained; in addition, the ubiquitous sitosterol (0·02%) and hexacosanol (0·006%), together with a trace of an unidentified yellow pigment were isolated. The leaves yielded hesperidin (0·17%), sitosterol (0·17%), and triacontanoic acid (0·013%) but the wood, only hesperidin (0·1%) and sitosterol (0·005%). A search for quaternary furoquinoline alkaloids of the type described by Price (1959), in each of the plant parts, gave negative results.

\* Manuscript received March 6, 1961.

† Department of Organic Chemistry, University of Sydney.

*Experimental*

The substances isolated were identified by direct comparison (mixed m.p.'s and i.r. spectra) with authentic specimens. The general procedure for extraction and isolation has been outlined in Part XII of this series (Ritchie, Taylor, and Wilcocks 1960).

(a) *Extraction of the Bark.*—The light petroleum extract of the bark (32·4 kg; C.S.I.R.O. SN 6261) on concentrating and keeping at 0 °C deposited a small amount of yellowish brown material, from which dilute NaOH extracted a yellow pigment. After repeated recrystallization from methanol, it formed yellow needles, m.p. 199–200 °C (Found: C, 62·7; H, 4·9; O, 32·2%; OCH<sub>3</sub>, nil. Calc. for C<sub>18</sub>H<sub>16</sub>O<sub>7</sub>: C, 62·8; H, 4·7; O, 32·5%) but insufficient material remained for further work.

The crude alkaloid fraction after combination with a similar fraction from the ether extract was chromatographed on alumina, yielding dictamine (0·1 g) and maclurine (0·1 g).

After removal of the acidic and phenolic fractions, which were dark intractable gums, the residual material was saponified. The neutral fraction chromatographed on alumina gave sitosterol (7·0 g).

The ether extract gave a crude alkaloid fraction which was combined with that from the light petroleum extract (see above). The acidic and phenolic fractions were again intractable, but the neutral material after saponification yielded hexacosanol (2·0 g) by chromatography on alumina.

The acetone extract on concentration deposited crude hesperidin (21 g), which was partially purified by washing with small quantities of warm acetone and methanol. The combined, dark filtrates yielded no further crystalline products.

The methanol extract behaved similarly, yielding only hesperidin (7 g).

(b) *Extraction of the Leaves.*—These (15·3 kg) were extracted with light petroleum, ether, and methanol.

The phenolic fraction obtained by shaking the concentrated light petroleum extract with dilute NaOH was methylated by diazomethane. On chromatographing the esters on alumina, a crystalline fraction was eluted by ether. After repeated recrystallization from light petroleum, methyl triacontanoate, m.p. 69–70 °C (1·2 g), was obtained. By saponification of the neutral fraction of this extract, sitosterol (15 g) was obtained.

The ether extract also yielded methyl triacontanoate (0·8 g) and sitosterol (10 g).

The methanol extract afforded crude hesperidin (25 g) on concentrating and keeping.

(c) *Extraction of the Wood.*—The milled shavings (6·5 kg) gave sitosterol in the light petroleum (0·1 g) and ether extracts (0·2 g) and hesperidin (6 g) in the methanol extract.

The authors are indebted to Mr. W. T. Jones, C.S.I.R.O., Brisbane, for the plant material.

*References*

PRICE, J. R. (1959).—*Aust. J. Chem.* **12**: 458.  
RITCHIE, E., TAYLOR, W. C., and WILLCOCKS, D. V. (1960).—*Aust. J. Chem.* **13**: 426.

## CHEMICAL STUDIES OF THE MYRTACEAE\*

### III. TRITERPENOIDS FROM THE WOOD OF *TRISTANIA CONFERTA* R.BR.

By E. RITCHIE,<sup>†</sup> DIANA SNAPE,<sup>†</sup> and W. C. TAYLOR<sup>†</sup>

*Tristania conferta* R.Br. is one of the most familiar trees of eastern Australia. It ranges from Port Stephens in New South Wales to Bowen in Queensland and is used very extensively in Sydney for street planting. The timber of this tree, which may reach a height of 120 ft, is close-grained, hard, and heavy. Commercially it is known as brush box and is used as decking for wharves and bridges and for flooring.

Preliminary tests by Simes *et al.* (1959) suggested that triterpenoids were present in the bark, leaves, and wood. In the present work, the wood has been systematically extracted. From the light petroleum extract a neutral fraction was obtained which after saponification yielded, in addition to the widespread sitosterol, cycloecalenol, previously reported by Cox, King, and King (1956) from the wood of *Eucalyptus microcorys*, and 24-methylenecycloartanol recently obtained by Ohta and Shimizu (1958) from a quite unrelated source, namely Japanese rice bran oil. The ether extract of the wood yielded large quantities (3·5%) of arjunolic acid, first isolated by King, King, and Ross (1954) from the wood of *Terminalia* species; the acetone and methanol extracts gave further small quantities of the same substance.

#### Experimental

Melting points are uncorrected.

(a) *Extraction with Light Petroleum.*—The milled wood (28 kg) was exhausted with light petroleum (b.p. 60–90 °C) at room temperature and the combined extracts concentrated to a thick reddish brown gum (360 g). This was dissolved in ether and the solution washed in turn with aqueous Na<sub>2</sub>CO<sub>3</sub> and NaOH. These reagents extracted only small amounts of gums which were discarded. The ether was removed and the residue saponified by refluxing with excess 10% alcoholic KOH for 8 hr. The reaction mixture was worked up as usual to yield an acidic and a neutral fraction. The former, a dark reddish brown gum, which apparently consisted of fatty acids, was discarded. The neutral fraction was dissolved in light petroleum and chromatographed systematically on alumina (7 kg). The early fractions eluted by ether–benzene consisted essentially of a mixture of cycloecalenol and 24-methylenecycloartanol, and later fractions eluted by ether–benzene and by ether, of sitosterol. By a combination of fractional crystallization from methanol and chromatography of the appropriate fractions, eventually sitosterol (0·3%), 24-methylenecycloartanol (0·12%), and cycloecalenol (0·004%) were separated. Cycloecalenol was eluted more readily than the other two substances. Each substance, together with its acetate, was identified by direct comparison (mixed m.p.'s and i.r. spectra) with an authentic specimen.

\* Manuscript received March 6, 1961.

† Department of Organic Chemistry, University of Sydney.

(b) *Isolation of Arjunolic Acid.*—Following the extraction with light petroleum, the wood was extracted with ether until almost no solid separated on concentration of the ether solution (about 8–10 times). The total extract was concentrated to a small bulk and the cream solid which separated, collected and washed with a little ether (3·5% yield).

The product could be purified either by recrystallizing its sodium salt from aqueous alcoholic NaOH followed by regeneration, or more satisfactorily, by direct crystallization as follows. The acid (10 g) was dissolved in a little methanol and ethyl acetate (700 ml) added. The filtered solution was boiled down on the steam-bath until bumping due to separation of crystals became bad. The mixture was allowed to cool, then quickly heated to boiling and the liquid decanted from the crystals which were collected with the aid of a little fresh ethyl acetate. Repetition of this procedure yielded a total of 5·6 g of crystalline acid, m.p. 320–322 °C (decomp.). Further recrystallization from ethyl acetate and then from a little methanol gave prismatic needles, m.p. 328–330 °C (decomp.), undepressed by admixture with an authentic specimen. The i.r. spectra of the two specimens were also identical, and the identification was confirmed by direct comparison of the triacetyl-lactones.

By re-working the mother liquors further quantities of arjunolic acid were obtained, but no other substance could be isolated. The acetone and methanol extracts of the wood on evaporation to a small bulk and dilution with ether also gave further small quantities of arjunolic acid.

The authors are grateful to the Forestry Commission of New South Wales for a supply of the plant material, and to Dr. T. J. King, University of Nottingham, and Dr. M. Shimizu, Daiichi Seiyaku Co. Ltd., Japan, for specimens of cyclo-eucalenol, arjunolic acid and its derived triacetyl-lactone, and of 24-methylene-cycloartanol, respectively.

#### References

COX, J. S. G., KING, F. E., and KING, T. J. (1956).—*J. Chem. Soc.* **1956**: 1384.  
KING, F. E., KING, T. J., and ROSS, F. M. (1954).—*J. Chem. Soc.* **1954**: 3995.  
OHTA, G., and SHIMIZU, M. (1958).—*Chem. Pharm. Bull. Japan* **6**: 325.  
SIMES, J. J. H., TRACEY, J. G., WEBB, L. J., and DUNSTAN, W. J. (1959).—An Australian phytochemical survey. C.S.I.R.O. Aust. Bull. No. 281.

## CHEMICAL STUDIES OF THE MYRTACEAE\*

### IV. CONSTITUENTS OF THE WOOD OF ANGOPHORA SUBVELUTINA F. MUELL.

By E. RITCHIE† and W. C. TAYLOR†

Following the isolation of the uncommon triterpenes, cycloeucaleanol, 24-methylenecycloartanol, and arjunolic acid, from the wood of *Tristania conferta* R.Br. (Ritchie, Snape, and Taylor 1961) it was decided to examine the woods of some species of related genera, and the present paper is concerned with the wood of *Angophora subvelutina* F. Muell. This medium-sized tree, commonly known as broad-leaved apple, is fairly common in the central and northern coastal regions of New South Wales, the timber often being used for fencing.

Several substances were isolated from the wood, but in small amounts only; ellagic acid (0·024%), sitosterol (0·025%), and 24-methylenecycloartanol (0·014%) were identified. In addition, fractions apparently consisting essentially of tetracosanoic acid (0·001%) and 24-hydroxytetracosanoic acid (0·021%) were obtained, but because of the small amounts available and the difficulties involved in purification (Murray and Schoenfeld 1955) their investigation was not pursued.

#### Experimental

Melting points are uncorrected.

(a) *Light Petroleum and Ether Extracts*.—The milled wood (10 kg) was extracted at room temperature with light petroleum (b.p. 60–90 °C; 4 × 15 l.) and then ether (3 × 15 l.). Evaporation of the extracts gave thick brown oils (23 and 9 g respectively) which were combined and saponified by heating under reflux with excess 10% alcoholic KOH for 6 hr. On working up in the usual manner neutral and acidic fractions were obtained together with an interfacial precipitate of insoluble potassium salts.

The neutral fraction, a thick reddish brown oil (11 g), was chromatographed on alumina (300 g). The ether-methanol (9 : 1) eluate crystallized from methanol, but the material (5·6 g) was obviously a mixture. On further chromatography on alumina (150 g) using benzene-ethyl acetate, 24-methylenecycloartanol (1·4 g) was first eluted, followed by sitosterol (2·5 g). The substances were identified by direct comparison (mixed m.p.'s and i.r. spectra) with authentic specimens. The acetates were also compared. No other substance could be isolated from the mother liquors.

The acidic fraction, a very dark reddish brown gum, was recycled with alkali, and then digested with light petroleum. The insoluble, dark, amorphous material was discarded and the filtrate evaporated to yield a brown gum (2·8 g) which was chromatographed in light petroleum on silica gel (100 g). The first eluates, on keeping, crystallized; repeated recrystallization from methanol, light petroleum, and ethanol gave colourless needles (0·1 g), m.p. 78–79 °C (Found: C, 78·5; H, 13·3%. Calc. for  $C_{21}H_{48}O_2$ : C, 78·1; H, 13·1%). The methyl ester crystallized from methanol in colourless plates, m.p. 56–58 °C. Tetracosanoic acid has m.p. 84 °C and its methyl ester, m.p. 59–60 °C.

\* Manuscript received March 6, 1961.

† Department of Organic Chemistry, University of Sydney.

The insoluble interfacial precipitate was recycled and the acid (2.1 g) liberated from the slimy precipitate. Recrystallization from acetic acid and light petroleum gave a colourless solid, m.p. 93–94 °C (Found: C, 74.7; H, 13.0%. Calc. for  $C_{24}H_{48}O_3$ : C, 74.9; H, 12.6%). The acetate of the methyl ester had m.p. 63–65 °C. The m.p. of the acid has not been recorded, but Murray and Schoenfeld (1955) give m.p. 63 °C for the acetate of the methyl ester.

(b) *Isolation of Ellagic Acid.*—The wood was then extracted with acetone ( $3 \times 15$  l.) and with methanol ( $7 \times 15$  l.).

The acetone extract was concentrated to a thick reddish brown syrup which was then digested with ethyl acetate (300 ml). The insoluble solid was collected, washed with ethyl acetate, and shaken with 5%  $Na_2CO_3$  (200 ml). The insoluble sodium salt was collected and washed with a little water. On treating with acid, ellagic acid (0.9 g) was regenerated. It was identified by the usual colour tests (Bate-Smith 1956) and by direct comparison of its acetyl derivative with authentic tetraacetyllellagic acid. The ethyl acetate filtrate failed to yield any crystalline substances.

The methanol extract on concentration yielded successive crops of crystalline material and eventually a very dark reddish brown syrup. Attempts to obtain crystalline substances from the syrup either before or after hydrolysis with acid or alkali, were unsuccessful. The crystalline precipitate consisted chiefly of inorganic material, which was removed by washing with water. The residue on purification as above gave more ellagic acid (1.4 g).

The authors are indebted to the Forestry Commission of New South Wales for a supply of the wood.

#### References

BATE-SMITH, E. C. (1956).—*Chem. & Ind. B.I.F.R.* **1956**: R32.  
MURRAY, K. E., and SCHOENFELD, R. (1955).—*Aust. J. Chem.* **8**: 437.  
RITCHIE, E., SNAPE, DIANA, and TAYLOR, W. C. (1961).—*Aust. J. Chem.* **14**: 471.

## FURTHER METABOLIC PRODUCTS OF *POLYPORUS TUMULOSUS* COOKE\*

By R. K. CROWDEN† and B. J. RALPH‡

When grown as a surface culture on a glucose-salts medium, the basidiomycete fungus *Polyporus tumulosus* Cooke produces a series of phenolic acid metabolites. These are secreted into the culture liquor, from which they can readily be obtained by exhaustive ether extraction. Identification of three of these metabolites, namely, 3,4-dihydroxyphenylacetic acid (I) (homoprotocatechuic acid), 2,5-dihydroxyphenylglyoxylic acid (II), and 2,4,5-trihydroxyphenylglyoxylic acid (III), has been reported previously (Ralph and Robertson 1950; Moir and Ralph 1954).

During investigations aimed at elucidating the possible metabolic interrelationships of these compounds, identification of some further metabolites has been made. Three of these, namely, *p*-hydroxybenzoic acid (IV), *p*-hydroxyphenylacetic acid (V), and 2,5-dihydroxybenzoic acid (VI) (gentisic acid), are well-known products of the activity of microorganisms. In addition to the above compounds, evidence has been obtained that 3,4-dihydroxyphenylglyoxylic acid (VII) is formed in small amount. To the authors' knowledge, this compound has not previously been reported as a fungal metabolite, although it has been cited as an intermediate in the breakdown of noradrenalin by chicken liver slices (Wada 1957).

These minor metabolic products make only a transient appearance in the culture liquor, corresponding to a phase of active growth of the organism, and they are not discernible in liquors from aged or autolysing cultures. A detailed discussion of the sequential production of metabolites in relation to the possible mode of biosynthesis of the phenylglyoxylic acids is the subject of a further paper, at present in preparation.

When liquor obtained from under comparatively young cultures (14–21 days) was examined spectroscopically, absorption peaks appeared at 254, 275, and 325 m $\mu$ , which could not be reconciled with those of any of the known metabolites. Corresponding spots of unknown identity appeared on paper chromatograms. The unknown compounds were subsequently isolated, and identified as (IV), (V), and (VI) respectively by their characteristic properties, and by the preparation of derivatives.

Spots corresponding to at least two other phenolic compounds in very minute amount also made irregular appearances on chromatograms. It was observed that one of these compounds, (VII), was formed in greatly increased amount

\* Manuscript received February 7, 1961.

† School of Biological Sciences, The University of New South Wales, Sydney; present address: Botany Department, University of Tasmania, Hobart.

‡ School of Biological Sciences, The University of New South Wales, Sydney.

TABLE I  
CHROMATOGRAPHIC DATA RELEVANT TO THE POLYPOURUS TUMULOSUS METABOLITES

Treatment or reagent	<i>R<sub>F</sub></i> Values						
	I	II	III	IV	V	VI	VII
Solvent							
(a) Butanol : acetic acid : water (4 : 1 : 3)	..	0.76	0.51	0.35	0.88	0.90	0.84
(b) Benzene : acetone : formic acid (20 : 4 : 1)	..	0.09	0.20	0.06	0.49	0.39	0.43
(c) Butanol : ethyl acetate : pyridine : water (3 : 2 : 1 : 4)	0.60	0.40	0.30	0.84	0.73	0.40	0.22
					Colours produced with visualizing reagent <sup>a</sup>		
(a) Visible light	..	..	..	..	Yellow	Yellow	Yellow
(b) Ultraviolet light	..	..	..	..	Dark	Dark	Dark
(c) Ferric chloride (0.2% aqueous)	..	..	..	..	Transient green	Brown	Blue-yellow
(d) 2,4-Dinitrophenylhydrazine (0.1% in 2N HCl)	..	..	..	..	Orange	—	—
(e) Diazoized <i>p</i> -nitroaniline	..	..	..	..	Brown	Red	Purple
(f) Diazoized sulphamic acid	..	..	..	..	Brown	Yellow	Red
(g) Triphenyltetrazoleum chloride	..	..	..	..	Pink	Orange	Dull pink

when *P. tumulosus* was cultured in the presence of 0·001M *p*-hydroxymandelic acid (added as a supplement to the usual culture medium), in fact in sufficient quantity to permit of its isolation and characterization. The other unknown metabolite is as yet unidentified, and further investigations into the nature of this compound are proceeding.

Spectroscopic and chromatographic data relevant to the *P. tumulosus* metabolites are presented in Tables 1 and 2.

TABLE 2  
ABSORPTION SPECTRA OF THE POLYPORUS TUMULOSUS METABOLITES IN WATER

Compound	Wavelength (m $\mu$ )		Compound	Wavelength (m $\mu$ )	
	Maxima	Minima		Maxima	Minima
I	280	252	V	275	250
II	230, 263, 360	249, 295	VI	323	267
III	242, 285, 348	226, 260	VII	234, 285, 310	255, 304
IV	253	224			

### Experimental

(i) *Paper Chromatography*.—Chromatograms for qualitative examinations were made on Whatman No. 1 paper, using the ascending technique at room temperature. Accordingly, the *R*<sub>F</sub> values quoted in Table 1 are only relative. The three chromatographic solvents used were:

- (a) Butanol : acetic acid : water (4 : 1 : 5)—the upper layer being used.
- (b) Benzene : acetone : formic acid (20 : 4 : 1)—water then being added dropwise to saturation, but maintaining only one phase.
- (c) Butanol : ethyl acetate : pyridine : water (3 : 2 : 1 : 4)—the upper layer being used.

The following visualizing reagents were used to detect the compounds on paper chromatograms:

- (a) Examination under visible light ; (b) examination under u.v. light ; (c) ferric chloride (0·2% aqueous) ; (d) 2,4-dinitrophenylhydrazine (0·1% in 2N HCl) ; (e) diazotized *p*-nitroaniline (Bray and Thorpe 1954) ; (f) diazotized sulphanilic acid (Bray and Thorpe 1954) ; (g) triphenyltetrazoleum chloride (Trevelyan, Procter, and Harrison 1950).

(ii) *Ultraviolet Spectra*.—Spectra of the compounds in water were recorded using a Cary recording spectrophotometer, model II.

(iii) *Identification of New Metabolites*.—The compounds (IV), (V), and (VI) were isolated from ether extracts of 14–27 days' culture liquors by repeated preparative-scale chromatography on Whatman 3MM paper. Chromatograms were developed with solvent (c), and, after drying, the appropriate bands were cut and eluted with acetone, the respective eluates then being evaporated to dryness under reduced pressure.

Compound (IV) was obtained as white prisms from ethanol–benzene, m.p. 213 °C, undepressed in mixture with an authentic sample (L. Light and Co.). Each of the *O*-acetyl derivatives, prepared from the isolated and authentic (IV) respectively had m.p. 185–186 °C, undepressed on admixture. (V) was obtained from ethyl acetate as white, microscopic crystals which took on a slight tinge after several weeks, m.p. 145–147 °C. A sample of (V) (Salkowski 1889) did not depress the melting point on admixture. The *O*-methyl ethers prepared from the isolated and synthetic (V) respectively were of identical m.p. 85–87 °C, and there was no depression of m.p. on admixture. The fraction, consisting principally of (VI), was purified by successive vacuum distillations yielding ultimately pure white microscopic needles, m.p. 201 °C, undepressed on admixture with an authentic sample (L. Light and Co.). The diacetyl derivatives of both

isolated and authentic materials had identical m.p. 118 °C, undepressed on admixture. The dimethyl derivatives were similarly identical, m.p. 76 °C. (VII) was obtained as dull yellow, microscopic needles from ethyl acetate-light petroleum (80–100 °C). The material charred and decomposed above 140 °C if heated slowly, but melted sharply at 160 °C when placed in a pre-heated bath. Synthetic (VII) (Barger and Ewins 1909) had m.p. 159–160 °C, undepressed in mixture with the naturally-occurring material. Decarboxylation of both samples of (VII) with *p*-methylaniline (Businelli 1950) in each case yielded protocatechualdehyde, m.p. 152 °C, identical with a synthetic sample prepared by demethylation of vanillin with aluminium bromide.

We are grateful to Mr. K. Schaffner, Department of Organic Chemistry, The University of New South Wales, for synthesizing *p*-hydroxyphenylacetic acid, and to Mr. I. Reece, Department of Physical Chemistry, The University of New South Wales, who operated the Cary spectrophotometer.

#### References

BARGER, G., and EWINS, A. J. (1909).—*J. Chem. Soc.* **95**: 560.  
BRAY, H. G., and THORPE, W. V. (1954).—“Methods of Biochemical Analysis.” pp. 1–35. (Ed. D. Glick.) (Interscience Press: New York.)  
BUSINELLI, M. (1950).—*Farmaco* **5**: 522–7. (*Chem. Abstr.* **45**: 3819f (1951).)  
MOIR, G. F. J., and RALPH, B. J. (1954).—*Chem. & Ind.* **1954**: 1143.  
RALPH, B. J., and ROBERTSON, J. (1950).—*J. Chem. Soc.* **1950**: 3380.  
SALKOWSKI, H. (1889).—*Ber. dtsch. chem. Ges.* **22**: 2137.  
TREVELYAN, W. E., PROCTER, D. P., and HARRISON, J. S. (1950).—*Nature* **166**: 444.  
WADA, M. (1957).—*Osaka Daigaku Igaku Zasshi* **9**: 279. (*Chem. Abstr.* **51**: 14138g (1957).)

